Methodology for the design of optimal processes : application to sugarcane conversion processes

Rami Bechara

Université Lyon I - Claude Bernard

Ecole Doctorale de Chimie

Thèse en vue de l'obtention d'un diplôme de DOCTEUR

Spécialité Procédés

Présentée par

BECHARA RAMI

METHODOLOGY FOR THE DESIGN OF OPTIMAL PROCESSES: APPLICATION TO SUGARCANE CONVERSION PROCESSES

DIRECTEUR DE THESE : SCHWEITZER Jean-Marc, Docteur, IFPEN Université Lyon I

CODIRECTEUR DE THESE : MARECHAL François, Professeur titulaire, EPFL

Le 17.11.2015, 10H30, AMPHITHEATRE AIGUE-MARINE IFPEN SOLAIZE, France

PRESIDENT: M. JALLUT Christian, Professeur des Universités, Université Lyon

RAPPORTEUR: M. ZOUGHAIB Assaad, Maître Assistant, Mines ParisTech

RAPPORTEUR: M. FAVRAT Daniel, Professeur honoraire, Ecole Polytechnique Fédérale de Lausanne

MEMBRES DU JURY

MEMBRE: Mme. BOIX Marianne, Maître de Conférences, Université de Toulouse

MEMBRE: MARECHAL François, Professeur titulaire, EPFL

MEMBRE: SCHWEITZER Jean-Marc, Docteur, IFPEN, Université Lyon I

=

Remerciements

Une thèse est une réussite certes individuelle mais qui se doit à la contribution d'un grand nombre de personnes. C'est pourquoi je me concentre dans cette section sur le remerciement de toutes les personnes qui ont contribué de près ou de loin à ce succès.

Je commence par remercier mes encadrants, collègues, rapporteurs et examinateurs, qui ont contribué à ce que la thèse soit un succès professionnel et scientifique.

Je désire remercier tout d'abord Adrien Gomez mon encadrant de thèse. Dr. Gomez était celui qui a proposé cet excellent sujet et & été responsable de ma sélection. Je salue aussi son encadrement impeccable, continu et professionnel tout au long des trois années et quelques de cette thèse.

Je remercie Valérie Saint-Antonin ainsi que ses collègues de la direction de Veille Economique : Frédérique Bouvart et Jérôme Sabathier. Leur support ainsi que leurs conseils m'étaient vraiment précieux lors de cette thèse.

Je remercie mon directeur de thèse Jean-Marc Schweitzer. Sa contribution était cruciale pour la définition conforme du procédé ainsi que du problème de l'optimisation ; des points clés dans le succès de cette thèse.

Je remercie aussi Professeur François Maréchal, mon directeur de thèse à l'EPFL. De par sa grande connaissance, son ouverture d'esprit et sa vue d'ensemble, Professeur Maréchal m'a appris l'art d'une approche systématique.. Tout échange avec Professeur Maréchal était fructueux, et tout conseil inestimable.

Je remercie de plus la direction de mon département et de ma direction à l'IFPEN, la direction de l'Ecole Doctorale IFP School et Chimie Lyon I, qui ont assuré un encadrement supplémentaire de ce travail.

Je remercie aussi mes collègues ingénieurs, post-docs, thésards et stagiaires pour leur support infaillible tout au long de cette thèse.

Mes remerciements s'étendent à mes collègues de l'EPFL, spécialement Adriano Ensinas et Juliana Albarelli, qui m'ont encadré pendant les premières phases de ma thèse.

=
Je remercie ensuite mes rapporteurs et examinateurs qui ont contribué à un manuscrit simple et didactique, surtout mes rapporteurs Dr. Assaad Zoughaib et Prof. Daniel Favrat

Je me tourne ensuite vers ma famille, mes amis ainsi quel les soldats inconnus.

Je commence par remercier mon père Bechara et ma mère Hala. Leur contribution à mon succès et ma croissance est incomparable. Cette contribution s'est concrétisée encore une fois dans l'effort mis dans le succès de ma soutenance de thèse et du pot qui a suivi. Je désire aussi remercier mes frères, Elie et Fadi, qui étaient toujours à mes côtés et qui ont toujours soutenu mes études malgré la distance qui nous séparait. Je remercie aussi mes oncles et tantes. De par leurs soucis de mon sort, ils me donnaient toujours le désir d'aller au-delà et de rester sain et sauf. Je remercie aussi mes cousins, surtout Georges. Sa grande appréciation de ma personne m'a toujours poussée à donner le mieux de moi-même et j'espère toujours rester un bon exemple pour lui. Je remercie finalement mon grand-père, Badih. Son support infaillible et ses conseils précieux se sont toujours présentés comme un phare sur mon chemin personnel et professionnel. Votre support et vos conseils m'ont aidé dans la poursuite de mes études en France qui ont culminé dans cette thèse réussie. Un grand MERCI à tous.

Je remercie dans un second lieu mes amis, à la fois proches et lointains, qui m'ont toujours donné le sentiment d'être apprécié et le plus important d'être près de chez moi, même dans des moments qui paraissaient difficiles. Un grand MERCI à tous.

Je remercie aussi les soldats anonymes qui m'ont aidé dans le bon déroulement de cette thèse.

=

Dédicace

Je conclus ce prologue par une dédiasse et un slogan.

Pour la dédicace, un artiste a sa muse, un héros sa princesse, mais moi j’ai la triade :

A ma FAMILLE, A mon PAYS, A mon EGLISE

Pour le slogan, je cite une personne qui m’est chère au monde :

« Que votre lumière luise ainsi devant les hommes, afin qu'ils voient vos bonnes œuvres, et qu'ils glorifient votre Père qui est dans les cieux. » Matthieu 5 :16

=

Titre

Méthodologie pour la conception de procédés optimaux : application aux procédés de conversion de canne à sucre

Résumé

L'adoption d'une méthodologie est cruciale pour la conception de procédés chimiques optimaux. L'optimisation multi-objective de modèles rigoureux en est un exemple, jouissant d'une application extensive dans la littérature. Cette méthode retourne un ensemble de solutions, dit de Pareto, présentant un compromis optimal entre les fonctions objectives. Ceci est suivi par une étape de sélection d'une solution d'intérêt répondant à des critères définis.

Cette méthodologie s'appliquait, dans le cadre de cette thèse, à deux procédés. Le premier consistait en une distillerie d'éthanol à partir de la canne à sucre, combinée à un système de cogénération et de combustion à partir de la biomasse de canne à sucre. Le deuxième contenait en plus un système d'hydrolyse enzymatique de cette biomasse.

Notre première contribution traitait de la construction d'une procédure pour la modélisation, simulation, intégration thermique et évaluation du coût des équipements.

La deuxième contribution traitait de l'analyse des résultats réalisée à travers un suivi de variables mesurées, une fragmentation de la courbe de Pareto, une hiérarchisation des variables de décision et une comparaison avec la littérature.

La dernière contribution traitait de l'étape de sélection qui s'est réalisée à travers une évaluation économique des solutions, sous des scénarii différents, avec la Valeur Nette Présente comme critère de sélection.

En conclusion, cette thèse constitue une première application intégrale de la méthodologie proposée. Elle représente, de par ses contributions, un tremplin pour des applications futures à des procédés chimiques ou biochimiques, plus spécialement pour la canne à sucre.

Mots clés

Conception, Procédés, Optimisation, Multi-Objectif, Sélection, Bioéthanol, Bioélectricité, Canne à Sucre, Hydrolyse, Distillation, Technico-économie, Exergie, Algorithmes Evolutifs, Intégration Thermique

=

Title

Methodology for the design of optimal processes: application to sugarcane conversion processes.

Abstract

The use of a systematic methodology is crucial for the design of optimal chemical processes, namely bio-processes. Multi-objective optimization of rigorous process models is therein a prime example, with extensive use in literature. This method yields a Pareto set of optimal compromise solutions, from which one optimal solution is chosen based on specific criteria.

This methodology was applied, in the course of this thesis, to two studied processes. The first consisted in a distillery converting sugarcane to ethanol, combined with a sugarcane biomass combustion and power cogeneration system. The second contained an additional biomass hydrolysis system.

Our first contribution deals with the construction of an organized procedure for the modeling, simulation, heat integration and equipment and capital cost estimation of chemical processes.

The second contribution deals with the analysis of the optimization results through a tracking of measured variables, the fragmentation of the Pareto curve, an ordering of optimization variables, and a comparisons with literature results.

The final realization deals with the selection step realized through an economic evaluation of optimal solutions for various scenarios, with the Net Present Value as the selection criterion.

In conclusion, this thesis constitutes a first integral application of the said methodology. It sets, through its contributions, a stepping stone for future application in the field of chemical and biochemical processes, namely for sugarcane processes.

Keywords

Design, Process, Optimization, Multi-objective, Selection, Bioethanol, Bioelectricity, Sugarcane, Hydrolysis, Distillation, technico-economic, exergy, evolutionary algorithms, heat integration

=

Thèse réalisée dans / Thesis realized at :

Département R121 Process Design,

Direction R12 Conception-Modélisation des procédés

Institut Français du Pétrole et des Énergies Nouvelles

BP3, Rond Point de l'Échangeur de Solaize

69360 Solaize, France

=

Résumé substantiel

Cette thèse est rédigée en anglais, ce qui oblige l'inclusion de ce résumé substantiel en Français.

Cette thèse traite du développement et de l'application d'une méthodologie multi-objective pour la conception de procédés optimaux. Cette méthodologie s'est appliquée sur deux procédés d'étude. Le premier procédé consiste en une distillerie de canne à sucre combinée à un système de cogénération, pour la production d'éthanol et d'électricité. La deuxième traite d'un procédé combinant la distillerie et la cogénération à une étape supplémentaire d'hydrolyse enzymatique, qui se dresse en compétition avec la cogénération.

Ce manuscrit de thèse est structuré comme suit. Dans le premier chapitre, nous présentons et défendons les différentes étapes de la méthodologie. Cette défense se base à la fois sur un raisonnement théorique et sur une expérience bibliographique. Ce chapitre se termine sur une spécification des étapes de la méthodologie, présentées dans le diagramme ci-dessous.

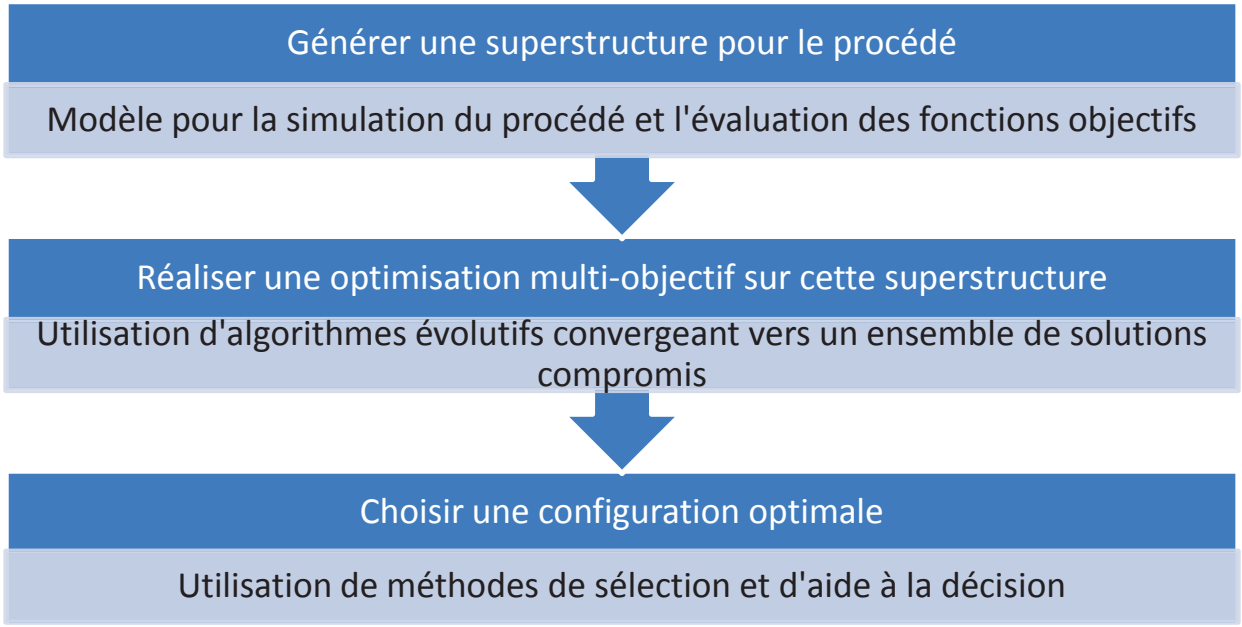

Les deuxième et troisième chapitres contiennent respectivement des informations relatives aux procédés en question, notamment : une revue bibliographique, le modèle de simulation choisi et le modèle d'évaluation associé. Ces chapitres se terminent par la génération d'une superstructure, qui constituera la base des chapitres suivants.

Les quatrième et cinquième chapitres traitent de l'application des deux dernières étapes de la méthodologie à savoir, optimisation et sélection, aux deux procédés en question. Ces chapitres se concluent avec une analyse des résultats optimaux en le comparant avec des résultats similaires extraits de la bibliographie.

Ceci étant dit, cette section présente un résumé des différents travaux réalisés dans cette thèse et des résultats obtenus. Ce résumé se structure autour des étapes de la méthodologie ci-dessus, et fait mention des plus grandes contributions et conclusions de ce travail.

=

Idées clés	Application aux procédés d'étude
Etape I : Générer une superstructure pour le procédé	
La construction d'un modèle de simulation correct pour le procédé est la pierre angulaire pour une implémentation réussie de la méthodologie	Les deux procédés ont été modélisés sur Aspen Plus®. Le choix des opérations unitaires, modèles thermodynamiques et des conditions opératoires s'est basé sur des données bibliographiques.
L'étape de conception du réseau d'échange est essentielle pour toute modélisation correcte du procédé	Ce modèle intervient après la convergence du modèle de simulation. Cette étape permet le calcul des besoins en utilités, la quantité d'électricité cogénérée ainsi que le coût du réseau d'échange pour une configuration de procédés donnée. Un algorithme d'optimisation linéaire (Mixed Integer Linear Programming) se basant sur la technique des cascades thermiques a été utilisé dans ce but, avec l'objectif de maximiser la production d'électricité dans les utilités.
Étape II : Réaliser une optimisation multi-objective	
Le choix des variables d'optimisation, dont les valeurs seront contrôlées, ainsi que leurs intervalles de variation est aussi une étape clé	Ces variables ont été choisies suite à une revue bibliographique sur l'optimisation des deux procédés en question. Trente-trois variables ont été choisies pour le premier et 36 pour le second. Ces variables appartenaient à toutes les sections du procédé et ont été choisies après une étude bibliographique exhaustive.
Le choix de fonctions objectifs adéquates est crucial pour une application fructueuse de la méthodologie	L'efficacité exergétique et les coûts d'investissement étaient les deux fonctions objectives choisies. Ces fonctions reflètent le conflit entre le profit et l'investissement.
L'évaluation correcte de fonctions objectives est une condition supplémentaire pour une bonne application de la méthodologie.	L'efficacité exergétique est calculée comme le ratio du contenu exergétique des produits (éthanol et électricité), à celui de la matière première (canne à sucre, feuilles pour les deux procédés et enzymes en plus pour le deuxième). Les coûts d'investissement sont calculés comme la somme des coûts d'équipements installés dans une unité neuve. Ce calcul s'est basé sur la méthodologie Chauvel utilisé à travers l'industrie.
L'inclusion de variables mesurées dans l'optimisation est de grande importance, autant plus si les variables ont un lien direct avec les fonctions objectives	Quatre variables ont été choisies pour le premier procédé : production d'éthanol, production d'électricité, coût du réseau d'échange, coût des équipements hors échangeurs de chaleur. Une variable supplémentaire a été choisie pour le deuxième procédé : la consommation d'enzymes. L'analyse de ces variables nous a permis de comprendre plus en profondeur les résultats obtenus.
Les algorithmes évolutifs étaient la technique d'optimisation choisie pour notre problème bi-objectif	Ces algorithmes commencent avec un nombre initial de configurations pour lesquels les valeurs des variables d'optimisation sont choisies aléatoirement. Ces configurations évoluent à travers des opérations bien définies vers des solutions optimales. Ces opérations sont :

	évaluation, classement, élimination et création.
Le modèle de conception du réseau d'échange se comporte comme un problème d'optimisation esclave	Ce modèle contrôle un nombre de variables, notamment les débits dans les diverses utilités afin d'optimiser une fonction sous-objectif : maximiser la production d'électricité. Son utilisation réduit ainsi le nombre total des variables contrôlées par l'algorithme évolutif.
La courbe de Pareto obtenue reflète la nature du procédé étudié	Les deux courbes obtenues pour les deux procédés d'étude présentent une croissance de l'efficacité exergétique accompagnée d'une croissance en coûts d'investissement. La première courbe contient 32 points avec une efficacité entre 37,3 et 41,7% et un coût entre 155 et 209 M$. La deuxième courbe contient 44 points avec une efficacité entre 39,2 et 44,4% et un coût entre 210 et 390 M$. De plus deux régions ont été identifiées pour le deuxième cas. La première région est définie par une production d'éthanol constante et d'une production d'électricité croissante. La deuxième est caractérisée par une production d'éthanol croissante et une production d'électricité décroissante. La première région est donc caractéristique d'une grande part de cogénération et intégration thermique, et une plus petite part d'hydrolyse. La deuxième région est caractérisée par une grande part d'hydrolyse et d'intégration thermique pour une plus petite part de cogénération.
La comparaison des résultats obtenus avec ceux de la bibliographie permet de caractériser notre problème et les avantages associés	La comparaison avec la bibliographie était difficile, notamment à cause des différences entre les diverses hypothèses, spécialement la composition de la canne à sucre, l'issue des feuilles, et la technologie adoptée. Cependant elle était possible. Cette comparaison a prouvé que nos résultats était meilleurs que ceux de la littérature pour des conditions similaires, mais moins bien pour des conditions plus favorables, et notamment des technologies plus avancées pour le cas de l'hydrolyse. Ces résultats ont aussi montrée les capacités de nos fonctions objectives, notamment l'efficacité exergétique qui a été rarement évaluée dans la bibliographie associée. Un cas intéressant s'est présenté : celui de la combustion des feuilles. En effet, les cas excluant cette combustion conduisaient à des solutions plus efficaces et moins coûteuses que des solutions incluant cette possibilité. Ceci souligne la nécessité de trouver une meilleure utilisation de cette entrée. Ces résultats soulignent les avantages derrière cette méthode d'optimisation et indiquent les résultats encore mieux qui peuvent être obtenus si elle est appliquée à des configurations plus avancées.
L'analyse des paramètres mesurés permet une compréhension plus approfondie des résultats d'optimisation	Pour le premier procédé, l'efficacité exergétique croît d'une manière linéaire avec la production d'électricité. Une dépendance similaire est observée entre le coût d'investissement et le coût du réseau d'échange. Ces résultats indiquent que des alternatives avec une intégration thermique avancée, caractérisée par une production d'électricité plus importante, conduit à des configurations plus efficaces mais plus coûteuses. De plus,

	la croissance en coûts d'investissement était plus importante que celle en efficacité. Pour le deuxième procédé, la production d'électricité a atteint un maximum pour avant de décroître pour des solutions plus efficaces. La production d'éthanol de l'autre côté demeurait constante pour les solutions avant le maximum d'électricité avant de croître pour les configurations plus efficaces que ce maximum. Ce dernier présente ainsi le passage vers une contribution importante de l'étape d'hydrolyse. Les coûts des équipements hors échangeurs présentaient la plus grande part du coût d'investissement. Ces résultats indiquent qu'une plus grande part d'hydrolyse conduit à des solutions plus efficaces, caractérisées par une production accrue d'éthanol et une production réduite d'électricité, mais avec des coûts d'investissement prohibitifs.
	Cette analyse commence par la caractérisation des intervalles finaux des variables. Des variables avec des intervalles plus rétrécis sont dénommés « variables de distance ». Ces variables de distance indiquent des conditions nécessaires d'optimalité. Ces résultats indiquent autant plus la proximité d'une configuration donnée des conditions optimales. 14 variables de distance ont été identifiées pour le premier problème et 15 pour le deuxième.
• **L'analyse des résultats obtenus pour les variables d'optimisation permet une compréhension plus détaillée des moteurs de l'optimisation**	La technique de fragmentation consiste à diviser la courbe de Pareto obtenue en des intervalles définis par des points d'inflexion ou coudes. Ces points sont caractérisés par un grand saut dans la valeur d'une fonction objective avec un plus petit saut dans la valeur de la deuxième. 7 fragments ont été identifiés dans le premier cas et 12 dans le deuxième. La visualisation de données statistiques des valeurs des variables dans les divers fragments permet une compréhension de l'évolution de la performance avec les valeurs des variables. Elle permet aussi de retrouver les variables les plus déterminantes ainsi que celles avec une moindre influence. Les premières sont caractérisées par une croissance ou décroissance de leurs valeurs à travers la courbe. On parle de variables de position. On distingue les variables de position primaire des variables secondaires. Les variables primaires voient une décroissance continue. Les variables secondaires voient une évolution un peu plus variable. Les deuxièmes sont caractérisées par une évolution aléatoire de leurs valeurs à travers la courbe de Pareto.

=

	11 variables de position primaires, 12 variables de position secondaires et 10 variables aléatoires ont été obtenues pour le premier cas tandis que 2 variables primaires, 18 variables secondaires et 16 variables aléatoires ont été obtenues pour le deuxième cas.
Étape III : Choisir les configurations optimales	
	La Valeur Actuelle Net était évaluée pour chaque alternative optimale sous quatre scénarios économiques différents. Le calcul de cette valeur part de l'évaluation des coûts opératoires, revenus, profit brut, amortissement, profit net et flux de trésoreries actualisés. La VAN est la somme de ces flux actualisés pour toute la durée du projet. Les scénarios de l'autre côté sont déduits de la littérature et englobent des conditions d'opération (vie du projet, nombre de jours d'opération, temps de construction) et des données économiques (prix des produits et de la matière première, autre). Une évolution de la NPV était ainsi attribuée à chaque scénario.
La Valeur Actuelle Net (VAN) était choisie comme critère de sélection. Ce critère permet de choisir la configuration la plus rentable et cela par le biais d'une évaluation économique complète.	Des évolutions similaires ont été observées pour les divers scénarios. Le premier cas était marqué par une VAN positive. Cette VAN augmente pour les points de faible efficacité pour arriver à un maximum à une efficacité de 41.6, après lequel cette valeur décroît pour les efficacités les plus élevées. On remarque aussi la présence de quelques pics de la VAN relatifs aux points d'inflexion ou coudes précédemment obtenus. Le deuxième cas était marqué par des VAN plutôt faible voire négatives avec une tendance similaire au premier pour les configurations de faible efficacité suivie par une tendance en chute pour les points de plus grande efficacité. Nous avons de plus observé une différence dans les valeurs de la VAN entre les scénarios. Cette différence a été attribuée aux conditions économiques et d'opération différentes. Ces différences n'ont pas changé la tendance pour le premier cas. Cependant, une différence dans cette tendance a été observée dans le deuxième problème entre le deuxième et troisième scénario. En effet, la VAN du deuxième scénario a eu des valeurs plus élevées pour des efficacités plus grandes, tandis que ces mêmes valeurs étaient plus faibles pour des efficacités plus petites. Ceci a été attribué au prix d'éthanol qui était plus élevé dans le deuxième scénario. Ceci étant dit, une modification dans la valeur d'une des variables peut conduire à une modification des tendances. Ceci est le cas pour le prix de l'électricité dans le premier cas, et pour le prix de l'éthanol deuxième génération ou cellulosique dans le deuxième. En effet, une augmentation du prix de l'électricité

	favorise les configurations les plus efficaces dans le premier cas, et vice versa, tandis que l'augmentation du prix de l'éthanol cellulosique favorise les configurations le plus efficace dans le deuxième cas. La solution choisie pour correspondait au maximum de la VAN. Elle correspondait pour le premier cas à une efficacité de 41.6% et un coût de 163 M$. Pour le deuxième cas, cela conduisait à des points correspondant à la région de cogénération et non pas à l'hydrolyse.
La recherche d'un prix convenable pour l'éthanol cellulosique permet	La solution choisie pour le deuxième cas correspondait à la configuration avec la plus grande part d'hydrolyse qui conduit soit à une VAN de zéro soit à une VAN maximale, et ceci en modifiant le prix de l'éthanol cellulosique. On parle dans le premier cas du minimum prix de vente de l'éthanol cellulosique, et dans le deuxième du minimum modifié du prix de vente de l'éthanol cellulosique. Ce deuxième critère était une innovation de notre travail. Ce travail a permis de définir les conditions économiques minimales pour garantir la faisabilité et la compétitivité des solutions avec une part d'hydrolyse importante.

En conclusion, ce travail exhaustif, détaillé et méthodologie souligne le grand potentiel derrière les procédés étudiés et la méthodologie utilisée. Ce travail peut conduire à plein de sujets intéressants. Ces sujets peuvent traiter d'avancements au procédé ainsi que des développements dans la méthodologie. Ces avancements incluent : des nouvelles variables d'optimisation, des intervalles de variation plus vastes, des technologies d'intégration thermique plus avancées, notamment pour la valorisation des pertes, ainsi que des technologies de valorisation de biomasse plus optimisées, incluant des prétraitements, hydrolyse, gazéification, methanation entre autre . Les développements à la méthodologie incluent la synthèse d'un réseau d'échange détaillé, la prise en compte de critères environnementaux, la prise en compte de la qualité des produits entrants, l'évaluation de la consommation en eau, parmi d'autres.

Je termine ce travail avec une citation traitant du travail scientifique et de on envergure :

« La connaissance scientifique possède en quelque sorte des propriétés fractales : nous aurons beau accroître notre savoir, le reste -- si infime soit-il -- sera toujours aussi infiniment complexe que l'ensemble de départ. » Isaac Azimov.

=

Contents

List of Figures

List of Tables

List of Equations

List of Symbols

Symbol	Explanation	Unit	Symbol	Explanation	Unit
eff_{var}	Conversion efficiency of variable var	%	n_{Prod}	Number of products	-
$var_{Prod,i}$	Value of variable var for product i	-	n_{inp}	Number of input streams	-
$var_{inp,i}$	Value of variable var for input i	-	ϵ, eff_{En}	Process energy efficiency	%
$n_{chem,Prod}$	Number of chemical products	-	$\dot{m}_{ch,Prod,i}$	Mass flow rate of chemical product i	t/h
$LHV_{ch,Prod,i}$	Lower Heating Value of Chemical Product i	MWh/t	W_{prod}	Net Power production	MW
Q_{prod}	Net Heat Production	MW	$n_{chem,inp}$	Number of chemical inputs	-
$\dot{m}_{ch,inp,i}$	Mass flow rate of chemical input i	t/h	$LHV_{ch,inp,i}$	Lower heating value of chemical product i	MWh/t
W_{inp}	Net Power Consumption	MW	Q_{inp}	Net Heat Consumption	MW
Ex_Q	Exergy of a heat stream	MW	Q	Heat duty	MW
η_C	Carnot efficiency	-	T_0	Ambient Temperature	K
T_{H}	Hot source Temperature	K	Ex_W	Exergy of Power stream	MW
W	Power content	MW	Ex_{cmp}	Exergy content of a chemical component	MW
$Ex_{ph,cmp}$	Physical exergy content	MW	$Ex_{ch,cmp}$	Chemical exergy content	MW
$\dot{m}_{cmp}$	Mass flow rate of chemical component cmp	t/h	$ex^0_{ch,cmp}$	Nominal chemical exergy content of component cmp	MWh/t
$\Delta_f G^0$	Gibbs free energy of formation	MWh/t	n_{elem}	Elements of formation reaction	-
ν_i	Stoechiometric coefficient of component i	-	$ex^0_{ch,elem,i}$	Nominal chemical exergy content of element i	MWh/t

η, eff_{Ex}	Process exergy efficiency	%	$ex^0_{ch,Prod,i}$	Nominal chemical exergy content of product i	MWh/t
$T_{H,prod}$	Temperature of heat produced	K	$ex^0_{ch,inp,i}$	Nominal chemical exergy content of input i	MWh/t
$T_{H,inp}$	Temperature of heat input	K			
ε_{chem}, $eff_{chm,Ex}$	Chemical exergy efficiency	%	$n_{chem,Prod}$	Number of chemical products	-
$\dot{m}_{ch,Prod,i}$	Mass flow rate of chemical product i	t/h	η_{NGCC}	Exergy efficiency of natural gas combined cycle	%
LHV_{SNG}	Lower heating value of synthetic natural gas	MWh/t	ex^0_{SNG}	Nominal exergy content of SNG	MWh/t
$Ex_{W,prod}$	**Exergy of produced electricity**	**MW**	$Ex_{Q,prod}$	**Exergy of produced heat**	**MW**
η_{HP}	Exergy efficiency of a heat pump	%	$Ex_{W,inp}$	Exergy of input electricity	MW
$Ex_{Q,inp}$	Exergy of input heat	MW			
$C_{BM,equip}$	Equipment Bare Module Cost	M$	$C_{base,equip}$	Equipment base cost	M$
H_{equip}	Characteristic equipment size	m, m^2, m^3, kg, MW,…	i	i^{th} secondary parameter affecting equipment cost	-
$f_{i,equip}$	Equipment i^{th} Correction factor	-	equip	Reference to equipment type	-
$C_{BM,equip,actua}$	Actualized Bare Module cost	M$			
$Cost_{ind,act}$	Cost index for the actual year	-	$Cost_{ind,calc}$	Cost index for the calculation year	-
$C_{TM,equip}$	Equipment total module cost	M$	$c_{1,equip}$	Total module correction factor	-
$C_{GR,equip}$	Equipment Grass Roots Cost	M$	$c_{2,equip}$	Grass root costs correction factor	-
C_{FC}	Process fixed capital cost	M$	C_{WC}	Process working capital cost	M$
f_{WC}	Working capital correction factor	-	C_{TCI}	Process total capital investment cost	M$
n_{dop}	Number of operating days	d/y	$\mathrm{C_{OP}}$	Process yearly operating costs	M$/y
C_{RM}	Raw Material Cost	M$/y	n_{RM}	Number of input raw materials	-

$C^0_{RM,i}$	Nominal cost for ith raw material	\$/l, \$/t, \$/MWh, etc.	$Cons_{y,RM,i}$	Yearly consumption rate for ith raw material	t/y
C_{cc}	Cost of chemicals and catalysts	M\$/y	n_{cc}	Number of catalysts and chemicals employed	-
$C^0_{CC,i}$	Nominal cost for ith chemical or catalyst	\$/t	$Cons_{y,CC,i}$	Yearly consumption rate for ith chemical or catalyst	t/y
C_{UT}	Utilities Cost	M\$/y	n_{UT}	Number of utility streams employed	-
$C^0_{UT,i}$	Nominal cost for ith utility stream	\$/m^3, \$/MWh, etc.	$Cons_{y,UT,i}$	Yearly consumption rate for ith utility stream	t/y, MWh /y, etc.
C_{labor}	Labor cost	M\$/y	$n_{emp_{cat}}$	Number of employee categories (operators, engineers, etc.)	-
$n_{employee,i}$	Number of employees in ith category	-	$C^0_{employee,y,i}$	Yearly salary of one employee in ith category	M\$/y
C_M	Maintenance cost	M\$/y	f_{CM}	Maintenance cost fraction	Year^{-1}
C_{exp}	Overheads, insurance and other expenses	M\$/y	f_{exp}	Other expenses fraction	Year^{-1}
$C_{TCI,ann}$	Annualized total capital investment	M\$/y	$a_{i_r,LT}$	annualization factor	-
i_r	Interest rate	%	n_r	Reimbursement period	y
$C_{tot,y,prod}$	Process total annual production costs	M\$/y			
$C_{tot,y,rev}$	Total yearly revenue	M\$/y	$n_{Products}$	Number of products	-
$P^0_{Prod,i}$	Nominal price of ith product	\$/l (t, MWh, …)	$Prod_{y,Prod,i}$	Production rate of product i	l (t, MWh) /y,
$Margin_{tot,y}$	Total yearly margin	M\$/y	$\mathrm{Profit}_{gross,y}$	Total yearly Gross profit	M\$/y
$C_{FC,dep}$	Depreciated Fixed Capital Cost	M\$/y	n_{dep}	number of depreciation years	y
$if_{dep,y}$	Depreciation factor	-	y	Year of operation	-
tax_{rate}	Taxation rate	-	$Proft_{tax,y,de}$	Taxable profit accounting depreciation	M\$/y
$\mathrm{Profit}_{net,y}$	Total yearly net profit	M\$/y	t_{c-s}	Construction and start-up	y
CF_y	Cash flow in year y	M\$/y	DCF_y	Discounted cash flow in	M\$/y

				year y	
$\mathbf{PV}_y$	Present Value in year y	M$/y	$f_{dc,y}$	Discount factor in year y	-
r_{dc}	Discount rate	-			
SRR	Simple Rate of Return	%	NPV	Net Present Value	M$
EAC	Equivalent Annual Cost	M$	IRR	Internal Rate of Return	%
DPT	Discounted Pay Back Time	y			
MOO	Multi-objective optimization	-	SOO	Single-Objective Optimization	-
x	Decision vector in multivariate optimization	-	x_{i}	i[th] optimization variable in decision vector	-
$x_{\mathrm{i},min}$	Minimum bound for optimization variable	-	$x_{\mathrm{i},max}$	Maximum bound for optimization variable	-
X	Search space	-	f, v, u	Objective function vector	-
$f_{\mathrm{i}}, \mathrm{v_i}, \mathrm{u_i}$	i[th] objective function	-	n	Number of objective functions	-
F_x	Set of feasible solutions	-	P_f	Pareto front	-
EA	Evolutionary Algorithms	-	QMOO	Queuing Multi-Objective optimization	-
P	Population of points in optimization	-	t	Optimization time	hours
I	Individual in population P	-	s_I	State of individual I	-
r_I	Ranking of individual I	-	I_{i}	i[th] individual in population P	-
$x_{sg,conc}$	Sugars content in concentrated juice fraction	kg/kg	$x_{sg,in}$	Sugars content in input juice	kg/kg
$x_{sg,f}$	Pre-hydrolysis sugar concentration	kg/kg	spl_{syr}	Fraction of juice to concentration	-
$M_{wat,rem}$	Quantity of water to be removed	t/h	$M_{tot,in}$	Total input mass flow rate	t/h
$M_{vap,i}$	Quantity of water evaporated at effect i	t/h	$r_{ev,i}$	Vaporization rate in effect i	-
$T_{ev,i}$	Vaporization temperature at effect i	°C	$N_{evap,units}$	Number of evaporators	-
T_{out}	Temperature of output cold streams	°C	T_{ster}	Upper sterilization temperature	°C

RT_{ster}	Duration of sterilization	min	$conv_{scr,hyd}$	Sucrose to glucose conversion	mol.%
$T_{scr,hyd}$	Temperature of sucrose hydrolysis reaction	°C	$P_{scr,hyd}$	Pressure of sucrose hydrolysis reaction	atm
$RT_{scr,hyd}$	Residence time of sucrose hydrolysis reaction	h	T_{Ferm}	Fermentation temperature	°C
$x_{v,yst,in}$	Yeast content in input yeast stream	vol.%	P_{Ferm}	Fermentation pressure	atm
$vfr_{yst,ferm}$	Fraction of yeast stream in fermentation volume	vol.%	RT_{Ferm}	Fermentation time	h
$x_{v,yst,cen}$	Cake yeast content after centrifugation	vol.%	V_{Ferm}	Fermentation reactor volume	m^3
rat_{wat}	Quantity of wash water/ quantity of yeast	-	$conv_{gluc,et}$	Yield of ethanol production reaction	mol.%
$conv_{gluc,acet}$	Yield of acetic acid production reaction	mol.%	$conv_{glc,glyc}$	Yield of glycerol production reaction	mol.%
$conv_{gluc,yst}$	Yield of yeast production reaction	mol.%	yst_{rec}	Yeast recycling ratio	%
$x_{v,yst,wash}$	Cake yeast content after washing	vol.%	$loss_{et,scrub}$	Ethanol loss in purge stream	wt.%
sep_{CO_2}	CO2 purged/CO2 produced	wt.%	$W_{0,Ferm}$	Fermentation power consumption	kW/m^3
rat_{NH_3}	NH_3 to glucose ratio	mol.%			
P_{AAD}	Operating pressure in stripping column	atm	$Vfr_{F,AAD}$	Vapor fraction of feed to stripping column	mol.%
N_{AAD}	Number of stages in stripping column	-	$N_{F,AAD}$	Feed stage in stripping column	-
$x_{et,vin}$	Ethanol content in stripping bottoms	wt.%	$x_{CO2,aad}$	CO_2 content in post-purge tops	wt.%
$x_{et,aad}$	Ethanol content in post-purge tops	wt.%	$Vfr_{F,BB1}$	Vapor fraction of feed to rectifying column	mol.%
N_{BB1}	Number of stages in rectifying column	-	$N_{F,BB1}$	Number of stages in rectifying column	-
$etrec_{BB1}$	Ethanol recovery in rectifying column	wt.%	$x_{et,bb1}$	Ethanol content in rectifying tops	wt.%
$Vfr_{D,BB1}$	Vapor content of rectifying distillate	mol.%	ΔP_{dis}	Pressure drop in distillation columns	atm
P_{ext}	Operating pressure in extraction column	atm	$MGHYDR$	MEG to input feed ratio	kg/kg
N_{ext}	Number of stages in extraction column	-	$N_{F,ext}$	Feed stage in extraction column	-
$x_{et,top}$	Ethanol content in extraction tops	wt.%	$ettowat$	Ethanol to water content in extraction	0.3 mol.%

				bottoms	
T_{MEG}	MEG input temperature	°C	N_{Rec}	Number of stages in recovery column	-
$N_{F,REC}$	Feed stage in recovery column	-	$megrec$	MEG recovery in recovery column	wt.%
$megbot$	MEG content in recovery bottoms	wt.%			
$hum_{dry-bag}$	Dried bagasse humidity	mol.%	AFR	Air to fuel ratio	-
$T_{AIR-HOT}$	Air heating temperature	°C	$T_{FLUE-HOT}$	Post-combustion flue gas temperature	°C
$T_{FLUE-OUT}$	Output flue gas temperature	°C	$conv_{comb}$	Conversion ratios of combustion reactions	mol.%
Ash_{SEP}	Ash separation in leaves washing	%	Lea_{Loss}	Loss of biomass in leaves washing	%
Sol_{SEP}	Extension of solid separation in bleeding	%	Gas_{Loss}	Extent of gas loss in bleeding	%
$M_{wat,in}$	Mass flow rate of water in boiler	t/h	$M_{tur,i}$	Mass flow rate in ith turbine	t/h
$\mathbf{P}_{steam}$	Steam pressure	atm	$\mathbf{Super}_{heat}$	Superheating temperature	°C
$T_{Tur,i}$	ith turbine temperature	°C	$M_{Tur,i}$	ith turbine mass flow rate	t/h
$\mathbf{T}_{col-wat-in}$	Input cold water temperature	°C	$\Delta\mathbf{T}_{col-wat}$	Increase in cold utility temperature	°C
SHF	Separate hydrolysis and fermentation	-	SSF	Sequential Hydrolysis and Fermentation	-
WAT: **BAG**	Mill water to bagasse ratio	Kg/kg	T_{mill}	Mill operating temperature	°C
$hum_{to-stex}$	Humidity to steam explosion	wt.%	$\eta_{solb-mil}$	Fraction of soluble solids remaining in cake stream after mill	%
$\eta_{sol-mil}$	Fraction of input cake remaining in cake stream after mill	100%	$\mathbf{C}_{\mathbf{cat}}$	Catalyst concentration	9.5 mg/g dry matter
DM	Dry Matter	-	$\mathbf{Res}_{\mathbf{stex}}$	Residence time in steam explosion reactor	min
T_{prt}	Pretreatment temperature	°C	ΔT_{sheat}	Input steam superheat temperature	°C
$\eta_{hem-xyl}$	Efficiency of xylose production reaction	mol.%			
$\eta_{hem-acet}$	Efficiency of acetic acid production	mol.%	P_{prt}	Pretreatment pressure	atm

	reaction				
$\eta_{xyl-furf}$	Efficiency of furfural production reaction	mol.%	$\eta_{cel-dex}$	Efficiency of glucose production reaction	mol.%
hum_{to-cen}	Humidity of centrifugation input stream	wt.%	$hum_{postcen}$	Humidity of centrifuged cake	wt.%
C_{xylose}	Xylose content in centrifuged cake	g/L	$\eta_{solb-cen}$	Fraction of input soluble solids remaining in cake stream after washing	%
$\eta_{sol-cen}$	Fraction of input cake remaining in cake stream after washing	%	ΔT_{sheat}	Input steam superheat temperature	90°C
$T_{hyd-wat}$	Water heating temperature	°C	$W_{0,hyd}$	Nominal power consumption in hydrolysis reactor	kWh/ m^3
sld_{load}	Hydrolysis Solids loading	wt.%	$hum_{cake,hyd}$	Humidity of centrifuged cake	wt.%
P_{hyd}	Hydrolysis pressure	atm	$\eta_{solblosscen}$	Loss of soluble material in centrifugation step	%
$\mathbf{enzload}_{hyd}$	Enzymes loading	0.1 g enzymes / g cellulose	$\eta_{sol-sep-cen}$	Solids recovery in centrifugation	%
hyd_{res}	Residence time in hydrolysis reactor	24 h	$\eta_{solblosspres}$	Loss of soluble material in press filtration step	0%
$C_{gluc,hyd}$	Glucose concentration in hydrolysis product stream	18 g/L	$\eta_{sol-sep-pres}$	Solids recovery in press filtration step	100%
$\eta_{hem-xyl,hyd}$	Efficiency of xylose production reaction	41 mol.%	$hum_{cake,hyd}$	Humidity of output hydrolysis cake	70 wt.%
T_{hyd}	Hydrolysis temperature	40 °C	P_{fls}	Flash pressure	1 atm
T_{dig}	Biodigestion temperature	40 °C	$P_{air-comp}$	Compressed air pressure	18 atm
P_{dig}	Biodigestion pressure	1 atm	$T_{gas-bur}$	Gas burner temperature	1127 °C
$\eta_{conv,dig}$	Efficiency of organics conversion reaction	70 mol%	$T_{pre-gas-tur}$	Turbine entry temperature	827 °C
$\mathbf{Res}_{\mathbf{dig}}$	Residence time in biodigestion reactor	48 h	$P_{gas-tur}$	Turbine outlet pressure	1 atm
T_{air-in}	Input air temperature	25°C	$\eta_{comb-conv}$	Combustion efficiency	100 mol.%
SSC	Specific steam consumption	(kg steam /L	OPEX	Operating expenditures	M$/y

		ethanol)			
CAPEX	Capital expenditures	M$/y	TAC	Total Annual Cost	M$/y
MINLP	Mixed Integer Non Linear Programming	-	TAP	Total Annual Profit	M$/y
MILP	Mixed integer linear programming	-			
RR_c	Reflux ratio	-	Q_{reb}	Reboiler heat duty	MW
reg_{solv}	Proportion of reused entrainer	%	N_{stages}	Number of stages	-
S/F	Solvent to feed ratio	kg/kg	T_{solv}	Solvent feed temperature	°C
$\dot{m}_D$	Column distillate flow rate	t/h	N_{feed}	Feed stream position	-
$C_{inv,ann}$	Annualized investment cost	M$/y	$\Delta C_{evap,i}$	Increment in sugar concentration in evaporator i	kg/kg
$U_{evap,i}$	Heat transfer coefficient in evaporator i	kW/(m^2.°C)	$C_{evap,i}$	Sugar concentration after evaporator i	kg/kg
CHP	Combined heat and power production	-	TC	Tone sugarcane	t/h
MESP	Minimum Ethanol Selling price	$/l	MPSP	Minimum Power Selling Price	$/MWh
$\dot{m}_{cane}$	Sugarcane mass flow rate	t/h	ex_{cane}	Sugarcane nominal exergy content	MWh/t
Ex_{cane}	Sugarcane total exergy content	MW	$\dot{m}_{leaves}$	Leaves mass flow rate	t/h
ex_{leaves}	Leaves nominal exergy content	t/h	Ex_{leaves}	Leaves total exergy content	MW
W_{net}	Net power production	MW	$\dot{m}_{ethanol}$	Mass flow rate of ethanol	t/h
$ex_{ethanol}$	Ethanol nominal exergy content	MWh/t	$ex_{W_{out}}$	Output power nominal exergy content	-
$Ex_{W_{out}}$	Output power total exergy content	MW	Ex_{Prod}	Exergy content of product streams	MW
Ex_{in}	Exergy content of input streams	MW	$C_{capital,GR}$	Capital costs for a grass root facility	M$
N_{blocks}	Number of process blocks	-	$C_{capital,GR_i}$	Capital cost of process block I (excluding heat exchange equipment)	M$
$C_{HEN,GR}$	Grass root cost of heat exchange equipment	M$	$A_{hen,tot}$	Total heat exchange area	m^2
dT_{ev_i}	Temperature decrement in evaporator i	°C	x_{sgcc}	Juice concentration at the outlet of concentration step	kg/kg

p_{strip}	Pressure in stripping column	atm	p_{rect}	Pressure in rectifying column	atm
$V_{fr,rect,top}$	Vapor fraction in rectifying distillate	mol/mol	S/F	Solvent to feed ratio in extraction column	kg/kg
T_{solv}	Solvent input temperature	°C	p_{tur_i}	Operating pressure in turbine i	atm
$\dot{m}_{water}$	Mass flow rate of water in boiler	t/h	$\dot{m}_{steam,i}$	Mass flow rate of steam in turbine i	t/h
P_{boiler}	Boiler pressure	atm	T_{sheat}	Temperature of superheating	°C
hum_{bag}	Bagasse humidity	mol/mol	$\dot{m}_{cold,ut}$	Cooling water mass flow rate	t/h
$\dot{m}_{frig,ut}$	Refrigeration utility mass flow rate	t/h	$\dot{m}_{et}$	Ethanol mass flow rate	t/h
$r_{ev,i,corrected}$	Corrected vaporization rate in evaporator i	-	$r_{ev,i,proposed}$	Vaporization rate I proposed by the optimization algorithm	-
$error$	Value of error due to divergence, non meeting of specs or non heat integration	-	$var_{calc,i}$	Calculated value for design variable i	-
$var_{spec,i}$	Specified value for design variable	-	Tol	Tolerance for error	-
$penalty_i$	Penalty function due to error type i	-	r_i	Penalty factor associated with error type i	-
$obj_{I,j}$	Value for jth objective function for individual I	-	$sign$	Indicator of function to be minimized or maximized	-
$Prob_{selection,I}$	Probability of selecting individual I	-	$rank_I$	Rank of individual I	-
$obj_{i,norm,j}$	Normalized value for objective function i at point j	-	$obj_{i,value,j}$	Actual value for objective function i at point j	-
$obj_{i,min,j}$	Minimal value for objective function i at point j	-	$obj_{i,max,j}$	Maximal value for objective function i at point j	-
$\Delta obj_{i,norm,j}$	Difference between normalized values for objective function i at point j	-	$obj_{i,norm,\mathrm{j}}$	Normalized value for objective function i at point j	-
$obj_{i,norm,j-1}$	Normalized value for objective function i at point j-1	-	$ratio_{var,\mathrm{j}}$	Variation ratio at point j	-
$\Delta ex_{eff_{norm,\mathrm{j}}}$	Difference between normalized values for exergy efficiency	-	$\Delta(C_{inv})_{norm,\mathrm{j}}$	Difference between normalized values for fixed capita costs at	-

	at point j			point j	
$point_j$	j[th] point in the Pareto curve	-	$knee_{points}$	Set of knee points in Pareto curve	-
Frag	Fragment of Pareto curve with points between two knee points	-	$var_{mean_{frag}}$	Mean value of variable var in frag k	-
var_j	Value of variable var for j[th] point in kth fragment	-	$obj_{i,norm_{frag,}}$	Normalized value of ith objective function in kth fragment	-
$obj_{i,mean_{frag,k}}$	Mean value of ith objective function in kth fragment	-	$obj_{i,mean_{min}}$	Minimum mean value of ith objective function	-
$obj_{i,mean_{max}}$	Maximum mean value of ith objective function	-	$var_{norm_{frag,}}$	Normalized value for variable var in kth fragment	-
$var_{mean_{frag,k}}$	Mean value of variable var in kth fragment	-	var_{low}	Lower bound for variable var	-
var_{up}	Upper bound for variable var	-	$maxNPV$	Maximum NPV value obtained on the Pareto curve	M$
NPV_I	NPV value for Pareto individual I	M$	I_{Profit}	Most profitable Pareto individual	-
$ex_{eff,I_{Profit}}$	Exergy efficiency of most profitable Pareto individual	%	$C_{\mathrm{FC},I_{Profit}}$	Fixed Capital Cost of most profitable Pareto individual	-
LT	Project lifetime	y	SV	Salvage equipment value	M$
λ	Depreciation rate	-	SCP	Sugarcane price	$/t
LP	Leaves Price	$/t	ESP	Ethanol selling price	$/l
PSP	Power selling price	$/MWh	N_{alt}	Number of profitable alternatives	-
$maxIRR$	Maximum internal rate of return	-	$maxSCP$	Maximum sugarcane selling price	$/t
$maxLP$	Maximum leaves price	$/t	$ex_{sucrose}$	Nominal chemical exergy content of sucrose	MWh /t
$x_{sucrose}$	Sucrose content in input sugarcane	kg/kg	$ex_{bagasse}$	Nominal chemical exergy content of bagasse	MWh /t
$x_{bagasse}$	Bagasse content in input sugarcane	kg/kg	et_{prod}	Specific ethanol production rate	l/TC
$\rho_{ethanol}$	Ethanol mass density	kg/l	bag_{toet}	Fraction of bagasse diverted to ethanol production	%

W_{prod}	Specific power production	MWh/TC	$\dot{m}_{enz}$	Enzymes input mass flow rate	t/h
ex_{enz}	Nominal exergy content of enzymes	MWh/t	Ex_{enz}	Exergy content of enzymes	MW
$GlcEq$	Glucose concentration in concentrated stream	g/L	k_{hyd}	Hydrolysis kinetic factor	-
hyd_{Res_0}	Nominal hydrolysis residence time	h	$GlcEq_0$	Glucose concentration at nominal residence time	-
$a_{var}, b_{var}, c_{var}, d_{var}, e_{var}, f_{var}$	Coefficients for hydrolysis reaction correlation of variable var	-	$mminESPc$	Modified minimum cellulosic ethanol selling price	$/l

General Introduction

This doctorate thesis deals with the application of optimal process design methodologies to the production of ethanol and electricity from Brazilian sugarcane. Two processes are investigated in this endeavor: a combined distillery + cogeneration unit and a combined distillery + cogeneration + hydrolysis unit. Work was realized in collaboration between the Process Design Department of IFP Energies Nouvelles, Solaize, France and the Industrial Process and Energy Systems Engineering (IPESE) lab at Ecole Polytechnique Fédérale de Lausanne (EPFL).

We begin this introductory section with a description of the context of this doctorate work.

The choice of the methodology

The need for a structured methodology for optimal process design has been a key issue ever since the advent of chemical engineering. This is due both to the complexity of processes at one hand, involving a great number of design conditions, and the complexity of their evaluation, namely with regards to competition between efficiency and costs.

This has led the designers to an ever expanding research work, which started from heuristics and rules of thumb, was incremented by the use of process simulation tools, and capped off by the application of process optimization tools.

Multi-objective optimization by the use of evolutionary algorithms is a variant therein that has gained increased application in the field of optimal process design.

This interest is due to several key points. The optimization returns to the designer optimal compromise designs with regards to the chosen objective functions. Evolutionary algorithms enable the applications of this method to any investigated process, namely those exhibiting hard to find optima.

With this in mind, the IPESE lab at EPFL has been a pioneer in this field and this for more than a decade.

This optimization leads to the generation of a set of optimal compromise solutions, otherwise termed as Pareto set. Select decision support techniques, of which profitability analysis is a prime example, can then help the decision maker pick but one solution out of the obtained lot.

Considering this, this methodology, consisting in multi-objective optimization coupled with detailed process design and final process selection was chosen in the context of our thesis.

The choice of the process

Sugarcane is the world's largest crop by production quantity. Moreover, its use for the production of biofuels, particularly bioethanol, is a consolidated practice, namely in Brazil. The conventional process contains the following steps: sugarcane juice extraction and treatment, concentration, sucrose hydrolysis, glucose fermentation, ethanol distillation and dehydration.

This practice however is still prone to improvements, which deal mainly with the reduction of heat demand and investment cost. This is done by optimizing the separation steps: concentration, distillation and dehydration.

Other improvements deal with the use of sugarcane's main by-product: bagasse. Two uses were investigated in this study.

The first application consisted in the combustion of bagasse, and leaves, and subsequent heat and power cogeneration via a Rankine cycle. This use is directly linked to the reduction in heat demand through a higher power production.

The second application consisted in the hydrolysis of this bagasse for additional ethanol production. A part of this hydrolyzed bagasse is sent for biodigestion, another fraction for ethanol production, whilst the unhydrolyzed fraction is sent to the cogeneration unit. Part of this bagasse still needs to be sent to cogeneration in order to meet process heat requirements. This use is directly linked with a reduction in heat demand linked with a higher hydrolyzed fraction.

Both these cases benefit from a multiplicity of related literature work, albeit with limited application of the chosen methodology.

Main Achievements

Our achievements in the course of this thesis can be divided as follows:

- **Our first contribution relates to the optimal process selection step taking place once the optimization run is done**. This step was seldom invoked in literature, and even less in the context of our work. Nonetheless, it is of prime importance since only one, or a handful of alternatives are actually of interest to the decision maker. The advocated and chosen selection criterion was, profitability, expressed by the Net Present Value (NPV) function. This value was calculated for each alternative, under chosen economic conditions. The alternative which maximizes this NPV is the most profitable one, and was hence chosen.
- **Our second contribution relates to the optimal process analysis step taking place once the optimization run is done**. This analysis was also seldom invoked in literature, and to our understanding never before in the context of our work. This was realized to have a better understanding of the obtained optimization results. Another incentive was to make required comparisons with other bibliographic works dealing with the studied processes. This analysis was done by taking a look at a group of variables: measured variables which have a direct relation with the objective function, and optimization variables which define the optimization problem. The optimization variables were split into four groups, as inspired by certain literature works in the field.
- **Our third contribution dealt with the implementation of the methodology**. This contribution consisted in the following: (1) parallelization of evaluations on a single computer, (2) the automated interaction between evaluation and optimization sheet and process simulation tool, (3) the construction of an equipment sizing and cost evaluation sheet based on the Chauvel manual.
- We built a simulation models for both processes inspired from a diverse and state of the art bibliographic review. These models were hence adapted for the performance of the required multi-objective optimization step.
- The two chosen objective functions, exergy efficiency and capital cost, were never applied for the investigated processes. This choice was realized in accordance with common practice found in literature concerning the optimization of other processes.
- We constructed a model taking into account the effect of certain hydrolysis parameters (solids loading and hydrolysis time) on the hydrolysis reaction. We then integrated this model into the simulation and subsequent optimization runs.

- We included as optimization variables for the optimization run operating parameters pertaining to all process sections. This differs from past research works that optimized only one specific section or at most two sections therein.
- We introduced a novel economic indicator, the modified product minimum selling price. This represents the product price beyond which a given high efficiency high cost system is the most profitable alternative. This parameter was found to provide a better representation than the traditional minimum selling price, and this because it takes into consideration the competition between the various alternatives.

Scientific Contributions

This thesis work led to a series of contributions and presentations in a list of scientific and technical venues:

- Presentation given at the 2nd Franco-Swiss Forum for innovation in Energy Transition, June 24th 2014, Lyon, France.
-
- Paper and oral presentation held 17th Conference on Process Integration, Modeling and Optimization for Energy Saving and Pollution Reduction PRES 2014- Prague, Czech Republic. Paper published in conference proceeding:
- Bechara R, Gomez A, Saint-Antonin V, Albarelli J, Ensinas A, Schweitzer JM, et al. Methodology for minimizing the utility consumption of a 2G ethanol process. Chem Eng Trans 2014;39:91e6.
-
- Paper and oral presentation held at 28th International Conference on Efficiency, Cost, Optimization, Simulation and Environmental Impact of Energy systems ECOS 2015- Pau, France.
- Heat integration of ethanol from sugarcane production process through modifications to separation sections.
- Paper submitted in Energy, as a special issue for the ECOS2015 conference
- Systematic methodology for the optimal design of a combined sugarcane distillery and cogeneration plant for ethanol and power production
- Paper to be submitted in Biotechnology for Biofuels.
- Methodology for the optimal design of an integrated first and second generation ethanol production plant combined with power cogeneration

Breakdown of the thesis

This thesis starts with an initial description and defense of the chosen methodology. This defense is realized both from a theoretical and bibliographic stand points. This chapter culminates with a diagram specifying the various steps of the employed methodology. This diagram is quickly described below.

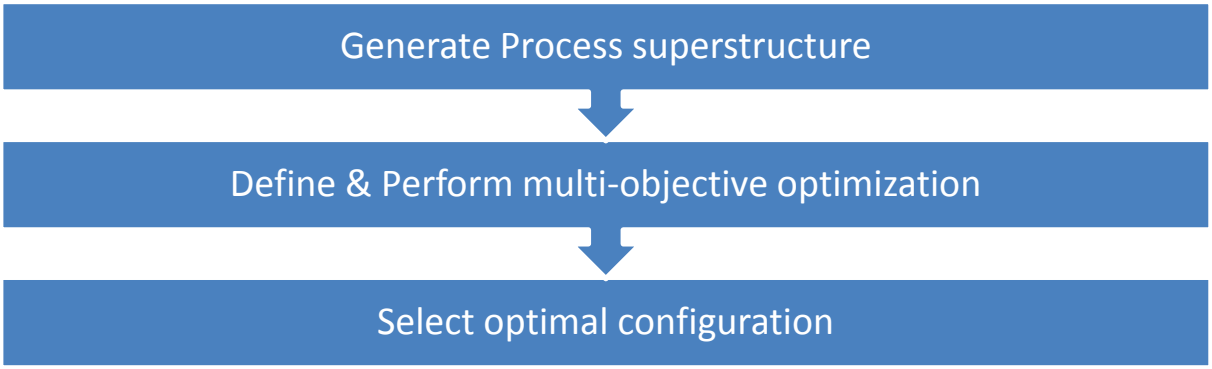

The second and third chapters detail the process simulation and evaluation flowsheets for the two investigated processes respectively. These flowsheets constitute the basis for the next two chapters.

The fourth and fifth chapters consist in the demonstration of the application of the methodology presented in Chapter 1 to the two processes defined in Chapters 2 and 3. This application goes from an initial search for potential optimization variables, to the definition and performance of the optimization run and finally the selection of the optimal process.

With this in mind, we wish all the readers of this document have a fruitful endeavor.

Chapter 1 Methodologies for the synthesis of optimal chemical processes

"Suppose one of you wants to build a tower. Won't you first sit down and estimate the cost to see if you have enough money to complete it?" Luke 14:28-30

The *decision* on whether to *undergo* any given enterprise always requires both 'sitting down' and 'estimating' its potential costs, benefits and associated risks. This must be realized in order to plan for most adequate design, avoid hazardous choices, and to make provisions against "unwelcome" surprises down the road. This is also the case for chemical processes and plants. To the delight of the engineer, rigorous and robust methods and tools, with numerous proven applications, were developed for this sake. These methods and tools will first be presented in this section before being compiled in a structured methodology, constituting the basis for our subsequent work.

1.1 Process design: Generation of process superstructure

Process design is a stage within plant conception occurring between process development and equipment design [1]. Information from the development stage are assimilated, integrated and synthesized into a total process. Multiple alternatives are drawn with the use of tools such as heuristics and mathematical modeling, with the constraint that the process must not stray outside the information field defined by the experience gained in the development stage. Moreover, within an engineering project, it is expensive to go back and modify an issued process design, making this step even more important. This section can be broken down into the smaller elements highlighted in Figure 1:1. The loop arrow stresses the need for iteration in this endeavor to enhance the optimality and accuracy of the proposed designs. The constitutive elements are detailed below. The choice of a capacity, topography, operating conditions and equipment defines a *process configuration*.

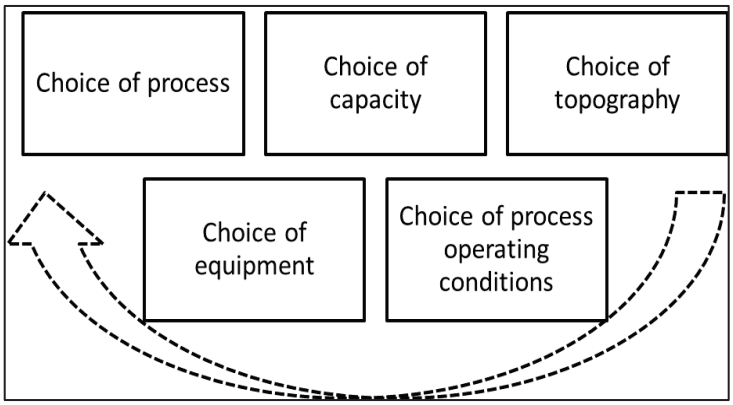

Figure 1:1 Elements of process design [1]

1.1.1 Choice of process

This step consists in choosing the process. The first point is the definition of key process inputs and outputs. This step is usually associated with the definition of a *battery* limit (BL) thereof. This limit is important in defining the process structure and evaluating its performance. The second point consists in defining key process components, placed within this battery limit. Examples of such components are: pretreatment/reaction, separation/recycle, heat exchange/recovery, side stream valorization, waste stream treatment and utility production. As a result, the input/output structure and process components are intrinsically linked. Moreover, the pretreatment/reaction sub-system is largely predetermined at the development stage, whereas the other sections are usually less well defined, and are left to the designer's knowledge and expertise. At this level, a rough process scheme can be drawn. The designer can define mandatory and optional components. We speak of a *Process Block Diagram* (*PBD*). Multiple process schemes are hence made possible.

1.1.2 Choice of capacity

The plant capacity needs to be fixed first because all numerical work depends on it. It usually intervenes at the beginning of the design step. It is a company-wide decision and is usually accompanied with a level of uncertainty. This uncertainty means that the plant could be too small or too big. Moreover, such a capacity can be defined for the main input stream or the main product stream. Finally, this choice depends directly on the investment cost of the differently sized plants.

1.1.3 Choice of topography

In addition to the presence of optional and mandatory components, diversity is introduced into the process scheme by virtue of competing technologies for the same process component. For example, distillation vs. adsorption for a given separation task, batch vs. continuous operation for a given reaction task, etc. This complexifies even more the nature of the input/output streams. Process topography, i.e. the order in which the various process sub-systems are assembled to form the desired process, is hence defined. Various decisions are made at this level: use of parallel

or serial units, use of single or multiple streams, choice of investigated technologies etc. This defines a *superstructure* for the process. Moreover, these are integer problems with a multitude of combinations to investigate before the true optimum can be located. Literature experience and heuristic rules are commonly used to tackle this problem. Moreover, the designer can profit from automated synthesis methods namely related to the design of heat exchange networks, the sequence in trains of distillation columns and the choice of an optimal utility system. The use of adequate predictive methods can also help explore novel possibilities.

A topology can also be defined for each process block. This topology or layout is denoted as the *Process Flow Diagram* (PFD). It is constructed by associating *unit operations* such as: distillation columns, reactor vessels, flash tanks, dryers, heat exchangers, etc. These physical unit operations are usually approximated by the use of process models which depict some form of reality. The design should hence build both robust and accurate models, with attention given to the adequate trade-off between the details of the unit models and the degree of freedom left to the process design.

1.1.4 Choice of process operating conditions

The choice of process operating conditions intervenes once the capacity and the topography for the studied process are identified. At this level, values of process conditions such as temperatures, pressures, concentrations, approach temperatures, recoveries and residence times are sought. These conditions intervene in the various sub-systems. This question is of great importance considering the effect these variables have on the process' performance. Some rules guide this step and help to choose initial values from which finer investigations can be made. These rules can be grouped under (i) rules of thumb namely for conversion efficiencies, recoveries, approach temperatures etc., (ii) Industry and company standards concerning operating pressures, equipment size, etc. , and (iii) results from the development stage, namely concerning reaction conditions. These said rules either provide initial guesses or an interval from which adequate values are extracted. The tuning of these parameters and the exploration of these intervals is a delicate matter, even more when one seeks to respect the knowledge gained in the development stage. The use of adequate predictive mathematical models is hence crucial if one wants to leave the beaten track. The main output of this level is a default value for operating conditions along with a variation interval for certain process parameters.

1.1.5 Choice of equipment

At this level, the designer makes a preliminary choice concerning the type of equipment to perform the desired unit operations. This choice has a direct impact on process performances. For example, the pressure drop in a distillation column increases the heat duty in the reboiler and may cause problems that affect process cost and safety such as reboiler fouling or vacuum distillation. A choice of distillation equipment with a low pressure drop can hence reduce this problem. This stresses even more the need for an iterative procedure to juggle between the various choice levels. The process engineer must hence have a good understanding of the equipment items in the

process. Moreover, we note as *design parameters* the parameters that are intrinsically linked to the equipment in question: pressure drop in heat exchangers and distillation columns, efficiencies in turbines and compressors, etc. A detailed equipment characterization is not needed at this level; however the designer must not leave many unexpected problems for the equipment designer to encounter. The designer must again make a trade-off between the details of the equipment model and the degrees of freedom left for design.

1.1.6 Use of process simulators

Process simulators are computer tools that transcribe the process along with its topology, operating conditions and to a certain extent equipment design into a computerized structure, known as a *flowsheet*. Notorious examples are Vali®, Aspen Plus®, Pro II®, Prosim®, etc. These simulators offer several characteristics:

- Databanks which contain a multitude of components, with their associated thermodynamic data. The designer has also the possibility to introduce novel components along with their associated data.
- Thermodynamic methods which enable the modeling of interactions between various components of a given mixture.
- Mass, heat and power streams which can be included in the flowsheet model. Operating conditions are usually defined for input streams, whereas output and intermediary streams are calculated in the simulation.
- Models for unit operations which help include these operations in the flowsheet. Interconnection between these units is hence made possible. Moreover, design constraints are embedded within each provided model. The designer can include additional "home-made" models. Operating conditions for each equipment model must also be specified.
- Design targets, such as purities or recoveries, can also be specified. These targets are met by controlling other operating conditions via algorithms embedded in the flowsheet.
- The various sub-systems and technologies can be organized into process blocks, enabling hence the presentation of the block flow diagram.
- Mass and heat balances are systematically performed around each unit operation, and for the entire process.
- Communication with data analysis tools such as Excel®, Matlab® and others is possible, enabling further thermo-economic calculations

We speak of *convergence* when a given configuration is resolved whilst respecting all design targets, equipment constraints and mass and heat balances. The simulators are able to render information concerning the state of convergence of the simulated configuration.

1.1.7 Step-wise optimization

Optimization work in literature was often turned towards one specific process step, were it reaction, separation, heat exchange or utility production. This will be highlighted in the various literature works mentioned in the course of this thesis. These works led to the development of

optimal configurations and to the identification of key operating parameters and their optimal operational ranges. Nevertheless, such works failed to consider a holistic view of the process and therefore capture its different aspects and their interactions.

1.1.8 Integrated Process Design

Integrated Process Design has been a recurring issue in literature related to optimal process synthesis, as highlighted in [2, 3]. Through this method, the process is considered as a system in a holistic fashion.

1.1.8.1 Hierarchical approach

In this context, the hierarchal approach, symbolized by the onion diagram highlighted in Figure 1:2, is considered as the first endeavor in this design method. This approach evolves in a sequential manner from the design of the reaction system, to separation, to the heat exchange network, to utility production, and ultimately effluent treatment for an integral process design.

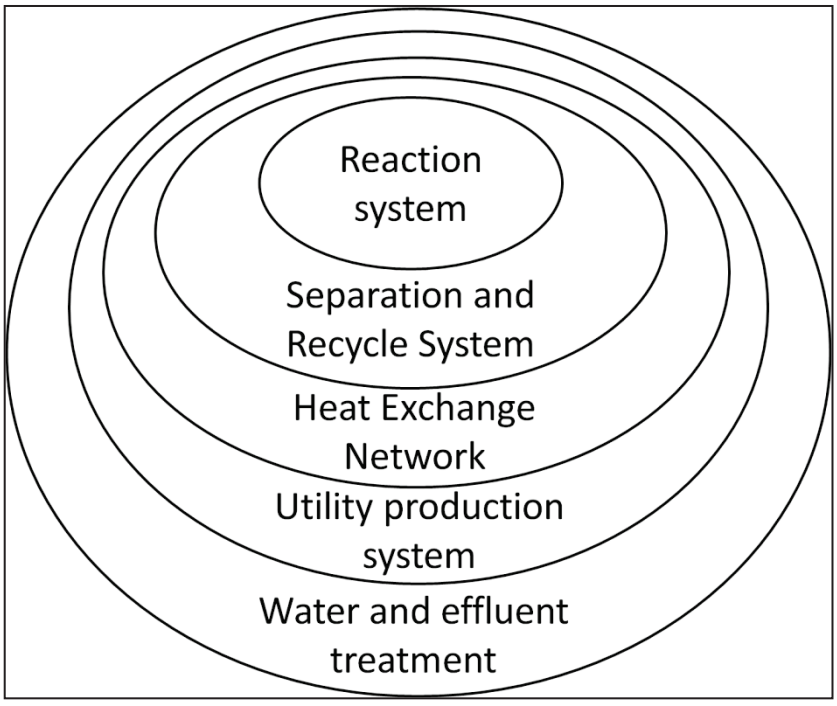

Figure 1:2 Graphic representation of onion model. Integral process design is obtained going from the reaction system outward to the effluent treatment system

1.1.8.2 Superstructure optimization

Superstructure optimization presents a more systematic approach than the hierarchical model, mainly because all process blocks are optimized simultaneously. This methodology enables a process designed from A to Z, or to the extent of the designer's scopes and interests. Its key benefits are highlighted as follows [4]:

- The superstructure is created and has embedded in it all options and interconnections
- Optimization of this superstructure is realized via computer aided techniques

- Many design options and multiple trade-offs can be taken into account

This approach comes however with its drawbacks namely: the finding of the optimum, the consideration of intangible criteria and the designs considered in the said superstructure[4]. These can however be overcome by an understanding of the process at hand.

1.1.8.3 Combined hierarchical and superstructure optimization

A third alternative entails the application of the previous methods for an efficient process design. A specific example, as will be highlighted later, entails the separation of the heat exchange network design from the actual process design problem. These concepts, will be our guiding principles throughout this thesis

1.1.9 Applications in literature

The Integrated Design Methodology was applied by [5] for the construction of a process model for the thermo-chemical production of Synthetic Natural Gas (SNG) from wood chips. A nominal capacity of 20 MW_{th} was assumed whereas the Swiss mandate on the quality of natural gas was chosen as a design specification. This process was broken down into three major steps: gasification, methanation and gas separation and other auxiliary steps: drying, pretreatment, gas cleaning, oxygen production, and CO_2 removal. These steps were organized into a *superstructure*, as highlighted in Figure 1:3. Moreover, alternatives were sought for each sub-section as highlighted also in Figure 1:3. In this figure, optional units are identified with dotted lines, whereas dashed lines investigate alternatives for various sections. Key material and heat streams are also indicated. However, the layout of each unit and alternative is not detailed at this level. We speak of a *block flow diagram.*

The chemical and physical transformations occurring in the units of the superstructure are defined at the energy-flow level along with the associated thermodynamic model. Robust and accurate models were constructed for the various technologies. As a result, key process assumptions and parameters were identified and process simulations were made possible. The chosen process simulator was VALI.

The heat exchange network was on the other hand determined in a post-simulation run leading to the calculation of key parameters such as utility consumption and heat exchange network area.

Equipment rating and design was then performed in preparations for capital cost evaluation. Finally, multiple process configurations with different choices for process topology and operating conditions were simulated.

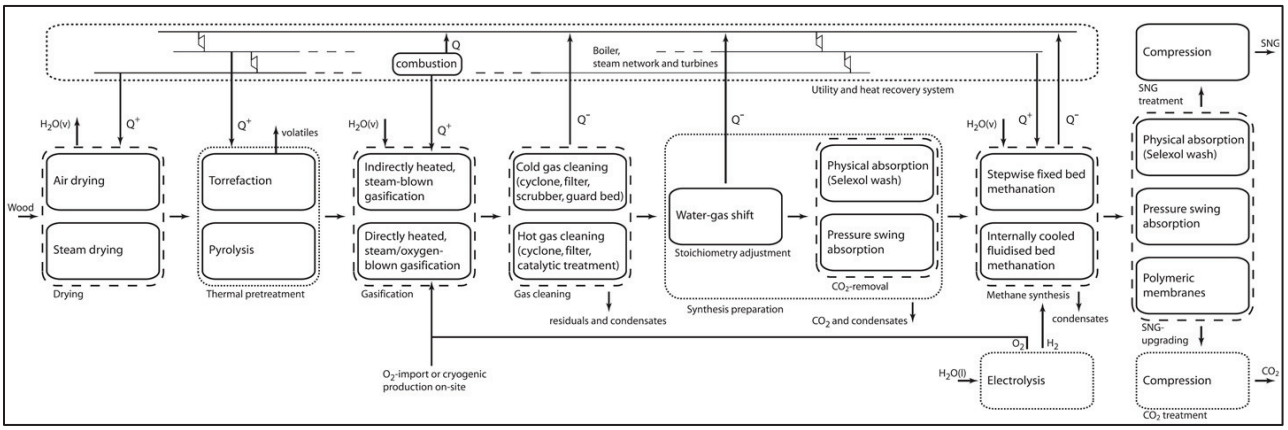

Figure 1:3 Superstructure for biomass methanation process [5]

1.2 Process evaluation: Performance indicators

Process evaluation aims to calculate the value of key performance indicators. Its goal is to enable adequate comparisons between process configurations, and ultimately selecting the better one. In this section, we highlight the said indicators as well as their calculation means. However, first of all, it is interesting to note that some of these indicators find application in the Heat Integration model (0), where an optimal utility system is sought and selected. The calculation of these indicators is also based on the key concept of process battery limits (BL) namely for determining the input/output streams, and the investigated equipment. Traditionally, utility production systems have been considered inside the battery limit (*ISBL)*. Moreover, in related literature work, process evaluation intervenes once a process configuration is chosen, simulated, converged and additionally its heat exchange network and utility system defined.

1.2.1 Conversion efficiency indicators

Conversion efficiency (eff_{var}) indicators measure the extent of the conversion of input streams to products. Mathematically, it is measured by the ratio of the values of a given variable for product and input streams, as highlighted in Equation 1:1.

Equation 1:1 General expression for conversion efficiency indicators

$$eff_{var} = \frac{\sum_{i=1}^{n_{Prod}} var_{Prod,i}}{\sum_{i=1}^{n_{inp}} var_{inp,i}} (\%)$$

The choice of input and product streams varies according to the chosen indicator and the chosen process battery limit. Nevertheless, certain streams are commonly found: raw material, non-recycled catalysts, utility streams, products, and by-products. Again at this level, the definition of a battery limit for the process is of great importance. Moreover, from their definition, we can see that these indicators are closely linked to profitability indicators such as margin, revenues and ultimately profit. For example, a configuration with a high conversion efficiency has higher chances of being profitable than a low conversion efficiency configuration. Likewise, at this level,

process by-products can be included as credit in the denominator. This makes it easier to calculate the actual efficiency associated with producing the main product.

In addition, by virtue of the laws of physics, second law of thermodynamics, limitations on chemical conversion, etc., the useful energy output is almost always smaller than the energy input. This implies that the calculated efficiencies are almost always smaller than 100%.

Considering this, we will present in this section the main indicators used in literature for efficiency evaluation.

1.2.1.1 Energy conversion efficiency

Energy conversion efficiency ϵ, otherwise termed as thermal efficiency, presents the ratio of the energy content in product streams to that in input streams. First, we provide a physical expression for this energy content, also utilized in Equation 1:17, Equation 1:18, Equation 1:19 and Equation 1:27, and then we provides a generic expression along with certain examples.

1.2.1.1.1 Calculating the energy content

The most common inputs and outputs of chemical processes are chemical products, steam and electricity. The energy content of steam is none other than its heat content (Q), whereas the energy content of electricity is none other than its power content (W).

Chemical products on the other hand contain what is termed as a *potential energy*, i.e. energy that must be converted to other forms before it can be utilized. For bioethanol or biodiesel, this utilization occurs in the combustion engine of automobiles. For biogas, this utilization occurs in automobile combustion engines or in Combined Heat and Power (CHP) production plants. In this context, the *heating value* (*HV*) expresses this (potential) energy content. By definition, it is the amount of heat released during the combustion of a specified amount of this component. It is usually expressed in units of energy per unit of the substance, usually mass, such as $\frac{kJ}{kg}, \frac{kcal}{kg}, \frac{Btu}{lb}$. In our case, the first expression $\frac{kJ}{kg}$ will be used in preference. Two different expressions for this heating value are normally used:

- the *higher (or total) heating value* (*HHV*) determined by bringing combustion products to the ambient temperature resulting in the condensation of the water contained therein, and heat below 150 °C is put to use.
- The *lower (or net) heating value (LHV)* determined by discarding the heat of vaporization of water vapor from the HHV. As a result, all water components are ultimately found in the vapor state. It is hence useful in comparing cases where operation below 150 °C is not feasible. Moreover, the use of LHV values in the case of condensing boilers can lead to efficiencies greater than 100%.

In Europe, the *LHV* is used whereas the *HHV* is employed in the USA. In our case, we choose to operate under the European standard, and hence employ the Lower Heating Value. The LHV of key fuels like natural gas, coal, ethanol, biodiesel etc., are tabulated, whereas specific formulae have

been developed to calculate the LHV of solids and other non-common fuels. Moreover, the LHV of fuels may be calculated either on a dry or on a wet basis. By definition, wet LHV is usually lower than dry LHV ($\frac{kJ}{kg}$).

1.2.1.1.2 Calculating energy efficiency

The general formula for calculating energy efficiency, highlighted in Equation 1:2, is a specific expression of Equation 1:1.

Equation 1:2 General expression for energy conversion efficiency

$$\epsilon = eff_{En} = \frac{\sum_{i=1}^{n_{chem,Prod}} \dot{m}_{ch,Prod,i} \times LHV_{ch,Prod,i} + W_{prod} + Q_{prod}}{\sum_{i=1}^{n_{chem,inp}} \dot{m}_{ch,inp,i} \times LHV_{ch,inp,i} + W_{inp} + Q_{inp}} (-)$$

Within Equation 1:2, both the numerator and the denominator are expressed in power terms (MW, kW, etc.). $\dot{m}_{ch,Prod,i}$ and $LHV_{ch,Prod,i}$ refer to the mass flow rate and lower heating value of the potential process chemical product stream i. $\dot{m}_{ch,inp,i}$ and $LHV_{ch,inp,i}$ refer to those same parameters for process chemical input stream i. Q_{prod} and W_{prod} refer to the potentially produced heat and electricity. Q_{inp} and W_{inp} refer to input values. Typical values for this efficiency are 40% for gas turbines (fuel input, power output), 60% for steam and gas turbines (fuel input, power output), 10-50% for combustion engines and >70% for electric motors.

1.2.1.2 Exergy conversion efficiency

Exergy conversion efficiency, otherwise termed second-law efficiency, η is another thermodynamic efficiency indicator. It presents the ratio of the exergy content in product streams to that in input streams. Like before, we provide first a physical expression for this exergy content, before explicating its formula.

1.2.1.2.1 Calculating the exergy content

Exergy as a thermodynamic concept is a measure of the maximum mechanical work that can be extracted from a given stream by bringing it to equilibrium with its environment, at temperature ($T_0 = 25\ °C$) and pressure ($P_0 = 1\ atm$). Consequently, it is expressed in energetic (kJ, kcal) or power terms (kW, MW, etc.). Moreover, this approach accounts for both the quantity and quality of the different forms of energy under consideration. In other terms, exergy takes into account both the first and the second law of thermodynamics.

For a heat stream, with heat content Q and temperature T_H, this is performed in an ideal Carnot heat engine, with the cold temperature equal to the ambient (T_0). The associated exergy content is noneother than the heat content multiplied by the Carnot efficiency as highlighted in Equation 1:3.

Equation 1:3 General expression for the exergy content of a heat stream with heat content Q and at the temperature level T_H

$$Ex_Q = Q \times \eta_C = Q \times \left(1 - \frac{T_0}{T_H}\right) (MW)$$

Considering that power is work, the exergy of an electricity stream is equal to its power content as highlighted in Equation 1:4.

Equation 1:4 General expression for the exergy content of an electricity stream with power content W

$$Ex_W = W\ (MW)$$

The exergy content of a chemical component (cmp), as highlighted in Equation 1:5 is the sum of its physical and chemical exergy contents. The physical exergy content is normally attributed to the changes of temperature, pressure and concentration of the substances. As a result, if one considers that chemical components enter and exit the system at ambient conditions, this term can be neglected.

Equation 1:5 Formula for the exergy content of a chemical component

$$Ex_{cmp} = Ex_{ph,cmp} + Ex_{ch,cmp} \cong Ex_{ch,cmp}\ (MW)$$

This leaves us with the chemical exergy, attributed to the chemical formation of the substances in question. More specifically, the chemical exergy content of a chemical component $Ex_{chm,comp}$ is defined as the shaft work or electrical energy necessary to produce one mol of this element in its standard state, in a reversible way, from reference materials present in the environment. For example, typical exergy reference components in the atmosphere air are oxygen $O_{2(g)}$, nitrogen $N_{2(g)}$, carbon dioxide $CO_{2(g)}$ and water vapour $H_2O_{(g)}$. Just as for energy content, a nominal chemical exergy ($ex^0_{ch,cmp}$) can be expressed, in $\frac{MWh}{t}$ for any component. As a result, the component's actual chemical exergy (MW) is the product of its mass flow rate $\frac{t}{h}$ and its standard chemical exergy, as in Equation 1:6.

Equation 1:6 General expression for the chemical exergy content of a chemical component

$$Ex_{ch,cmp} = \dot{m}_{cmp} \times ex^0_{ch,cmp}\ (MW)$$

The chemical exergy values of key elements and components have been tabulated in literature [6]. However, the standard chemical exergy of a non-tabulated component is equal to the sum of its Gibbs free energy of formation ($\Delta_f G^0$) and the standard chemical exergy of its constitutive elements ($ex^0_{ch,elem,i}$) multiplied by the element's stoechiometric coefficient (ν_i), as highlighted in Equation 1:7. This calculation can further be extended to mixtures and solutions

Equation 1:7 General formula for calculating the standard chemical exergy of a component

$$ex^0_{ch,cmp} = \Delta_f G^0 + \sum_{i=1}^{n_{elem}} \nu_i \times ex^0_{ch,elem,i}\ (MWh/t)$$

1.2.1.2.2 Calculating exergy efficiency

The general formula for calculating exergy efficiency, highlighted in Equation 1:8, is also a specific expression of Equation 1:1.

Equation 1:8 General expression for exergy conversion efficiency

$$\eta = eff_{Ex} = \frac{\sum_{i=1}^{n_{chem,Prod}} \dot{m}_{ch,Prod,i} \times ex^0_{ch,Prod,i} + W_{prod} + Q_{prod} \times \left(1 - \frac{T_0}{T_{H,prod}}\right)}{\sum_{i=1}^{n_{chem,inp}} \dot{m}_{ch,inp,i} \times ex^0_{ch,inp,i} + W_{inp} + Q_{inp} \times \left(1 - \frac{T_0}{T_{H,inp}}\right)} (-)$$

Within Equation 1:2, both the numerator and the denominator are expressed in power terms (MW, kW, etc.). $\dot{m}_{ch,Prod,i}$ and $ex^0_{ch,Prod,i}$ refer to the mass flow rate and exergy content of the potential process chemical product stream i. $\dot{m}_{ch,inp,i}$ and $ex^0_{ch,inp,i}$ refer to those same parameters for process chemical input stream i. Q_{prod} and W_{prod} refer to the potentially produced heat and electricity. Q_{inp} and W_{inp} refer to input values. $T_{H,prod}$ and $T_{H,inp}$ refer to the temperature levels of product and input heat streams The exergy efficiency of a combined cycle system is typically equal to 54%

1.2.1.3 Chemical exergy conversion efficiency

The chemical exergy efficiency or fuel-based efficiency indicator is a modification of the exergy efficiency indicator defined in Equation 1:9. This modification consisted in replacing the contribution of heat and power streams by the equivalent amount of natural gas that is consumed (or saved) in a reference technology [7]. For power, this reference technology is the (synthetic) Natural Gas Combined Cycle (NGCC), whereas for heat it is the electricity-driven Heat Pump (HP), both with exergetic efficiencies ($\eta_{NGCC}\ and\ \eta_{HP}$) equal to 55%. This was realized in order to asses the value of the products with respect to the technical feasibility of their further conversion into final energy services and competing technologies. The general formula for the chemical exergy efficiency is provided in Equation 1:9. $Ex_{W,prod}$, $Ex_{W,inp}$, $Ex_{Q,prod}$ and $Ex_{Q,inp}$ are the exergy contents of input/output power and heat streams. LHV_{SNG} and ex^0_{SNG} refer to the lower heating value and standard chemical exergy of synthetic natural gas. Finally, η_{HP} and η_{NGCC} are the exergy efficiencies of the chosen reference technologies.

Equation 1:9 General expression for energy conversion efficiency

$$\varepsilon_{chem} = eff_{chm,Ex} = \frac{\sum_{i=1}^{n_{chem,Prod}} \dot{m}_{ch,Prod,i} \times ex^{0}_{ch,Prod,i} + \frac{1}{\eta_{NGCC}} \times \frac{LHV_{SNG}}{ex^{0}_{SNG}} \times (Ex_{W,prod} + \frac{Ex_{Q,prod}}{\eta_{HP}})}{\sum_{i=1}^{n_{chem,inp}} \dot{m}_{ch,inp,i} \times ex^{0}_{ch,inp,i} + \frac{1}{\eta_{NGCC}} \times \frac{LHV_{SNG}}{ex^{0}_{SNG}} \times (Ex_{W,inp} + \frac{Ex_{Q,inp}}{\eta_{HP}})} (-)$$

1.2.1.4 Comparison between the various efficiency indicators

The energy efficiency indicator is rather an intuitive straight-forward evaluation of the conversion efficiencies of a process. For this reason, it was used early on in process evaluation works. However, the different degrees of usefulness of the various energy forms are not taken into account by this indicator. As a result, this indicator can be used only in cases where entropy-free energy is produced or consumed. This is rarely the case in industrial processes, and as a result, the exergy efficiency indicator rapidly saw an increase in its application. Moreover, exergy efficiency being based on both the first and second thermodynamic laws permits the quantitative evaluation of energy degradation, an endeavor not possible with the energy efficiency formulation. This indicator is capable of measuring thus the usefulness of the obtained products. It also allows obtaining a primary assessment of the environmental performance of the investigated process. Finally, it can be an indicator of economic performance. For this reason, it was the chosen indicator in our case.

The chemical exergy content even though of interest is recent applications was not adopted in our case, mainly because of its need for comparison with hypothetical conversion strategies: namely the heat pump and the combined gasification cycle.

1.2.2 Investment Costs

The investment cost presents the cost of purchase and installation of the required equipment, along with other indirect costs. [8] employed the method developed by [9], and which breaks down as follows.

1.2.2.1 Equipment Purchase Cost

The first evaluated variable is the equipment purchase cost, denoted as the *Bare Module Cost*, $C_{BM,equip}$. This cost is calculated via equipment-specific correlations. This cost is the basis for the employed method. As a result, it should be determined as accurately as possible. In [9], a base cost ($C_{base,equip}$), was deduced from a characteristic equipment size (H_{equip}) via log-log plots. The obtained cost was then corrected with factors ($f_{i,equip}$). Such factors take into account the influence of operating pressure, operating temperature and type of material, among others, to obtain the real cost. This formulation is expressed in Equation 1:10. The cost of specialized equipment, unavailable in literature, is usually estimated from the cost of its constitutive components. This method approximates the actual cost by a ±25/30% margin.

Equation 1:10 – Expression for an equipment's total module cost [10]

$$C_{BM,equip} = C_{base,equip}(H_{equip}) \times \prod_i f_{i,equip}\ (M\$)$$

1.2.2.2 Cost actualization

The base equipment cost, and subsequently the bare module cost, are usually specified in most economic evaluation methods for a given calculation year. This year is generally different from the actual evaluation year. For this reason, a cost actualization is required. The latter is usually performed by the use of cost indices [11], and the actual costs are obtained as is highlighted in Equation 1:11.

Equation 1:11 – Actualization of equipment cost [10]

$$C_{BM,equip,actual} = C_{BM,equip} \times \frac{Cost_{ind,act}}{Cost_{ind,calc}}\ (M\$)$$

Multiple cost indices exist in literature and they mostly depend on the working sector. [5] employ the Marshall and Swift Index (M&S) and this for its suitability for paper (a ligno-cellulosic material) production processes. With this in mind, it is this actualized parameter that will be used for the subsequent cost calculation steps.

1.2.2.3 Equipment Total Module Cost

The installed cost is denoted as the *Total Module Cost*($C_{TM,equip}$). It takes into account, in addition to the Bare Module Cost, indirect costs like freights and engineering expenses. Its expression is available in Equation 1:12, where $c_{1,equip}$ accounts for contingencies and fees during construction, and is deduced from literature correlations. The *equip* subscript indicates that this factor might depend on the equipment. In the work of [8], this factor was considered constant for all equipment at 18%, in accordance with the works of [10].

Equation 1:12 – Expression for an equipment's total module cost [10]

$$C_{TM,equip} = \left(1 + c_{1,equip}\right) \times C_{BM,equip,actual}(M\$)$$

1.2.2.4 Equipment Grass Root Cost

The grass-roots facility presents the case for a totally new site. Its cost, denoted C_{GR}, is expressed in Equation 1:13, takes into account site development and auxiliary facilities, expressed in $c_{2,equip}$, along with indirect costs, expressed in $c_{1,equip}$. Again, the equip subscript is used in cases where indirect costs are dependent on the considered equipment. In the works of [8], $c_{2,equip}$ was also considered at 35%, in line with the works of [10]. Also, in Equation 1:13, the first term is denoted as Inside Battery Limit (ISBL) cost, whereas the second term is the Outside Battery Limit (OSBL) cost.

Equation 1:13 – Expression for a grass root process cost [10]

$$C_{GR,equip} = C_{TM,equip} + c_{2,equip} \times C_{BM,equip,actual}(M\$)$$

1.2.2.5 Fixed Capital Cost

The Fixed Capital Cost (C_{FC}) is defined as the total cost of processing installations, contained inside the process battery limit (ISBL), and involved in the creation of a new plant. As a result, it can be calculated, in the case of grassroots facility, as the sum of the grass roots cost of all of the equipment contained inside the battery limit, $C_{GR,equip}$, as highlighted in Equation 1:14.

Equation 1:14 Expression for the fixed capital cost of a process

$$C_{FC} = \sum_{equip} C_{GR,equip} \text{ (M\$)}$$

1.2.2.6 Working Capital Investment

The *Working Capital Investment* (C_{WC}) is usually added to the fixed capital investment (C_{GR} in the case of a grassroot site, C_{TM} in the case of revamps or additions). This cost accounts for interest, storage of raw materials and end-products, accounts payable, and taxes payable [12]. This parameter is usually obtained from the fixed capital investment by virtue of a correction factor, f_{WC}, as highlighted in Equation 1:15.

Equation 1:15 – Expression of working capital cost

$$C_{WC} = f_{WC} \times C_{FC} \ (M\$)$$

The factor f_{WC} equals 10 to 20 percent for most chemical plants. It can however increase to as much as 50 percent for seasonable production processes, like bioprocesses.

1.2.2.7 Total Capital Investment

The *Total Capital Investment (C_{TCI})* is obtained as the sum of the fixed capital cost and the working capital cost as highlighted in Equation 1:16.

Equation 1:16 – Expression of total capital cost

$$C_{TCI} = C_{FC} + C_{WC} = (1 + f_{WC}) \times C_{FC} \ (M\$)$$

1.2.3 Economic performance indicators

Economic indicators provide information about the process performance for a given reference. . These indicators are usually calculated on one of three bases: daily, unity of product (or raw material), or annual. According to [12], the third formulation is the most adequate. The main reason is its capacity to take into account seasonality as well as infrequent large expenses.

1.2.3.1 Plant availability

Plant availability refers mainly to the number of hours a process is in operation in a given day. In the case of seasonable production, availability can also reflect the number of days, n_{dop}, the plant

is in operation for a given year. This parameter, combined with simulation results, can help calculate the yearly production rates for the various products or consumption rates for the various raw materials and utilities. Considering this, this is a very important parameter for all subsequent calculations.

1.2.3.2 Annual Operating Costs

Operating costs (C_{OP}), are another key process performance indicator. As a result, yearly consumption rates are of great importance at this level.

These costs are calculated as the sum of the following components, whose equations are provided in Table 1:1:

- The costs of raw material (C_{RM}), expressed as the sum of: the nominal cost of the n_{RM} raw materials consumed, ($C^0_{RM,i}$), which can be expressed in \$/L, \$/t or \$/MWh, multiplied by their yearly consumption rate ($Cons_{y,RM,i}$), as highlighted in Equation 1:17
- The cost of catalysts and chemicals (C_{CC}) expressed as the sum of: the nominal cost of the n_{cc} catalyst or chemicals employed, $C^0_{CC,i}$, multiplied by their yearly consumption rate, ($Cons_{rate,y,CC,i}$), as highlighted in Equation 1:18.
- The cost of utilities (C_{UT}), expressed as the sum of: the nominal cost of the n_{UT} utility streams, ($C^0_{UT,i}$), multiplied by their yearly consumption rate, $Cons_{y,UT,i}$, as expressed in Equation 1:19.
- The operating labor cost (C_{labor}), expressed as the sum of: the employee count ($n_{employee,i}$) in the ith category of the $n_{emp_{cat}}$ employee categories (operator, supervisor, manager, engineer, overhead) multiplied by their respective yearly salary, $C^0_{employee,y,i}$, as highlighted in Equation 1:20. This number is mostly dependent on the process at hand.
- The Maintenance Cost (C_M), expressed as a fraction, f_{CM}, of the fixed capital cost, C_{FC}, as in Equation 1:21.
- Other expenses (C_{exp}), including overheads, insurance, research and innovation among others. These costs are expressed as a fraction, f_{exp}, of the fixed capital cost, C_{FC}, as in Equation 1:22.

The sum of these costs yields the total operating costs, whose mathematical expression is provided in Equation 1:23.

Table 1:1 Expressions for components of process operating cost on an annual basis

Cost	Expression	Equation
C_{RM} (M$/y)	$C_{RM} = \sum_{i=1}^{n_{RM}} C_{RM,i}^{0} \times Cons_{y,RM,i}$	Equation 1:17 Expression for raw material cost
C_{CC} (M$/y)	$C_{CC} = \sum_{i=1}^{n_{cc}} C_{CC,i}^{0} \times Cons_{y,CC,i}$	Equation 1:18 Expression for chemicals cost
C_{UT}(M$/y)	$C_{UT} = \sum_{i=1}^{n_{UT}} C_{UT,i}^{0} \times Cons_{y,UT,i}$	Equation 1:19 Expression for utilities costs
C_{labor} (M$/y)	$C_{labor} = \sum_{i=1}^{n_{emp_{cat}}} n_{employee,i} \times C_{employee,y,i}$	Equation 1:20 Expression for labor cost
C_{M} (M$/y)	$C_{M} = f_{CM} \times C_{FC}$	Equation 1:21 Expression for maintenance costs
C_{exp} (M$/y)	$C_{exp} = f_{exp} \times C_{FC}$	Equation 1:22 Expression for additional expenses costs
C_{OP} (M$/y)	$C_{op} = C_{RM} + C_{CC} + C_{UT} + C_{labor} + C_{M} + C_{exp}$	Equation 1:23 Expression for operating costs

In most processes, raw material costs are the largest contributor to operating costs, with utility costs in second spot. Moreover, all components, save maintenance and additional expenses, depend to a large extent on commercial considerations. An example thereof is whether materials are bought under a contractual market or on the open market. Another case is related to the location of the plant and the associated labor costs. Moreover, utilities costs are usually used as a selection criteria or "objective function" for the case of optimal utility design.

1.2.3.3 Annualized Total Investment cost

This annualized cost is defined when the company borrows money from the bank with a predefined interest rate (i_r), and a predefined reimbursement period (n_r), evaluated in years. This is taken into account by the *Annualization* method. In this method, the annual cost ($C_{TCI,ann}$) is equal to the total capital investment cost, C_{TCI} divided by an annualization factor ($a_{i_r,\mathrm{LT}}$), as highlighted in Equation 1:24. $a_{i_r,\mathrm{LT}}$ is function of the reimbursement period (n_r) and the interest rate (i_r), as highlighted in Equation 1:25.

Equation 1:24 – Annualization of equipment cost: Annualization method

$$C_{TCI,ann} = \frac{C_{TCI}}{a_{i_r,LT}} \left(\frac{M\$}{y}\right)$$

Equation 1:25 – Expression for the annualization factor

$$a_{i_r n_r} = \frac{((1+i_r)^{n_r} - 1)}{i_r \times (1+i_r)^{n_r}} \ (-)$$

This method has found application for process design in the works of [8]. However, it comes with its own drawbacks. The first drawback concerns the need for defining a financing scheme, debt vs. equity, and for defining the terms, interest rate and reimbursement period. Moreover, this annualization could not be taken into account when the company uses internal assets and capital.

Even though, this annualization procedure is of great importance, it was not investigated in the context of our work. Considering this, there was no decision to annualize the investment cost.

1.2.3.4 Total annual production cost

The total yearly production cost ($C_{tot,y,prod}$) is the total cost incurred to produce the desired products. It is calculated as the sum of the annual operating costs (C_{op}) and of the annualized total investment cost ($C_{TCI,y}$). The later is weighted by the annualization decision (ann_{dec}). With this in mind and seeing that there was no decision for annualization, the annualized total investment cost contribution equaled zero and the total yearly production cost equaled the annual operating cost, as evidenced in Equation 1:26.

Equation 1:26 Expression for total annual production costs

$$C_{tot,y,prod} = C_{op} + ann_{dec} \times C_{TCI,y} = C_{op}(\frac{M\$}{y})$$

1.2.3.5 Total yearly revenues

Revenues for a project are the incomes earned from sales of products and byproducts. In addition to process specific parameters such as plant availability, the calculation of these values is to a large extent dependent on market conditions. Contractual situations versus open market situations can be considered as in the case of raw materials. Price estimation and forecasting is hence pivotal at this level. The expression for total yearly revenue, $C_{tot,y,rev}$, is similar to that of the raw material costs, C_{RM}, and is available in Equation 1:27. The factors in this equation are: the number of process products, ($n_{Products}$), the nominal selling price for product i, $P^0_{Prod,i}$, and the yearly production rate of product i, $Prod_{rate,y,Product,i}$. Whereas $P^0_{Prod,i}$ can be expressed in \$/l, \$/t or \$/MWh among others, $Prod_{y,Prod,i}$ can be expressed in l/y, t/y or MWh/y among others. Nonetheless, the employed units for these two variables should be coherent. As a result, the total yearly revenue expressed in M\$/y.

Equation 1:27 Expression for total annual revenues

$$C_{tot,y,rev} = \sum_{i=1}^{n_{Products}} P^0_{Prod,i} \times Prod_{y,Prod,i} \, (\frac{M\$}{y})$$

However, as indicated previously, byproduct revenues may be included in the total production costs instead of the total yearly revenue.

1.2.3.6 Total yearly margin

Margin, Gross Margin or Product Margin, $Margin_{tot,ann}$, is defined as the difference between yearly revenues and the yearly raw material costs, and is expressed in Equation 1:28. It is a useful concept for the following reasons: (1) raw materials costs are almost always the largest contributor to production costs. (2) Both revenues and raw material costs are dependent on nominal component prices and are hence subject to variability. They are hence useful in price forecasting.

Equation 1:28 Expression for margin

$$Margin_{tot,y} = C_{tot,y,rev} - C_{RM}(\frac{M\$}{y})$$

1.2.3.7 Gross Annual Profit

Gross profit is the difference between main revenues and total production cost as highlighted in Equation 1:29. It should not be confused with gross margin, since it contains all production costs and not just those of raw materials [13].

Equation 1:29 Expression for Gross Profit

$$Profit_{gross,y} = C_{tot,y,rev} - C_{tot,y,prod}(\frac{M\$}{y})$$

1.2.3.8 Investment depreciation

Depreciation, in its broad sense, refers to the loss of value of an item. For chemical processes, it refers to the loss of value due to the "wear and tear" of the components and facilities of the plant. As a result, depreciation only takes into consideration the fixed capital costs, and does not include working capital or land.

The straight line depreciation is the most used method for approximating depreciation. In this method, the depreciable value , $C_{FC,dep}$, is calculated as the ratio of the Fixed Capital Cost, C_{FC}, to the number of depreciation years (n_{dep}), as highlighted in Equation 1:26.

Equation 1:30 – Investment Depreciation according to the straight line method

$$C_{FC,dep} = \frac{C_{FC}}{n_{dep}}\ (\frac{M\$}{y})$$

Depreciation is however only accountable for the years preceding the end of the associated depreciation period, n_{dep}. This leads us to consider an additional factor , $if_{dep,y}$, which indicates whether depreciation is to be included or not in a given yearly evaluation. This factor is equal to 1 in the case of a year preceding the end of depreciation, and to 0 for a post-depreciation year, as highlighted in Equation 1:31.

Equation 1:31 – Expression for depreciation factor

$$if_{dep,y} = \begin{cases} 0 \; if \; y > n_{dep} \\ 1 \; if \; y < n_{dep} \end{cases}$$

1.2.3.9 Annual Taxable profit

Taxable profit refers to the fraction of profit that is subject to taxation by the government. This value is considered equal to the gross profit, minus the possible depreciation cost, as highlighted in Equation 1:32.

Equation 1:32 Expression for annual taxable profit

$$Profit_{tax,y,dep} = \left(Profit_{gross,y} - if_{dep,y} \times C_{FC,dep}\right) \times tax_{rate}$$

The presence of the depreciation factor leads thus to two cases. The first consists in a taking into account of depreciation, and occurs for years prior to the end of the depreciation period. The second consists in a zero depreciation cost, and occurs for the years after the depreciation period.

Finally, it should be indicated that taxation is also a delicate matter. Tax codes vary by countries and locations. Also, taxation may not apply to the entire of the components of the gross profit.

1.2.3.10 Net Annual Profit

The net profit expressed in Equation 1:33, is the amount left after taxes are paid.

Equation 1:33 Expression for Net Profit

$$Profit_{net,y} = Profit_{gross,y} - Proft_{tax,y,dep}\left(\frac{M\$}{y}\right)$$

This is a key parameter since chemical plants, like any other industrial endeavor, are designed and built to make a profit.

1.2.3.11 Plant construction and start-up time

Plant construction refers to the activities required in order to establish the process as an actual facility. Start-up on the other hand intervenes after construction. Its goal is to bring the plant into steady-state operation. These definitions entail that the process cannot be considered as operational during the construction and start-up period. This is aggravated by the fact that the main fixed and working capital expenses occur within this period.

As a result, the construction and start-up time (t_{c-s}), usually evaluated in years, is a key design parameter.

1.2.3.12 Cash Flow

The *Cash Flow* for a given year y *(CF_y)* is the operating balance for a given process configuration at year y of the plant's lifetime.

In the first years, namely the construction and start-up period, investments are made, and plant availability is not at its fullest. Negative cash flows are hence obtained. This pattern is turned in later years where the need for investment is reduced and operation is at maximum availability.

The case is also different for the years occurring before the end of depreciation and the years occurring after it. In the former, depreciation is included in the net profit calculations. It is however absent in the latter formulation.

A final difference also concerns the choice for spending the investment cost, namely annualization vs. direct pay.

Considering these points, its evaluation is delicate and closely related to the process at hand. Moreover, its calculation formula can only be made by the decision maker.

1.2.3.13 Discounted Cash Flow-Present Value: Time value of money

The concept of the time value of money is of importance in all projects where cash flows occurring at different years are to be evaluated. Its two base principles are depreciation of money and risk. The first principle relates to the fact that a dollar earned today is worth more than a dollar earned at a later time. The second principle includes the uncertainty associated with any future cash-flow.

This time value is intrinsically linked to prevalent interest rates or industry-norm return on investment rates, represented by the discount rate, r_{dc}. Evaluating the present value of a future cash flow is termed *discounting*. As a result, the *discounted cash flow* presents the *Present Value* (PV) of a future cash flow. A discounted cash-flow/year diagram can hence be drawn. Finally, discounting in year i usually occurs by virtue of the *discount factor* $f_{dc,i}$, calculated from the discount rate r_{dc}. The discounted cash flow in year i DCF_i is expressed as in Equation 1:34. This expression accounts for both time value of money and varying annual cash flows.

Equation 1:34 Expression for Discounted Cash Flow in year i

$$DCF_y = PV_y = CF_y \times f_{dc,y} = \frac{CF_y}{(1+r_{dc})^y} \left(\frac{M\$}{y}\right)$$

This discounted cash flow is the ultimate indicator for the economic performance in a given year I, since it takes into account the totality of the previous indicators.

1.2.4 Process profitability indicators

Profitability indicators enable the appraisal of the opportunity associated with a given process configuration. They also enable a comparison between processes, and ultimately the selection of a most profitable alternative. Multiple indicators are available in literature, and will be detailed hereafter.

1.2.4.1 Simple Rate of return on investment

The Simple Rate of Return is referred to as the yearly net profit generated, divided by the total capital investment, as highlighted in Equation 1:35. Other methods consider a different

investment function accounting for equipment depreciation [12]. As a result of this definition, this value is expressed on a yearly percentage basis.

Equation 1:35 Expression for the Simple Rate of Return on Investment

$$SRR = \frac{Profit_{net,y}}{C_{TCI}}(\%)$$

Other variants for this equation exist, namely through the consideration of a yearly net profit value, averaged across the project lifetime.

This method is one of the most commonly used methods for investment appraisal, and ultimately project selection. Considering this, a value ranging between 15 and 25 percent is common for many food and agri-business companies. The typical range for renewable energy applications ranges however between 8 and 12%.

It comes however with its drawbacks, cited below:

- This method uses net profit rather than *cash flows*. The latter approach is however as a better method since it accounts for non-cash transactions, such as depreciation, and for varying profits along the project lifetime.
- This method does not take into account the *Time value of money*. It assumes thus that a net income earned at a later time of the project lifetime has the same value as an income earned at an earlier time.
- This method is influenced by the size of the equipment. Hence a project with high profit values can be rejected if it has a high investment cost, when compared to a low profit low investment alternative.

1.2.4.2 Net Present Value (NPV)

The Net Present Value (NPV) represents the sum of the present values or discounted cash flows over the project lifetime (LT). It represents hence the excess or shortfall of cash flows, in present term values, in comparison to cost of funds. As a result, it is a useful tool to determine the net profitability of a project or investment, as highlighted in Table 1:2. Moreover, in the case of limited capital funding such in process design, the project, or configuration, with the highest NPV is the most interesting, as shown in Table 1:2.

Table 1:2 NPV and project/configuration selection

Case	Interpretation	Outcome
$\mathbf{NPV} > 0$	The project creates economic value	The project can be accepted
$\mathbf{NPV} < 0$	The project destroys economic value	The project is to rejected
$\mathbf{NPV} = \mathbf{0}$	The project neither creates nor destroys value	Decision based on other factors
$\mathbf{NPV_1} > \mathbf{NPV_2}$	The first project creates more value	The first project is preferred

The formula for calculating the Net Present Value of a project is highlighted in Equation 1:36. The Net Present Value method can further be extended to compare projects with varying lifetime by the use of the Equivalent Annual Cost (EAC), which is the product of the NPV and the annuity factor ($a_{i_r,LT}$), as highlighted in Equation 1:37.

Equation 1:36 Expression for Project Net Present Value

$$NPV = \sum_{i=1}^{LT} DCF_i = \sum_{i=1}^{LT} \frac{CF_i}{(1+r_{dc})^i} (\$)$$

Equation 1:37 Expression for Project Equivalent Annual Cost

$$EAC = NPV \times a_{i_r,LT} (\$)$$

1.2.4.3 Internal Rate of Return

The internal rate of return (*IRR*) is another term used in capital budgeting to measure and compare the profitability of competing projects. It is equal to the value of the discount rate where the NPV of a given project is null. In this context, the *hurdle rate,* r_{hur} is the company's or the designer's minimum acceptable discount rate. In general, the following rule applies: when NPV is positive IRR is greater than the hurdle rate, r_{hur}, and vice-versa. For simple cash flows, the IRR can be approximated by the rate of return RR [14].

Equation 1:38 Expression for Internal Rate of Return

$$IRR(\%) \backslash\ NPV(IRR) = \sum_{i=1}^{LT} \frac{CF_i}{(1+IRR)^i} = 0$$

1.2.4.4 Break-even cost

The break-even cost is usually calculated for a chosen raw material or a chosen product, when all other parameters are considered known. In the context of discounted monetary values, it can be considered as the nominal cost which makes the NPV equal to zero. Hence, a higher raw material cost leads to an unprofitable configuration. The same applies for a lower product price.

1.2.4.5 Discounted payback time

Discounted payback time (PBT) defines the minimum length of time necessary to recover the initial capital investment in the form of discounted cash flow. It refers hence to the case where the cumulative discounted cash flow is positive or null, as expressed in Equation 1:39. It is obvious that the investor or designer would like an alternative with a rather small payback time. On another note, the Payback Time can also be calculated with no consideration for the discount rate. In this case, the obtained value is none other than the ratio between the initial investment and the yearly profit.

Equation 1:39 Expression for Discounted Payback Time

$$DPT(y)\backslash \sum_{n_y=1}^{PBT} DCF_i \geq 0 \;\&\; \sum_{n_y=1}^{PBT-1} DCF_i < 0$$

1.2.4.6 Comparison between the various indicators

Revenue and total production cost considered alone cannot determine the profitability of a process. Both should be equally considered in any evaluation of profitability. However, total profit alone cannot determine the profitability behind a given investment and this for the following reasons [12]: (1) This parameter does not take into account neither the initial investment nor the project scope and lifetime. (2) Comparison is not possible between different competing processes, a case typically encountered in process design. **In all cases, a designer ideally seeks configuration with maximum revenues, margins and profits, and with minimum total production costs.**

Moreover, the simple rate of return SRR gives "point values", applicable either to one particular year or for some sort of average year. However, as previously indicated, this parameter does not consider the time-value of money, neither the variability cash flows across the project lifetime, and is greatly influenced by equipment size. The use of time dependent indicators making use of discounted cash flows, such as the NPV, the IRR and the DPT, is hence more appealing?

From the previous analysis, we can deduce that the higher the values of NPV and IRR for a given alternative, the more attractive it is. However, the essential distinction between these two parameters is: (1) NPV measures profit but does not indicate how efficiently capital is being used. It is hence more interesting when the goal is to maximize profit. (2) IRR measures how efficiently capital is used but gives no indication on profit. It is more useful in cases with restricted supply of capital, and reflects which projects will use the capital more efficiently. In process engineering, designers would look for alternatives that have both a small investment requirement and a large profit. Finally, the PBT parameter has two shortcomings: (1) it cannot differentiate between projects having a low IRR (or NPV) and projects having a high IRR (or NPV). (2) It ignores cash flows occurring after the payout year. However, it can prove useful when used in conjunction with other parameters, namely IRR and NPV [14].

In all cases, we remind that all of the previous indicators depend to a large extent on the financial and operating assumptions made for the total scope of the project, in addition to estimations on prices and specific process parameters. Some of these indicators were applied by [15] to compare and select various configurations of a small sized fictitious Williams-Otto Process, with three variable parameters. Two cases were realized: (1) seek configurations with maximum Net Present Value (NPV) and maximum gross profit, Profit_{gross} and (2) seek configurations with maximum NPV and minimum PBT (non-discounted in this case). Both cases yielded different configurations, but with comparable results. The first yielded a 7.2 M$ NPV for a 2.37 M$ gross profit, whereas the second yielded a 7.21 M$ NPV for a 1.37 year payback time.

1.2.5 Environmental indicators

The inclusion of environmental indicators in process evaluation has become an ever more common practice. These indicators stretch from a simple material balance around process boundaries to an extensive lifecycle analysis concerning the main product. Within these various works, exergy efficiency has once again proven to be a good tool in this endeavor, as indicated in [16]. In fact, increasing exergy efficiency leads to a reduced environmental impact. This is realized by limiting order destruction, resource degradation and waste exergy emissions. [17] argue however that the exergy of waste emissions cannot be solely evaluated by physico-chemical parameters. Proposed evaluation alternatives consist of (1) an evaluation related to the exergy consumption that is necessary to abate the emissions in a waste treatment facility, (2) an evaluation related to the loss of exergy in the environment and society due to health effects. The former formulation resembles that found within the chemical exergy indicator. As a result, exergy will be used as a compound indicator to measure and ultimately reduce a process's environmental impact.

1.2.6 Coupling exergy efficiency indicators and economics

[18] indicate that exergy is a more consistent measure of economic value than energy. This is a direct consequence of the concept of usefulness and "utility" considered solely in the exergetic formulation. However, the exergy balance differs from the economic balance in the fact that the first is dependent on technological and scientific considerations whereas the second is based on market conditions. A direct result of this observation is the benefits of the voluntary inclusion of exergy analysis components into process design. Moreover, [19] highlighted the existence of correlations between exergy efficiency and capital costs: (1) lower exergy efficiency is obtained with low capital costs, and vice versa. (2) A balance exists between exergy efficiency and capital costs in real systems. (3) Energy conversion devices operate at an appropriate "trade-off" between exergy efficiency and capital cost. This trade-off was exploited in the works of [7].

1.2.7 On the hierarchy of indicators: exergy efficiency and Fixed Capital Cost as ultimate performance indicators

This section deals with the relative adequacy of the various indicators.

From the previous analysis, it was established that profitability and economic performance indicators depend to a large extent on financial and market considerations. They cannot hence be utilized as generic process evaluation tools, even more in the context of multiple products. They prove however useful for the ultimate 'appraisal' of processes prior to the final selection phase. This is due to the great level of detail, and the great number of financial decisions involved in their calculation.

Fixed Capital costs on the other hand suffer to a lesser extent from market variations, and company decisions, making them a universal indicator for basic process evaluation.

Exergy efficiency is another adequate indicator for process evaluation. This adequacy is emphasized by its close link to margins and profits. The exergy efficiency indicator provide a better evaluation of value creation within the process since it does not depend on market considerations. In addition, this exergy efficiency indicator is a good indicator of environmental performance. Finally, the conflicting nature between exergy efficiency and capital costs was also proven.

For these reasons, exergy efficiency and capital costs were chosen as primary indicators of process performance in many literature works [7, 8, 20, 21].

1.3 Process optimization: optimal process design

Process optimization, otherwise termed optimal process design, is concerned with the finding of optimal process configurations with regards to chosen indicators or *objective functions*. This optimization consists in modifying the values of certain *optimization variables* related either to system structure or to operating conditions of unit operations, in order to obtain better values for the said objective functions. This optimization work can be split into two groups: manual and computerized optimization.

1.3.1 Manual process optimization

Manual means have always been a chosen method to handle the process optimization problem. The designer has multiple tools and approaches at his disposition to perform this task. His first approach is the proper investigation of the simulation model, the resulting heat integration model, and the obtained values for chosen indicators, namely exergy efficiency and capital costs. *Pinch analysis* is a widely used tool at this level, namely to increase the exergy efficiency of the process. The basis for the application of this method for a manual optimization of the heat demand of processes are provided in [2]. This tool does not however take into account process capital costs. As a result, the designer must use it cautiously.

Another tool consists in applying heuristics developed by process engineers through experience and practice. These heuristics concern the choice of operating conditions, the sequencing of operations and the design of equipment. These heuristics are however often conflicting, and a certain prioritization or selection needs to be performed by the designer. This difficulty limits the applicability of these heuristics.

This manual optimization rapidly presents its limits to the process designer either in the extent of configurations to be evaluated or in the conflictive nature between the obtained solutions. Its use has hence rapidly made way for the use of computerized techniques. Nonetheless, this approach remains essential for the proposition of process alternatives susceptible of improving process performance and in ultimately pinpointing the range of variation of key optimization variables

1.3.2 Computerized optimization

Computerized optimization signifies the use of computer algorithms for the selection of optimal process configurations. These algorithms are usually associated to the process simulation model and perform the desired optimization by multiple iterations with the said model.

1.3.3 Single vs. Multiple objective optimization

Two optimization approaches exist for any process optimization endeavor, namely computer-aided optimization. The first consists in a Single Objective Optimization (SOO), whereas the second consist in a Multiple Objective Optimization (MOO).

The main difference between these two approaches is the fact that only one objective function is to be optimized in the former, whereas two or more, usually conflicting, objective functions are optimized in the latter [16]. This difference leads to interesting some interesting results.

A direct result is the presence of a spectrum of optimal solutions, in our case process configurations, in the MOO case in opposition to just one ,or at most a handful, in the SOO case [16] This spectrum extensively illustrates the trade-offs between the various objective functions. This comes in opposition to a pure SOO which provides one optimal solution, that is usually but at an exception of the MOO spectrum [22].

An additional result relates to the quality of the investigated model. In fact, the multiplicity of objective functions in the MOO approach leads to a more realistic representation of the problem at hand, than in the SOO approach. This is due to the greater level of detail and precision that accompanies the evaluation of multiple objective functions.

A third result deals with decision making. The SOO approach witnesses a transfer of the decision making process from the decision maker to the modeler. This is realized by selecting one specific objective function. In opposition, the MOO approach keeps the responsibility of balancing between the various objective function in the hands of the decision maker, and this by virtue of the optimal trade-off curve [16].

On the other hand, the SOO approach presents key advantages: (1) a given SOO run converges to a given solution considerably faster than a complex MOO approach. (2) The SOO approach benefits from age long applictions and consolidated algorithms. (3) Specific formulations were developed in the case of SO approaches namely for heat exchange network design and synthesis of optimal separation sequences. A specific example is the choice of the optimal utility system in the heat integration methodology 0. As a result, even though SOO and MOO are essentially distinct, they can be complementary in a multitude of cases.

Considering this, a comparison of these two approaches with respect to key issues is provided in Table 1:3. As a result of this difference and complementarity, the approach utilized in a handful of literature work, namely [7, 8], consists in embedding the Heat Integration methodology, resolved by the SOO approach, within a global MOO resolution. This approach is discussed more in detail

in 1.3.6. Finally, the multi-objective approach has been thoroughly applied in literature. We cite below a few examples of this application:

- [7] optimized of the polygeneration of biogas, power and natural gas from softwood via gasification and methanation with regards to exergy efficiency and capital costs as objective functions
- [23] optimized of a combined cycle power production system, with regards to operating costs and capital costs as objective functions
- [20]optimized a generation IV nuclear power production system with regards to exergy loss and capital costs.

Table 1:3 Comparison between single objective and multiple objective optimization

Nature of optimization	Single Objective Optimization	Multiple-Objective Optimization
Chronological positioning	Traditional approach	More recent approach
Number of objective functions	One objective function (one indicator or a weighted average of indicators)	Multiple objective functions (usually at odds)
Nature of solution	One optimal (extreme) configuration – possibly the first 5-10 optimal solutions	A spectrum of optimal trade-off configurations
Positioning in decision making	Decision made by the modeler	Decision made by the decision maker
Additional benefits	Faster convergence – Consolidated formulations – Problem specific formulations	A wider range of considered alternatives – More realistic models
Application in literature	Heat Exchange Network Design – Synthesis of optimal distillation sequences	Complex energy systems (sugarcane processes, biomass processes) design of unit operations (heat exchanger, membrane separator)

1.3.4 The Pareto approach for Multi-objective Multivariate optimization

A typical multi-objective multivariate problem is defined by both a decision vector *x* and an objective function vector *f*. The *decision vector x* contains the various optimization variables ($x_k, k = 1, \dots, n$), as highlighted in Equation 1:40. This vector normally operates within a confined space X ($x \in X$), defined by the upper and lower bounds specified for the various optimization variables also as highlighted in Equation 1:40. On the other hand, the *objective function vector* f is made up of the several of objective functions (f_k, k=1… n, n≥2) as highlighted in Equation 1:41.

Equation 1:40 General expression for a decision vector in Multivariate optimization

$$x = \left(x_1, \dots, x_{n_{var}}\right) \in X = \left(\left[x_{1,min}; x_{1,max}\right], \dots, \left[x_{n_{var},min}; x_{n_{var},max}\right]\right)$$

Equation 1:41 General expression for the objective function vector [20]

$$f = \big(f_1(x), \dots, f_n(x)\big)$$

The set of feasible solutions, i.e. the list of points that are images of decision points $x \in X$, is denoted as F_x and is mathematically defined in Equation 1:42.

Equation 1:42 Mathematical expression for the set of feasible solutions

$$y \in F_x \; iff \; y = f(x) \;\; x \in X$$

On another note, each objective function f_k may be nonlinear, and even discontinuous with respect to some components of the decision vector. Moreover, the chosen objective functions are often at odds. As a result, this problem formulation does not have a unique solution in general. On the contrary, its solution is a set of *non-dominated* solutions termed *Pareto-optimal set* or *Pareto optimal front* [20]. Domination is described in Equation 1:43, for the case where all objectives are to be maximized. This formulation translates into: objective function vector $v \in F_x$ dominates objective function vector $u \in F_x$ if and only if each component of v is equal to or greater than each component of u, with at least one component strictly greater.

Equation 1:43 Expression of Pareto domination [20]

$$v = f(x_v) \succ u = f(x_u) \; iff : \; \forall i \in [1, \dots, n]: v_i \geq u_i \;\; \bigwedge \exists i \in [1, \dots, n] : \; v_i \; > u_i$$

To that definition we can add that of *Weak Pareto Domination* defined in Equation 1:44 which translate into: objective function vector $v \in F_x$ weakly dominates objective function vector $u \in F_x$ if and only if each component of v is equal to or greater than each component of u. We can easily that if v dominates u then v weakly dominates u, but not the other way around.

Equation 1:44 Expression of Weak Pareto domination

$$v = f(x_v) \succcurlyeq u = f(x_u) \; iff : \; \forall i \in [1, \dots, n]: v_i \geq u_i$$

On the opposite side, *mutual non-domination* occurs when v outranks u for at least one objective function whereas u outranks v for also at least one objective function. This notion is translated in Equation 1:45. v and u are hence *mutually non-dominating.*

Equation 1:45 Expression of Pareto non-domination

$$v = f(x_v) \approx u = f(x_u) iff : \; \exists i \in [1, \dots, n]: v_i > u_i \;\; \bigwedge \exists i \in [1, \dots, n] : \; v_i < u_i$$

The *Pareto Front* $P_f \subset F_x$ can be thus defined based on these formulations. A given point $v \in F_x$ belongs to this front, ($v \in P_f$), or in other terms is *Pareto optimal*, if and only if there is no feasible point $u \in F_x$ that dominates it. This is equivalent to saying that v either dominates (or weakly

dominates depending on the formulation) or is mutually non-dominating with any solution $u \in F_x$ both these definitions are highlighted in Equation 1:46.

Equation 1:46 Expression of Pareto optimality [20]

$$v \in P_f \; iff : \nexists u \in F_X / v \succ u \;\Leftrightarrow \forall u \in F_X, (v \succ u \; (or \; v \succcurlyeq u) \; \bigvee v \approx u)$$

From this definition, we conclude that the said Pareto front contains multiple solutions. Moreover, all these points are mutually non-dominating ($v \approx u$). This is why the Pareto set is defined as *non-dominated*. The notion of *Pareto efficiency* is a direct result of this mutual non-domination: it is impossible to optimize the value of a given objective function without deteriorating the value of at least one other function. As a result, the Pareto set represents a frontier for optimization: it is impossible to obtain a better value for a given objective having all other objectives constant. We speak hence of an *ultimate trade-off* between the objective functions.

Figure 1:4 provides an illustration for the previous statements. In this case, the two objective functions are to be minimized. Members of the Pareto set are indicated by blue points. Point (a) represents the optimum of OF_1 for a given value of OF_2. The opposite is true for point (b). Moreover, point (a) has a lower value for OF_1 than point (b), whereas pont (b) has a lower value for OF_2, stressing hence their mutual non-domination. Accordingly, we can see that desiring a better value for a given objective function (say for OF_2 choose point (d) over point (c)) comes at a worse value for the other function (point (c) performs better than point (d) for objective OF_1). Finally, as indicated on this figure, all points "beyond" the Pareto optimal frontier are impossible to obtain.

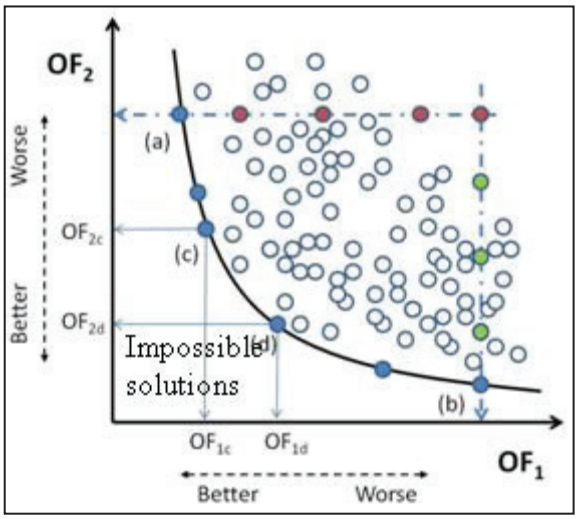

Figure 1:4 Illustration of Pareto Front in a Generic optimization problem [24]

1.3.5 Solving Multi-objective optimization Problems: Evolutionary Algorithms

In this section, we will provide a brief review of technologies employed for resolving multi-objective multivariate optimization problems. We will then concentrate on our chosen techniques with proven applications: Evolutionary Algorithms.

1.3.5.1 Brief description of Multi-Objective optimization algorithms

Multiple algorithms exist for the resolution of Multiple-Objective Optimization problems; with respect to the Pareto optimality concept highlighted previously. We mention, among others: the ε-constraint method, Population Simulated Annealing (PSA), Taboo Search (TS), Particle Swarm Optimization (PSO), Differential Evolution (DE) and Evolutionary Algorithms (EA). These methods share various common attributes:

- All these methods are heuristic, i.e. they require little knowledge of the problem to be optimized.
- All these methods are population based, i.e. multiple points are evaluated simultaneously at the opposite of just one.
- All these methods converge towards optimal solutions by virtue of an ordered knowledge of the search space.
- All these methods are probabilistic, in the sense that the generation of points depends on probabilistic tools.
- All these methods require a great computational time, albeit to a varying extent.
- All these methods present a time vs. quality compromise, i.e. more computation time necessary for a better solution

Seeing that all of these methods are comparable, and none of them is perfect, choosing a particular algorithm is a rather delicate matter, which depends to a great extent on the requirements of the particular design [20]. The analysis of literature pertaining to optimization of chemical processes shows that Evolutionary Algorithms were applied in 40% of the cases with other methods ranking far behind [20]. As an illustration, these methods were applied in the following works [7, 15, 20, 21, 23]

For these reasons, we chose this class of algorithms as the optimization tool for our work.

1.3.5.2 QMOO: an EA dedicated to process optimization

Evolutionary Algorithms (EA) are a specific set of heuristic algorithms widely used for the multi-objective optimization of engineering problems in general and chemical processes in particular. In this context, QMOO (Queuing Multi-Objective Optimization) is an Evolutionary Algorithm developed at Ecole Polytechnique Fédérale de Lausanne by the research team of Daniel Favrat and François Maréchal [25] and dedicated for optimization of chemical processes and energy systems.

Within a generic EA , a *population* of *individuals evolves* toward an *approximation* of the desired Pareto set by means of *operations* which *evaluate* and *rank* the said individuals, remove bad individuals and *create* new better ones [25]. Within this context, QMOO adds the following characteristics: *steady-state, queuing, elitism and parallelism.* We provide in this section a concise description of this algorithm, and this by highlighting the various terms of the previous description.

As the name suggests, a *population* is a collection of individuals as highlighted in Equation 1:47. The constitution of this population is time dependent and this because its constitutive individuals

($I_1, \dots, I_{N_{POP}}$) are prone to change in the course of the evaluation. An additional trait to QMOO is that the population's size can vary, albeit in a constrained manner, and this to guarantee a decent approximation of the desired Pareto set. However, in all cases, by virtue of these algorithms, this population will ultimately converge towards an *approximation* of the desired Pareto set.

Equation 1:47 Definition of a population in QMOO [25]

$$P(t) = \{I_1(t), \dots, I_{N_{POP}(t)}(t)\}$$

An *individual I* is conventionally defined by a specific value for the decision vector x_I, belonging to the predefined search space X, to which is associated a specific value for the objective function vector $f(x_I)$.Within the QMOO algorithm, [25] includes additional attributes for a given individual: (1) its state s_I which determines the impending fate of an individual: evaluation, ranking or removal and (2) its ranking r_I which determines its positioning within the actual population. s_I and $r_I$vary in the course of the evaluation whereas x_I and $f(x_I)$ remain constant. Moreover, an individual is no longer considered part of the population once it is removed. Finally, a mathematical definition for the said *individual* is provided in Equation 1:48.

Equation 1:48 Definition of an individual in QMOO [25]

$$I = \{x_I, f(x_I), s_I, r_I\}$$

Evolution suggests an iterative and progressive procedure which, mimicking nature, takes the most promising individuals as originators of new test individuals. In this sense, evolutionary algorithms make use of probabilistic tools and black-box approaches. In this sense, only the inputs and the outputs of the model are taken into account at the expense of its constitutive equations. This is opposite to the conventional analytical methods [25] where the model's derivatives are sought. The main advantage of evolution is the overcoming of common pitfalls of such formulations, namely concerning models where derivative is not straight forward or even impossible. This is exactly the case for chemical processes, whence the extended application of evolutionary algorithms.

The desired Pareto set, otherwise termed Pareto Optimal Frontier (POF), is only *approximated* through this procedure. This is because the working population has but a finite number of individuals [25]. Moreover, this approximation is largely dependent on the elapsed optimization time. The quality of this approximation increases with the elapsed time, albeit to a certain extent. In all cases, the top-ranked individuals of a given population, otherwise termed as the *Non-Dominated Set*, always provide the best current approximation.

Operations within an EA normally occur on the individuals of a population and are hence related to its ranking and state. Those operations are defined in [25] and are briefly described in Table 1:4. This listing provides, in the case of QMOO, the various phases of the "life" of an individual and this in chronological order. Whereas the "creation" operation is rather trivial, the simulation operation was detailed in previous sections. The operations of assignment, ranking and removal will hence

be dealt with in more detail. Moreover, all operations depend on the entire population at hand, except evaluation which depends only on the individual. As a result, an important step at this level is the choice of a working number of individuals. The population will be ranked, individuals removed, and new ones created and assigned values only once that number of individuals is evaluated.

1.3.5.3 Detailed description of the operations in QMOO

In this section, we will provide more detail concerning the operations highlighted in Table 1:4.

Table 1:4 Key operations in Evolutionary Algorithm for Multi-Objective Optimization (EA-MOO)

Creation		
New individuals are created	Allocation of memory space	Default values given to decision vector
Assignment		
Values given to decision vector	if initialization, values randomly chosen	Else, deduced from population via specific operators
Evaluation		
Process simulation	Heat integration	Evaluation of objective functions
Ranking		
Individual is ranked	Pareto optimality and diversity	Participates in the generation of new individuals
Removal		
Removal from population	If individual is lacking	low ranking, duplicate

1.3.5.3.1 Ranking

Ranking on the other hand is key in determining the *position* (or rank) of an individual within the current population. The Pareto optimality criterion described in 1.3.4 constitutes the core of this

ranking method, as described in [25] and illustrated in Figure 1:5. Its working principle is based on the Goldberg ranking method highlighted below:

- "The NDS of the entire population is found, given the top rank 1, and temporarily removed from the population"
- "The NDS of the remaining population is found, given rank 2, and temporarily removed from the population"
- "The process continues until the entire population is ranked"

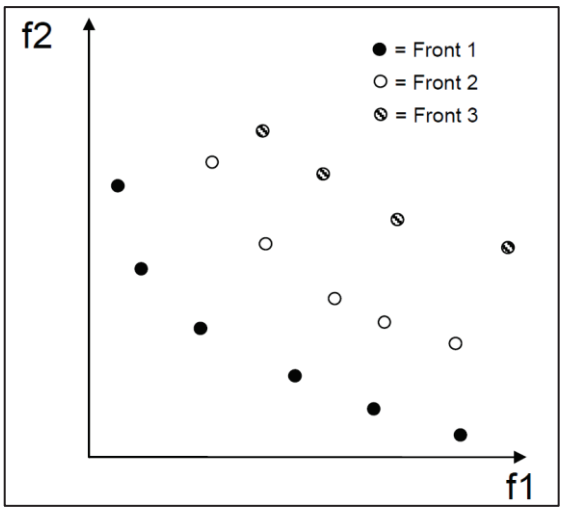

Figure 1:5 Formation of ranks (or fronts) within the current population [26]

We can see in Figure 1:5 the first three fronts of a generic population, wherein Front 1 dominates Front 2, which dominates Front 3. It is interesting to note that the Pareto weak optimality criterion can also be used for population ranking. In this case, rank 2 are not necessarily dominated by all rank 1 points. They might be only weakly dominated by these points.

Other criteria that determine the ranking of individuals within a population are diversity and tail preservation. Diversity, both in the search space X and image space F(X), guarantees: (1) the spread of the population in the search space, and ultimately (2) the approximation of the POF over a larger space, for a better presentation of the various trade-offs [25]. Tail preservation on the other hand ensures that, in later evaluations, extreme points of the working population retain a high ranking.

1.3.5.3.2 Removal

Removal of 'lacking' individuals is important for three reasons: (1) avoid an explosion of the population size, (2) guarantee the generation of new individuals from good-ranking ones, (3) eliminate redundancies or close individuals. Whereas the first point is key for computational practicality, the second is important to guarantee convergence towards the POF in a reasonable time frame, and the third is important to promote diversity. In this context, thinning is employed at later phases of the optimization, where the maximum rank approaches 1, in order to enlarge

the scope of the final NDS [25]. Finally, a given point may ultimately not be removed, if it keeps its high ranking status.

1.3.5.3.3 Additional characteristics of QMOO

We now consider more in detail the special characteristics of QMOO. QMOO is a steady-state algorithm, in opposition to a generational one. Within the first class, only a few individuals are replaced at a given time, whereas the entire population is removed at each time lapse in the latter. The *queuing* mechanism on the other hand is related to the state s_I of a given individual. A newly created individual is *queued* for assignment. An assigned individual is queued for evaluation, and so on. QMOO is elitist in the sense that its single population contains only the best individuals found so far. This is due both to its steady-state nature and to its removal strategy. Finally, QMOO can be *parallelized* namely concerning the evaluation scheme, which helps to reduce the desired computation time.

The QMOO algorithm has been widely used in literature and this for a variety of cases, [7, 21, 27]. For this reason, it was chosen as the algorithm for our work.

1.3.5.4 Pareto filters

A *Pareto Filter* is an algorithm that extracts the Non-Dominated Set out of a given set of points in the objective space. In other terms, the Pareto filter *filters* out dominated points from a given set of points. This tool is of great importance in generational algorithms. This is because select old individuals are removed at the end of an iteration, making way for new individuals. The said filter extracts high ranking individuals from the old population, before its removal, and this in order to preserve them in a separate set. This separate set provides the ultimate approximation of the Pareto Optimal Frontier.

This use is however not possible in the case of steady-state algorithms like QMOO. This is because the algorithm utilizes just one population that contains all the *current* top ranking individuals.

On the other hand, the use of Pareto Filters may intervene in later stages of the QMOO optimization run. This is realized in order to speed up the generation of the NDS approximation to the Pareto frontier. Local optimization techniques may also be applied to generate non-dominated points from certain high-ranked dominating points.

1.3.6 Heat exchanger Network Synthesis: example of single objective optimization embedded into MOO

The synthesis of an optimal heat exchanger network is a prime example of a single-objective optimization problem embedded into a more global multi-objective optimization context. This was adopted in the works of [7, 8, 21, 27, 28] among others. Its goal is to find the heat exchange configuration or an approximation thereof which optimizes a chosen objective function. This task is performed within the evaluation sub-step as highlighted in Table 1:4. We will briefly discuss hereafter the methodology normally adopted for this task.

The methodology adopted in these works, and in this thesis, is based on the following precepts:

Calculate the *minimum energy requirements* (MER) via the *temperature interval* (TI) method [29].This method has the advantage of operating on thermodynamic rather than combinatorial bases. It has thus a significantly reduced computational time, and provides key information concerning the process minimum energy requirements (MER). This MER, both hot and cold, highlights the bounds for the process's external energy needs.

Mixed Integer Linear Programming (MILP) optimization methodology which seeks the optimal utility system for a given configuration, with regards to a chosen optimization function [30, 31]. This function can be the maximization of process power cogeneration, the minimization of operating costs or the minimization of exergy consumption.

Approximation for the HEN cost by virtue of the *enthalpy-interval* (HI) method [32]. This method provides an adequate approximation of the cost of the heat exchange network and this in a reasonable time frame.

Considering this, a breakdown of the employed methodology is provided in Figure 1:6.

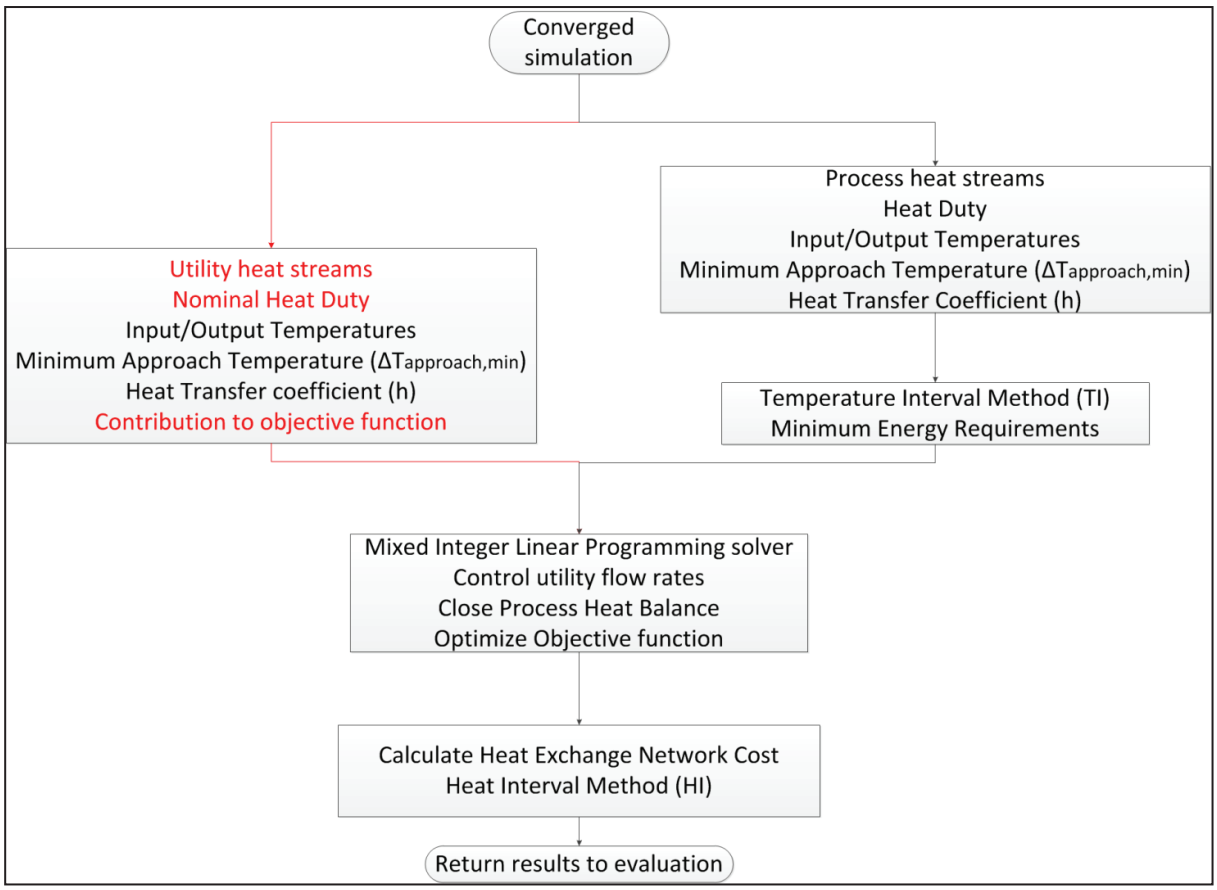

Figure 1:6 Breakdown of employed methodology for synthesis of optimal heat exchange network

Heat streams are extracted from a converged process simulation. They are then classified into process and utility heat stream with the former having a constant heat duty and the latter having a

varying duty, by virtue of controlled utility mass flow rates. Both stream types are nonetheless characterized by constant input/output temperatures, constant minimum approach temperatures ($\Delta T_{approach,min}$ and constant heat transfer coefficients (h). Moreover, whereas the input/output temperatures are provided from simulation results, the minimum approach temperatures and heat transfer coefficients are design choices. These choices concern the employed heat exchange technologies as well as the streams in question. Heat exchange technologies include shell and tube exchangers, Robert type evaporators, among others. Types of streams with varying heat transfer coefficient are: steam, air and flue gases and aqueous liquids. Finally, we note that the approach temperature is added to the temperatures of a heat stream in need of heating and subtracted from the temperatures of a heat stream in need of cooling.

The minimum approach temperature has a direct impact on the process minimum energy requirements. In this aspect, a smaller approach temperature offers greater potential for heat transfer than a greater approach temperature. This is because greater temperatures inhibit heat exchange between streams with operating temperatures closer than their given values. Moreover, this temperature has an impact on heat exchanger cost considering that a smaller temperature difference leads to a greater heat exchange area, and hence to greater costs.

It should however be noted that a smaller minimum approach temperature is a better design choice since it gives the possibility of adopting higher approach temperatures, to the contrary of a greater minimum approach temperature which forbids the use of smaller approach temperatures.

The heat transfer coefficient does not impact the process minimum energy requirements, namely because the Temperature Interval method for calculating these requirements reflect only the quality of the heat exchange and not its cost. Nonetheless, these coefficients are used for the calculation of the heat exchange network cost by virtue of the Heat Interval Method. In this context, a greater heat transfer coefficient leads to a smaller heat exchange area, and hence to greater costs.

The contribution of the utility stream to the objective function is expressed in nominal terms like($\frac{\$}{\frac{kg}{h}}$) in the case of operating costs objective function or $\frac{kWh}{kg}$ in the case of exergy consumption or electricity cogeneration objective function. It is hence a discriminatory criterion namely for choosing between utility systems. This parameter, combined with process minimum energy requirements help determine the utility flow rates by virtue of maximizing the objective function and closing the process heat balance.

Finally, this step returns information to the evaluation step namely concerning utility flow rates, values for the objective function and heat exchanger network area. These steps enter directly in the calculation of the process performance indicators and objective functions.

1.4 Process selection: MCDM techniques

"What are you exactly going to do after you've done all this assessing and formulating?"
The Bland Encounter

The presence of multiple solutions to multi-objective optimization problems, albeit interesting for thorough process analysis, presents an important setback for the designer. In fact, whereas single-objective optimization yields but one solution, its multi-objective counterpart yields a multitude of solutions, from which the designer would like to choose but a few, or even one. For this sake, multiple techniques were developed and applied in literature, and are detailed in this section.

Multiple Criteria Decision Methods (MCDM) are techniques which select Pareto optimal solutions with respect to the values of their objective functions, and to preferences issued by the *designer* or the *expert*. At this level, the notions of criteria and objective functions can be merged. Two types of MCDM methods exist: compensatory and non-compensatory. The latter do not permit trade-offs between objective functions, but rather require that each function stands on its own. To the contrary, compensatory methods allow for trade-offs between alternatives.

Seeing that a trade-off analysis is key for process design, we will only discuss the compensatory methods in our current work. Such methods can be broken down into the following families [33].

1.4.1 Analysis and visualization of Pareto frontier

Analysis of the Pareto frontier enables the designer to access wealthy knowledge about his chemical process. This analysis can be realized both on the objective functions and the design variables.

A first distinction is to be made on the nature of the Pareto fronts.

Another important point is the analysis of *extremums.* These points have the particularity of offering the best achievable value for a given objective function, with relatively bad values for other objective functions. In this sense, they offer little to no trade-off between the various objectives. As a result, they might be avoided if objectives are of equal importance.

To this we can add the analysis and determination of *knee* points. A knee point is characterized by a steep deterioration in one objective for a slight improvement of another. As a result, knee points are nearly always a most preferred solution.

Another important point is the analysis of discontinuities within the obtained curve, which are very common for such curves. These discontinuities occur namely in the case of constraints, in the case of the use of integer variables and in the case of the implementation of embedded single-objective optimizations.

Clustering is a common technique used for the analysis of Pareto curves. Therein, similar Pareto-optimal solutions are grouped within *clusters.* This similarity can either pertain to the objective

functions or the optimization variables. This clustering yields patterns for the process, which will help the designer in understanding the process's behavior and in ultimately selecting a solution.

All of these attributes render the analysis and visualization of the Pareto Frontier indispensable for correct decision making.

1.4.2 Scoring methods: HAP

Scoring methods select or evaluate an alternative according to its score. The calculation of this score is dependent both on the performance of a given alternative and on the decision maker's preferences. Values of objective functions are transformed into a common preference scale so that comparisons between different attributes are made possible. The Analytical Hierarchy Approach (*HAP*) is a popular variant of these methods. This method derives the weighs of objective functions and ultimately the scores of the various alternatives via pair wise comparisons between criteria and alternatives. This comparison is realized by a survey presented to an *expert*. Moreover, heuristics are often applied to avoid extensive comparisons.

1.4.3 Compromising methods: TOPSIS

Compromising methods selects an alternative that is closest to a hypothetical ideal solution and farthest from a hypothetical nadir solution. Ideal and nadir solutions mimic in this sense the concept of ultimate profit and ultimate risk. TOPSIS (Technique for Order of Preference by Similarity to Ideal Solution) [34] is a popular variant. (1) First weights are assigned to each objective function. (2) Then, a weighted normalized decision matrix $M_{i,j}$ is constructed (i refers to the considered alternative, and j to the objective function in question). (3) Later, the positive and negative ideal solutions are determined (the positive ideal solution has the best values for all objectives, whereas the nadir has the worst values for all objectives). (4) The distance of each alternative I to the positive ideal and the nadir points are then calculated. (5) Finally, the point with the smaller relative closeness to the ideal solution is selected.

1.4.4 Outranking methods: ELECTRE, PROMETHEE, GAIA

Outranking methods build a preference relation, otherwise termed as *outranking relation*, among alternatives evaluated on several objectives. This relation is defined as follows : x outranks y if given the preferences of the decision-maker, and the various alternatives and the nature of the problem, there are enough arguments to declare that alternative x is at least as good as y, with no essential reason to refute that statement [35]. We speak of concordance and non-discordance, and mimics in this sense certain voting mechanisms [35]. This method has however a strong non-compensatory dimension. It has been largely developed in the French school. ELECTRE, PROMETHEE and GAIA are prominent examples.

1.4.5 Multi-Attribute Utility Functions: SMART

Multi-Attribute Utility Functions strongly resembles the weighting approaches briefly mentioned in 1.3.2. Such methods take into consideration the decision maker's preferences in the form of

utility functions defined over a set of objective functions. SMART (Simple Multi-Attribute Rating Technique) is the simplest form of such algorithms. One utility function is chosen defined as the weighted algebraic mean of the associated objective functions. Other methods proposed the use of generalized mean functions , whereas further methods proposed a multiplication of the weighted geometric mean [36]. Moreover, actual real world utility functions (such as net present value, environmental impact, break-even costs or others) can also be applied by the use of such methods. These methods can be extended to using multiple utility functions, treading the way to another compromise situation. These techniques are amongst the earliest developed and the most widely used tools, namely in the field of operations research.

1.4.6 Application to optimal process selection

Cited MCDM techniques differ from the analysis and visualization of the Pareto Curve by the use of quantitative rather than qualitative choice methods. These methods include appraisal and ranking of the obtained solutions. Applications of MCDM techniques to process design have been rather scarce in literature. We record below research works related to each proposed family of techniques.

[15] makes use of TOPSIS and a variation thereof to select the optimal points in a series of bi- and tri-objective optimization runs for two different hypothetical chemical processes. Albeit this selection was realized for illustrative purposes, it highlighted the importance of both multi-objective optimization and multiple-criteria decision making.

[37] on the other hand utilizes the HAP approach for a VOC (toluene ethyl acetate) recovery/recycle process. Two criteria were assessed: one economic (the NPV) and one environmental (the composite process index). This work did not make use of multi-objective optimization, but rather employed a brute-force approach where a multitude of points was evaluated. Two cases were considered: (1) search for the optimal combination of two process operating parameters and (2) search for the optimal value of the minimum heat exchange temperature.

[38] utilizes the ELECTRE approach coupled with multi-objective process optimization for a specialty extrusion process. Three objectives and two optimization variables were considered. Moreover, the ELECTRE approach was put to application via a dedicated program. A tri-dimensional Pareto set was obtained, and best and worst alternatives were deduced.

Finally, [7] utilize a utility function to determine the optimal biomass gasification and methanation process. This function was the *break-even biomass* cost for a specified plant capacity and under different pre-defined economic conditions. This decision was made after multi-objective optimization runs were performed. This work resulted in the proposal of optimal configurations (choice of technologies and operating conditions) for the said process. This work also highlights the importance of chosen economic conditions on the obtained optimal solutions.

On the other hand, [18] identifies yet another utility function characterizing the optimal performance of coal fired power plants: the ratio of exergy loss to capital costs. This ratio merges two conflicting objectives loss efficiency (and subsequently efficiency) and capital cost.

The use of quantifiable and measurable real world utility functions makes the *Multi-Attribute Utility Functions* approach far more interesting than its computational counterparts. For this reason, it will be both detailed and applied in the course of our work, in tandem with analysis techniques.

The said utility functions will be chosen from amongst the financial appraisal indicators. A trade-off between these various indicators can be sought as a result. Moreover, multiple economic scenarios can also be considered.

1.5 Conclusions and presentation of the methodology

From the previous sections we can conclude the following concerning the design of chemical processes:

- Chemical process design is an iterative procedure which takes into account both the technological and economical contexts, and depends on the contribution of various fields. It benefits from a variety of tools in the form of heuristics and computer programs. It ultimately results in a process *superstructure*, modeled in process simulation tools, encompassing a process *topology* as well as a set of *operating conditions* and *equipment*. A *configuration* within this structure is defined by a choice of topology, operating conditions and equipment. It is defined, simulated and converged by virtue of process simulators. Moreover, for each configuration there exists but one heat exchange network design minimizing its external energy requirement.
- Adequate process evaluation is important seeing the iterative nature of chemical process design. This is facilitated by the use of economic, financial, chemical and environmental indicators. We distinguish between basic evaluation indicators, and selection indicators.
- Our evaluation indicators are exergy efficiency and capital costs
- Our selection indicators are: Net Present Value, Pay Back Time, Internal Rate of Return and Break-Even Cost.
- Process optimization is crucial in order to bring out the most promising process configurations. This optimization can be performed either manually or via computer algorithms.
- Manual optimization is based on an analysis of the process at hand. It plays a great role in identifying important process operations and influential process indicators. However, it falls short when faced with the complexity of chemical processes.
- Two types of computerized optimizations exist: single-objective and multi-objective. It was demonstrated that multiple-objective optimizations were preferred to their single-objective counterparts. This is because the former offer a greater understanding of (1) process performance, (2) the trade-offs between evaluation indicators and a better provision for informed decision making. However, because of their consolidated application, single objective

approaches may be integrated into multiple-objective ones. Finally, Evolutionary algorithms are an excellent tool for performing multiple-objective optimizations.

- The Pareto frontier is the result of multiple-objective optimizations. It contains multiple solutions representing the ultimate compromise between the various objective functions.
- Exergy efficiency and capital costs are common objective functions for the multi-objective optimization case.
- The modified operating conditions are usually termed as optimization variables.
- Process selection is the ultimate objective of this endeavor. It is the direct aftermath of process evaluation and optimization. Going from the process Pareto Curve, the designer disposes of a variety of techniques for adequate decision making. We retain two of those techniques:
- Analysis of the Pareto curve consists of visualizing both the optimization variables and the objective functions, identifying regions of interest and discontinuities. This is an inevitable step for informed process selection.
- Multi-Attribute Utility Functions are a specific case of multi-criteria decision techniques where solutions are ranked based on their values for one or more utility functions. These functions are defined over a set of objective functions. In the case of process design, selection indicators are chosen to be such functions.

Going from this enumeration, we were able to construct a structured methodology for optimal process design, highlighted and broken down in Figure 1:7. This methodology will be thoroughly developed and applied in the course of this thesis and this for a study problem: conversion of sugarcane and sugarcane bagasse to energy products through biochemical means.

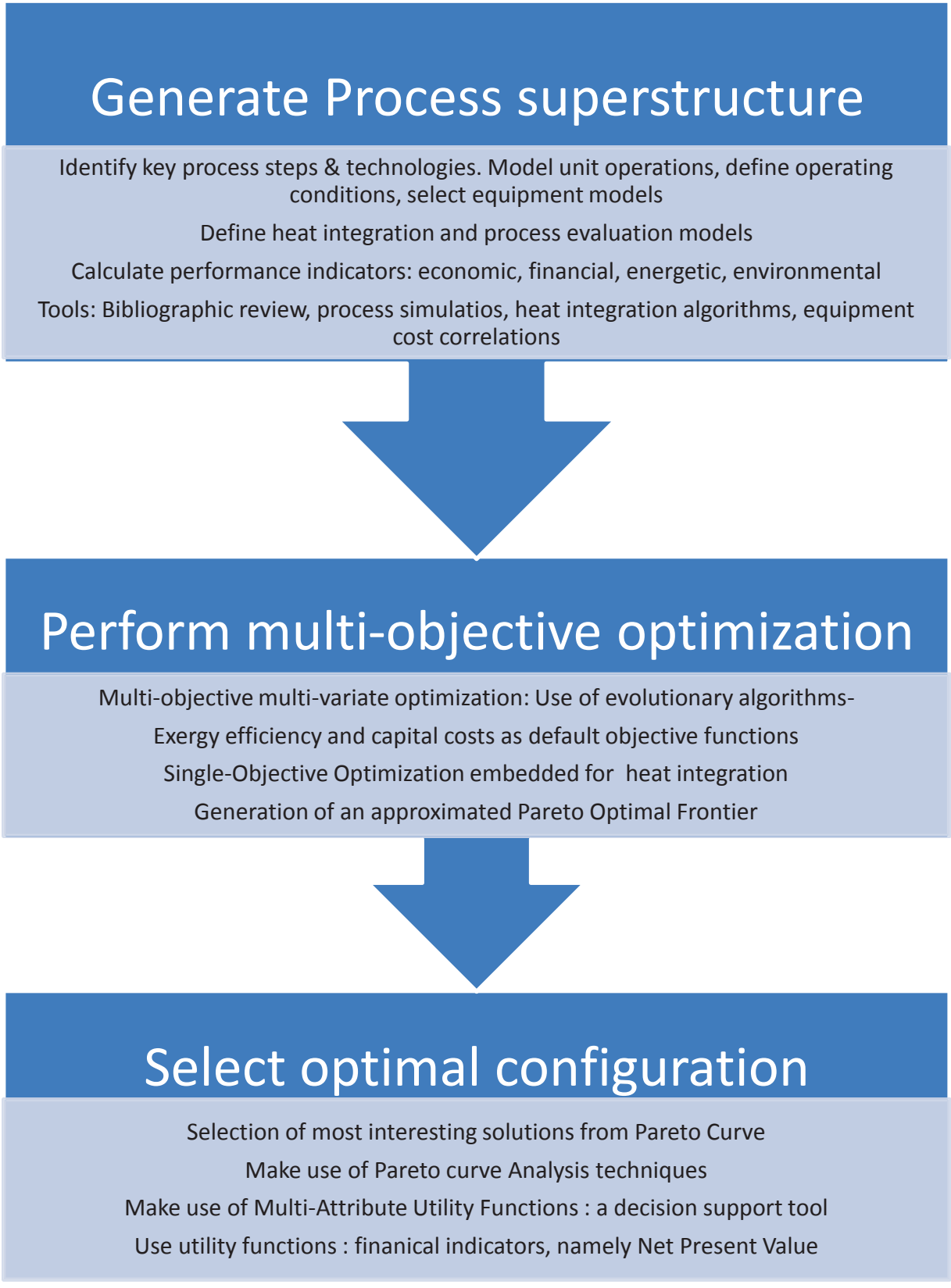

Figure 1:7 Break-down of methodology for the synthesis of optimal processes

Chapter 2 Case study I: combined ethanol from sugarcane distillery and power cogeneration plant

Sugarcane is the world's largest crop by production quantity, with Brazil as the main producer followed by India and China. It was historically used for the production of white sugar, along with alcoholic beverages, in sugarcane mills. However, in the modern context of energy diversification, it has seen increased use for the production of bio-energy, namely bio-ethanol and bio-electricity, especially in Brazil, and this thanks to the following attributes:

- Its great yield (2 times greater than corn, its US counterpart).Yield is defined as the liters of ethanol per hectare of land.
- Its great energy balance (7 times greater than that of corn). This balance is defined as the ratio of the energy contained in a given volume of ethanol divided by the fossil energy required for its production
- Its high energy content, namely its by-products bagasse and leaves, responsible for its great energy balance,
- Government policies favorable for the introduction of ethanol in the car fleet.

As a result, sugarcane is today the first source of renewable energy in Brazil, providing 15.4% of the country's energy demand, second to petroleum with 39.2% (UNICA). In addition, the "Brazilian experience" has become a reference for bioenergy and biofuels and this for all levels: harvesting, processing and policy making. More specifically, processing plants provide engineers today with a prototype for future biorefineries, where multiple products are extracted from bioresources in the image of oil refineries. In addition, this success went hand in hand with technological developments also at all levels, ever enhancing the industry's efficiency. This development led to consolidated and optimal process design and operation. Finally, attempts for continuous development led to a wealth of literary work related to these processes, increasing hence both their potential and related scientific knowledge.

In this context, bioethanol has long been established as the world's top biofuel. Moreover, its production has more than quintupled in the last 20 years, with more than 85% of the world's production concentrated in the United States and Brazil. However, whereas the US produces a larger quantity, ethanol has a greater share in the Brazilian national fuel market. Moreover,

Brazilian ethanol profits from greater performance parameters than its American counterpart, and this thanks to its source crop: Sugarcane.

Bioelectricity produced in sugarcane mills is however a rather novel practice, which replaced the burning of bagasse for heating purposes only. Its inclusion was the result of power decentralization practices and the desire for greater profitability. With this in mind, the current production level in Brazil is around 16 TWh of power from bagasse.

Thus, thanks to its solid foundation, and to the extent of its investigation in literature, the *ethanol and power production from sugarcane* process was chosen as the study case for the application of our methodology, previously specified in Chapter 1.

More specifically, this chapter will deal with the first part of this methodology: the construction of the process superstructure. We will first present and discuss the conventional process before including proposed modifications. We will then describe in more detail the various building blocks of the superstructure.

2.1 Composition and flow rate of input materials: sugarcane and leaves

The conventional production process has two key input materials: sugarcane and leaves. Whereas the first is the main harvest product, the second is collected once the harvest is over as valuable waste. Sugarcane received in the factory, contains water, sugars, fibers otherwise termed as bagasse, dirt along with other impurities. Within the studied process, only sugars are converted to ethanol. Water is seen as the main “impurity” to be removed, along with other minor components such as dirt and impurities. Bagasse is conventionally diverted for heat and power production as previously stated. Modern large scale production units run with a sugarcane input of 500 t/h. As a result, this will be our chosen input capacity.

Sugarcane leaves enter the process at the rate of 70 kg/t-SC, which translates into a flow rate of 35 t/h for our chosen capacity. It contains namely water, ash, and biomass. Its humidity content is at 15% [39] whereas the mass content of ash is equal to 2%.

Moreover, the various components were modeled using the NREL (National Renweable Energy Laboratory) model detailed in [40]. Also, the related process, along with its constitutive streams and operations was modeled using the Aspen Plus V7.2™ process simulator, and the built-in UNIQ-RK (UNIQUAC-REDLICH-KWONG) thermodynamic method.

Table 2:1 Flow rate and composition of inputs to processing plant [39]

Sugarcane Input Flow rate	500 t/h	Component	Content in sugarcane (wt.%)
Trash input flow rate	35 t/h	Water	71.57
Component	Content in trash (wt. %)	Sugars	13.92
Water	15%	Bagasse	11.92
Ash	2%	Dirt	0.6
Biomass	83%	Impurities	1.99

2.2 Overall scheme of sugarcane to ethanol and power process

Considering the composition of input materials and the fate of their respective components, we can now draw a global scheme for our conventional process. This scheme can be seen in Figure 2:1. In this figure, input materials, sugarcane, and leaves are highlighted in green; output materials, ethanol and power, in red; waste products, water and impurities, in grey, and intermediary streams, bagasse, heat, steam and power in purple. We also distinguish between blue contoured and green contoured process sections. The first pertain to core process steps, whereas the latter pertain to process utilities. All these sections are detailed in the paragraphs below.

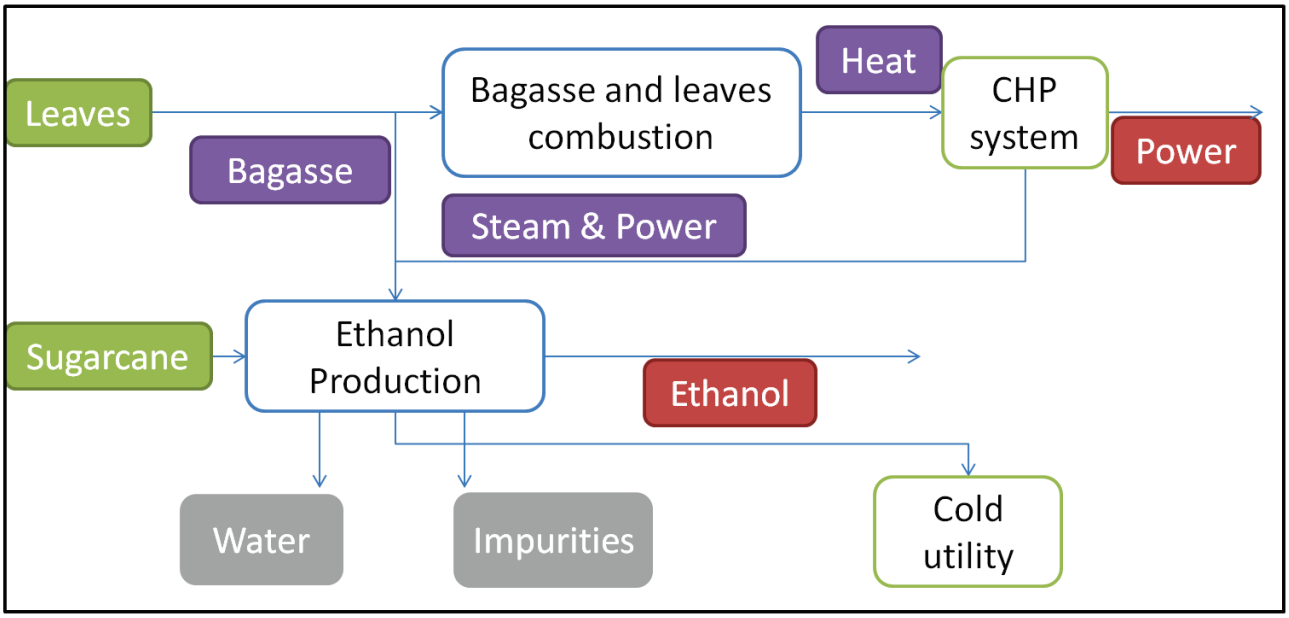

Figure 2:1 Overall scheme of sugarcane to ethanol and power process

2.3 Scheme for ethanol distillery

The ethanol production section is comprised of the following steps: (1) sugarcane cleaning, juice treatment and sugar extraction (3) juice concentration and sterilization, (4) fermentation, (5) distillation and (6) dehydration [41] Its *block flow diagram*, with key input, product, intermediate and waste streams, is specified in Figure 2:2. As we can see, two conversions take place:$sucrose \rightarrow glucose \rightarrow ethanol$. Moroever, water is the most abundant in this process, and

its elimination is necessary for the production of anhydrous ethanol. Finally, we provide below details concerning these various steps

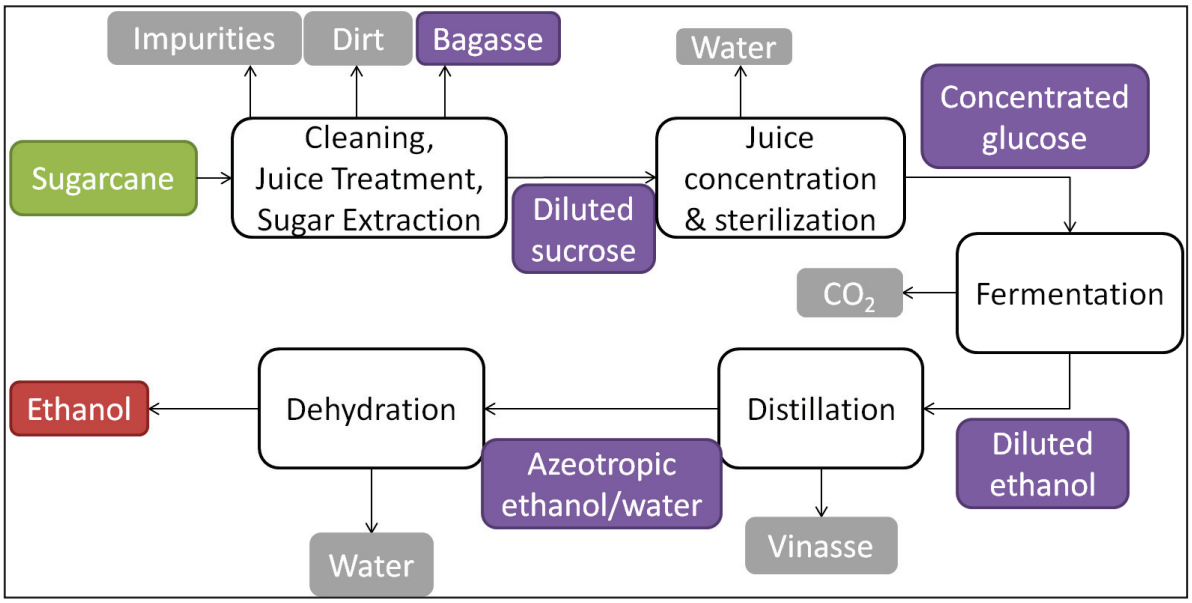

Figure 2:2 Block Flow Diagram for ethanol production section

2.3.1 Cleaning, treatment and extraction

Sugarcane cleaning is needed in order to remove dirt dragged along with the sugarcane from the fields. Dry cleaning, the industry norm, is chosen as the cleaning technology for our process. On the other hand, sugar extraction on the other hand is performed in mills through a process termed imbibition where water is injected to enhance sugar recovery. As a result of this step, the bagasse fraction is separated from the remaining juice. Moreover, juice treatment, both physical and chemical, removes remaining impurities in order to enable the use of sugarcane juice as a raw material for ethanol production. Finally, key design parameters specific for this section are provided in Table 2:2

Table 2:2 Design parameters for cleaning, treatment and extraction section [41]

Design Parameter	Default Value
Dirt removal efficiency	70%
Sugarcane recovery in cleaning	99.5%
Extraction water flow/sugarcane flow	28%
Sugar extraction efficiency	97%
Bagasse humidity	50%
Recovery of sugars in treatment step	99.7%

2.3.2 Juice concentration, sterilization and hydrolysis

The obtained clarified juice is too diluted to be introduced to the fermentation step. As a result, it needs to be concentrated.Concentration is realized by splitting the juice stream into two fractions: one sent to concentration whilst the other remains intact. Afterwards, the two streams are mixed and sent for sterilization [41] A material balance around the concentration section yields the split fraction ($\mathrm{spl_{syr}}$), based on the sugar content of the concentrated stream ($\mathrm{x_{sg,conc}}$), the desired sugar content in the final mixture ($\mathrm{x_{sg,f}}$), and the initial sugar content ($\mathrm{x_{sg,in}}$), as indicated in Equation 2:1. Moreover, following a similar mass balance, the mass flow rate of water evaporated in the concentration operation ($M_{wat,vap}$) can be calculated based on total input mass flow rate ($\mathrm{M_{tot,in}}$) and input and output sugar contents ($x_{sg,f}$, $\mathrm{x_{sg,in}}$), as in Equation 2:2.

Equation 2:1 Expression for the sugar content of the concentrated juice stream

$$spl_{syr} = \frac{x_{sg,conc} \times (x_{sg,in} - x_{sg,f})}{x_{sg,f} \times (x_{sg,in} - x_{sg,conc})}$$

Equation 2:2 Expression for the mass flow rate of water removed in concentration section

$$M_{wat,rem} = M_{tot,in} \times (1 - \frac{x_{sg,in}}{x_{sg,f}})$$

The juice concentration step occurs, in most industrial applications, by employing multiple-effect evaporators. The associated concept is simple and its application extensive: instead of evaporating the needed quantity of water ($M_{wat,vap}$) in one given evaporator, this evaporation is spread along multiple units ($N_{evap,units}$) working with a pressure gradient. As a result, evaporation occurs at temperatures with specific decrements ($\Delta T_{ev,i}, i = 1 \dots N_{evap,units}$) within the multiple-effect evaporator. Thus, condensing part or the entire vapor produced in one level can provide heat for vaporizing water in the next level. Other important variables in multi-effect evaporation relate to the quantity of water evaporated at each effect ($M_{vap,i}$). This quantity is calculated as a fraction ($r_{ev,i}$) of the total quantity of removed water ($M_{wat,vap}$), as in Equation 2:3. Finally, the sum of the quantities of water leaving each effect needs to equal the total amount of evaporated. This translates into the relationship for ($r_{ev,i}$) expressed in Equation 2:4. The simplicity and linear aspect of this expression are the reasons why evaporation fractions ($r_{ev,i}$) have been chosen instead of more conventional output concentrations ($C_{ev,i}$).

Equation 2:3 Quantity of water evaporated a given effect as a function of total evaporated water

$$M_{vap,i} = r_{ev,i} \times M_{wat,vap}$$

Equation 2:4 Governing relationship for evaporation fractions

$$\sum_{i=1}^{N_{evap,units}} M_{vap,i} = M_{wat,vap} \Rightarrow \sum_{i=1}^{N_{evap,units}} r_{ev,i} = 1$$

Figure 2:3 shows the *Process Flow Diagram* for the juice concentration section, with the main operations, streams (mass, heat and power), design parameters highlighted (16) and controlled parameters. As a result, specifications on evaporation temperatures are met by controlling valve pressures, whereas those concerning evaporation rates are met by controlling the vapor content in the evaporators. We can also see in this figure the use of six evaporator units. This figure also highlights the employed thermodynamic method UNIQ-RK as highlighted in [41]. This figure finally provides a list of related research works: (Ensinas et al. 2007) [42], (Dias et al. 2009) [41], (Higa et al. 2009) [43], (Morandin et al. 2010) [28] and (Palacios-Bereche et al. 2015) [44].

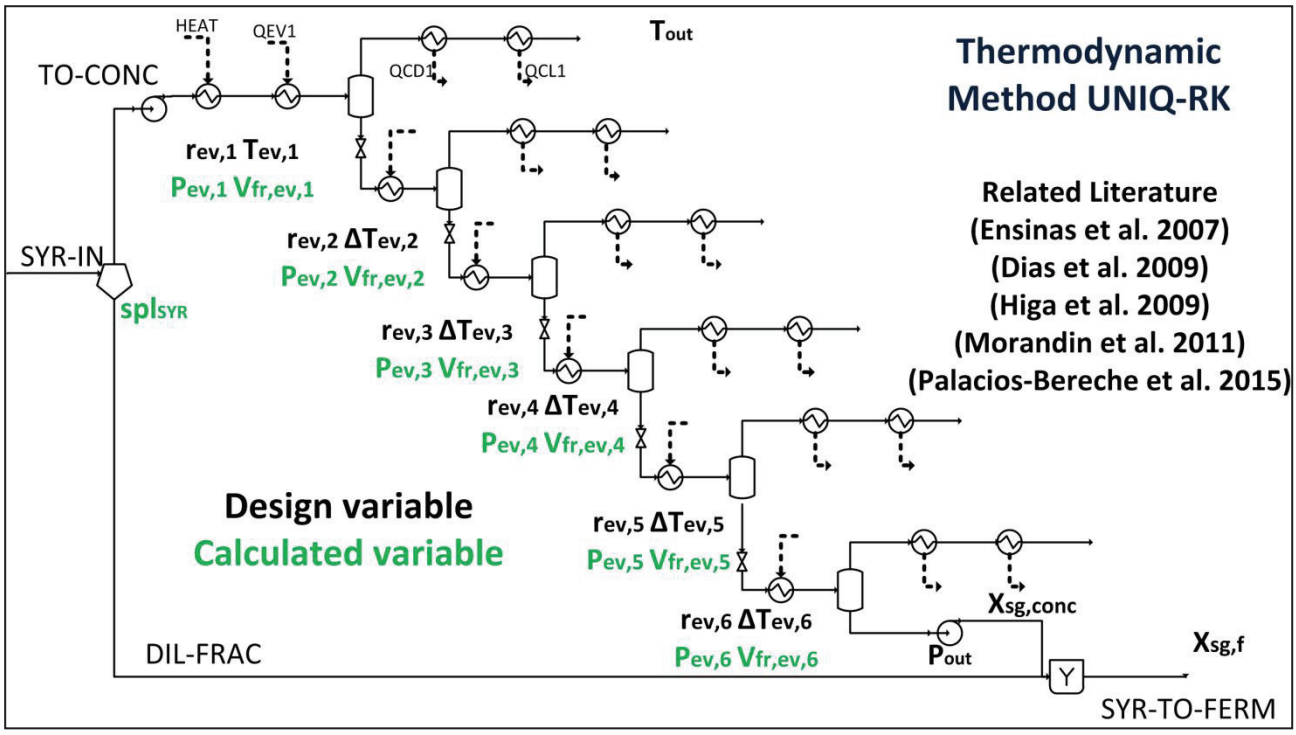

Figure 2:3 Process Flow Diagram for juice concentration section

On another hand, Table 2:3 provides the default values for the design variables highlighted in Figure 2:3. We note namely the constant evaporation rates as highlighted in [45] and constant temperature decrements as highlighted in [28]. The temperature of the first evaporator is bound by limits on sucrose decomposition. The final sugar concentration is provided by [46] and the intermediate concentration by [42].

Table 2:3 Design parameters for juice concentration and sterilization step [41]

Design Parameter	Symbol	Default Value
Sugar fraction in concentrated stream	$x_{sg,conc}$	65%
Final sugar concentration	$x_{sg,f}$	22.5%
Number of evaporation effects	$N_{evap,units}$	6
Evaporation fraction in each effect	$r_{ev,i}$	$\frac{1}{6}$
Temperature of first effect	$T_{ev,1}$	120 °C
Temperature decrement in 2nd to last effect	$\Delta T_{ev,i}$	10°C
Temperature of output cold streams	T_{out}	35 °C
Output stream pressure	P_{out}	1 atm

Finally, we count 19 heat streams in Figure 2:3, with feed preheating and stream vaporization as heat sinks and condensation and cooling as heat sources.

2.3.3 Sterilization and Fermentation

Fermentation deals with the conversion of input sugars to ethanol. Sterilization on the other hand is required prior to fermentation in order to kill off bacteria, molds and slow down natural yeasts, allowing specialty yeasts to outperform them. Moroever, input juice is made mostly of sucrose ($C_{12}H_{22}O_{11}$), (c.a. 95 wt.% of sugar content) [41]. This sugar cannot be readily converted to ethanol. It needs thus to be broken down (hydrolyzed) to glucose, which is on the other hand fermentable. Although, parallel reactions are common in the industry, we chose to model these reactions in two separate units performing respectively: sucrose hydrolysis and glucose (dextrose) to ethanol conversion.

Sterilization is realized by heating up the juice to a given temperature (T_{ster}) during a given amount of time (RT_{ster}) and then rapidly cooling it down to hydrolysis temperature ($T_{scr,hyd}$). Sucrose hydrolysis then occurs in a batch reactor with total conversion ($conv_{scr,hyd}$) of sucrose to glucose, under specified temperature ($T_{scr,hyd}$), pressure ($P_{scr,hyd}$) and retention time ($RT_{scr,hyd}$).

Glucose fermentation is finally realized in a fed-batch reactor with cell recycling technology, otherwise termed the Melle-Boinot process. This process has widespread application in the Brazilian context (75% of distilleries, [46]). This is thanks to yeast recycling which reduces the need for intensive yeast propagation, leading to less sugar being deviated for biomass formation [46]. As a result, great glucose to ethanol conversion yields ($conv_{gluc,et}$) can be obtained. Other minor reactions were considered within the fermenter albeit at greatly lower yields. Table 2:4 indicates the equations for these various reactions, as well as their main product. As we can see in this table, CO_2 is an important by-product of the fermentation reaction. As a result, all ethanol distilleries are equipped with a CO_2 scrubber, where water is used to absorb ethanol and VOCs from the gaseous fermentation stream. On another note, the yeast content exiting the fermenter needs to be separated from the obtained wine and recycled back to the reactor; thus the

additional reactors: (1) yeast separation: via staged centrifugation; (2) yeast dilution and addition of nutrients (NH_3), (3) recycling part of the yeast to the fermentation reactor. Figure 2:4 provides the Process Flow Diagram for the fermentation section. We can visualize the main operations previously indicated. It was proposed in this configuration to heat the fermentation wine in order to obtain the desired CO2 separation yield. Key design parameters for this step are available in

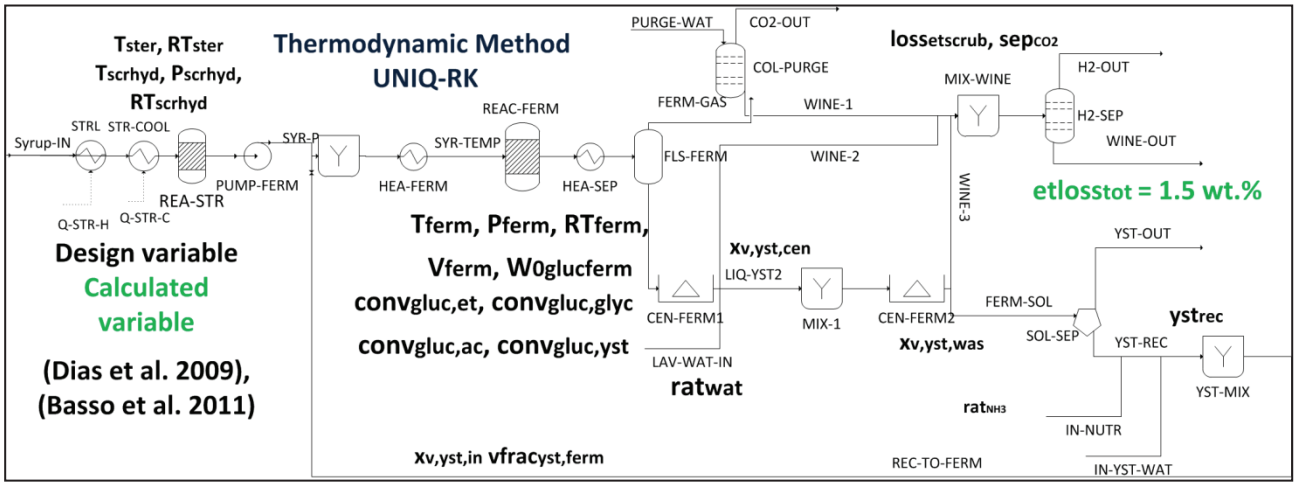

Figure 2:4 Process Flow Diagram fermentation section

Figure 2:4 highlights the two research articles that proved of great importance for this section: (Dias et al.2009) [41] and (Basso et al. 2011) [46]. The used thermodynamic method was on the other hand UNIQ-RK.

Table 2:5. The total resulting ethanol loss is equal to 1.5%. Output wine streams, both from centrifugation and scrubbing, are mixed before being sent to the distillation section for ethanol separation. This output stream has an ethanol mass content in the range of [8-12] wt.%. It also contains a variety of minor components, namely, impurities, unfermented glucose, and fermentation by-products.

Table 2:4 Equation and reaction extent of main process reactions [39]

Main Product	Reaction equation
Ethanol	Glucose → 2*Ethanol + 2*CO_2
Acetic Acid	Glucose +2*H_2O→ 2*Acetic Acid + 2*CO_2+4*H_2
Glycerol	Glucose+2*H_2 → 2*Glycerol (H_2 from acetic acid formation)
Yeast	Glucose+0.79*NH_3+0.73*CO_2 → 6.73*Yeast+ 1.4*H_2O

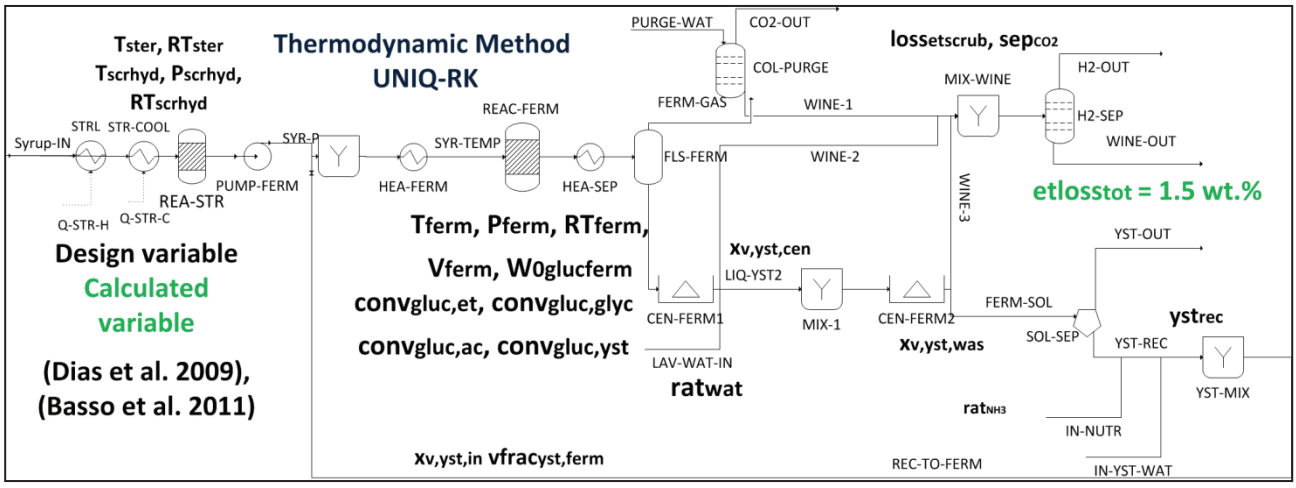

Figure 2:4 Process Flow Diagram fermentation section

Figure 2:4 highlights the two research articles that proved of great importance for this section: (Dias et al.2009) [41] and (Basso et al. 2011) [46]. The used thermodynamic method was on the other hand UNIQ-RK.

Table 2:5 Design parameters fermentation step [46]

Design Parameter	Symbol	Default Value	Design Parameter	Symbol	Default Value
Upper sterilization temperature	T_{ster}	130 °C	**Duration of sterilization**	RT_{ster}	30 min
Sucrose to glucose conversion	$conv_{scr,hyd}$	100 mol. %	**Temperature of sucrose hydrolysis reaction**	$T_{scr,hyd}$	32 °C
Pressure of sucrose hydrolysis reaction	$P_{scr,hyd}$	1 atm	**Residence time of sucrose hydrolysis reaction**	$RT_{scr,hyd}$	3
Fermentation temperature	T_{Ferm}	32 °C	**Yeast content in input yeast stream**	$x_{v,yst,in}$	30 vol.%
Fermentation pressure	P_{Ferm}	1 atm	**Fraction of yeast stream in fermentation volume**	$vfrac_{yst,ferm}$	25 vol.%
Fermentation time	RT_{Ferm}	12 h	**Cake yeast content after centrifugation**	$x_{v,yst,cen}$	35 vol.%
Reactor volume	V_{Ferm}	500 m^3	**Quantity of wash water/ quantity of yeast**	rat_{wat}	1
Yield of ethanol production reaction	$conv_{gluc,et}$	92 mol.%	**Cake yeast content after washing**	$x_{v,yst,wash}$	70 vol.%
Yield of glycerol production reaction	$conv_{gluc,glyc}$	2.58 mol.%	**Yeast recycling ratio**	yst_{rec}	95%
Yield of acetic acid production reaction	$conv_{gluc,acet}$	1.15 mol.%	**Ethanol loss in purge stream**	$loss_{et,scrub}$	0.076 wt.%
Yield of yeast production reaction	$conv_{gluc,yst}$	1.79 mol.%	**CO2 purged/CO2 produced**	sep_{CO_2}	98 wt.%
Agitation power consumption	$W_{0,Ferm}$	0 kW/m^3	$\boldsymbol{NH_3}$ **to glucose ratio**	rat_{NH_3}	1.79 mol.%

2.3.4 Distillation for Ethanol Concentration

The ultimate goal of this section is to increase the ethanol concentration in the product stream. The second goal is the purification of the ethanol stream of minor components, namely CO_2, glucose, and fermentation products [47]. This section is constituted of two distillation columns: (1) a stripping column (termed AAD) where ethanol is separated from the bulk of the fermentation wine, and (2) a rectifying column (termed BB1) where the remaining water content is removed from the rising bioethanol stream. An additional (3) purge system is however inserted between the two columns in order to remover volatile components, namely CO_2. This configuration is

inspired from the works of [48] which proved its accuracy compared to industrial set-ups and other simulation models. Figure 2:5 shows the *Process Flow Diagram* for this section, with the main operations, streams (mass, heat and power) and design parameters. The related ethanol loss at 2.6% is also highlighted. Within the related simulation model, these specifications are met by controlling variables such as: reflux and distillate to feed ratios for columns, and vapor fraction for the purge cooler. This figure also provided details concerning the related thermodynamic method which was based on the works of [47, 48]. We can also find therein literature works related to this section: (Batista et al. 2012) [47],(Bessa et al.2012) [48], (Bessa et al. 2013) [49], (Ponce et al. 2015) [50], and (Palacios-Bereche et al. 2015) [44].

In addition, Table 2:6 and Table 2:7 summarize the design parameters for the stripping column (AAD) of the distillation section and the rectifying column (BB1) respectively.

Finally, Table 2:8 provides values for parameters common to both columns.

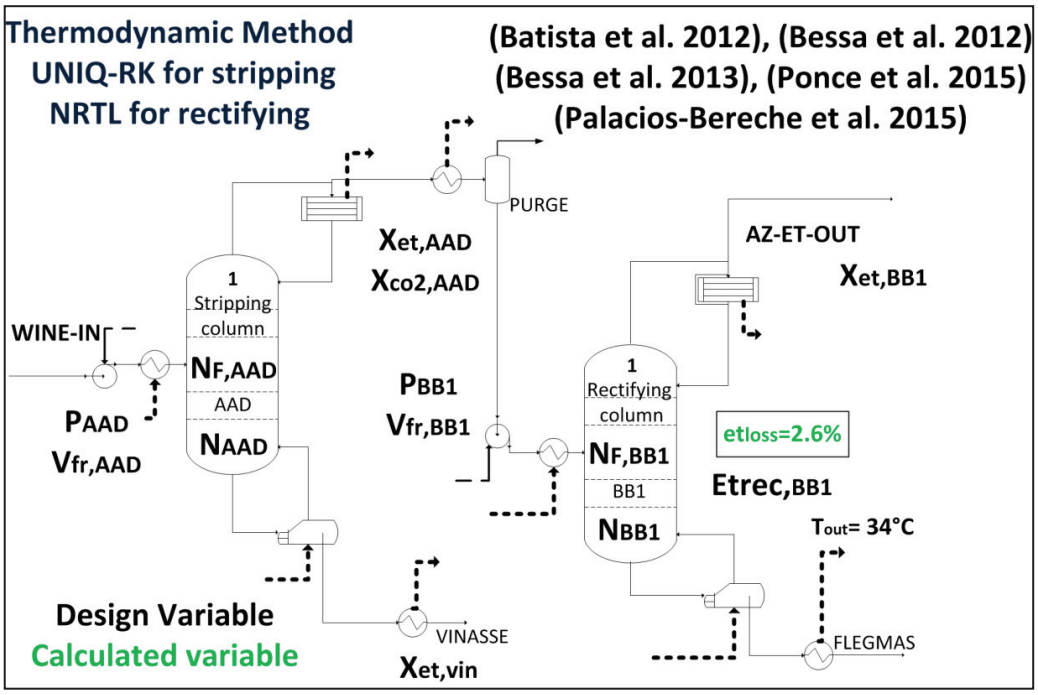

Figure 2:5 Process Flow Diagram for ethanol distillation section

Table 2:6 Design parameters for the stripping column of the distillation section [48]

Design Parameter	Symbol	Default Value	Design Parameter	Symbol	Default Value
Operating pressure	$\mathrm{P_{AAD}}$	1.275 atm	**Ethanol content in bottoms**	$x_{et,vin}$	0.02 wt.%
Feed vapor fraction	$\mathrm{Vfr_{F,AAD}}$	0	**Ethanol content in post-purge tops**	$x_{et,AAD}$	40 wt.%
Number of stages	$\mathrm{N_{AAD}}$	30	**CO2 content in post-purge tops**	$x_{CO2,\mathrm{AAD}}$	0.3 wt.%
Feed stage location	$N_{F,AAD}$	25			

Table 2:7 Design parameters for the rectifying column of the distillation section [48]

Design Parameter	Symbol	Default Value	Design Parameter	Symbol	Default Value
Operating pressure	P_{BB1}	1.373 atm	**Feed stage location**	$N_{F,BB1}$	43
Feed Vapor Fraction	$Vfr_{F,BB1}$	0	**Ethanol recovery in distillate**	$etrec_{\mathrm{BB1}}$	99.8 wt.%
Number of stages	N_{BB1}	63	**Ethanol content in distillate**	$x_{et,BB1}$	93.6 wt.%

Table 2:8 Parameters common to stripping and rectifying columns

Design Parameter	Symbol	Default Value
Pressure drop in distillation columns	ΔP_{dis}	0 atm
Temperature of output cold streams	T_{out}	35 °C

On another note, we count 10 heat streams. Reboilers and feed heaters are heat sinks, whereas the condensers purge streams, and bottom stream coolers are heat sources. Finally, as we can see, ethanol does not exit the system in a completely dehydrated state. This is due to the water-ethanol azeotrope which forms for the given rectifying column pressure at 4 wt. % water content. This azeotrope cannot be removed by thermal means and as a result, an additional dehydration section is required. In this context, as we can see in Figure 2:5, only a partial condensation is considered for column BB1. This is because the vapor fraction in this column's distillate is a design variable for the subsequent dehydration section

2.3.5 Dehydration by extractive distillation

The goal herein is the production of fuel grade anhydrous ethanol. With all impurities being removed in the distillation section, the main obstacle remains the removal of remaining water content. [51] notes three methods for this endeavor of which extractive distillation using ethylene-glycol (MEG) is the most economic. [52] adds that this technology is simple in operation and allows handling of mixtures far from the azeotrope. For these reasons, it was chosen for our process. This technology consists of two distillation columns: (1) an extraction column in which the solvent MEG is added; ethanol is obtained in a dehydrated form at the column top, and water is entrained to

the bottom with the solvent. (2) a recovery column in which MEG is separated from water and recycled back to the extraction column. A MEG make-up stream is also included.

Figure 2:6 shows the *Process Flow Diagram* for the dehydration section, with the main operations, streams (mass, heat and power) and design parameters. Within the related simulation model, these specifications are met by controlling reflux and distillate to feed ratios for the columns. The employed thermodynamic methods are also highlighted therein, along with the main related research works. We cite: (Errico et al. 2013a) [53], (Errico et al. 2013b) [54], (Garcias-Herreros et al. 2011) [55], (Vazquez-Ojeda et al. 2013a) [56] and (Vazquez-Ojeda et al. 2013b) [57]. In addition, Table 2:7 summarizes the design parameters for this section. On another note, we count 6 heat streams. Reboilers and feed heaters are heat sinks, whereas the condensers purge streams, and bottom stream coolers are heat sources. Dehydration is the last step of the ethanol distillery.

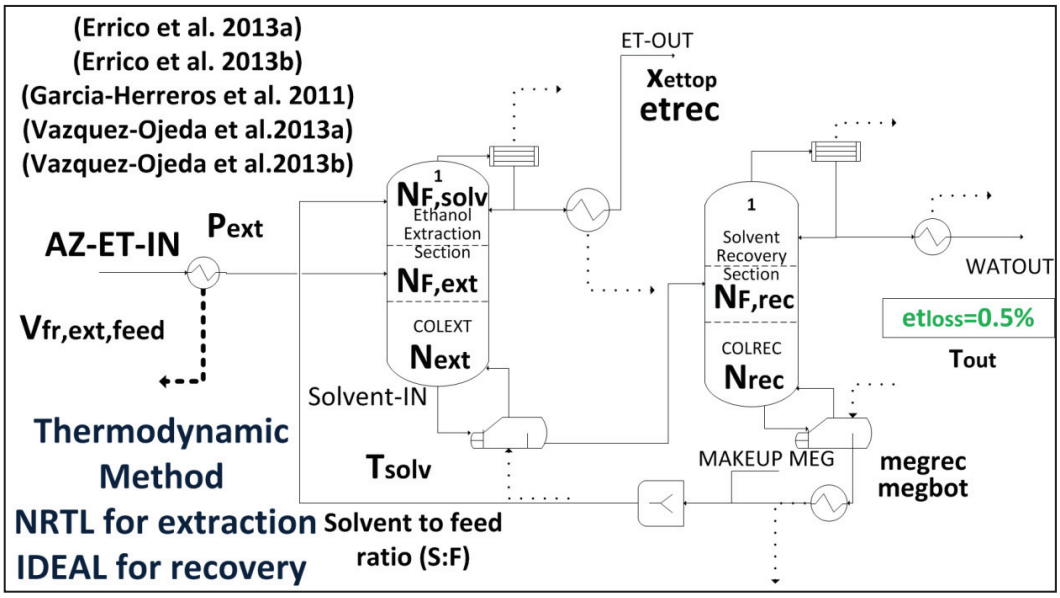

Figure 2:6 Process Flow Diagram for ethanol dehydration section: extractive distillation technology

Table 2:9 Design parameters for the dehydration section [48]

Design Parameter	Symbol	Default Value	Design Parameter	Symbol	Default Value
Operating pressure in extraction column	P_{ext}	1 atm	**Number of stages in extraction column**	N_{ext}	35
Feed stage in extraction column	$N_{F,ext}$	21	**Solvent feed stage**	$N_{F,solv}$	3
Solvent to feed ratio	$S:F$	0.52	**Vapor fraction of input to extraction column**	$V_{fr,ext,feed}$	0
Solvent input temperature	T_{solv}	100 °C	**Ethanol content in extraction tops**	$x_{et,top}$	99.3 wt.%
Ethanol recovery in extraction tops	$etrec$	99%	**Number of stages in recovery column**	N_{Rec}	10
Feed stage in recovery column	$N_{F,REC}$	6	**MEG recovery in recovery column**	$megrec$	99.5 wt.%
MEG content in recovery bottoms	$megbot$	99.9 wt.%	**Output temperature for cold streams**	T_{out}	35 °C

2.4 Bagasse and leaves combustion

We highlight in this paragraph the process blocks dealing with the valorization of the bagasse and leaves. Conventionally, these materials were burnt in solids boilers to provide heat for the system. A bagasse drying step is usually performed in order to reduce its moisture content and enhance boiler performance. It is possible to use output combustion gases to perform this drying step.

2.4.1 Block Flow Diagram

The *Block Flow Diagram* for this process section is highlighted in Figure 2:7. In this image, we can visualize the section's main operations, process input (in green), intermediary (purple) and waste (grey) streams. Streams in blue are exchanged with the ethanol production section. Also, the conventional route is presented in plain lines and the proposed modifications in dashed lines. The various building blocks are detailed below.

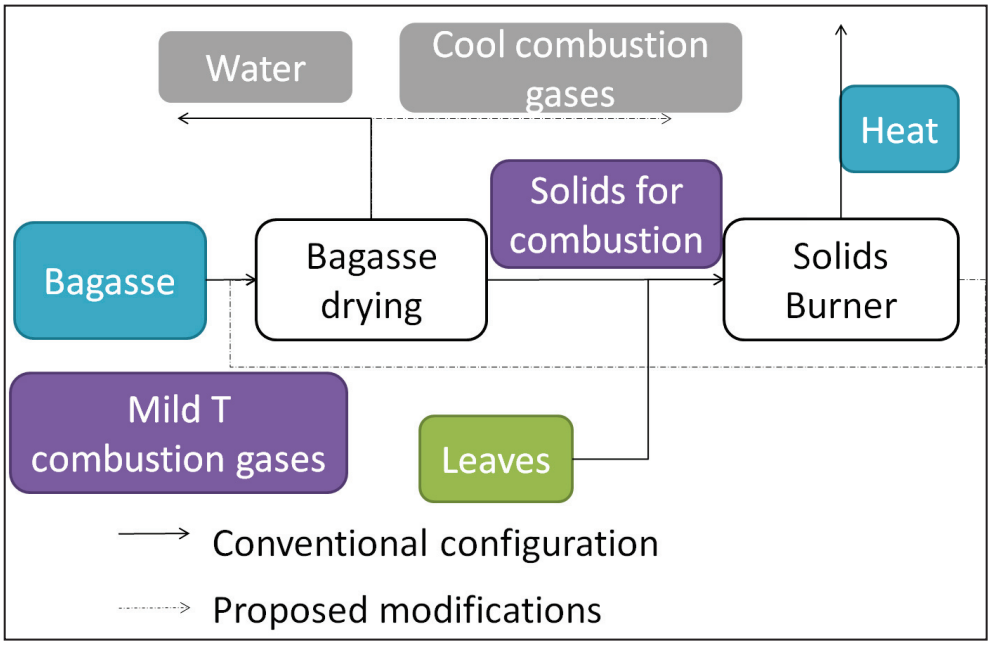

Figure 2:7 Block Flow Diagram for bagasse and leaves conventional valorization section

2.4.2 Process flow diagram

The process flow diagram for this step is provided in Figure 2:8. We recognize first the inputs: bagasse, leaves and air.

Bagasse is first subject to drying via flue gas recirculation, highlighted in red. The reduction of bagasse moisture realized via drying increases its combustion capability by increasing its total lower heat value (LHV). At the same time, it reduces the volume of the boiler exit gases, along with related heat losses. In addition, drying the sugar cane bagasse could reduce air pollution and air demand in the furnace [58]. As a result, bagasse drying is a good course of action for large mills with a bagasse moisture content superior to 50%, as in the case of our studied process.

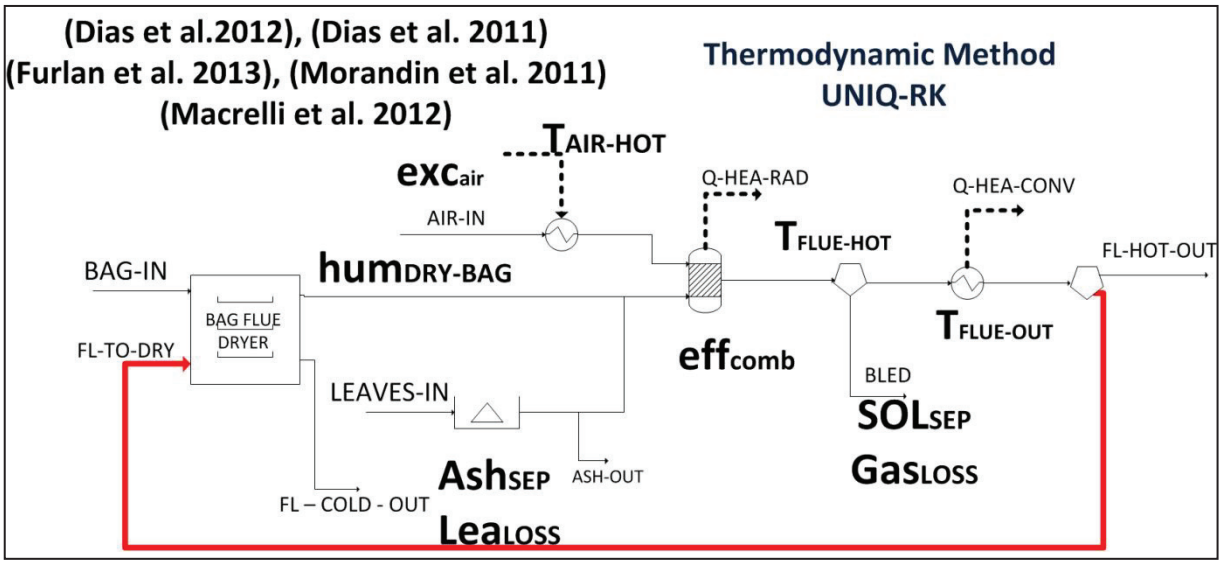

Figure 2:8 Process Flow Diagram for biomass burner

This drying is realized via recirculation of low temperature flue gases, which have already exchanged heat with the process. This technique is advocated by [58–60] and namely because it utilizes the exhaust heat of exhaust flue gases. The novelty in our case is related to the splitting of output flue gas. Exhaust flue gases are first separated. One fraction (FL_{SEP}) goes to flue drying whereas the other does not. Within this section, this fraction is calculated based on the desired bagasse humidity ($hum_{dry-bag}$). It is however also dependent on combustion related parameters. The drying operation was modeled as a RADFRAC column with no condenser, and no reboiler, two input and two products streams. Given this design, $hum_{dry-bag}$ is the only process parameter related to this step, which has no related heat streams.

Input leaves have a moisture content lower than that of input bagasse (15 wt.% vs. 50 wt.%). For this reason, their drying is not a required step. Nevertheless, this biomass needs to be washed in order to reduce its ash content.

The solids burner is used to valorize the LHV content of input biomass constituted of dried bagasse and washed leaves. Combustion air at ambient conditions and no moisture content is first heated to $T_{AIR-HOT}$ before being injected with the biomass to the burner. The post-combustion flue-gas temperature is set to $T_{FLUE-HOT}$. A bleeding stream is also included to recover non-combustible solids, namely ash and dirt. We can also view in Figure 2:8 that this section has three heat streams: two heat sources, one related to radiation heat $Q_{HEA-RAD}$ and one related to convection heat $Q_{HEA-CONV}$; and one heat sink $Q_{HEA-AIR}$ related to combustion air pre-heating.

In addition, the design variables intervening in this process section are summarized in Table 2:10.

Table 2:10 Design parameters for biomass combustion step

Design Parameter	Symbol	Default Value	Design Parameter	Symbol	Default Value
Excess air ratio	$\mathrm{exc_{air}}$	0.3	**Ash separation in leaves washing**	Ash_{SEP}	70%
Air heating temperature	$T_{AIR-HOT}$	250 °C	**Loss of biomass in leaves washing**	Lea_{Loss}	0.5%
Post-combustion flue gas temperature	$T_{FLUE-HOT}$	527 °C	**Extension of solid separation in bleeding**	Sol_{SEP}	100%
Output flue gas temperature	$T_{FLUE-OUT}$	160 °C	**Extent of gas loss in bleeding**	Gas_{Loss}	0%
Conversion ratios of combustion reactions	eff_{comb}	98 mol.%	**Dried bagasse humidity**	$hum_{dry-bag}$	0.25

Finally, Figure 2:8 provides certain literature references. We cite: (Dias et al.2012) [61], (Dias et al.2011) [62], (Furlan et al. 2013) [63], (Morandin et al. 2011) [28]and (Macrelli et al. 2012) [64].

2.5 Utility production system

Utility production is needed by the process for three reasons: (1) providing heat for the process in the form of steam, (2) providing power for the system and (3) cooling down process streams. This need is however dependent on [65]

- The chosen process configuration (technology + values for design variables)
- The chosen heat exchange network and its parameters and constraints
- The extent of heat recovery within the available utility systems.

For this reason, we will provide in this paragraph the layout for these process sections along with the main design variables. However, only nominal flow rates were chosen, seeing that the actual rates, which translate the relative need, can only be obtained once the heat integration problem is resolved.

2.5.1 Combined Heat and Power system

A variation of the Rankine cycle is conventionally used for combined heat and power production in sugarcane plants[59, 62, 66]. High pressure superheated steam is first produced in a steam production system. Then, [67] proposed the use of two turbines: one back-pressure and one condensing. Steam is extracted in the first in order to meet process heat demands, whereas excess steam is withdrawn in the second for a greater power production. We speak of steam network targeting [68]: the flow rates associated with water production and steam extraction are determined based on chosen process configuration. In this context, [28] proposed a total of 5 steam levels, a configuration that was used in [21] and will employed in our work. This was realized in order to enable a greater range of extraction temperatures and a more targeted extraction, and ultimately higher conversion efficiency

Considering this, the process flow diagram for our chosen combined heat and power production system is presented in Figure 2:9. As we can see, five turbines are used in our case: four back-pressures and one condensing. Steam pressures were chosen as the design variables in our work in line with literature [28]. Operating temperatures are controlled so as to obtain saturated steam at the desired pressure levels.

The mass flow rates at this level are nominative and not effective. In fact, the true values can be obtained only once the heat integration profile for the configuration at hand is computed. This leads to nominal heat and power production rates, which are also directly dependent on the chosen temperature levels.

Nonetheless, a mass balance around the steam splitter/water mixer yields the equality constraint specified in Equation 2:5. Consequently, the sixth parameter can be calculated according to this equation once the other five parameters are specified.

Equation 2:5 Mass balance for steam splitter

$$M_{wat,in} = \sum_{i=1}^{5} M_{tur,i}$$

After condensation, all water streams are pumped to first turbine pressure before being recycled back to the cycle. The employed thermodynamic method as highlighted in Figure 2:9 is STEAM-TA. Figure 2:9 also provides certain bibliographic references. We cite (Dias et al.2012) [61], (Dias et al. 2011a) [62], (Dias et al. 2011b) [69] and (Morandin et al. 2011) [28].

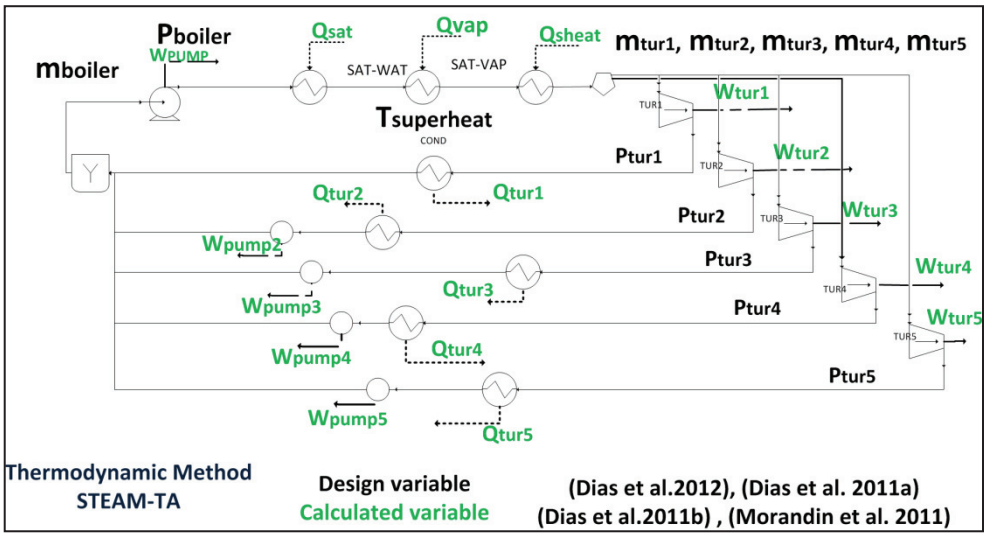

Figure 2:9 Process Flow Diagram for combined heat and power production system

Finally, Table 2:11 provides details concerning the key design variables for this step.

Table 2:11 Design parameters for combined heat and power production step

Design Parameter	Symbol	Default Value	Design Parameter	Symbol	Default Value
Steam pressure	P_{boiler}	90 atm.	**3rd turbine pressure**	P_{tur3}	1.73 atm
Superheating temperature	$T_{super,heat}$	200 °C	**4th turbine pressure**	P_{tur4}	0.71 atm
1st turbine pressure	P_{tur1}	20.55 atm	**5th turbine pressure**	P_{tur5}	0.12 atm
2nd turbine pressure	t_{tur2}	2.72 atm	**Input water rate***	m_{boiler}	1 kg/h
1st turbine rate	m_{tur1}	0.2 kg/h	**2nd turbine rate**	m_{Tur2}	0.2 kg/h
3rd turbine rate	m_{tur3}	0.2 kg/h	**4th turbine rate**	m_{tur4}	0.2 kg/h
5th turbine rate	m_{tur5}	0.2 kg/h			

* Nominal values

2.5.2 Cold utility system

2.5.2.1 Cooling water utility

Cooling water was chosen in our system in line with other research works. This utility system recovers process waste heat, up to a certain temperature level. As in the case of the CHP system, the amount of cooling water depends on the chosen problem configuration and related heat integration problem. This section is modeled by a simple heat exchanger as highlighted in Figure 2:10. The values for this section's key parameters are highlighted in Table 2:12. This utility system was based on IFPEN's guidelines

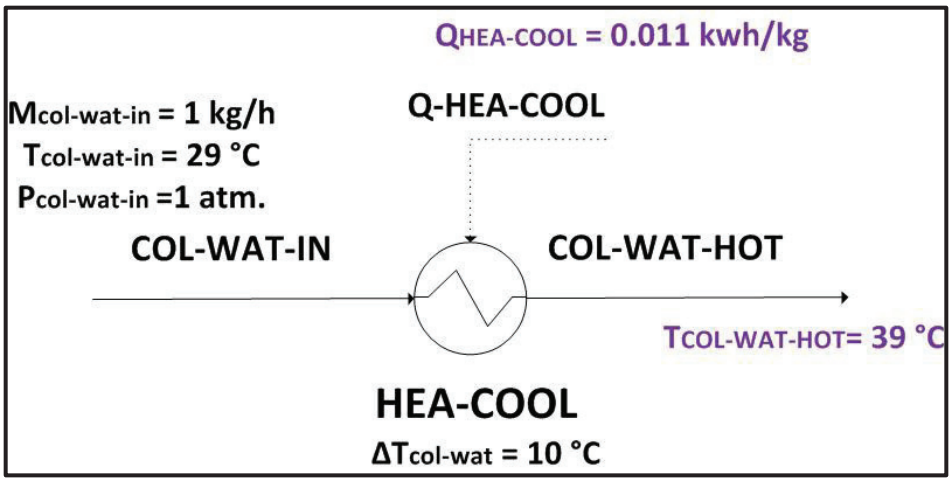

Figure 2:10 Process flow Diagram for process cooling water utility

Table 2:12 Design parameters for cold utility system

Design Parameter	Symbol	Default Value
Input Water temperature	$T_{col-wat-in}$	29 °C
Increase in cold utility temperature	$\Delta T_{col-wat}$	10 °C

2.5.2.2 Refrigerant utility

The refrigerant is required for our case, to cool the fermentation reactor as highlighted in the works of [62] and to condense column tops in case of heat integrated distillation as highlighted in the works of [44]. Moroever, as in the case of other utility systems, its flow rate depends directly on the chosen problem configuration and related heat integration problem. This section is however modeled as an evaporator with input refrigerant entering at saturation as highlighted in Figure 2:10. This utility system was based on IFPEN's guidelines.

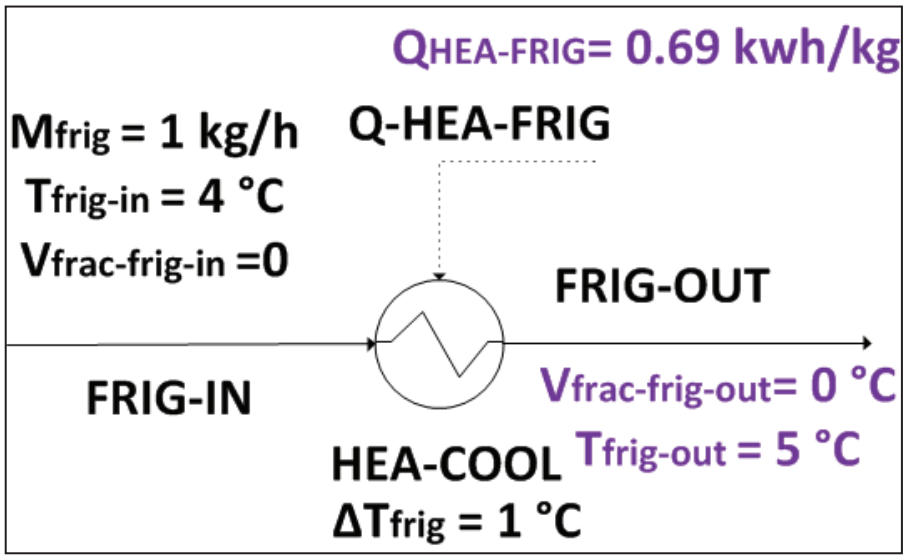

Figure 2:11 Process flow Diagram for process refrigerant utility

Finally, the values for this section's key parameters are highlighted in Table 2:13.

Table 2:13 Design parameters for cold utility system

Design Parameter	Symbol	Default Value
Input Refrigerant temperature	$T_{col-frig-in}$	4 °C
Increase in refrigerant temperature	ΔT_{frig}	1 °C

2.6 Conclusion concerning conventional sugarcane to ethanol biorefinery

We presented in this section the chosen superstructure for the conventional process of cogenerating power and ethanol from sugarcane. The capacity and content of input material was presented. Moreover, 9 process blocks along with their process flow diagrams were highlighted:

Blocks related to ethanol production: (1) Sugarcane cleaning, treatment and sugar extraction, (2) juice concentration through multi-effect evaporation, (3) glucose fermentation through the Melle-Boinot process, (4) Ethanol concentration through distillation and (5) ethanol dehydration by extractive distillation.

Blocks related to bagasse and leaves valorization: (1) Bagasse drying through flue gas recirculation and (2) bagasse and leaves combustion in a conventional biomass burner

Blocks related to utility production: (1) Combined Heat and Power Production system consisting of a Rankine cycle with a high pressure boiler and a multi-level steam turbine and (2) the cold utility consisting of cold water heated to a predefined extent.

This process, along with its constitutive streams and operations was modeled using the Aspen Plus V7.2™ process simulator, following the UNIQ-RK thermodynamic method and the NREL model for component modeling.

The process flow diagrams provided also information concerning the related unit operations which consist of: evaporators, reactors, centrifuges, condensers/heat exchangers, distillation columns, mix tanks, dryers and burners. We count a total of 49 operations and this whilst excluding heat exchangers and sugarcane handling operations; the first because the number of heat exchanger can only be determined once the heat integration problem is resolved; the second because it remains intact in our case.

Design variables were specified for each section. We count a total of 99 design variables relating to separation/recovery efficiency, humidity content/sugar or ethanol concentrations, evaporation rates, operating temperatures and pressures and mass flow rates. These variables were highlighted both in dedicated tables and on the images relating to the various process flow diagrams.

Simulation results were also highlighted in the process flow diagrams, namely concerning the main input and output flow rates of the various sections. One should note that nominal values were provided to utility system flow rates. This is because these results depend on the resolution of the process heat integration problem which will be detailed in a later paragraph.

The process heat and power streams were also highlighted in the various process flow diagrams. We count a total of 50 heat streams and 15 power streams. This information is summarized in Table 2:14.

Table 2:14 Main sugarcane to ethanol process information along with related count

Process information	Related count
Simulation Program	Aspen Plus™
Thermodynamic Method	UNIQ-RK
Component modeling	NREL model
Process blocks	9
Number of unit operations*	47
Number of design variables	99
Number of heat streams	50
Number of power streams	15

*excluding sugarcane handling section and heat exchangers

Chapter 3 Case study II: Combined distillery, hydrolysis and cogeneration plant

In this chapter, we will investigate the integration of a lignocellulosic material conversion system into a more global conversion process. The material in question as will be detailed later is bagasse, the conversion system, hydrolysis, and the global conversion process is the combined ethanol distillery and power cogeneration system highlighted in Chapter 2. The novel scheme is denoted hereafter: combined distillery, hydrolysis and cogeneration plant.

3.1 Lignocellulosic material and their valorization

Lignocellulosic materials constitute the most abundant biomass material with approximately 50% of world biomass production at 10-50 billion ton/year [19]. Moreover, with a lower heating value of 18 MJ/kg, the global energy content of this material is equal to 5.78 TW, equivalent to that of petrol. However, these materials are not available for immediate consumer, namely in the form of liquid or gaseous fuels. Therefore these materials require the performance of dedicated chemical transformation operations. The main possible operations are highlighted in Figure 3:1. These operations can be broken down into thermo-chemical and biochemical. Excluding combustion, the first set makes use of high pressure and temperature conditions to break down the biomass before transforming the intermediary product into the required fuel. The second set makes use of biochemical reactions occurring at mild conditions to transform the input material into output fuels, mainly bioethanol and biodiesel.

Hydrolysis is an example of a biochemical conversion route, which breaks the carbohydrate biomass fraction into base sugars. Enzymatic hydrolysis is a variant thereof which has gained increased interest in literature due to its following advantages:

- Mild reaction conditions of temperature and pressure
- Theoretically high conversion yields
- Little or no formation of inhibitory by-products
- Easy separation of hydrolyzed and non-hydrolyzed fractions
- A wide variety of related literature work
- The fermentation of glucose, a hydrolysis product, is a consolidated technology in Brazil

For these reasons, this technology was chosen as the investigated route in our study case.

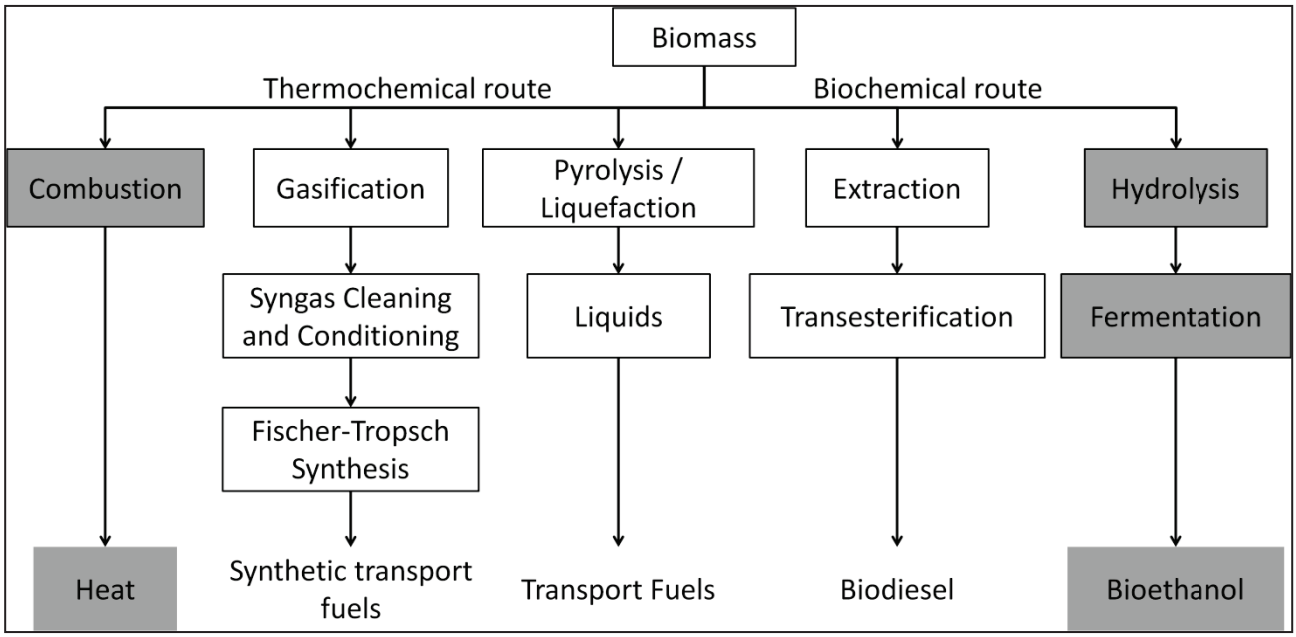

Figure 3:1 Diagram of the main biofuel production pathways [70] – Pathways considered in this chapter highlighted in grey

3.2 Lignocellulosic material: sugarcane bagasse

Sugarcane bagasse is a prime example of lignocellulosic material. This is thanks to its low cost, great abundance (150 metric tons/year in Brazil-280 kg of bagasse at 50% humidity per ton of sugarcane), absence of competition with food or animal feed applications, direct availability in sugarcane facilities. This availability is namely due to the great energy balance of sugarcane processing plants and the high energetic content of bagasse (c.a. 2/3 of sugarcane energy content). In fact, even though this material is usually burnt to provide both heat and power to operate such plants, a great excess (c.a. 50%) of it remains. The traditional approach, highlighted in Chapter 2, consists in entirely burning the excess bagasse to produce power that is later sold to the grid. An alternative that has gained increased attention is its partial conversion to ethanol via enzymatic hydrolysis. This conversion ultimately raises the overall ethanol yield. In this paragraph, we will highlight this process as integrated with the conventional sugarcane conversion process highlighted in Chapter 2.

As indicated earlier, sugarcane bagasse is a lignocellulosic biomass consisting of an insoluble solid fraction and a soluble liquid fraction. The solid fraction consists of: carbohydrate polymers, mainly cellulose and hemicellulose, aromatic polymers, denoted lignin, and ash. The liquid fraction on the other hand consists mainly in water and sucrose. Table 3:1 highlights the various information of the input bagasse stream. Such information includes temperature, pressure, flow rate, composition and energy and exergy contents. Moreover, it is interesting to note that the bagasse composition depends on the variety and maturity of the sugarcane feedstock as well as the applied harvesting and milling methods. The results of this work are based on the works of [71, 72].

Table 3:1 Flow rate, composition and energy content of input bagasse [71]

Parameter	Value	Parameter	Value
Temperature	37 °C	Solid content	52 wt. %
Pressure	1 atm	Cellulose content (in solid fraction)	21% (43%)
Input bagasse to Input sugarcane ratio	11.92 ton bagasse/ ton sugarcane	Lignin content	13% (26%)
Water content (in liquid fraction)	48 wt. % (96 wt.%)	Hemi-cellulose content	13% (26%)
Sucrose content (in liquid fraction)	2% (4%)	Ash content	3% (5%)
Nominal energy content (kWh LHV/kg total)	2.82	Nominal exergy content (kWh LHV/kg total)	2.945

The thermodynamic data for the various materials was based on the NREL databank [40], developed under Aspen PLUS. The stream class *MIXCISLD* was used to model the soluble and insoluble solid fractions. Moreover, the chemical formulae and components used to model the biomass components are highlighted in Table 3:2

Table 3:2 Model component and chemical formula adopted for non-conventional process components

Process component	Model component	Chemical Formula
Cellulose	Dilactic-Acid	$C_6H_{10}O_5$
Hemicellulose	Glutaric-Acid	$C_5H_8O_4$
Lignin	Vanillin	$C_8H_8O_3$
Ash	Silicon Dioxide	SiO_2

3.3 Overall scheme of hydrolysis process

As indicated earlier, enzymatic hydrolysis is our chosen bagasse conversion route and this thanks to its enumerated advantages. However, it should be noted that only the carbohydrate fraction, namely cellulose, is readily available for ethanol production through this method. Moreover, two techniques are possible for performing the hydrolysis and subsequent fermentation [71]:

- SHF: separate hydrolysis and fermentation. Hydrolysis and fermentation reactions occur in separate reactors.
- SSF: simultaneous saccharification and fermentation. Both reactions occur in the same reactor.
- Separation of un-hydrolyzed solids from post-hydrolysis sugar juice
- Keeping un-hydrolyzed solids in the post-hydrolysis sugar juice

In addition, the original biomass cannot be easily hydrolyzed, and this due to its rigid structure. Consequently, it is almost always preceded by a pretreatment step. This step seeks to increase the *digestibility* of the processed biomass whilst remaining cost-effective. This is done by the following

methods: decomposing hemicellulose, breaking the lignin structure, reducing cellulose crystallinity, increasing material porosity. Cost-effectiveness is guaranteed by reducing the formation of inhibitors and preserving the utility of hemicelluloses [73, 74]. Several pretreatment technologies are available and can be classified into the following categories [75]:

- Biological pretreatment namely by the use of fungi. Advantages: attack hemi-cellulose and lignin but not cellulose, low energy, low capital cost, mild conditions. Inconvenient: low hydrolysis rate.
- Physical pretreatment: chipping, milling, grinding. Advantage: increase in surface area. Inconvenient: high energy cost.
- Chemical pretreatment (addition of solvent): alkaline pretreatment, dilute acid pretreatment, organosolv (a pulping technique that uses an organic solvent to solubilize lignin and possibly hemicellulose). Advantages: breaks down hemi-cellulose and lignin, easily recoverable products, high hydrolysis rate. Inconvenient: necessity to separate and recycle the solvent.
- Physico-chemical pretreatments: combination of harsh operating conditions, and addition of catalysts. Examples of such methods are: liquid hot water, wet oxidation, CO_2 explosion and steam explosion. Advantages: cost-effective, degradation of hemi-cellulose, modification of lignin structure. Drawbacks: Generation of toxic components, hemicellulose degradation.

Steam explosion, a physico-chemical pretreatment, is the most widely employed technology. It is a hydrothermal pretreatment in which the biomass is subjected to pressurized steam for a period of time (in the order of minutes), and then suddenly depressurized. An acidic catalyst (SO_2, H_3PO_4, H_2SO_4) may also be added to enhance its performance. This technology ultimately leads to the autohydrolysis of hemicellulose, the reordering of the lignin structure and the increase in cellulose hydrolysis rate [75]. Finally, key design parameters include: the catalyst concentration, the residence time and the pretreatment temperature. These steps ultimately result in the following:

- One or more liquid streams, containing pretreatment by-products
- One solid stream, containing the cellulose and ash fraction alongside remaining input components.

Multiple possibilities exist for the fate of this step's products:

- Separating pre-treatment soluble products (hydrolysates or soluble lignin) from the biomass stream entering hydrolysis.
- Keeping pre-treatment products in the biomass stream entering hydrolysis

In the context of our work, we chose to operate with the Separate Hydrolysis and Fermentation (SHF) technology, whilst separating pre-treatment products from hydrolysis biomass and separating un-hydrolyzed solids from the produced sugar juice. This was realized in order to guarantee that the obtained glucose juice can be easily integrated with the conventional sugarcane to ethanol distillery. This approach was also adopted in all related research works.

Another important issue in bagasse hydrolysis is the utilization of by-products: namely pre-treatment hydrolysates and the un-hydrolyzed solid fraction. The chosen configuration consists in:

- For xylose: biodigestion of xylose and the rerouting of the obtained biogas to a gas turbine
- For biomass: concentration via press filter and rerouting to solids combustion system.

Other possibilities may exist for these streams. We cite namely the conversion of xylose fraction into ethanol as highlighted in [64] or butanol as highlighted in [76]. We cite also the further conversion of hydrolysis biomass, namely gasification as highlighted in [77]. These technologies suffer however from relative immaturity, and their inclusion adds further complexity to the investigated processes, which goes beyond the requirements of the current thesis.

Considering this, Figure 3:2 provides the block flow diagram for this section. We notice the bagasse input, the steam explosion pretreatment followed by solid/liquid separation. The stream is then split into a liquid stream containing xylose, rerouted to biodigestion, and a solid stream sent to enzymatic hydrolysis, with enzymes and water as additional input. The obtained stream is separated into solid and liquid fractions. The solid fraction is press filtered and sent to combustion whereas the liquid fraction, which contains hydrolysis glucose is sent to the distillery.

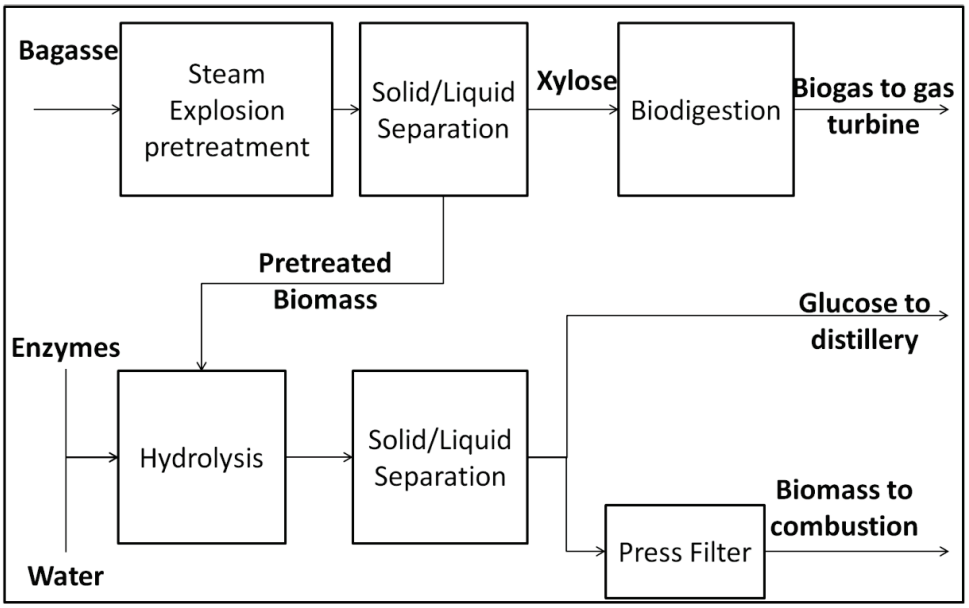

Figure 3:2 Block Flow Diagram for chosen bagasse hydrolysis scheme

3.4 Overall scheme of studied process

The integration of this technology into the conventional sugarcane distillery and cogeneration system, detailed in Chapter 2, leads to a novel global process scheme. This novel scheme is provided in Figure 3:1. We note the existence of distillery, cogeneration and cooling systems common with the combined distillery and cogeneration process. We also note the additional presence of the hydrolysis step. Two points should be considered at this level. The first is that the fraction of hydrolyzed bagasse is a key design variable and the second is that the cogeneration system is not exactly the same as that in Chapter 2.

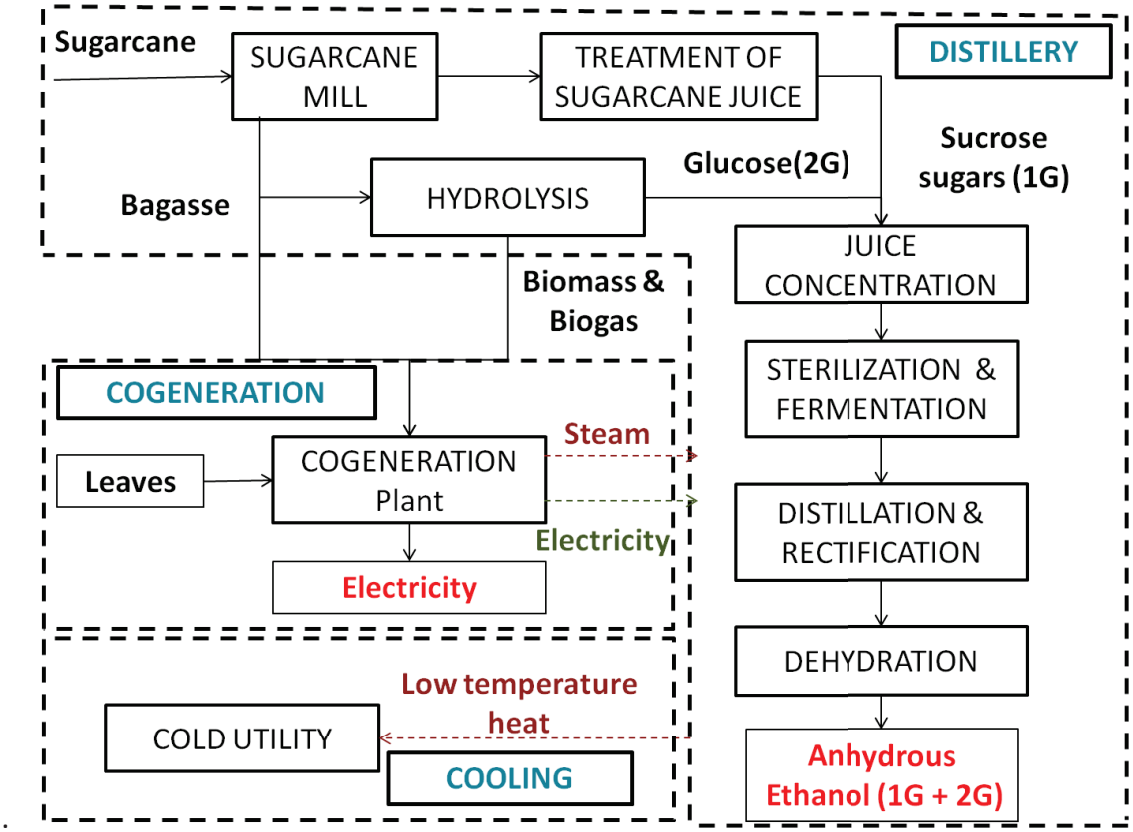

Figure 3:3 Overall scheme for bagasse hydrolysis process

3.5 Description of hydrolysis sections and associated models

3.5.1 Bagasse Pretreatment: catalyzed steam explosion

For our process, we adopted the model for steam explosion pretreatment used by [71, 72]. This model consists in applying dilute acid (H_3PO_4 or SO_2) catalyzed steam explosion to sugarcane bagasse. This technology was developed and validated under the Cane Biofuel joint European-Brazilian project [78]. This pretreatment leads to the conversion of the hemi-cellulose fraction to xylose (C5 sugars), with other components remaining in the solid fraction. The soluble xylose fraction is later separated from the solid fraction by means of filtration and washing. Parameters for filtration and washing are based on the works of [72, 79]. Finally, this step is preceded by a milling step where soluble solids, namely sucrose, are separated from the humid biomass stream. Figure 3:4 highlights the chosen process layout. We recognize the milling, steam explosion, depressurization and xylose separation sections. This process section has 24 design variables relating to temperatures, pressures, humidity, concentrations and conversion rates. These variables, highlighted in Figure 3:4, are provided, along with their default values, highlighted in Table 3:4. Other variables, highlighted in green in Figure 3:4, are calculated as a result thereof.

Figure 3:4 also provides certain literature data. We cite (Palmqvist et al. 1996) [79], (Alvira et al. 2010) [75], (Carrasco et al. 2010) [72] and (Ramos et al. 2014) [71] among others. The thermodynamic method UNIQ-RK was adopted for this section.

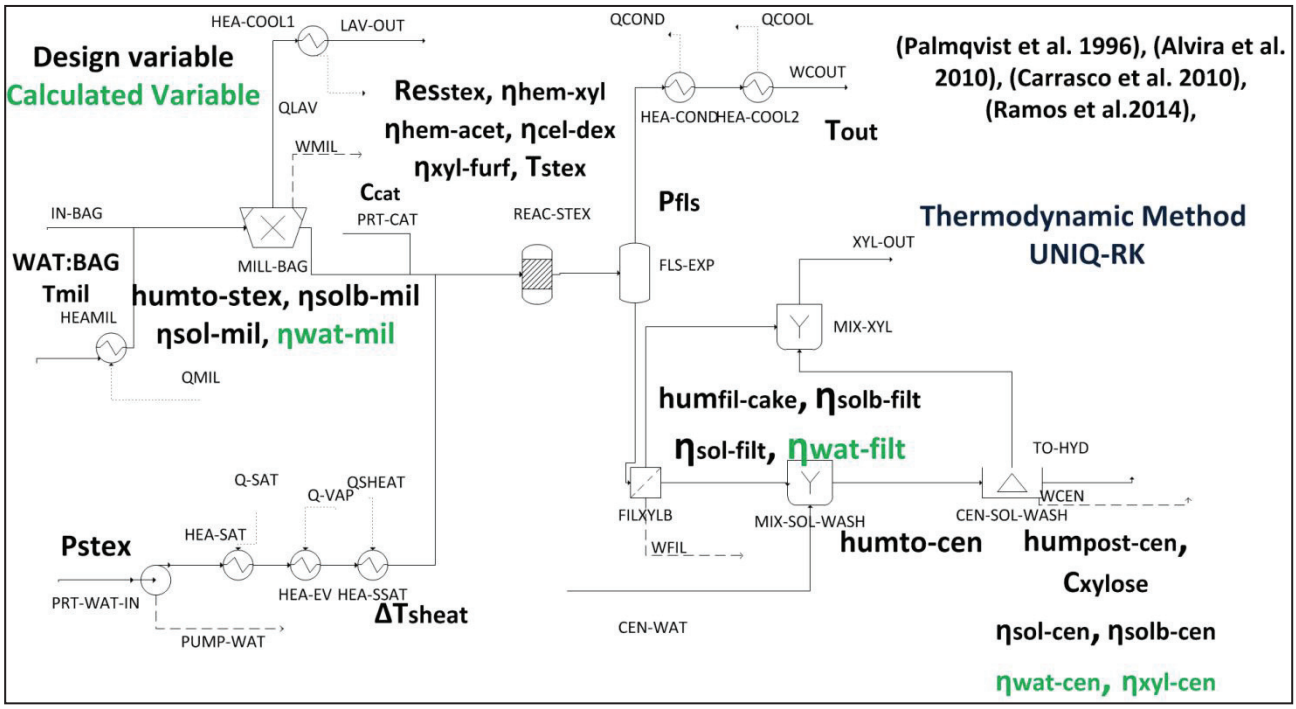

Figure 3:4 Process Flow Diagram for steam explosion pretreatment section

Moreover, as we can see from reaction parameters, cellulose degradation is kept at a minimum, and hemi-cellulose conversion is controlled. In addition, a great deal of water is required in the process, namely for the washing steps, resulting in a highly diluted xylose output stream (98.6 wt. % water concentration). Four different reactions, highlighted in Table 3:3 occur in the steam explosion reactor which was modeled as a steady-state reactor.

Finally, this process section has seven heat streams: 4 for heating and 3 for cooling. This section has also four power streams related to pumping, milling, filtration and centrifugation.

Table 3:3 Equations and main product for steam explosion reactions

Main Product	Reaction equation
Xylose (C5 sugars)	Hemicellulose + Water → Xylose
Acetic Acid	Hemicellulose + Water → 2.5*Acetic Acid
Glucose (C6 sugars)	Cellulose + Water → Glucose
Furfural	Xylose → Furfural + 3*Water

Table 3:4 Design parameters for the steam explosion pretreatment section

Design Parameter	Symbol	Default Value	Design Parameter	Symbol	Default Value
Mill water to bagasse ratio	WAT: BAG	3	**Efficiency of furfural production reaction**	$\eta_{xyl-furf}$	5 mol.%
Mill Temperature	T_{mil}	40 °C	**Efficiency of glucose reaction**	$\eta_{cel-dex}$	4 mol.%
Humidity to steam explosion	$hum_{to-stex}$	50 wt.%	**Flash pressure**	P_{fls}	1 atm
Fraction of soluble solids remaining in cake stream after mill	$\eta_{solb-mil}$	15%	**Output temperature**	T_{out}	34 °C
Fraction of input cake remaining in cake stream after mill	$\eta_{sol-mil}$	100%	**Humidity of filtration cake**	$hum_{fil-cake}$	27%
Steam Explosion pressure	P_{stex}	12 atm	**Fraction of soluble solids remaining in cake stream after filtration**	$\eta_{solb-filt}$	40%
Input steam superheat temperature	ΔT_{sheat}	90 °C	**Fraction of cake remaining in cake stream after filtration**	$\eta_{sol-filt}$	100%
Catalyst concentration	C_{cat}	9.5 mg/g dry matter	**Humidity of centrifugation input stream**	hum_{to-cen}	95 wt.%
Residence time in steam explosion reactor	Res_{stex}	5 min	**Humidity of centrifuged cake**	$hum_{post-cen}$	43 wt.%
Pretreatment temperature	T_{stex}	190 °C	**Xylose content in centrifuged cake**	C_{xylose}	0.25 g/L
Efficiency of xylose production reaction	$\eta_{hem-xyl}$	64 mol.%	**Fraction of input soluble solids remaining in cake stream after washing**	$\eta_{solb-cen}$	10%
Efficiency of acetic acid production reaction	$\eta_{hem-acet}$	24 mol.%	**Fraction of input cake remaining in cake stream after washing**	$\eta_{sol-cen}$	100%

3.5.2 Enzymatic hydrolysis of pretreated bagasse

As specified earlier, enzymatic hydrolysis is a technique for the conversion of biomass to liquid fuels, through the conversion of cellulose to glucose, ultimately fermented to ethanol. This technique is characterized by its selectivity, which results in an absence in the formation of inhibitors, and its mild conditions of temperature and pressure. However, through this method, a portion of input biomass, namely lignin and ash, remains intact. This fraction gets separated from the obtained liquid juice before downstream processing. Key parameters concerning this step are:

the solids loading, the enzymes loading, agitation power, residence time, and reaction temperature[71, 80].

For our superstructure, we based our work on the results obtained by c. In this work, different hydrolysis configurations with different input solids loading (sd_{load}), enzymes loading (Enz_{Load}), agitation power (W_a) and residence time (Res_{Hyd}) were considered and the glucose concentrations in the product stream were measured. As a result, the hydrolysis reactor was modeled as a steady state reactor. As for the design parameters, we chose to operate with the following values: 5% for the solids loading, 0.1 g/g for the enzymes loading, 0.3 kW/m^3 (200 rpm) for agitation power and 24h for the residence time. Moreover, we assumed that hydrolysis occurs under a temperature T_{hyd} of 40°C and a pressure P_{hyd} of 1 atm. These values resulted in a glucose concentration ($C_{gluc,hyd}$) in the output stream's liquid fraction of 18 g/L and a glucose content of 1.8 wt.%. The conversion rate ($\eta_{cel-gluc-hyd}$) associated to the cellulose to glucose conversion reaction is calculated as a result of this concentration, and was found equal to 65 mol. %. Moreover, a hemicellulose to xylose conversion reaction was considered in addition to the cellulose to glucose conversion reaction. A default rate ($\eta_{hem-xyl-hyd}$) of 41% was assumed for this reaction resulting in a xylose concentration ($C_{xyl,hyd}$) of 2 g/L for a 0.2 wt.% xylose content. Through this method, the lignin and ash contents remain intact. As a result, the stream leaving the hydrolysis reactor contains both a liquid with soluble solids fraction and a insoluble solids fraction. A centrifuge is then used to separate both fractions, with a 65 wt.% specification for the lignin cake humidity ($hum_{lig-cake}$), and a 10% loss of organics in the cake stream. The resulting cake is then passed through a press filter in order both to recover lost organics and to reduce the humidity level of the unhydrolyzed cake to 50 wt.%. The resulting glucose filtrate has a glucose concentration of 49 g/L and a glucose content of 5.4 wt.%, with a flow rate equal to 3.8% the value of the main glucose stream, for 10% of its glucose content. In the chosen design, these two flows are mixed together priori to downstream steps.

In addition, the required enzymes are added to speed up the hydrolysis and are not depleted. As a result, they end up in the pressed cake which has the following composition: $x_{cellulose} = 27\ wt.\%$, $x_{hemicellulose} = 7\ wt.\%$, $x_{lignin} = 47\ wt.\%$, $x_{ash} = 10\ wt.\%$ and $x_{enz} = 9\ wt.\%$. As indicated earlier, this cake is sent to the plant cogeneration system.

Finally, Figure 3:5 highlights the chosen process layout. We recognize the stream mixing, hydrolysis, centrifuge and press filter steps. Moreover, as we can see, only 0.7 t/h of hemicellulose remain, pertaining to an 84% conversion of the initial hemi-cellulose flow rate. Moreover, 27% of input biomass (4.8 t/h of cellulose) is converted to ethanol producing glucose. Two different reactions occur in the hydrolysis reactor, as previously cited and highlighted in Table 3:3. This reactor was modeled as a steady-state reactor. The absence of by-product formation reactions highlights the great selectivity associated with enzymatic hydrolysis.

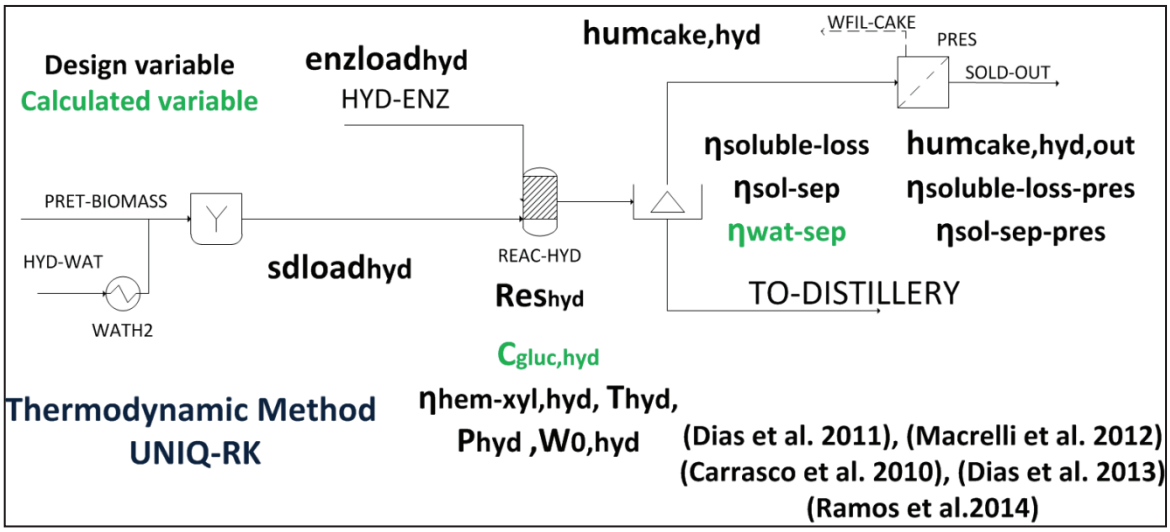

Figure 3:5 Process Flow Diagram for enzymatic hydrolysis section

Table 3:5 Equations and main product for enzymatic hydrolysis reactions

Main Product	Reaction equation
Xylose (C5 sugars)	Hemicellulose + Water → Xylose
Glucose (C6 sugars)	Cellulose + Water → Glucose

This process section has 13 design variables relating to temperatures, pressures, humidity, concentrations and conversion rates. These variables along with their default values are highlighted in Table 3:6. Other variables are calculated as a result, like input water flow rates, separation efficiencies along with output flow rates. On another note, this process section has one heat stream for heating input water, and four power streams related to pumping, hydrolysis, centrifugation and filtration.

Moreover, the chosen thermodynamic method is UNIQ-RK. Finally, Figure 3:5 provides also certain literature references related to this step. We note: (Dias et al. 2011) [69], (Macrelli et al. 2012) [64], (Carrasco et al.2012) [72], (Dias et al.2013) [81], and (Ramos et al. 2014). [71].

Table 3:6 Design parameters for the enzymatic hydrolysis section

Design Parameter	Symbol	Default Value	Design Parameter	Symbol	Default Value
Hydrolysis Solids loading	sdload_{hyd}	5 wt.%	**Nominal power consumption in hydrolysis reactor**	$W_{0,hyd}$	0.3 kWh/m^3
Hydrolysis pressure	P_{hyd}	1 atm	**Humidity of centrifuged cake**	$hum_{cake,hyd}$	65 wt.%
Enzymes loading	$\mathrm{enzload}_{hyd}$	0.1 g enzymes / g cellulose	**Loss of soluble material in centrifugation step**	$\eta_{soluble-loss}$	10%
Residence time in hydrolysis reactor	$\mathrm{Res}_{\mathrm{hyd}}$	24 h	**Solids recovery in centrifugation**	$\eta_{sol-sep}$	100%
Glucose concentration in hydrolysis product stream	$C_{gluc,hyd}$	18 g/L	**Loss of soluble material in press filtration step**	$\eta_{solb-loss-pres}$	0%
Efficiency of xylose production reaction	$\eta_{hem-\mathrm{xyl},hyd}$	41 mol.%	**Solids recovery in press filtration step**	$\eta_{sol-sep-pres}$	100%
Hydrolysis temperature	T_{hyd}	40 °C	**Humidity of output hydrolysis cake**	$hum_{cake,hydout}$	70 wt.%

3.5.3 Xylose biodigestion step

We detail in this section the characteristics of the xylose stream biodigestion step. First off, Table 2:11 highlights the two main conversion reactions occurring in the biodigestor.

Table 3:7 Main conversion reactions occurring in the biodigestor

Consumed organic compound	Reaction equation
Xylose	2 Xylose → 5 CH_4 + 5 CO_2
Glucose	Glucose → 3 CH_4 + 3 CO_2

These reactions involve the conversion of xylose and glucose, the two products of steam explosion, into methane and carbon dioxide. The process flow diagram associated to this step is on the other hand highlighted in Figure 3:6.

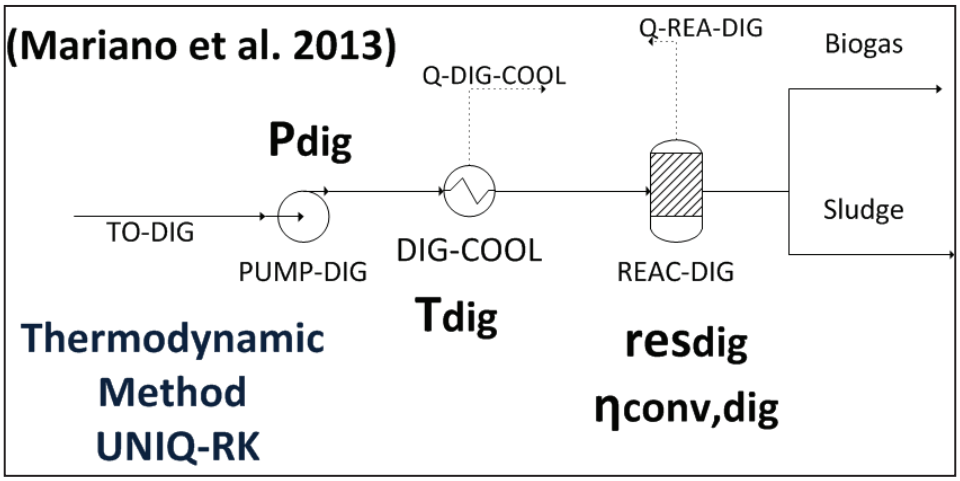

Figure 3:6 Process Flow Diagram for biodigestion section

Finally, the step's design specifications are provided in Table 3:8

Table 3:8 Design parameters related to biodigestion of xylose stream

Design Parameter	Symbol	Default Value
Biodigestion temperature	T_{dig}	40 °C
Biodigestion pressure	P_{dig}	1 atm
Efficiency of organics conversion reaction	$\eta_{conv,dig}$	70 mol%
Residence time in biodigestion reactor	$\mathrm{Res}_{\mathrm{dig}}$	48 h

3.6 Modifications to ethanol distillery: Outcome of glucose rich stream

As indicated earlier and highlighted in Figure 3:3, the glucose rich stream is an additional raw material for ethanol production. This stream enters the distillery at the concentration step and is mixed with the input sugarcane juice. The following steps as well as their related design parameters are identical to those detailed in Chapter 2.

3.7 Modifications to combustion system: outcome of biomass and biogas

The block flow diagram for the cogeneration section is provided in Figure 3:7. We notice first the biogas which is combusted in a gas turbine. This turbine produces electricity along with heat and hot flue gases. We then notice the three biomass streams: leaves, subjected to washing, and bagasse and hydrolysis biomass, subjected to drying via flue gas recirculation. Hydrolysis biomass is mainly composed of the unhydrolyzed biomass fraction combined with the enzymes used for cellulose hydrolysis. These biomass streams are then introduced into a solids burner which produces heat and hot flue gases, later used by the Rankine multi-level steam cycle to produce both steam and electricity. This cycle outputs mild temperature flue gases that are, as indicated earlier, used for drying.

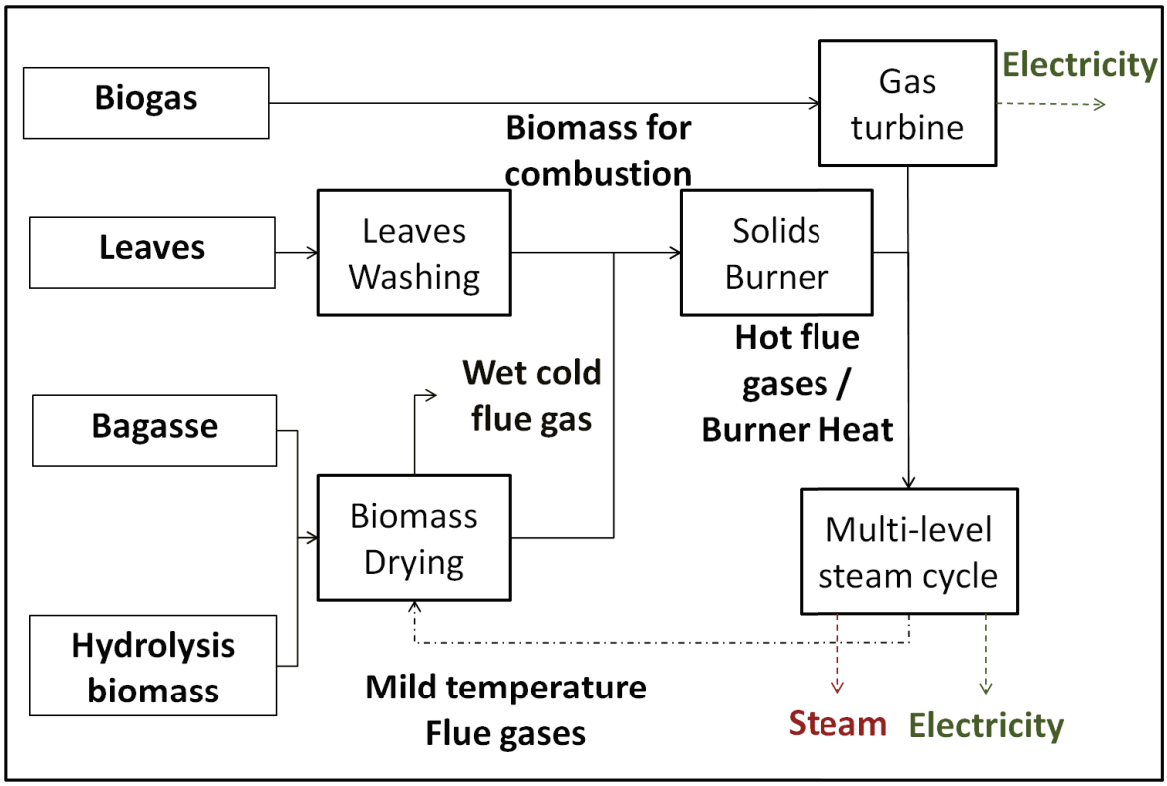

Figure 3:7 Block flow Diagram for the Cogeneration section

With this in mind, Table 3:9 highlights the main reactions occurring in the combustion reactor. These reactions involve the combustion of cellulose, hemicellulose, lignin and enzymes. We should indicate at this level that these reactions are also used in the process related in Chapter 2, save for the enzymes combustion namely due to their absence in the said process.

Table 3:9 Main combustion reactions occurring in solid cake burner

Spent fuel	Reaction equation
Cellulose	Cellulose + 6 O_2 → 6 CO_2 + 5 H_2O
Hemicellulose	Hemicellulose + 5 O_2 → 5 CO_2 + 4 H_2O
Lignin	Lignin + 10.125 O_2 → 7.3 CO_2 + 6.95 H_2O
Enzyme	Enzyme + 1.6825 O_2 → 1 CO_2 + 0.785 H_2O + 0.29 NO_2

Finally, Table 3:10 provides values for design parameters related to the gas turbine, whereas Figure 3:8 highlights its related Process Flow Diagram.

We should indicate that both process sections made use of the UNIQ-RK thermodynamic method and were based on the works of (Mariano et al. 2013) [76]

Table 3:10 Design parameters for the biodigestion ad gas turbine section

Design Parameter	Symbol	Default Value	Design Parameter	Symbol	Default Value
Input air temperature	T_{air-in}	25°C	**Turbine entry temperature**	$T_{pre-gas-tur}$	827 °C
Compressed air pressure	$P_{air-comp}$	18 atm	**Turbine outlet pressure**	$P_{gas-tur}$	1 atm
Gas burner temperature	$T_{gas-bur}$	1127 °C	**Combustion efficiency**	$\eta_{comb-conv}$	100 mol.%

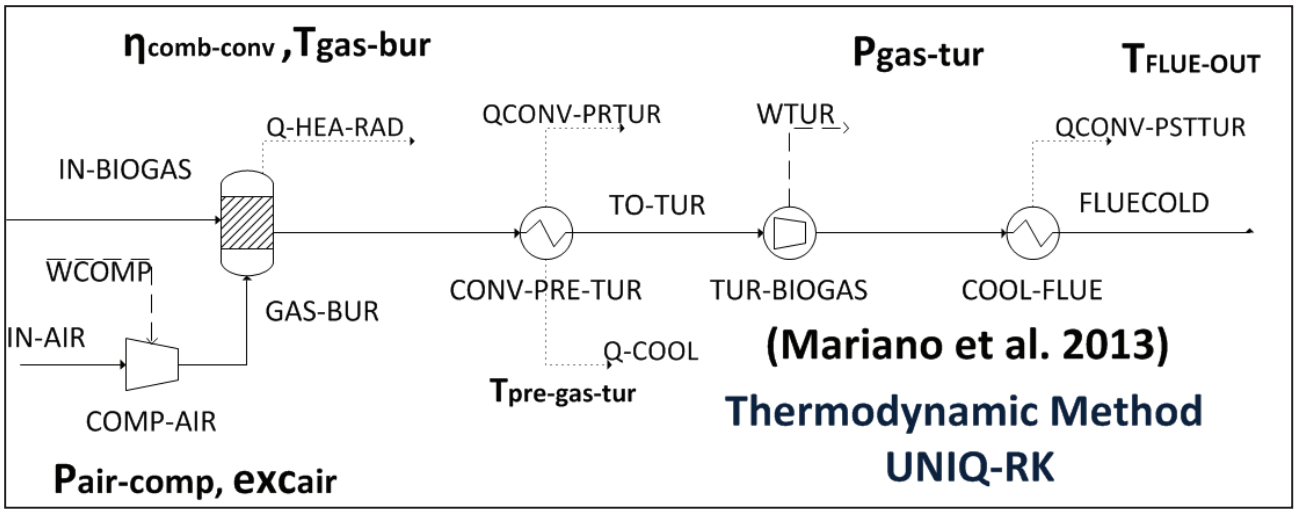

Figure 3:8 Process Flow Diagram for gas turbine section

3.8 Cold utility system

The cold utility system is similar to that highlighted in Chapter 2 and more specifically in Paragraph 2.5.2. In brief, this system has two components: cooling water for regular cooling needs, and refrigeration for low temperature cooling n

3.9 Conclusions for combined distillery, hydrolysis and cogeneration plant

We presented in this section the superstructure for our second studied process: combined distillery, hydrolysis and cogeneration plant. This plant differs from the plant highlighted in Chapter 2 by the presence of a bagasse hydrolysis steps. This steps takes in a fraction of sugarcane bagasse and employs steam explosion pretreatment and enzymatic hydrolysis to obtain a glucose juice which is then considered as an additional raw material for the distillery. This process has two by-products: (1) unhydrolyzed solid fraction which is pres filtered and sent to the conventional combustion system, (2) xylose C5 sugar juice which is biodigested and the biogas burnt in a gas turbine for heat and power production. The downstream distillery, cold utility and steam cycle components of this process are exactly similar to those of the first studied process. For this reason also, only novel steps, like steam explosion pretreatment, enzymatic hydrolysis and organics biodigestion and burning, were discussed in detail and their Process Flow Diagrams shown This

process, along with its constitutive streams and operations was modeled using the Aspen Plus V7.2™ process simulator, following the UNIQ-RK thermodynamic method and the NREL model for component modeling. The process flow diagrams provided also information concerning the related unit operations which consist of: evaporators, reactors, centrifuges, condensers/heat exchangers, distillation columns, mix tanks, dryers and burners. We count 21 unit operations in addition to the operations occurring in the process sections common with the sugarcane to ethanol process, leading to a total of 70 unit operations, whilst excluding the heat exchangers. esign variables were also specified for each section. We count 64 design variables in addition to those related to process sections common with the sugarcane to ethanol process, leading to a total of 140 different design variables. These variables were highlighted both in dedicated tables and on the images relating to the various process flow diagrams. Simulation results were also highlighted in the process flow diagrams, namely concerning the main input and output flow rates of the various sections. One should note that nominal values were adopted (1 kg/h) to utility system flow rates. This is because these results depend on the resolution of the process heat integration problem which will be detailed in a later paragraph. The process heat and power streams were also highlighted in the various process flow diagrams. We count 32 heat streams and 11 power streams in addition to the streams related to process sections common with the sugarcane to ethanol process. This leads to a total of 84 heat streams and 25 power streams. This information is summarized in Table 3:11.

Table 3:11 Main bagasse to ethanol process information along with related count

Process information	Related count
Simulation Program	Aspen Plus™
Thermodynamic Method	UNIQ-RK
Component modeling	NREL model
Process blocks	14
Number of unit operations*	70
Number of design variables	140
Number of heat streams	84
Number of power streams	25

*excluding heat exchangers

This work has allowed us to obtain a solid superstructure for the production of ethanol (and possibly power) from sugarcane bagasse in an integrated facility through the enzymatic hydrolysis route. As a result, this process is now ready for the application of the subsequent parts of the methodology as highlighted in Chapter 1.

Chapter 4 Application of optimal process design methodology to combined distillery and cogeneration process

In this chapter, we will investigate the application of the methodology for optimal process design highlighted in Chapter 1 to the process defined in Chapter 2. In a first step, we will provide a brief review of the employed methodology and the studied process. We will then present a bibliographic review of the main bibliographic works dealing with the studied process. We will then present the application of our methodology, and analyze the obtained results. Finally, comparisons will be made with results from bibliography, and conclusions will be made.

4.1 Reminder of employed methodology

The employed methodology is presented in detail in Chapter 1. Nonetheless, a brief reminder thereof is provided in this section. Considering this, a brief description of the methodology's main points and their operating principle are provided in Figure 4:1, with further details in this paragraph. We notice on this figure the one run simulation, multi-objective optimization and optimal process selection steps. All of these steps are fed by bibliographic data which deal either with the design of the process superstructure as highlighted in Chapter 2 or to the choice of optimization variables, objective functions or selection criteria and scenario. With this in mind, the previously highlighted steps are discussed below.

4.1.1 One Run Simulation

A One Run simulation can be realized once specific values are assigned to process variables. This step starts by first performing a process simulation in ASPEN PLUS ®: the chosen values for process variables are transferred to the Aspen simulation flow sheet; mass and energy balances are performed for each process block. Convergence of this simulation occurs when all design specifications are met, and all balances are respected. In this case, values for controlled operating parameters are calculated for each unit operation as well as parameters for mass, heat and power streams.

Going from heat stream results, we proceed to resolve the process heat integration problem which consists in determining the process heat cascade and the corresponding utility system by the use of a specific linear optimization algorithm, as highlighted in [28] This algorithm operates in

two levels: in a first step, the process streams heat exchange network which minimizes external heat demand is deduced by the use of the heat cascade methodology; then the flow rate of the various utility streams is chosen such that it maximizes a chosen objective function, in our case the cogenerated power stream. Finally, this algorithm deduces also a corresponding cost for the heat exchange network.

Once this is realized, we can proceed to perform a thermo-economic evaluation based on a predefined thermo-economic calculation procedure pertaining to the studied superstructure. This evaluation takes as inputs the results of both process simulation and thermo-economic evaluation, and ultimately returns values for the process performance indicators, otherwise denoted as objective functions.

4.1.2 Process optimization

Multi-objective multi-variable evolutionary optimization can then be performed on the defined system. This optimization converges towards a Pareto set of solutions presenting a compromise between the various objectives. The chosen objective functions are as highlighted in Chapter 1 the maximization of exergy efficiency and the minimization of capital costs. These objectives are conflicting and both contribute to the optimal design of a given process.

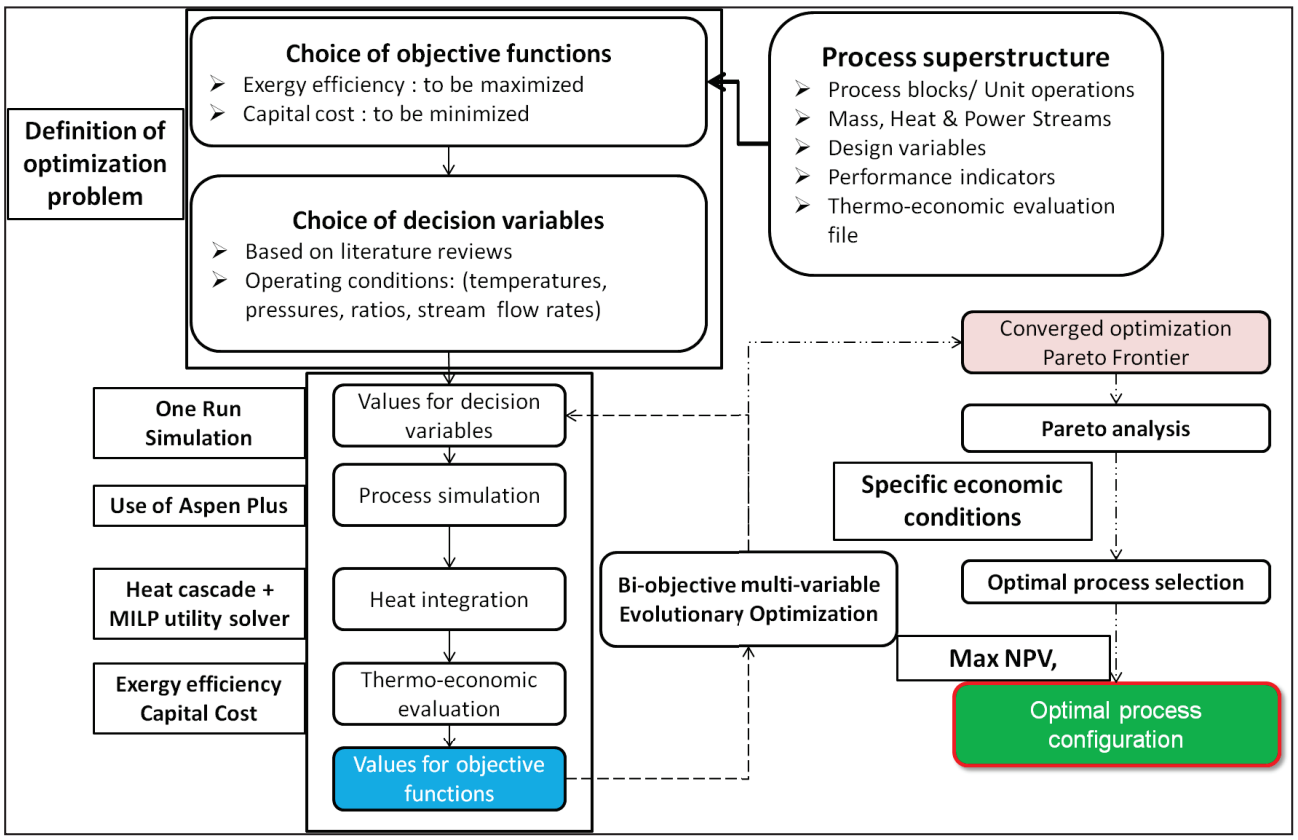

Figure 4:1 Overall scheme for proposed multi-objective optimal process design

4.1.3 Optimal process selection

Specific analysis and selection techniques are finally applied on the obtained Pareto curve in order to deduce one single optimal process configuration. As indicated in Chapter 1, our chosen technique resorts to a profitability analysis under specific or varying economic conditions. This profitability is expressed notably by the maximization of the Net Present Value (NPV) criterion

4.2 Studied process: Combined sugarcane distillery and cogeneration plant

The employed methodology starts off from a given process superstructure, with defined process blocks, unit operations, mass streams, heat streams, power streams and design variables. Considering this, Figure 4:2 provides an illustration of the studied combined sugarcane distillery and cogeneration process superstructure in the form of a Block Flow Diagram, which is decomposed, as we can see, into four sections.

The first section is the ethanol production sections comprising all process blocks leading from sugarcane milling to anhydrous fuel grade ethanol production. These blocks are: sugarcane handling and sugar extraction yielding a diluted sucrose stream (c.a. 12 wt. %), juice concentration via multi-effect evaporation and subsequent sterilization yielding a higher concentration glucose stream (c.a. 22wt. %), glucose fermentation via the Melle-Boinot process yielding a diluted ethanol stream (c.a. 8 wt. %). This wine stream is then sent to a concentration step employing two-column distillation where an azeotropic ethanol-water mixture is produced (c.a. 93.6 wt. %). Finally, the ethanol dehydration stream employing the extractive distillation technology yields a fuel grade anhydrous ethanol stream (c.a. 99.3 wt. %).

The second section takes in sugarcane bagasse extracted from the sugarcane handling section. With a 50 wt.% humidity, this stream is sent through a bagasse drying by flue gas recirculation step and reaches a 25 wt.% humidity. This stream is then coupled to the leaves stream, extracted from the sugarcane field, and burnt in a traditional biomass boiler, which produces both radiative and convective heat streams. Moreover, in most designs, the produced heat has the potential of fuelling all process heat streams, excluding the need for an additional natural gas boiler.

The third section consists of a steam boiler and extracting condensing steam turbine cycle. This system takes in the heat produced by the biomass burner and converts it to lower temperature steam and power. The balance between steam and power production is directly dependent on the process heat integration and power demands. Produced steam, with multiple possible pressure levels, has the objective of heating process cold streams which do not exchange heat with the hot streams. The produced power on the other hand has the potential of being sold to the grid as an additional product, once all process power demands have been met. This is why this section has been labeled as a hot utility for the process.

The final section includes, the cold utility unit consisting of a cold water input stream (c.a. 29°C) heated by the cooling of process hot streams which do not exchange heat with other cold streams.

As a result, the amount of cooling water depends on the heat integration potential of the process. It also depends on the output water temperature, set at 39°C in our case. This section also contains an electricity input stream, which can be potentially used in the case of a positive power demand associated with a given design for the bagasse valorization and ethanol production sections. This is for example the case for a poorly integrated system or for a low pressure steam boiler.

This process is further detailed in Chapter 2 in the form of Process Flow Diagrams containing unit operations along with design variables and design specifications for each process block. As a result, the investigated superstructure has a total of **47** unit operations, **99** design variables, **50** heat streams and **15** power streams.

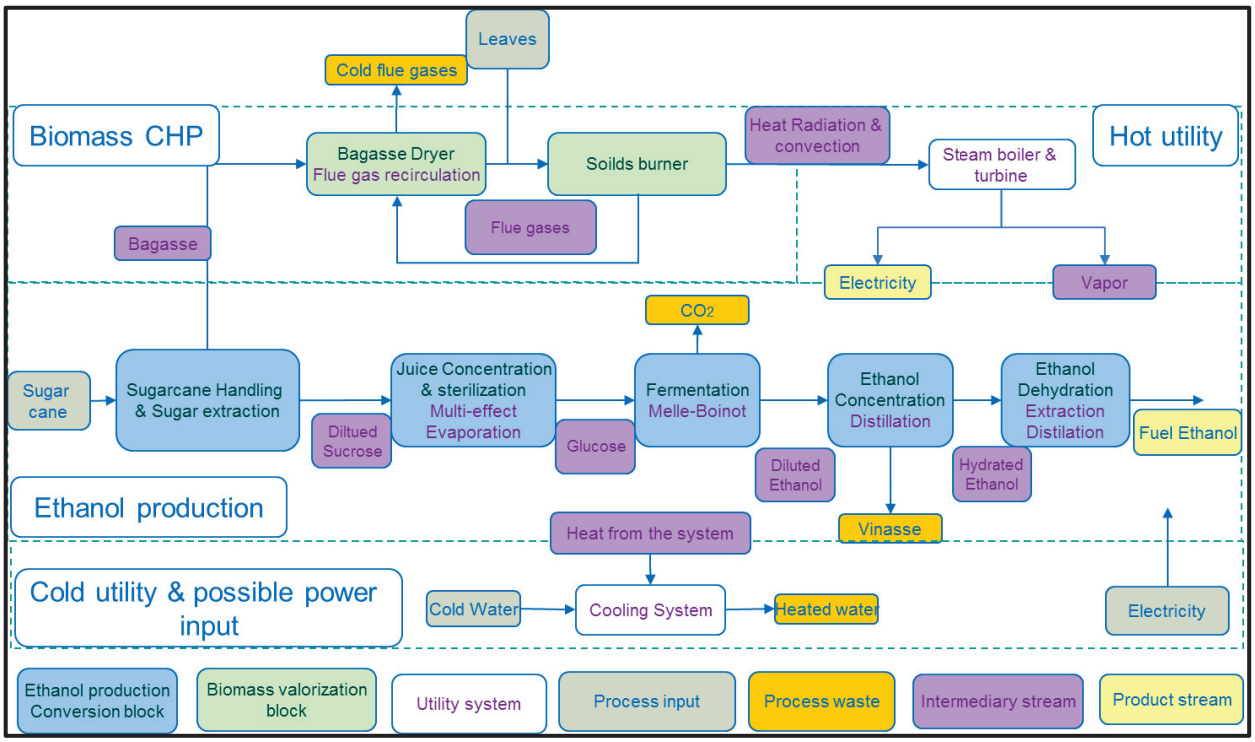

Figure 4:2 Block Flow Diagram for ethanol and power from sugarcane production process

4.3 Bibliography concerning process optimization

With the context of our work defined, we now move towards a review of the key bibliographic works related the optimization of this process

The sugarcane to ethanol process is a consolidated industrial practice. However, its optimization has gained increased interest in recent times. With sugarcane to ethanol conversion presenting a rather mature technology, recent optimization works have concentrated on the production of bioelectricity from bagasse. This interest has increased namely with the possibility of selling power to the Brazilian grid. As highlighted in Chapter 2, this electricity is produced by burning sugarcane bagasse and leaves in a heat and power cogeneration system (CHP). The very nature of this

cogeneration implies the presence of a competition between the energy demands of the process and the extent of power production. This translates to the fact that a greater heat or power demand in the process leads to a smaller power production. The reduction of this energy demand has hence constituted a key aspect of process optimization works. This reduction is realized by operating on three key process sections, pertaining to separation: distillation, dehydration and multi-effect evaporation. Another key optimization aspect found in literature deals with the energy conversion or CHP technology used for bagasse valorization. This aspect translates into the fact that an optimized conversion system leads to a greater power production for the same design of the ethanol production section. Finally, both these aspects were combined in hopes of obtaining an even greater power production. Moreover, these optimizations are often accompanied with an increase in capital and operating costs. This impact was also studied in various literature works. It will hence be highlighted in the course of this review. Considering this, we will present in a first paragraph the ethanol production rates obtained in various literature works along with values for key optimization variables. We will then proceed to highlight works dealing with the optimization of the distillation, dehydration, multi-effect evaporation and CHP production systems before providing the results of a process thermo-economic evaluation. This bibliographic review will enable us to draw conclusions concerning key design parameters related both to ethanol and CHP production. This will ultimately help us define the optimization variables pertaining to our global multi-objective evolutionary optimization problem. We will also be able to identify values for our objective functions, values that will later be compared with our optimization results.

4.3.1 Ethanol production rates as obtained in literature

Sugarcane is the second most important crop for the production of ethanol, making Brazil the second most important global ethanol producer, with the particular characteristic of having a profitable ethanol industry. This importance is ensured in part by the optimal sugarcane to ethanol conversion process, which makes use of a highly efficient sugar extraction process, an optimized fermentation process and a high recovery ethanol separation process. Considering this, the optimization of this conversion process has seen little improvement in recent times, with more interest being directed to the reduction in heat consumption and the increase in power production. Nonetheless, this production rate remains a key performance parameter playing an important role in the global thermo-economic process evaluation. Consequently, Table 4:1 provides values for ethanol production rates, as deduced from literature, along with values for process parameters with a direct impact on this flow rate. From this table, we can see that the main design parameter impacting final ethanol production rate is the sugar content in the input stream. In fact, by comparing [62, 69] we can see that a 7% increase for this variable leads to a 5% increase in ethanol production rate. This parameter however cannot be determined by process conditions and is solely a factor of the input sugarcane quality. On another note, by comparing [69, 82], we can see that a 5% increase in fermentation efficiency leads to an additional 2% increase in ethanol production. Finally, for 13% water content, we can see that the average

ethanol production is equal to 83.5 L/TC, whereas for a 15% concentration, this value is equal to 90.6 L/TC.

Table 4:1 Ethanol production rates and main design parameters as extracted from key research works

Article	[61]	[69]	[62]	[82]	[64]	[63]	[44]
Input sugar content (wt. %)	13.92%	15%	13.92%	15%	13.92%	15.86%	13.85%
Sugar extraction efficiency		96%		95%		96%	96%
Sugars recovery on juice treatment				99.5%			
Glucose to ethanol conversion yield (mol. %)		90%		95%	90%	89%	0.89
Ethanol recovery in separation (wt. %)				99.7%			
Ethanol produced (L/TC)	85	89.3	81.8	83.2	91	85	91.6	82.6

Considering this, we will now proceed to present optimization works dealing with the minimization of the energy consumption and consequent maximization of power production for the sugarcane distillery.

4.3.2 Works dealing with the optimization of the ethanol concentration section

Ethanol concentration is the main process section to be investigated in literature. This is due its great energy demand and its important role concerning the separation of impurities, the recovery of ethanol and the production of a near azeotropic ethanol graduation. As explained in Chapter 2, this section is composed of two distillation columns: one for stripping and the other for rectification. A key aspect dealt with in literature is the heat integration of these two columns by controlling their operating pressures.

[48] studied the thermal integration of two ethanol concentration systems, the first operating at a high pressure (1.52 atm) and the second at a low pressure (0.219 atm), resulting in what is called a forward integrated distillation scheme The wine feed is first equally split between these two systems, and the split fraction is then varied to minimize the specific steam consumption. (SSC) expressed in kg steam/L ethanol produced. Integration was possible, and it resulted in a 54% decrease in SSC with 38% of wine fed to the high pressure column. The authors indicated that this integration resulted in a high heat transfer area, without specifying the obtained value. Moreover, the cooling of low pressure hot streams required the use of an additional water cooling system. This temperature drop was linked to the condensation of CO_2 found in the distillate.

[44] on the other hand assessed the use of backward double-effect distillation as highlighted in Figure 4:3. (b). In the investigated scenario, the stripping column operated under vacuum, and the rectifying column under atmospheric pressure, resulting in a heat transfer from the rectifying column to the stripping column. As a result, the stripping distillation was pumped (compressed for vapor stream) before entering the rectifying column. Moreover, a washing column was added at the top of the stripping column due to the greater loss of ethanol in the degassing stream. A

portion of the phlegmasse was rerouted for the scrubbing performed at atmospheric pressure, leading to the inclusion of a compressor on top of the stripping column. These modifications lead to a small increase in ethanol production (+1%) a 37% reduction in specific steam consumption in the concentration section, and ultimately a 4% increase in power production. This improvement resulted in a 2.69 times higher investment cost for the distillation section. However, the total annual cost for the global process with the optimized configuration was equal to that with the conventional configuration.

[49] built on the previous work and further considered obtaining an almost ethanol-free bottoms stream, using a larger degassing stream for CO2 removal and scrubbing the CO2 gas stream for ethanol recovery. The associated configuration is highlighted in Figure 4:3. (a). Response Surface Methodology (RSM), an optimization technique based on Central Composite Design, was implemented with the goal of reducing the specific steam consumption. The chosen variables were: the ethanol split ratio between the two columns, the number of stages in each column, feed stage location in the rectifying column, ethanol concentration in bottoms, and ethanol purity. The authors concluded that the ethanol split ratio was the most influential factor with other parameters having a smaller impact. The optimization resulted in a 37% reduction in specific steam consumption. A cost analysis on the investigated was also performed with the total annual cost (sum of operating and annualized capital costs) as the chosen indicator. The optimized cases (with and without scrubbing) led to 19% and 25% increases in capital costs, met with 31% and 32% savings in operating costs leading to 8% and 6% savings in total annual cost. This made double-effect distillation with the scrubber the most economical case, followed by the simple double-effect distillation, and finally the conventional configuration.

On another note, [50] studied the use of a Heat Integrated Distillation Column (HIDiC) on the studied system. This configuration acts by raising the rectifying section pressure and placing it in direct contact with the stripping section, enabling interpolate heat exchange, as highlighted in Figure 4:3.(c). In the investigated work, 15 stages were assumed for both sections with 13 heat exchanging stages. Reboiler duty was reduced by 82%, whereas the condenser duty increased by 32%. Also, the condensation temperature was increased by 25 °C. This was counterbalanced by an increase in compressor power consumption, leading to a 70% reduction in total energy consumption. A sensitivity analysis concluded that the pressure difference between the column sections ΔP is the most important parameter. The total annual costs were not calculated, even though related parameters were evaluated. In conclusion, even though this work did not study an industrial situation with an industrial type feed, it presented a solid framework for the application of HIDiC and provided proof for its promising advantages.

Table 4:2 provides a summary of the previous research works. As we can see, the pressure differential was handled in all of the mentioned works. [48, 49] considered forward heat-integrated distillation; [44] backward heat-integrated distillation; and [50] Heat Integrated Distillation Columns (HIDiC). It was shown that the presence of this differential leads to a lower

heat consumption. Other investigated variables were: the number of trays in the columns; ethanol graduation recovery and purity; and feed tray location. These parameters had however a smaller impact, with the exception of ethanol purity and recovery. Moreover, their values were retained for our default process design. Finally, the ethanol split ratio was an additional influential factor in the works of [48, 49].The main performance indicator was the Specific Steam Consumption (SSC) reflecting the energy consumption in the system. A similar indicator, power surplus, was used in [44]. Finally, in cases where economic evaluations were performed the total annual cost TAC was considered as an additional indicator.

Table 4:2 Summary of research works dealing with optimization of ethanol concentration step

Article	Studied scenario	Controlled Variable	Performance indicator
[48]	Study of forward-integrated double-effect distillation, sensitivity analysis	Ethanol split ratio Pressure in both columns	Specific steam consumption
[44]	Backward double-effect distillation Economic evaluation	Pressure in both columns	Specific steam consumption, power surplus, Total Annual Cost
[49]	Forward double-effect distillation, Optimization through CCD and RSM Economic evaluation Study of stream temperatures	Ethanol split ratio, feed stage, number of stages Pressure in both columns	Specific steam consumption, Total Annual Cost
[50]	Study of Heat Integrated Distillation Columns	Pressure differential in columns	Reboiler duty, total heat consumption, heat exchange area

Table 4:3 on the other hand provides a summary of the main operating conditions along with the results for the main performance indicators. As we can see, the lowest value for steam consumption was obtained in the works of [50]. The next lowest value is for the case of double-effect evaluation in [48, 49]. This is due to the less stringent condition on the ethanol content in the phlegmasse. Reductions in specific steam consumption are similar for [44, 49]. Looking on the economic side, we can see that integrated distillation schemes provide a smaller total annual cost with the forward integrated double-effect case having the smallest cost. Finally, Figure 4:3 provides an illustration taken from the bibliographic works concerning the design of the optimized processes.

Table 4:3 Summary of results of research works dealing with optimization of ethanol concentration step

Article	[48]		[49]		[44]		[50]	
Case	Classic	2-effect	2-effect	2-effect w/wash	Base Case	2-effect	Classic	HIDiC
$\dot{m}_{in}$(t/hr)	200				522		245	
$x_{et,in}$(%)	8.10%				6.30%		8.00%	
P_{AA1D}(atm)	1.177	1.52	1.177		0.28		1	
P_{BB1} (atm)	1.013	0.219	0.288		1.16		1	
Ethanol content in phlegmasse (mg/kg)	200	200	59.06		200	200	200	200
SSC (kg steam / L ethanol)	2.15	0.995	1.431		2.67	1.67	2.62	0.78
SSC savings		-54%	-33%	-33%		-38%		-70%
OPEX M$/yr	3.72		2.48		8.08	5.05		
OPEX savings			-33.5%	-33.5%		-37.4%		
CAPEX M$/yr	0.65		1.10	1.08	0.914	2.46		
CAPEX savings			68.5%	66.2%		169.1%		
TAC M$/yr	4.37		3.57	3.56	8.99	7.51		
TAC saving			-18.3%	-18.7%		-16.5%		

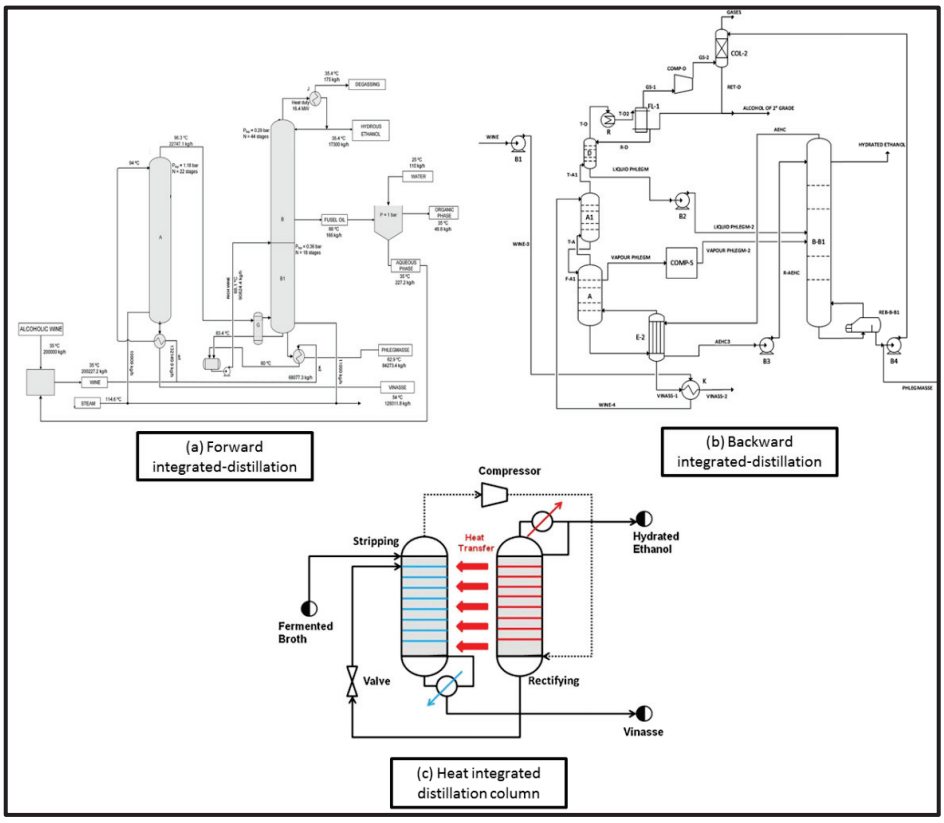

Figure 4:3 Illustrations of process design for (a) forward integrated distillation [49] ,(b) backward integrated distillation [44], and (c) heat integrated distillation column [50].

4.3.3 Works dealing with the optimization of the ethanol dehydration section

The next investigated process section is the ethanol dehydration section. This process takes hydrated ethanol as input and produces fuel grade ethanol at 99.3 wt. % content. The chosen technology in our case was extractive distillation by the use of methyl-ethyl glycol (MEG) as highlighted in Chapter 2. In brief, the ethanol-water azeotrope is broken down in the first column by the action of the MEG solvent. Ethanol is obtained as a pure top product, whereas water leaves with the solvent in the bottoms stream. The solvent is then recovered in a recovery column and recycled back to the extraction column. We will present in this process section research works dealing with this technique.

[83] compared different configurations using a sequence of simple column designs. Total reboiler and condenser duties (Q_{reb}, Q_{conc}) were calculated for each case along with the annualized capital cost($C_{inv,ann}$). They concluded that the use of a partial condenser at the ethanol concentration step, and the liquid (or vapor) recycling of recovery column distillate to the ethanol concentrator were the optimal cases, presenting reductions of 19% (22%) in total reboiler duty, 23% (27%). in total condenser duty and 18% (17%) in total capital costs, when compared to the conventional scenarios.

[54] studied the use of complex column configurations, with the inclusion of thermal couplings. Those configurations included: substituting the extraction column reboiler by a thermal link with the recovery column, replacing the extraction column by a side rectifier, employing one single column with three product streams for both ethanol extraction and solvent, and finally the Divided Wall Column configuration. However, the introduction of these complex configurations did not bring any considerable benefits. This was also confirmed by the works of [84, 85] where the reductions in energy demands or economic costs were minimal compared to an optimized conventional sequence.

More interestingly, optimization techniques were employed for the optimization of this process section. In fact, [55] employed a two-level Mixed Integer Non Linear Programming (MINLP) strategy to **maximize the Total Annual Profit (TAP)** associated with this section. This parameter included the annual value of products, the annual raw material costs and the annualized capital cost. This system was modeled using Matlab® as five separate distillation columns (3 for the extractive column and 2 for the recovery column). Design variables included: the reflux ratio (RR_c), reboiler heat duty (Q_{reb}), the number of stages in each section (N_{stages}), the proportion of reused entrainer (reg_{solv}), the solvent to feed ratio (S/F) and the solvent feed temperature (T_{solv}). Whereas the number of stages is discrete, the remaining variables are continuous. Also, the model has some constant parameters, namely: operating pressure and ethanol purity. The optimization process was initialized from a feasible operating point in order to favor the achievement of the optimum. The two-step optimization methodology breaks down as follows: (1) Values for discrete variables are proposed in a first stage. (2) Values for continuous variables which maximize the objective function and respect model equations are sought. (3) The system

turns in a loop until a satisfactory optimum is obtained. The obtained configuration was 60% more profitable than the original case, however with a higher reboiler energy consumption in comparison to similar works.

Furthermore, [56] employed differential evolutionary programming, a stochastic global optimization algorithm, coupled with process simulation in Aspen Plus, a methodology similar to parts of our chosen methodology as defined in Chapter 2. The chosen objective function was the **minimization of the Total Annual Cost (TAC)**. The authors considered both the ethanol concentration and dehydration sections in two different configurations. The first included a three column sequence (1 for concentration, 1 for extraction and 1 for solvent recovery), whereas the second included an additional liquid–liquid extraction step before the concentration column. Moreover, simulations were realized for four different ethanol concentrations, with the fourth one at 5wt. % ethanol concentration being the closest to our default design. Design variables included: number of stages (N_{stages}), reflux ratios (RR_C), column distillate flow rates ($\dot{m}_D$), and feed stream positions (N_{feed}). Moreover constraints were put on product purities and recoveries. As a result, it was found that the conventional sequence was more optimal than the alternative one for low ethanol concentrations. However, very tall distillation columns (c.a. 90 stages) were obtained.

Finally, [57] applies heat integration methodology on the optimized configurations obtained in [56]. A Mixed Integer Non Linear Programming (MINLP) model was employed for this sake with the goal of **minimizing the total annual costs (TAC)** of the Heat Exchange Network (HEN). For the conventional separation sequence, energy Integration enabled a 5% reduction in reboiler heat duty and a 56% reduction in the heat requirement for the cooling of the solvent recovery stream. This led to a 10% reduction in utility costs and specific steam consumption. This was however accompanied by a 50% increase in heat exchange area. The resulting in-process heat exchange resulted in the heating of the concentration column reboiler via the recovery column condenser and the recycled solvent stream. Finally, the authors also applied mass integration techniques in order to reduce the on the other hand led to an average 96.8% solvent recycle.

Table 4:4 provides a summary of the previous research works dealing with this section. First, we mention that all these works included an ethanol concentration step, and considered similar constraints on ethanol purity and recovery. Key design variables considered in the various works are: the solvent to hydrated ethanol feed ratio (S/F), reflux ratios (RR_c) , the number of stages (N_{stages}), the location of the hydrated ethanol and solvent feed stages (N_{Feed}) and the solvent feed temperature (T_{solv}). [83] [83]included additionally the vapor content of distillate streams and recycle of recovery ethanol distillate. Key performance indicators on the other hand included: reboiler and condenser duties (Q_{reb}, Q_{conc}), annualized investment costs ($C_{inv,ann}$), Total Annual Profit (TAP), and Total Annual Cost (TAC). All those parameters were minimized in the cited works except the Total Annual Profit which was maximized. On a second note, whereas [54, 57] utilized a scenario evaluation procedure, where different cases were evaluated and compare,[55, 56] made use of process optimization techniques in order to seek optimal configurations. In

addition, [57] performed heat integrated on the previously optimal solutions obtained in [56]. Finally, it is interesting to note that the methodology utilized in [56, 57] shares similar points with the methodology adopted in the context of our work. In fact, we find the key steps of process simulation, optimization via evolutionary algorithms and heat integration.

Table 4:4 Summary of research works dealing with optimization of ethanol dehydration (and concentration)

Article	Studied scenario	Controlled Variable	Performance indicator
[83]	Use of Partial or Total Condensers Recycle of recovery column distillate to the concentration column	Nature and position of condensers, Nature of recycle stream	$Q_{reb}, Q_{conc}, C_{inv,ann}$
[54]	Use of complex column configurations : thermal couplings, process intensification, dividing wall columns	Several different process designs were considered	Specific steam consumption
[55]	Two-level Mixed Integer Non Linear Programming strategy. Use of glycerol as solvent	$N_{stages}, N_{Feed}, S/F, RR_C, Q_{reb}, , T_{solv}, reg_{solv}.$	Total Annual Profit (TAP)
[56]	Stochastic global optimization method. Optional use of a liquid-liquid extraction system.	N_{stages}, N_{Feed} $RR_C, \dot{m}_D,$	Total Annual Cost (TAC)
[57]	Heat (and Mass) integration using MINLP models	Possible exchanges between process heat (and mass) streams	Total Annual Cost (TAC)

Table 4:5 on the other hand provides a summary of the main operating conditions along with the results for the main performance indicators. As we can see, a large disparity exists between input stream conditions, and input parameter values. From this table, we can deduce that: the concentration column has a higher reboiler (and condenser) duty than the extraction and recovery columns combined. This heat duty is mainly function of input temperature and ethanol content. Moreover, the solvent to feed ratio seems to have a greater impact on heat demand than the number of stages in the different columns. As we can see, the use of vapor recycles and partial condensation reduces both the condenser and reboiler duties. As a result, the modification of the number of stages, feed stages and reflux ratios alone does not yield optimal results. Moreover, the rather unsatisfactory results displayed by [56] may be related to their poor initial design. On another note, we can see that the results obtained by [54, 83] are even slightly better with those obtained by [55] indicating the importance of proper design. Figure 4:4 highlights two configurations chosen from these works. As we can see, the second configuration highlights an intensified scheme with one column for ethanol extraction and solvent recovery. Finally, it should be noted that only the works of [57] considered the operating temperatures of the various streams by virtue of heat integration. The optimal heat integrated configuration, whose results are shown in Table 4:5, is highlighted in Figure 4:5. In this configuration, we can see that the

concentration column reboiler exchanges heat with the recovery column condenser and the solvent stream cooler. Other heat streams do not inter-exchange heat indicating the potential for further heat integration with the rest of the process. As a conclusion, the control of solvent to feed ratio, partial condensation recycling to concentration column and heat integration will be retained as possible optimization strategies along with the entrainer feed temperature.

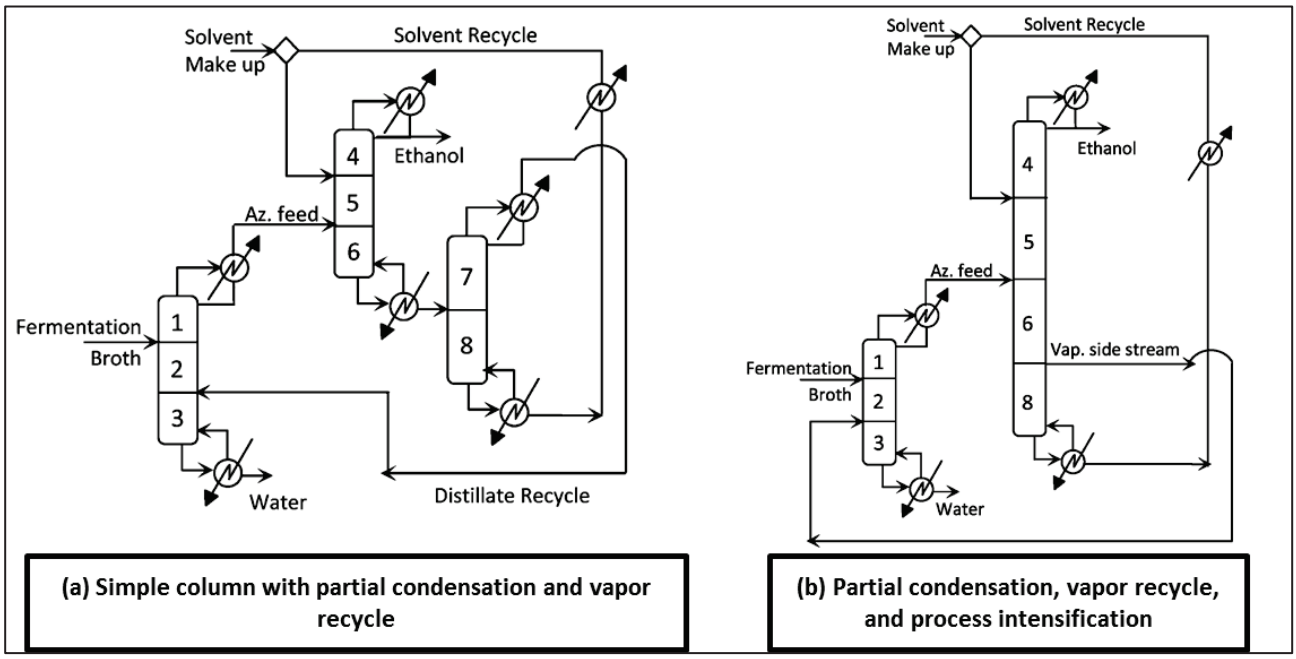

Figure 4:4 Illustration of the distillation configurations as extracted from (a) [83] and (b) [54]

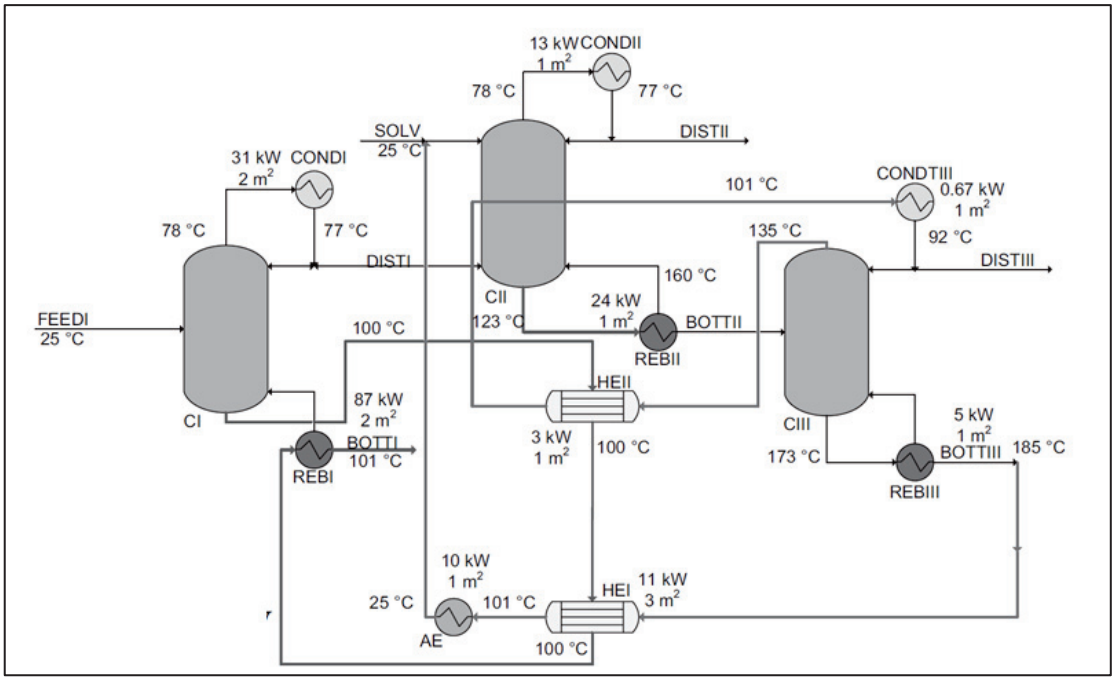

Figure 4:5 Optimized conventional scheme with heat integration as shown in [57]

Table 4:5 Summary of main results of research works dealing with optimization of ethanol concentration (light grey) and dehydration (medium grey) and solvent recovery (dark grey)

Parameters	[83]	[54]	[56]	[57]	[55]
Process description	Simple columns with vapor recycle and partial condensation	Ethanol extraction and solvent recovery	Classic + optimization ([57] with heat integration)		Ethanol extraction and solvent recovery-use of glycerol as solvent
Mass flow rate (t/h)	32		0.8		4
Input ethanol content (wt, %)	12%		12%	5%	93.50%
Ethanol production (kg/h)	4		0.1	0.04	4
Nstages *	44		50	80	-
Feed stage	30		20	35	-
Feed Temperature (°C)	90		25		
Reflux ratio (molar)	0.42	0.25	1.11	1.46	-
Nstages	41	28	77	86	18
Hydrated ethanol Feed Stage	25		58	63	11
Solvent to feed ratio (mol/mol)	0.87		1.56	1.6	0.52
Entrainer feed temperature (°C)					32
Solvent Feed Stage	5		10	27	2
Reflux ratio	0.42	0.25	0.41	0.31	0.04
Nstages	17		26	13	6
Feed Stage	7		19	4	2
Reflux Ratio	0.51		0.3	0.42	0.12
Reboiler duty**	0.99	0.96	1.37	2.40 2.1	
Condenser duty**	0.66	0.65	0.67	0.74	
Reboiler duty**	0.11	0.28	0.62	0.57	0.42
Condenser duty**	0.29	0.33	0.34	0.31	
Reboiler duty**	0.14		0.15	0.12	0.09
Condenser duty**	0.02		0.10	0.07 0.02	
Cooling duty**			1.10	1.12	
Total reboiler duty**	1.24	1.24	2.133	3.095 2.071	0.51
Total Condenser duty**	0.97	0.98	1.11	1.12 1.06	
CAPEX (k$/y)	133.1	107.8	666.2	842.1	

**All duties are expressed in kWh/kg ethanol produced

4.3.4 Works dealing with the optimization of the sugar concentration section

The sugar concentration step is another heat demanding process section. Within the ethanol production process, part of the sugar stream extracted from input sugarcane is brought to a higher concentration before being mixed with the remaining sugar stream faction and sent to sucrose hydrolysis and glucose fermentation, as highlighted in Chapter 2. Higher concentrations are sought in order to reduce the volume of fermentation reactors and reduce the heat requirement for the distillation step and this by producing a higher ethanol content fermentation broths. As a result of this step, the sugar content is brought from an initial concentration of around 11 wt. % to a final concentration in the order of 65%, resulting in a final post-mixing concentration in the range of [18-22.5wt. %]. Multiple-effect evaporation is the traditional technology employed for this sake. This technology has many other applications, namely in sugarcane juice concentration for sugar production where it plays a key role in the said process. As discussed in Chapter 2, this technology makes use of a sequence of multiple evaporators operating in a heat cascade configuration, with the vapor of the i^{th} effect providing heat for the i+1 effect. In addition, a common design condition is the use of steam produced in the first evaporator unit to provide additional heat for other process sections. We speak of vapor bleeding. However, a direct result of this configuration is the fact that other evaporation effects do not exchange heat with the remaining process sections. Considering this, and in an endeavor to reduce the process heat consumption, research works have mainly dealt with the optimal integration of the evaporation step with the rest of the process, along with optimization to the evaporation step per say. Moreover, most of these works have dealt with the sugar production process, with applications to the ethanol production process appearing more recently.

[86] proposed a decomposition of the thermal system by considering the evaporator and the process heating equipment as two interacting subsystems. As a result, the generated vapors are regarded as utilities, and their flow rates were controlled in a targeting scheme with the objective of ***minimizing the total annual cost*** and the constraints of having their sum equal to the amount of discarded water as defined by input and output conditions.

[43] further discussed and highlighted its application on a sugar production process. The following steps were realized: (1) calculation of the heat demand of process steps while excluding multi-effect evaporation, (2) choice of evaporator parameters : number of effects, temperature levels and corresponding vapor bleeds, and finally (3) use of heat integration technique and construction of process composite curves including both process and evaporation streams. It was shown that vapor bleeding at low temperature effects reduces the global consumption of the process. These results also showed that the increase in vapor effects or the increase in vapor bleeding do not necessarily lead to a reduction in global heat demand. The authors hence emphasized the importance of considering an integrated systems analysis.

[42] employed this technique for the thermo-economic optimization of the evaporating system of a sugar producing sugarcane factory, with the objective of ***minimizing the total annual cost*** of the process. Optimization variables included the saturation temperature of the steam generated in the various effects and the vapor bleed in each effect. Constraints were also introduced namely concerning the output sugar concentration and the maximum and minimum possible operating conditions for the evaporators. Contrary to the base case where vapor bleeding occurred only in the first effect, this bleeding occurred across all effects in the optimized case save the last. This is because of this effect's low operating temperature (c.a.60 °C). This scenario led to a 31% reduction in total operating cost accompanied by a 52% increase in investment cost leading to an overall 23% reduction in total annual costs. [87] applied this technique in an optimized combined sugar and ethanol production process, with backward integrated distillation, leading to a 49% reduction in process steam consumption.

[44] applied this procedure to an optimized ethanol production process with backward integrated distillation, albeit by modifying the temperature levels in the various evaporators. It was found that raising the temperature level of the fourth and fifth evaporator results in evaporation with no additional heat consumption.

[28] built on previous works and proposed a different technique for the reduction of the heat demand of a combined ethanol and sugar production process. This technique employs a nested optimization algorithm similar to that highlighted in Chapter 1. The outer level evolutionary algorithm controls the values of process intensive parameters; whereas the inner level linear programming algorithm determines the minimum hot and cold utility consumptions, by the use of Heat Integration. Process parameters controlled by the outer algorithm included: the number of evaporators, along with the increment in solids content, and the decrement in temperature level in each effect. This optimization led to a design with a 39% reduction in minimum energy consumption. The obtained design had two characteristics. The first is the lower increment in solids content after the first level when compared to the base case, while the opposite is true for remaining levels. The other main difference is the decrease in temperature decrement between the evaporators, leading to higher evaporation temperatures when compared to the base case. Through these improvements, the evaporator system was capable of providing heat both for the distillation and the sugar production systems.

Finally, [88] proposed the use of vapor recompression technologies to heat high temperature levels with condensates from low temperature level. This technology however leads to negligible reductions in steam consumption at the expense of higher power consumption and a greater capital cost.

Table 4:6 provides a summary of the previous research works dealing with this section. As we could see; most works considered the heat integration of evaporation with other process streams. In most of these works, these units were considered as a utility system for the rest of the process

with the capacity to provide steam at various temperature levels. As a result, vapor flow rates (or bleedings) in the various evaporators (VF_i) and evaporator temperature levels ($T_{ev,i}$) were controlled with the goal of reducing either process energy requirements or total annual costs, and this for different numbers of units$N_{ev,i}$. Moreover, some of these works considered fixed heat exchange configurations, whereas others applied heat integration and generated process composite curves. Finally, [28] applies a nested optimization algorithm, similar to the one proposed in Chapter 1 with an outer evolutionary algorithm controlling evaporation parameters and an inner algorithm calculating minimum process energy requirements. However, instead ofVF_i, the increment in sugar concentration ($\Delta C_{evap,i}$) was the control variable. On a side note, It should be noted that all optimization systems included upper and lower on operating temperatures and vapor flow rates. On the other hand, only [87] included the investment costs in their optimization.

Table 4:6 Summary of research works dealing with optimization of multiple-effect evaporation steps

Article	Studied scenario	Controlled Variable	Performance indicator
[86]	Sugar production. Decomposition of thermal system. Evaporators and other process parts considered as two separate sub-systems	VF_i	Total Annual Cost (TAC)
[42]	Sugar Decomposition of thermal system Calculation of investment and operating costs	VF_i, $T_{ev,i}$	Total Annual Cost (TAC)
[87]	Sugar and ethanol production. Optimized vapor bleeding and backward integrated distillation.	VF_i	Minimum energy requirements (MER)
[43]	Sugar production. Decomposition of thermal system Evaporators considered as utility streams, heat integration	VF_i	Minimum energy requirements (MER)
[28]	Sugar and ethanol production, multi-objective optimization, heat integration	Δc_i, $T_{ev,i}$, $N_{ev,i}$	Minimum Energy requirements (MER)
[44]	Ethanol production, backward integrated distillation, heat integration	$T_{ev,i}$	Minimum Energy requirements (MER)

Table 4:7 on the other hand highlights the results of the works with ethanol production in their process scheme. As we can see, the optimization leads to an upward shift in the operating pressures of the evaporators and to a modification in the vapor flow rates of each effect, expressed in the vaporization rate as defined in Chapter 2. As we can see also, the combination of heat integration, optimized distillation and optimized multi-effect evaporation can lead to 50% reductions in steam consumption.

Finally, Figure 4:6 shows two composite curves from cited works. Figure 4.4 (a) highlights integrated composite curves plotting multi-effect evaporation streams against other process streams. As we can see, this section integrates perfectly with the remaining process. Figure 4.4 (b) on the other hand highlights the General Composite curves for a combined ethanol and sugar production process. As we can see, the first four effects operate at a temperature level greater than that of the distillation column whereas the last effect has a similar temperature level. In addition to their difference in representation, these two graphs differ in the fact that the first system does not include certain process heat streams namely distillation heat integrated stream (boiler of stripping column, condenser of rectifying column, feed preheating and product cooling), whereas the second system includes all possible heat streams in the heat integration problem. The last approach is the one chosen in our methodology. Finally, by analyzing the cold and hot heat demands of the process, we can see that both processes have a similar hot requirement of 60 MW, whereas the cold heat requirement in the first graph is 50% smaller at 25 MW, and this thank to the inclusion of double-effect distillation.

Table 4:7 Summary of main results for the optimization of multiple-effect evaporation steps for ethanol production

Process description	**Sugar and ethanol production half and half**				**Ethanol production**	
Article	**[87]**		**[28]**		**[44]**	
Case	Base case	Optimized case	Base case with heat integration	Optimized case	Base case	Optimized case
Pressures (atm)	1.69, 1.07, 0.76, 0.46, 0.16	1.69, 1.38, 1.12,0.75, 0.16	1.69, 1.07, 0.76, 0.46, 0.16	1.69, 1.16, 0.8, 0.53, 0.31	1.69, 1.31, 0.93, 0.54, 0.16	1.69, 1.31, 0.93, 0.71, 0.51
Vaporization rates			53%, 9%, 12%, 12%, 13%	15%, 30%, 30%, 11%, 13%	20% (x5)	
Steam consumption (kg/ t cane)	540	278	330	228	467	214
Reduction in steam consumption		-49%		-31%		-54%

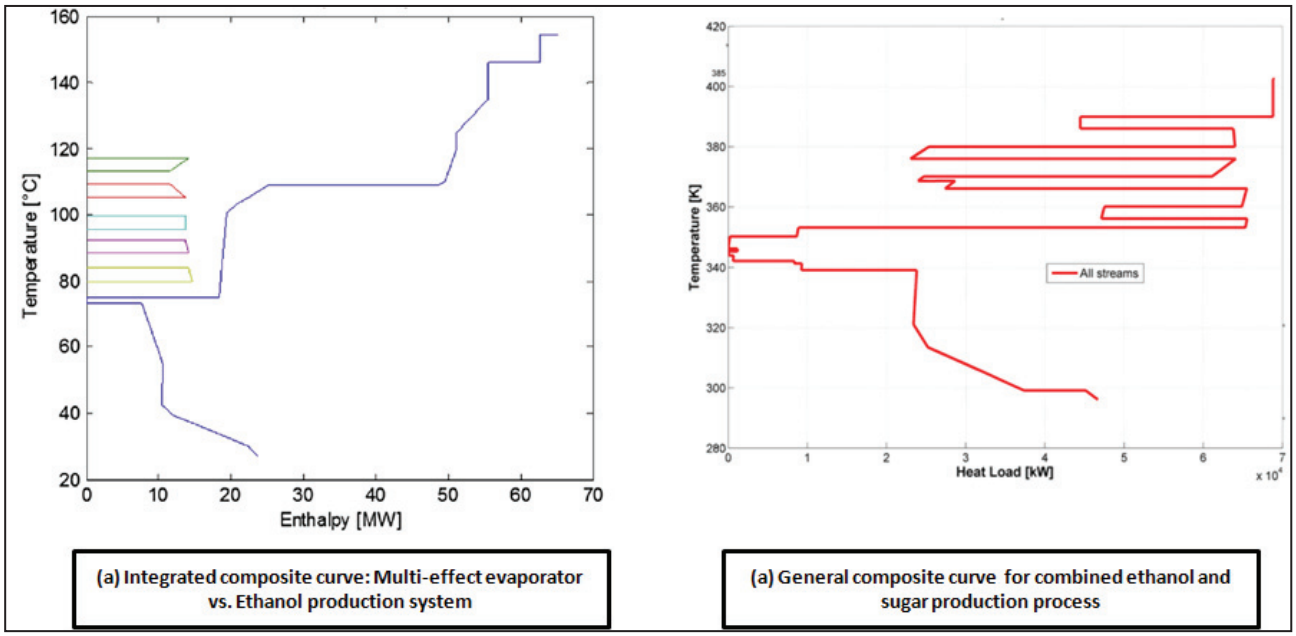

Figure 4:6 Composite curves for ethanol production process (a) Integrated composite curve [44], (b) General composite curve [28]

Moreover, concerning the calculation of investment costs, Ensinas et al. 2007a used the Robert equation highlighted in Equation 4:1 for the calculation of the heat transfer coefficient. By analyzing this equation, we can that this coefficient decreases with decreasing temperature levels ($T_{evap,i}$) and increasing solids concentration ($C_{evap,i}$). As a result, the inclusion of investment cost leads to a design with higher operating temperatures and a greater vapor bleeding in the first effects, contradicting the previous vapor bleeding concept. The importance of the inclusion of this cost is stressed by the authors who highlight its importance when compared to regular juice heaters. Moreover, this equation was adopted for our model as indicated in Equation 4:1.

Equation 4:1 Robert equation for calculating evaporator heat transfer coefficient

$$U_{evap,i}\left(\frac{kW}{m^2°C}\right) = \frac{0.465T_{evap,i}(°C)}{C_{evap,i}(wt.\%)}$$

Finally, the cited authors indicated the existence of several design issues related to multi-effect evaporation. The first issue deals with the elevation in evaporation temperature normally associated with the presence of sugars in the water stream [21, 45]. This point leads to an evaporation temperature greater than the corresponding condensation temperature. Moreover, this elevation is greater for the final levels where the sugar concentration becomes more important.

Another cited issue deals with the partial vaporization of sugar juice when throttled to a lower pressure level [43]. This point leads to a value for the energy of vaporization smaller than that for condensation.

4.3.5 Bibliographic work on combined heat and power production from bagasse

As highlighted earlier, bagasse, one of the main by-products of the ethanol production process, is usually burnt in biomass boilers in order to provide heat for the previously highlighted process sections. The traditional approach consisted in employing low pressure (22 atm) and low steam temperature (300°C) systems with back-pressure turbines to fuel the process. However, this produced heat was in most times greater than the required amount [61]. This has lead designers to include an optimized combined heat and power production section. This alternative has become even more interesting in the context of selling decentralized power to the grid, and of a reduced process steam consumption through an optimized design as highlighted in the previous paragraphs. This optimized CHP system contains: higher boiler pressures, higher steam temperatures, addition of an extraction-condensing turbine, and the use of leaves as an additional fuel. Moreover, the standard practice in most works is to simulate this step for a defined process design. As a result, this step is considered as a utility system, for which the optimal values yield a ***maximized net power production, whilst respecting process energy requirements***. Considering this**,** Table 4:8 presents the results for key research works making use of bagasse boilers and CHP technology. First of all, by comparing the results [69], we can see that an optimized process configuration, with backward integrated distillation and vapor bleeding in the multi-effect evaporator, leads to a 13% increase in power production, accompanied by a 20% decrease in steam consumption. Moreover, the additional inclusion of leaves leads to a 78% increase in power production, to a value of 186 kWh/TC (ton sugarcane). We can see a similar trend in the work of (Dias et al., 2012) where the power production reached 173 kWh/TC, for a similar optimized process with leaves combustion. Moreover, as we can see, there is no power production for low pressure boilers. The works of (Dias et al., 2011) and **(**Palacios-Bereche et al., 2015) on the other hand highlight the importance of including process-wide heat integration in addition to the optimized process configuration. This configuration leads to respective 22% and 27% increases in power production, with 50% reductions in steam consumption. In addition, by comparing the results of (Dias et al., 2011) [69] and (Palacios-Bereche et al., 2015) [44].we can see that the increase in boiler pressure and steam temperature leads to an additional increase in power production (32% for the non-optimized non-integrated case, and 27% for the optimized and integrated case). On another note, the works of (Seabra and Macedo, 2011) [58] and (Furlan et al., 2013) [63] provide additional literature results. Both works include an optimized process configuration with leaves combustion. However, both processes have low electricity surplus when compared to other processes with a similar configuration. This could be attributed to the lower operating pressures (65 atm vs. 90 atm.). We add to these process the results of [64] which highlighted a similar 142 kWh/TC power production.

On another note, [28] includes a process optimization work similar to that highlighted in Paragraph 4.3.4, with the objective of maximizing the net power production of the system. Like previous works, bagasse was burnt in a high pressure boiler (100 atm), with steam superheating (527°C) and an air excess of 0.3. This work however differs from previous works in the inclusion of

a bagasse drying step, bringing the bagasse moisture to a value of 25%. Optimization variables related to the multi-effect evaporator (temperature, concentration and number of units) were included in the outer evolutionary algorithm. The inner linear algorithm on the other hand sought the optimal heat integration configuration for a given set of optimization variables. Like other works, the authors made use of a back-pressure and condensing/extracting steam turbines. Moreover, whereas the operating pressure of the condensing turbine was set at 1.92 atm, that of the back-pressure turbine was chosen as a optimization variable to be controlled by the outer evolutionary algorithm. In addition, the steam mass flow rates at the various levels ($\dot{m}_{steam,j}$) were chosen as optimization variables for the inner linear algorithm, as highlighted in Chapter 1. The said optimization resulted in a 154 kWh/TC power production, with the same parameters for multi-effect evaporation as those found in the previous MER minimization problem, and an expansion of back-pressure steam to low levels (0.1 atm). By comparing these results to those obtained by [44], which operates at similar boiler conditions, we can see that [28] obtained a 50% increase in power production. This can be linked both to the optimization problem per say, but also to the cake drying step.

Finally, [28] realized this optimization on a cogeneration system based on an integrated gasification combined cycle. The optimized problem leads to a 234 kWh/TC power production, a 52% increase over the previous system. This substantial increase was also recorded by [81], where an 80% increase, from 79.61 kWh/TC to 144 kWh/TC, was noted. However, even though this alternative provides substantial benefits in power production, it is not as of today a commercially viable technology. Finally, [28] noted the positive impact of including more steam extraction levels. In fact, this inclusion resulted in an additional 5% increase in power production for the integrated gasification cycle, at a 245 kWh/TC power production.

Considering this, Table 4:8 and Table 4:9 provide both the main hypotheses and the key results respectively, as relating to the previous literature works and their considered scenarios. The recorded results pertain to the steam consumption and power consumption, as well as their respective reduction and increase through optimization in comparison to the recorded base cases. With this in mind, the inclusion of leaves combustion enables the highest increase in power production at 78%. The inclusion of heat integration on the other hand enables a 13 to 27% increase in power production, with a 20 to 54% percent reduction in steam consumption.

Table 4:8 Hypotheses for main works including a bagasse boiler and CHP production system

Article	[69]	[61]		[81]	[44]	[82]	[63]	[28]
Optimized process	x		x	x	x	x	x	
Leaves Combustion	x		x			x	x	
Heat integration				x	x			x
Optimization								x
Cake moisture (wt. %)				50%				25%
Water Pressure (atm)	90	22	90	80	100	65	65	100
Steam temperature (°C)	520	300	520	510	530	480	520	527

Table 4:9 Results for main works including a bagasse boiler and CHP production system in the evaluation

Article	[69]			[61]			[81]		[44]		[82]	[63]	[28]
Steam consumption (ton/TC)	0.4	0.3	0.5	0.3	0.4	0.2	0.4	0.4	0.2	0.3	0.3	0.2	
↓in steam consumption (%)		20%		28%			52%		54%				
Power surplus (kWh/ton SC)	93	105	186	0	173	63	80	83	84	102	130	144	154
↑ in power surplus (%)		13%	78%					27%		22%			

4.3.6 Summary of main thermo-economic results

With the previous points being considered, Table 4:10 provides a thermo-economic evaluation of the various processes for the production of power and ethanol from sugarcane as found in literature, joint with a brief reminder of the works' main hypothesis. By comparing, the main economic hypotheses, we can see that all works have considered a similar salvage equipment value (0 M$), a similar depreciation rate (10 years-linear), construction period (2 years) and tax rate (34%). Moreover, all works considered a project lifetime of 25 years except [64] who considered a 20 year period. Likewise, all works considered 167 days of operation in a year, except [63] who considered 210 days. Finally, the interest rate was highest for [44] at 15%. The average assumed sugarcane price was equal to 24.28 $/TC with a coefficient of variation of 19% ($\frac{STDEV}{AVERAGE}$). Only two works considered sugarcane trash prices which had an average value of 16 $/kWh and a coefficient of variation of 9%. Ethanol prices on the other hand had an average value of 0.536 $/L

with a coefficient of variation of 8%. Finally, electricity prices had an average value of 72.6 $/MWh and a coefficient of variation of 11.5%. Finally, it is interesting to note that all technologies took a sugarcane input rate of 500 TC/h.

Table 4:10 Thermo-economic results for main research works dealing with production of ethanol and power from sugarcane

Article	[69]			[89]	[64]	[63]		[44]	
Sugarcane rate (TC/h)	500								
Optimized process		x	x	x		x		x	x
Leaves combustion			x	x	x	x			
Heat integration									x
Ethanol produced (L/TC)		89.3		83.2	85	91.6	81.9	82.6	82.6
Electricity surplus (kWh/ton SC)	93	105	186	173	142	144	86	83	102
Investment cost (M$)	199	202	222	263	117	165	143.3	153.3	157.4
Project lifetime (years)		25			20		25		
Salvage equipment value (M$)	0								
Construction and start-up (years)	2								
Depreciation (years)	10- Linear								
Days of operation			167			210		167	
Tax rate (income and social contributions)	34%								
Interest rate (%)					10%	11%		15%	
Sugarcane price ($/TC)		19.41		23.25	20.40	28,76		29.40	
Sugarcane Trash Price ($/TC)			15	17.05					
Ethanol price ($/L)		0.5		0.60	0.53	0.513			
Electricity price ($/MWh)		70.5		84.88	66.00	69			
MESP ($ / L ethanol)	0.307	0.303	0.288	0.37	0.264	0.29			
MPSP ($/MWh)	45.26	44.97	44.7	52.63					
IRR (%)	15.70%	15.90%	16.90%	14.90%	32.10%	7.60%			
NPV M$						-34.5			

Table 4:10 also provides results for various economic indicators.

The first indicator is the Minimum Ethanol Selling Price (MESP), expressed in $/L ethanol. Two formulations exist for the calculation of this indicator. The first considers this indicator as the sum of all the operating costs and the annualized capital cost, whilst considering the electricity price as

an opportunity cost. This is the approach taken by [63, 64, 69, 89]. Another approach highlighted in [89] defines the MESP as the price required (at the factory level, without sales taxes) for a zero internal rate of return for a given electricity price. In both cases, the MESP can be seen as the minimum acceptable ethanol price if the plant does not want to lose money. By comparing the results of [69], we can see that the increased power production due to process optimization and additional leaves combustion lead to 1.3% and 6.2% reductions in MESP. From this analysis, we can see that the highest MESP value (0.37 $/L ethanol) was obtained by [89]. This value can be linked to the high sugarcane price (23.25 $/TC) and high investment cost (263 M$). The lowest value (0.264 $/L ethanol) on the other hand is obtained by [64]. This can be linked to both their low investment cost (117 M$) and low sugarcane price (20.4 $/TC).

The second indicator is the Minimum Power Selling Price (MPSP). The previous two formulations also exist for this indicator. The only difference being the fact that ethanol is considered as the fixed-price by-product in this case. Thus, the MPSP can be seen as the minimum acceptable ethanol price if the plant does not want to lose money. By comparing the results of [69], we can see that the increased power production due to process optimization and additional leaves combustion lead to 0.6% and 1.2% reductions in MPSP, variations that are lower than for MESP. From this analysis, we can see that the highest MPSP value (52.63 $/MWh) was obtained by [89]. This value can also be linked to the high sugarcane price (23.25 $/TC) and high investment cost (263 M$). The lowest value (44.7 $/MWh) on the other hand is obtained[69]. This can be linked to both their lower investment cost (222 M$) and sugarcane price (19.41 $/TC).

The third and fourth indicators are the Internal Rate of Return (IRR) and Net Present Value (NPV). Whereas the first is calculated as the cash flow discount rate yielding a zero Net Present Value (NPV) for the project lifetime, the second represents the sum of the various discounted cash flows at a given discount rate. As a result, a project is considered profitable if its IRR is greater than a designer-set value, denoted in Table 4:10 as the discount rate, or if its NPV is greater than zero. Moreover, when comparing two projects, a project is more profitable than another if it has a higher IRR, or a higher NPV.

By comparing the results of Table 4:10, we can see that the higher IRR (32.1%) is obtained in the works of [64]. This is due to a combination of high power production, low investment costs, low sugarcane prices, and high ethanol prices. Moreover, we can see, the second most profitable project (16.9%) is that of [69] involving an optimized process coupled with the combustion of leaves. This is due to a high power production and a low sugarcane price (the lowest). In addition, we can see that the results of [63] provide the lowest IRR values (7.6%). This is due to the high sugarcane prices (28.76 $/TC). We can also see that this value is lower than the chosen discount rate (11%), meaning that the project is not profitable. This is asserted by the negative value obtained for the NPV (-34.5 M$). Sadly, no other authors provide values for this variable. Moreover, the absence of economic calculations in the works of [44] prevented the analysis of the

chosen configuration. This present analysis provides a setting and a scope for our optimization work whose outcome will be compared against the previously highlighted results.

In summary, we see that, as expected, an increased power production leads, under constant ethanol production and fixed economic conditions, to a higher value process. The same applies to a lower investment cost. As a result, any optimization work will have the dual objective of increasing the net power production and reducing the process investment cost. However, the optimal profitability of any conversion process depends on the economic conditions. Namely, a lower sugarcane price along with higher ethanol and electricity selling prices lead also to a higher value project.

4.3.7 Summary of optimization work

The previously cited works give us a better idea of the main points to be handled in any optimal design work dealing with ethanol and power production from sugarcane. The main topic of the previous works was the reduction of process steam consumption, and as a direct result, the increase in its power production in the adjacent CHP system. This reaction, or increase, is however met by an increase in investment costs. Consequently, the ethanol and power production from sugarcane process is a prime example of a multi (double)-objective problem. This optimization can be realized by controlling several process design parameters pertaining to the distillation, dehydration, multi-effect evaporation and combined heat and power production steps. In addition, this process disposes of an optimal process selection criterion which is the Internal Rate of Return (or the Net Present Value).

Finally, Table 4:11 provides a definition of the ethanol and power optimization from sugarcane optimization process, with the objective functions and main decision variables, as deduced from the previous literature review. Comments and indications are also provided for each parameter as deduced from the analysis of literature. References are finally provided for works dealing with the various sections.

On another note, Table 4:11 considers a decomposition for the optimization problem into an outer evolutionary algorithm and an inner linear algorithm as realized in [28]. To this nested formulation, we can add the lower layer of process simulation by the use of Aspen as is done by [57] and an additional intermediary layer for process thermo-economic evaluation cost similar to the one realized by [42].

Finally, most of the previous works dealt with only the optimization of only one process section, with the remaining works dealing with these optimizations in a sequential way, with the exception of [28] who performed a global optimization with optimization variables pertaining to both multi-effect evaporation and CHP production. As a result, a global optimization problem considering optimization variables pertaining to different process sections may lead to uncharted territories in both increasing net power production and reducing investment costs.

Table 4:11 Definition of the ethanol and power optimization problem as deduced from literature

x		Comments and indications	References
Objective functions	Reduce Minimum Energy Requirement	↓steam consumption	
	Increase net power production	↓ steam consumption, ↓conversion efficiency, greater profit from sales,	
	Reduce capital cost	↓ initial investment, ↓ maintenance costs	
Process section	**Optimization variables**	**Controlled by the outer-evolutionary algorithm Key trends**	
Distillation	Rectifying and striping column pressures Vapor content of rectifying column distillate Wine feed split ratio in case of double-effect distillation	A pressure differential, a ↑ vapor content and an optimal feed split lead to ↓ steam consumption and ↑ power production, but with ↑capital costs, namely for back-ward integrated distillation	[44, 47, 49, 50, 83]
Dehydration	Solvent temperature Solvent to hydrated ethanol ratio	A ↓ solvent temperature and an optimal solvent ratio lead to a ↑ power production. Their effect on investment cost was not documented	[54–57, 83]
Multi-effect evaporation	Temperature levels in evaporators Vapor bleedings in evaporators Number of evaporators Sugar content in concentrated juice	↑ pressure levels, a ↑ potential for vapor bleeding, namely in the lower levels and a greater sugar concentration lead to ↑ power production rates, albeit for ↑ capital costs. The ↑in number of evaporators has little impact on power production with no recorded impact on capital costs	[42–44, 86, 87]
Bagasse boiler and CHP system	Boiler pressure Steam production temperature Number of turbine extractions Pressure levels in steam turbine	↑ boiler pressures, ↑ steam production temperatures lead to ↑ power , an ↑ in the number of turbine extractions and the appropriate placement of these extractions lead to ↑ power production with ↑ investment cost	[21, 44, 63, 69, 81, 82]
Process section	**Controlled variables**	**Comment**	
Bagasse boiler and CHP system **Heat integration**	Boiler water and steam mass flow rates Heat streams, defined for a given set of optimization variables	Controlled by the inner linear heat integration algorithm with the objective of maximizing net power production	[28, 44]

4.4 Definition of framework for optimization work

We provide in this section a definition of the framework for the optimization work. This framework includes: the choice of the objective functions along with their calculation method, the choice of optimization variables and the adaptations made to the optimization algorithm.

4.4.1 Choice and calculation of objective functions

The second step of the methodology consists in choosing the objective functions and defining their calculation routes and their desired fate. As indicated in Chapter 1 exergy efficiency, and capital cost are common examples of interesting and conflicting objective functions. In fact, the first needs to be minimized and the second to be maximized in any optimization endeavor. Considering this, we provide in this paragraph literal expression of their values for our studied process.

4.4.1.1 Calculation of process exergy efficiency

As indicated in Chapter 1, exergy efficiency is calculated as the ratio of the exergy of product streams to that of input streams. It is hence an indicator of the process' conversion efficiency, and ultimately of its profitability.

Considering this, the exergy input/output balance for the ethanol process is highlighted in Table 4:12. Input streams include: sugarcane and leaves. Output streams on the other hand include ethanol and power production activated only once the process net power is positive. Mass flow rates are expressed in tones/hour $\left(\frac{t}{h}\right)$ whereas energy rates are expressed in Megawatts (MW). Moreover, nominal exergy contents are expressed in $\frac{MWh}{t}$ for mass streams whereas it is unit less for power streams. The final exergy is but the multiplication of the specific rate by the nominal exergy content and is expressed in MW, as indicated in Chapter 1.

Table 4:12 Exergy balance for the ethanol and power from sugarcane production process

Component	Flow rate	Nominal exergy content	Total exergy content (MW)
		Input streams	
Sugarcane	$\dot{m}_{cane}(\frac{t}{h})$	$ex_{cane} = 1.582\ (\frac{MWh}{t})$	$Ex_{cane} = \dot{m}_{cane} \times ex_{cane}$
Leaves	$\dot{m}_{leaves}\ (\frac{t}{h})$	$ex_{leaves} = 4.4\ (\frac{MWh}{t})$	$Ex_{leaves} = \dot{m}_{leaves} \times ex_{leaves}$
		Output streams	
Ethanol	$\dot{m}_{ethanol}\ (\frac{t}{h})$	$ex_{ethanol} = 8.21\ (\frac{MWh}{t})$	$Ex_{ethanol} = \dot{m}_{ethanol} \times ex_{ethanol}$
Power production	$W_{out}(MW)$	$ex_{W_{out}} = 1\ ()$	$Ex_{W_{out}} = W_{out} \times ex_{W_{out}}$

Finally, considering the exergy contents of the various input and output streams defined in Table 4:12, provides the literal equation for the exergy efficiency of the ethanol and power from sugarcane production process.

Equation 4:2 Literal expression of exergy efficiency for the ethanol and power from sugarcane production process

$$\eta = ex_{eff} = \frac{Ex_{Prod}}{Ex_{in}} = \frac{Ex_{ethanol} + Ex_{W_{out}}}{Ex_{cane} + Ex_{leaves}} = \frac{\dot{m}_{ethanol} \times ex_{ethanol} + W_{out} \times ex_{W_{out}}}{\dot{m}_{cane} \times ex_{cane} + \dot{m}_{leaves} \times ex_{leaves}}$$

Finally, considering this formulation, the maximization of exergy efficiency is equivalent to maximization of power production, and ultimately minimization of process steam and energy requirement, in the case of fixed process inputs and fixed power production.

4.4.1.2 Calculation of process capital cost

As indicated in Chapter 1, capital costs are another key objective function used for process evaluation and optimization. In fact, this function provides an indication about the required investment. Considering this, this function is calculated for our objective function as the sum of the capital costs of the various process blocks, to which is added the cost of the heat exchange network. Moreover, in order to avoid a repetition in the calculation of heat exchange such as the biomass burner, juice evaporators, column reboilers and others, the costs of these items was excluded from the calculation route related to the block's costs. As a result, Equation 4:3 provides a literal equation for the Grass Root Capital cost for a given process configuration ($C_{capital,GR}$).

Equation 4:3 Literal equation for the calculation of process capital cost

$$C_{inv} = C_{capital,GR} = \sum_{i=1}^{N_{blocks}} C_{capital,GR_i}\,(excluding\ HEN) + C_{HEN,GR}\,(Area_{HEN})(M\$)$$

4.4.2 Choice of optimization variables

The optimization variables were chosen from amongst the variables investigated in literature and defined in Table 4:11. Considering this, details concerning the 25 optimization variables controlled by the outer Evolutionary Multi-Objective Optimization (EMOO) algorithm and their variation ranges are provided in Table 4:13. The 8 variables controlled by the M Mixed Integer Linear Programming algorithm for the resolution of the heat integration slave problem are provided in Table 4:14.

Table 4:13 Optimization variables and associated bounds for the multi-objective optimization problem

Section	Variable names	Unit	Variables description	N_{var}	min	max
Evaporation	r_{ev_i}	-	Vaporization rates in various evaporators	6	0	1
	dT_{ev_i}	°C	Temperature difference in evaporators	5	4	12
	x_{sgcc}	kg/kg	Juice concentration at the outlet of concentration step	1	0.65	0.7
Distillation	p_{strip}	atm	Pressure in stripping column	1	0.25	3
	p_{rect}	atm	Pressure in rectifying column	1	0.75	3.5
	$V_{fr,rect,top}$	mol/mol	Vapor fraction in rectifying distillate	1	0	1
Dehydration	S/F	kg/kg	Solvent to feed ratio in extraction column	1	0.5	1.75
	T_{solv}	°C	Solvent input temperature	1	365	470
Boiler and steam turbine	p_{tur_1}	atm	Operating pressure in various turbines	1	12	25
	p_{tur_2}	atm		1	2	12
	p_{tur_3}	atm		1	1	2
	p_{tur_4}	atm		1	0.4	1
	p_{tur_5}	atm		1	0.08	0.4
	P_{boiler}	kg/h	Boiler pressure	1	60	100
	T_{sheat}	°C	Superheating temperature	1	150	300
Cake drying	hum_{bag}	mol/mol	Bagasse humidity	1	0.2	0.45
$N_{var,MOO}$				25		

Table 4:14 Optimization variables and associated bounds for the MILP heat integration slave problem

Section	Variable names	Unit	Variables description	var_{MILP}	min	max
Boiler and steam turbine	$\dot{m}_{water}$, $\dot{m}_{steam,i}$	t/h	Boiler water and steam flow rates	6	0	10^3
Cold utility	$\dot{m}_{cold,ut}$	t/h	Cooling water mass flow rate	1	0	10^5
Refrigeration utility	$\dot{m}_{frig,ut}$	t/h	Refrigeration utility mass flow rate	1	0	10^3
$N_{var,MILP}$				8		

4.4.3 Choice of measured parameters

Keeping track of key parameters is of great importance for the correct understanding of optimization results. For this reason, five additional parameters were measured in our case as

highlighted in Table 4:15. These variables are: the produced ethanol flow rate, the net power production, the heat exchanger area, the heat exchanger cost and process capital cost without heat exchange network. These parameters were chosen because they are directly related to the chosen objective functions, and as such their evolution can be directly correlated to that of the objective functions. Another reason is the presence of a conflict between some of these variables as will be highlighted later. In fact, with other input/output streams having similar magnitudes, electric power production evolves in a linear fashion with exergy efficiency. Moreover, considering the chosen variables, the heat exchanger network cost and the cost of the process without the heat exchange network directly affect the process capital cost. Finally, seeing that the chosen variables have little to no effect on the sucrose to ethanol conversion, the ultimate ethanol production rate should stay fairly constant, save for small fluctuations.

Table 4:15 Process variables measured in Multi-Objective optimization problem

Variable names	Variables description	Unit
$\dot{m}_{et}$	Ethanol mass flow rate	t/h
W_{prod}	Total net power production	MW
$Area_{HEN}$	Area of heat exchanger network	m^2
C_{HEN}	Cost of heat exchange network	M$
$C_{non-HEN}$	Process capital cost without heat exchange network	M$

4.4.4 Model preparation

In this section, we present the main points introduced to the multi-objective optimization model in order to ensure that the model converges to optimal feasible solutions and this in a reasonable time span.

4.4.4.1 Setting of constraints on design variables

In order to ensure minimal feasibility of operation within the proposed variation ranges, several modifications were proposed and highlighted below:

- In the case of a vaporization rate for a given evaporator equal to zero, the heat duty of both the condensation and cooling streams associated to the said evaporator are also set to zero
- The refrigeration system is used in the case of low temperatures in the purge stream related to the stripping column. In fact this stream requires cooling in order to extract the carbon dioxide stream. With low pressure levels, cooling temperatures might be too low and thus require the use of a refrigeration unit.
- The variation in evaporation temperature is defined by two bounds: the first in relation with the sucrose degradation temperature set at 120°C. The second is in relation to the lower permissible pressure which yields a minimal temperature at 50°C. As a result, the maximal

temperature difference is set at 70 °C. None the less, this constraint is always respected with the chosen values for the design variables.

- In order to respect the constraints imposed on the vaporization rates, the various rates proposed by the algorithm are first normalized by dividing each specific original value by the sum of the original values, as highlighted in Equation 4:4. This new value is then returned to the optimizer as the actual value for these variables. As a result, the sum of the corrected vaporization rates is equal to 1.

Equation 4:4 Equation for the correction of the vaporization rates

$$r_{ev,i,corrected} = \frac{r_{ev,i,proposed}}{\sum_{i=1}^{6} r_{ev,i,proposed}} \Rightarrow \sum_{i=1}^{6} r_{ev,i,corrected} = 1$$

In the case of sub-atmospheric pressure in the rectifying column, the vapor content in the column's distillate is set to zero so to prevent the use of a compressor to bring the pressure up to atmospheric level. In fact, this alternative is to be avoided because it requires both additional investment in compressor and additional power consumption.

4.4.4.2 Error handling

Model preparation also includes an error handling step taking into account the three following types of errors:

The first error relates to non-convergent Aspen Simulations that do not meet mass and energy balances. No heat integration or thermo-economic evaluation can be performed on these points.

The second error pertains to Aspen Simulations that fail to respect imposed design specifications. Although these points have already met mass and energy balances, they are undesirable points because of this disrespect.

The third error pertains to the Heat Integration Problem convergence. Non-convergent points do not yield results for minimum utility consumption/maximum, for power cogeneration or for total heat exchange network cost. This occurs in the case of an excessive heat demand. No subsequent thermo-economic evaluation can be performed on these points.

A penalty method as presented in [90] will be employed for this sake. This technique consists in punishing infeasible individuals by equating the values of objective functions by a penalty term, reflecting constraint violation, leading to bad results in comparison to feasible points. By combining this technique with the elitist mechanism of evolutionary algorithms, the evaluated population will be steered towards feasible, optimal solutions in the course of the optimization. Considering this, the following penalties were defined for the previous error types:

An error evaluation function was introduced into the model. This function reflects the satisfaction of process design specifications pertaining namely to the ethanol separation step: ethanol purity

and recovery in the final product, vinasse content and recycled MEG purity. A generic expression thereof is provided in Equation 4:5. The tolerance,tol in this equation is the set precision on the difference between the calculated value and the specified value for the investigated variable. $N_{spec,var}$ reflects the number of variables whose value is set by design specifications that are involved in the error evaluation.

This error function is then used to calculate the imposed penalty functions as highlighted in Equation 4:6, where the subscript "i" refers to the type of error. For the first error type, i.e. non convergent Aspen simulations, this violation is set to$r_1 = 10^{20}$, for the second $r_2 = 10^{15}$ and the third $r_3 = 10^{12}$. This decreasing valuation is due to the decreased severity of the evaluated solutions. A non converged point is the most undesired situation, followed by a point that does not respect design specifications and finally a non-heat-integrated point.

Finally, the values of objective function (j) for the evaluated individual I is calculated as highlighted in Equation 4:7. For convergent point meeting design specifications, the true objective function values can be calculated and are hence specified for these functions. In non-convergent types, objective functions are given values according to their error type. Special attention is also given in the case of errors to the nature of the objective function and this through the sign operator defined in Equation 4:8.

Equation 4:5 Expression for error on design specifications

$$error = \max_i \frac{\left|var_{calc,i} - var_{spec,i}\right|}{tol(= 1E-3)}$$

Equation 4:6 Expression for penalty function

$$penalty_i = r_i \times error$$

Equation 4:7 Expression for objective function values

$$obj_{I,j} = \begin{cases} sign * error * penalty_i = \begin{cases} penalty_1 if\ non\ convergence \\ penalty_2 if\ error > 1 \\ penalty_3 if\ no\ heat\ integration \end{cases} \\ obj_{calc}\ if\ convergence\ and\ no\ error \end{cases}$$

Equation 4:8 Expression for the sign operator

$$sign = \begin{cases} +1\ if\ obj\ to\ be\ minimized \\ -1\ if\ obj\ to\ be\ maximized \end{cases}$$

From the definition provided in Equation 4:7, we can see that feasible points will always retain better values for the various objective functions than the unfeasible ones, guaranteeing hence their higher ranking. Moreover, the gradual penalization will yield better ranking for unfeasible points presenting a better performance characterized by a smaller constraint violation. This will guarantee a gradual convergence towards feasible points.

4.4.4.3 Selection pressure

Selection in evolutionary algorithms determines which individuals are to be chosen as parents for subsequent individuals [91]. The main underlying principle of selection strategy is "the better is an individual; the higher is its chance of being parent." Multiple specialized techniques exist for this endeavor, each with its advantages and disadvantages. In our case we chose to operate with a rank-based roulette wheel selection procedure like the works of [92]. In this algorithm, each individual has a selection probability related to its rank in the population as highlighted in Equation 4:9. From this definition, we can see that higher ranking individuals (rank→1) have a higher selection probability than lower ranking points.

Equation 4:9 Expression for selection probability of individual I

$$Prob_{selection,I} = \frac{1}{rank_I}$$

A random weighted selection procedure based on the obtained probability distribution is then implemented to deduce parent individuals. [92] indicated that this method is faster in convergence to the Non Dominated Set than a value based method. This is because this method overcomes the bias towards an optimal solution discovered early on, an event that may lead to a loss of diversity and possibly to wrong solutions, resulting in a steadier and faster algorithm.

4.4.4.4 Parallelization

A key aspect of the QMOO algorithm is its propensity for parallelization namely concerning the evaluation of a given individual through a one run simulation, heat integration and thermo-economic evaluation. This parallelization has been discussed in [25] extensively utilized in past research works. Standard parallelization normally requires the use of supercomputers and associated clusters, albeit this option is not viable under Aspen Plus which operates solely on Windows Platform. For this reason, a customized Matlab parallelization algorithm [93] was put into practice, permitting the running of up to three simulations in parallel with one master and two slave programs. Considering this, whereas the evaluation task is split between the various programs, the ranking, elimination and selection tasks are performed solely by the master program.

4.5 Results of multi-objective optimization

A total number of 1000 evaluations were performed. The population count was controlled by the use of elimination and creation techniques in order to move towards an optimized population. We detail in this paragraph aspects of the optimization run mainly relating to the evolution of the investigated population and its characteristics.

4.5.1.1 Evolution of Population

We decided to start with an initial population of 25 individuals, whose values were generated randomly from the design space defined in Table 4:13. Each individual was evaluated according to the one run methodology and the values of its objective functions and modified design variables recoded. At the end of this iteration, the individuals were ranked, generating hence the seed for a thorough multi-objective optimization.

This population was then permitted to grow towards a population of around 100 individuals and this by the intermittent addition and elimination of points occurring after each iteration. This population was then permitted to evolve towards a smaller population of high ranking individuals. Considering this, the evolution of the number of points in the population with the number of evaluations is provided in Figure 4:7. The evaluation was halted after 1000 evaluations yielding hence the range for the highlighted graph.

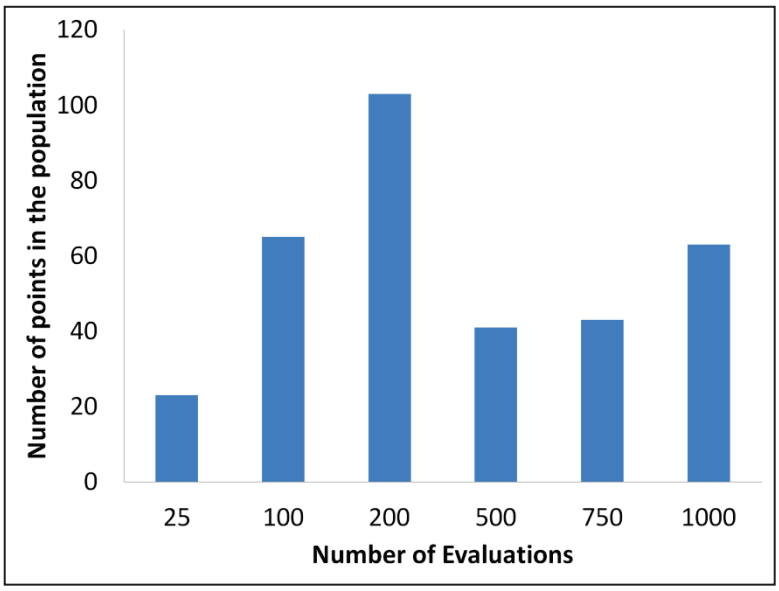

Figure 4:7 Evolution of population count with the number of evaluations

As we can see, the population count stabilizes around 100 for an evaluation count between 100 and 500 evaluations before dropping to a value around 75 for the final evaluations. Ultimately, this population count will converge towards the number of points with ranking equal to 1.

4.5.1.2 Evolution of highest ranking

The evolution of the maximum (worst) ranking with the number of evaluations was also evaluated, and its value highlighted for chosen points in Figure 4:8. As we can see, after witnessing a net increase in this maximum ranking, this value witnessed a continuous decrease until reaching the value of two for the final recorded population.

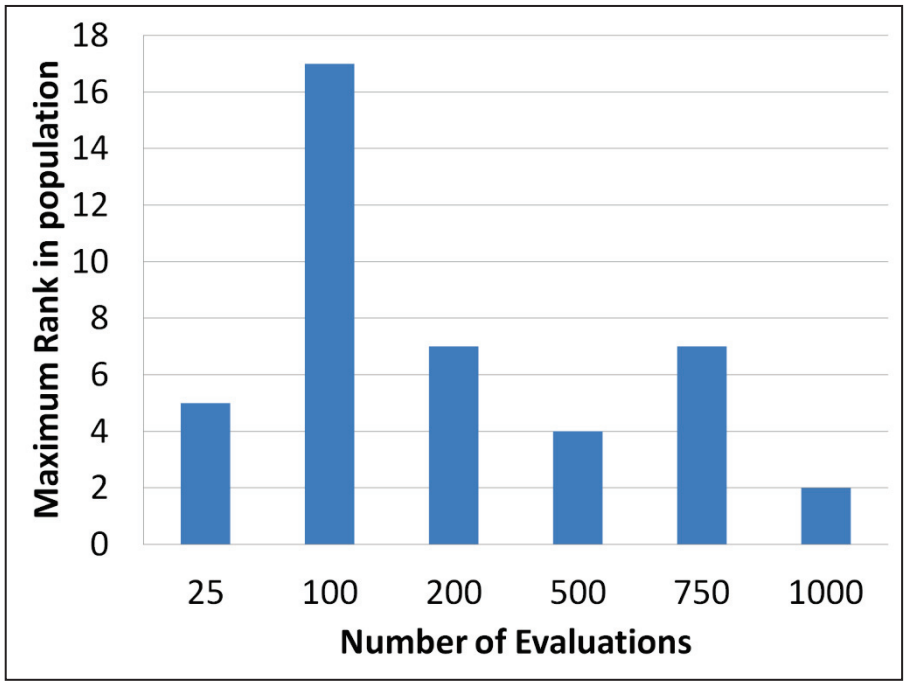

Figure 4:8 Evolution of the maximum ranking with the number of evaluations

Considering this, we can see that a high maximum ranking is characteristic of an explorative phase, whereas a low ranking is characteristic of convergence. Ultimately, if the population was left to evolve in an infinite time period, this maximum ranking will equal 1.

4.5.1.3 Evolution of the number of rank 1 points

Another important characteristic of the used algorithm is the evolution of the number of rank 1 points. These points constitute the non dominated set obtained after a given number of evaluations. Its evolution is hence a characteristic of convergence and its count is a direct characteristic of the efficiency of the algorithm. Considering this, the evolution of the number of rank 1 points and their percentage of the total population with the number of evaluations is highlighted in Figure 4:9.

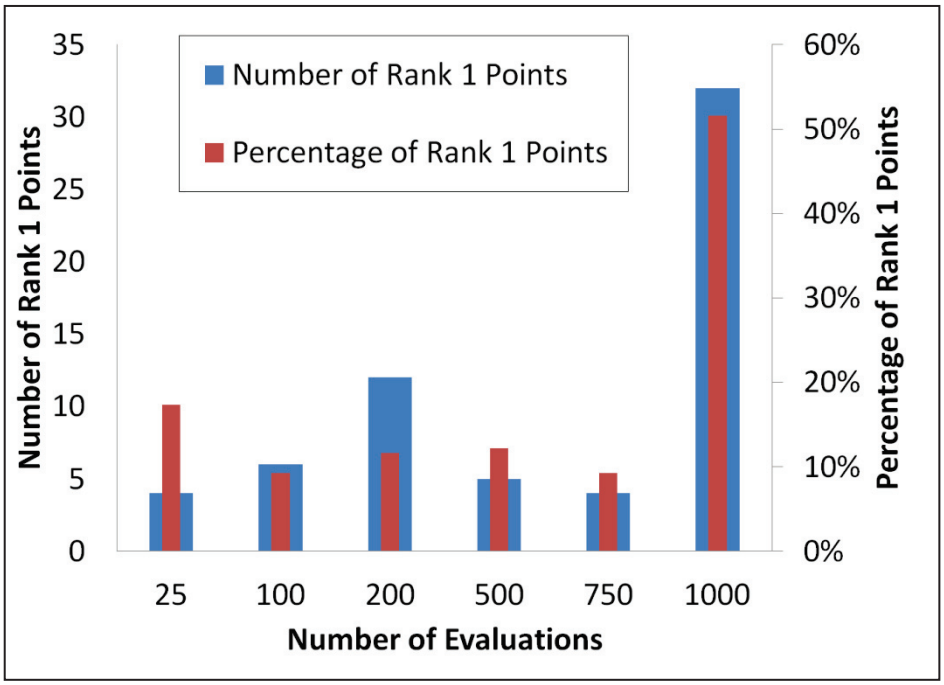

Figure 4:9 Evolution of the number of rank 1 points with the number of evaluations

As we can see, the number of rank 1 points keeps on increasing with the increasing number of evaluations. The percentage of rank 1 points witnesses however a decrease between the 25th and 100th evaluation. This can be linked to the increased maximum ranking witnessed in Figure 4:8, which also can be linked to the explorative phase. Besides this, this percentage witnesses a spike in its value between the 500th and 750th evaluation. This is due both to the increase in the top ranking individuals and to the decrease in total population count as highlighted in Figure 4:7.

4.5.1.4 Evolution of objective function values

All of the previous sections and graphs presented the evolution of statistical measures describing the state of the algorithm. What is more interesting however is the evolution of the objective function values with the number of evaluations. This evolution for the investigated process is highlighted in Figure 4:10. The blue arrows in this figure express the pressure exerted by the optimization algorithm on the evaluated population, which seeks to obtain a greater exergy efficiency for a smaller capital cost. This pressure is however met by the physical limits of the studied process and the impact of the design variables. These competing forces lead to the formation of the obtained population spread. We can also see that the evaluated population converges more and more towards to a non dominated set approximating better and better the Pareto curve relative to the studied process and the chosen variables.

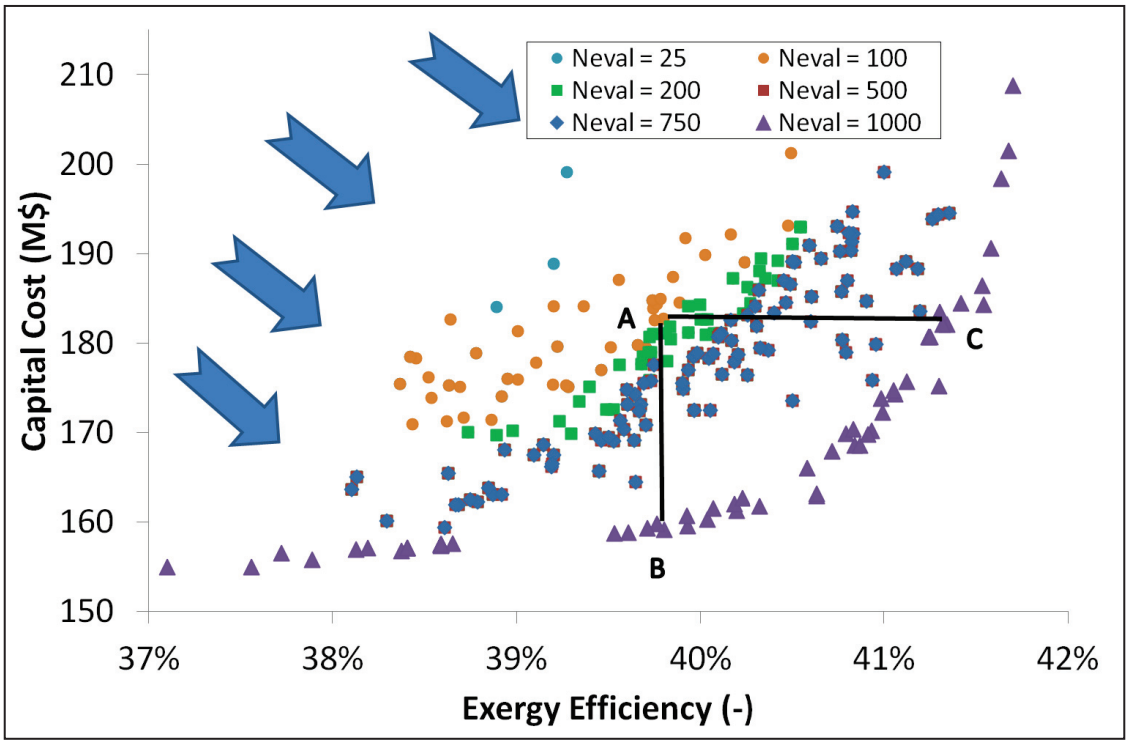

Figure 4:10 Evolution of objective function values for the total population with the number of evaluations

Moreover, in order to illustrate the impact of the optimization algorithm, we decided to visualize the evolution of objective function values of a (ex_{eff}, C_{inv}) couple A obtained before the 100th evaluation. Points B and C represent, respectively, the lowest cost alternative for a similar exergy efficiency and the highest exergy efficiency for a similar capital cost. Before going further in our analysis, it should be interesting to note that all the points existing in the domain defined by points A, B and C fare better than point A since they all have a higher exergy efficiency and a lower investment cost. None the less, we will focus our attention on the two directions defined by AB and AC.

With this in mind, we can see that point B has a smaller investment cost for a similar exergy efficiency, whereas point C has a greater exergy efficiency for a similar investment cost.

4.5.2 Analysis of optimization results: last population

Whereas we focused in the previous section on the evolution of the algorithm towards the final optimal solution, we turn our attention in this section towards the last population and its corresponding solutions. As highlighted in Chapter 1, this optimal fraction corresponds to the best approximation of the Pareto set, and as a result, yields the solutions with the optimal trade-offs between the two competing objectives.

4.5.2.1 Graphical presentation of last population

Figure 4:11 highlights the contents of the final population of the optimization problem for the ethanol and power from sugarcane optimization problem, under the design space highlighted in

Table 4:13. As we can see, the maximum obtained rank is equal to 2 as highlighted in Figure 4:8. Moreover, the obtained results are rather close depicting the convergence of the optimization problem. Finally, this population was obtained by removing both redundant points and points that did not respect the constraint of having zero vapor content for the rectification column distillate in the case of sub-atmospheric pressure. The final population count was hence equal to 57 points of which 34 points were of rank 1.

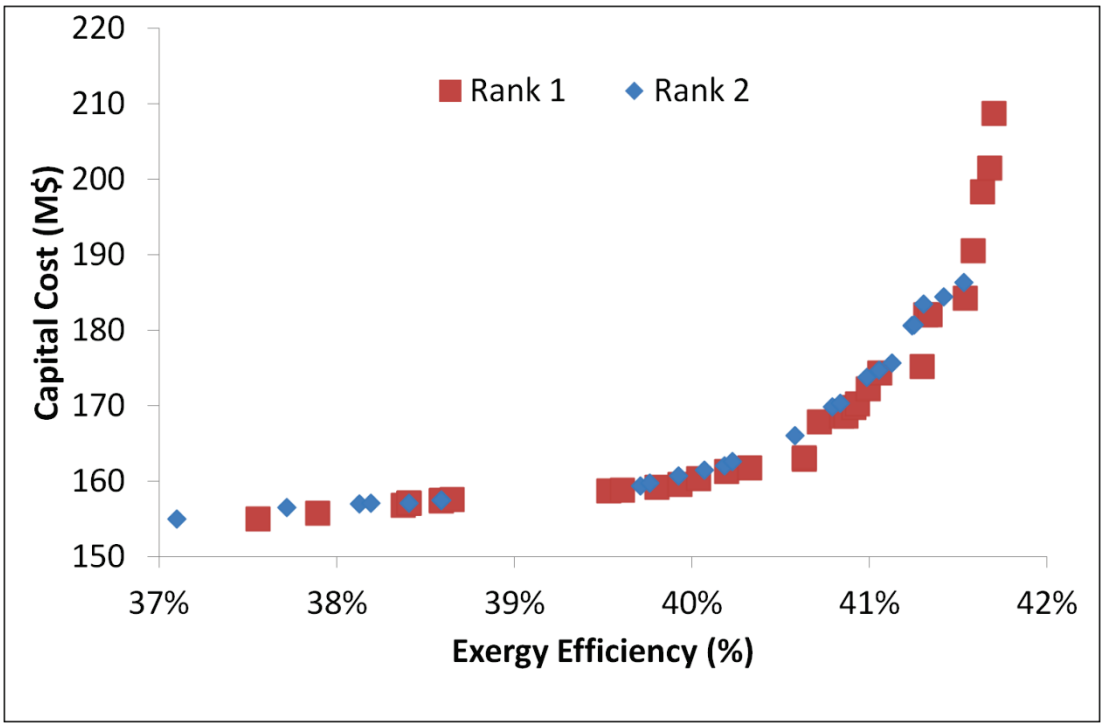

Figure 4:11 The contents of the final population for the ethanol and power from sugarcane optimization problem

4.5.2.2 Graphical presentation of final Non-Dominated Set

Figure 4:12 on the other hand provides a graphical representation of the final Non-Dominated Set for the ethanol and power from sugarcane optimization problem. As we can see the exergy efficiency evolves between a minimal value of 37.6% and a maximal value of 41.7%. Capital costs on the other hand evolve between a minimal value of 155 M$, corresponding to the smallest exergy efficiency and a maximal value of 210 M$, corresponding to the greatest exergy efficiency. A clear observation can be made at this level: the scope of variation of capital cost is greater than that of exergy efficiency (35.5% for the first vs. 11% for the second).

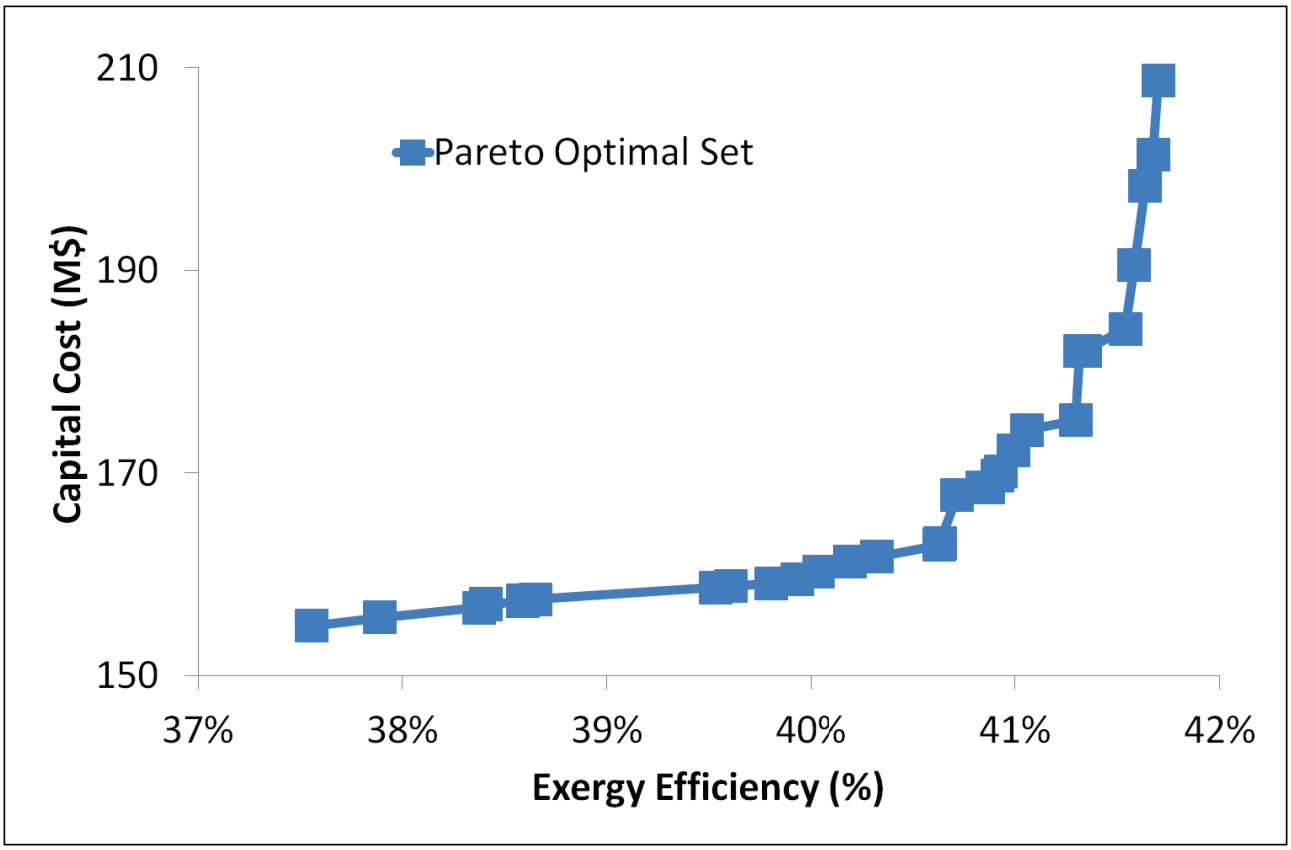

Figure 4:12 Graph for the final Pareto optimal Non Dominated Set: optimization of combined sugarcane distillery and cogeneration process

4.5.2.3 Explanation of the obtained results: Measured Variables

The obtained trade-off curve can be explained by taking a closer look at the measured variables. Given the previous choice of the design variables along with the various specifications and design constraints, the most dependent variables are net power production W_{prod} (MW) and heat exchanger network area $Area_{HEN}$ (m^2) or cost C_{HEN} (M$). As a matter of fact, these two variables present the main trade-off associated with the approach of the proposed optimization: a greater power production leads to a greater exergy efficiency. This same increase, presented by a better heat integration, is met by a greater heat exchanger area and a subsequent capital cost. To highlight these relationships, Figure 4:13 highlights the relationship between exergy efficiency and net power production. As we can see, all of the obtained alternatives present a largely positive (>60 MW) net power production. Moreover, a higher efficiency system is characterized by a higher net power production and this in a nearly linear factor (determination factor $R^2 = 0.9951$). This is due to the fact that both input flow rates and composition (sugarcane and leaves) are constant, whereas the ethanol production rate is bound by a myriad of specifications. The tolerance for these same specifications is the reason behind the small deviance from linearity, and this by a slightly variable ethanol production rate, as highlighted in Figure 4:14. Albeit small (0.6 t/h maximal variation), this variation is responsible for the observed deviation from linearity.

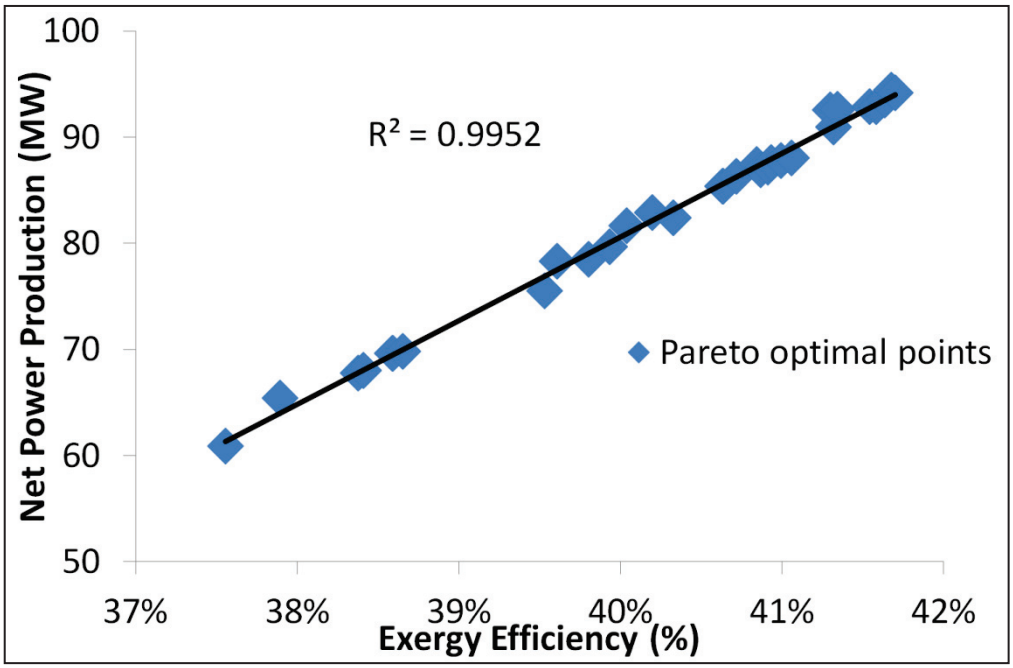

Figure 4:13 Net power production vs. exergy efficiency for Pareto-optimal solutions

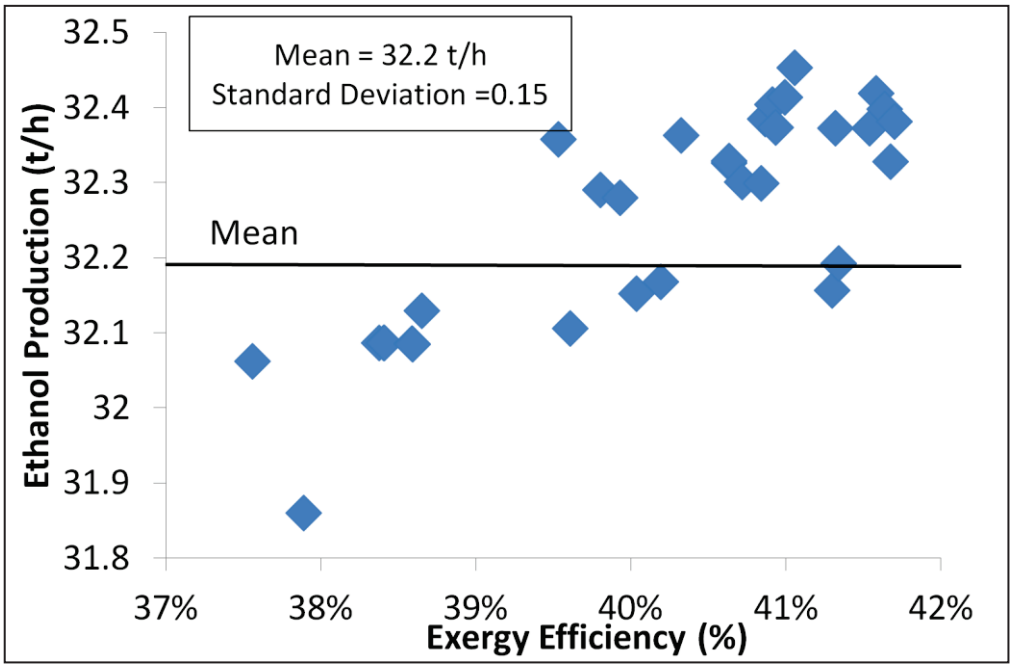

Figure 4:14 Ethanol production vs. exergy efficiency for Pareto-optimal solutions

Figure 4:15 on the other hand presents the relationship between the heat exchanger cost and the process capital cost. As we can see, a higher capital cost is associated with a greater heat exchanger network cost. This relationship is also nearly linear ($R^2 = 0.96$), albeit with a greater deviation than the $W_{prod}\ vs.\ ex_{eff}$ relationship. This is due to the contribution of other process

sections to the total capital cost, namely the distillation/dehydration section, the steam turbines, and the dryer.

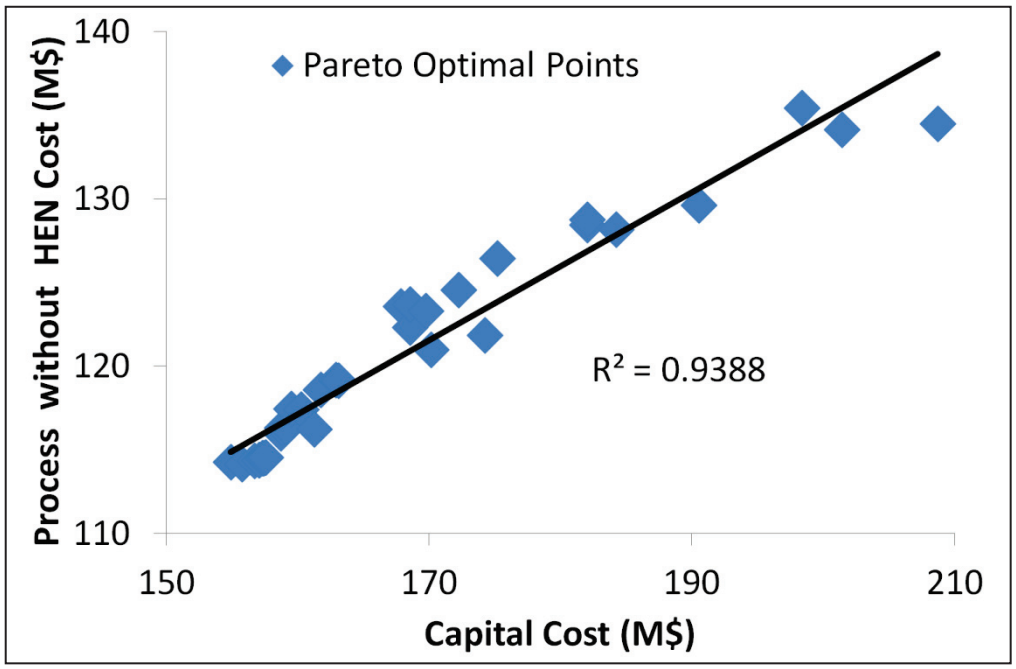

Figure 4:15 Heat Exchanger Cost vs. Capital Cost for Pareto-optimal solutions

Figure 4:16 presents the relationship between the investment cost of process sections different from the heat exchange network. As we can see, this cost also increases indicating the role the various process sections play in increasing process efficiency at the detriment of a higher investment cost, and this mainly by a lower heat demand. We can see however that this increase stops for high cost systems indicating the limits of the process in reducing its heat demand. At this level, in-process heat exchange is responsible for the increase in efficiency and in capital cost.

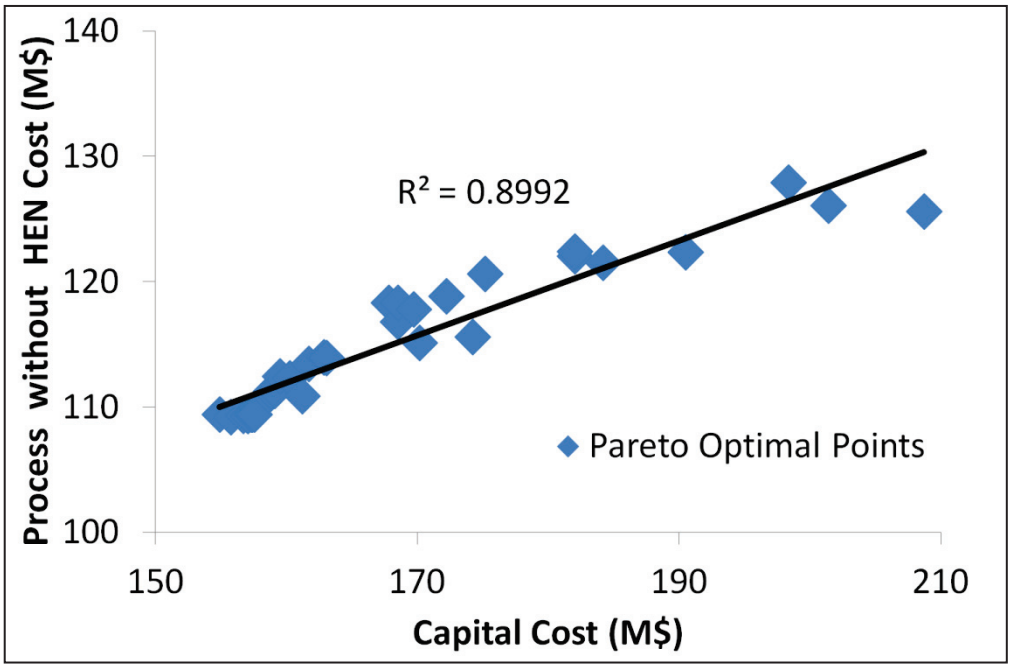

Figure 4:16 Process Cost vs. Capital Cost for Pareto optimal solutions

Figure 4:17 highlights the evolution of the percentage of heat exchanger and process cost with increasing capital cost process alternatives. As we can see, both these percentages remain constant for alternatives with capital costs smaller than 163 M$. In this interval, the Heat Exchange Network (HEN) Cost makes about 26% of the process capital cost, whereas the cost of the process without the HEN makes around 74% of the process capital cost. The trends vary after the process with a capital cost of 163 M$. The percentage of the cost of the process without the HEN decreases whereas that of the HEN increases with increasing capital cost. Nonetheless, the process part remains largely more considerable with a minimum of 64% for a maximum of 36% for heat exchanger cost.

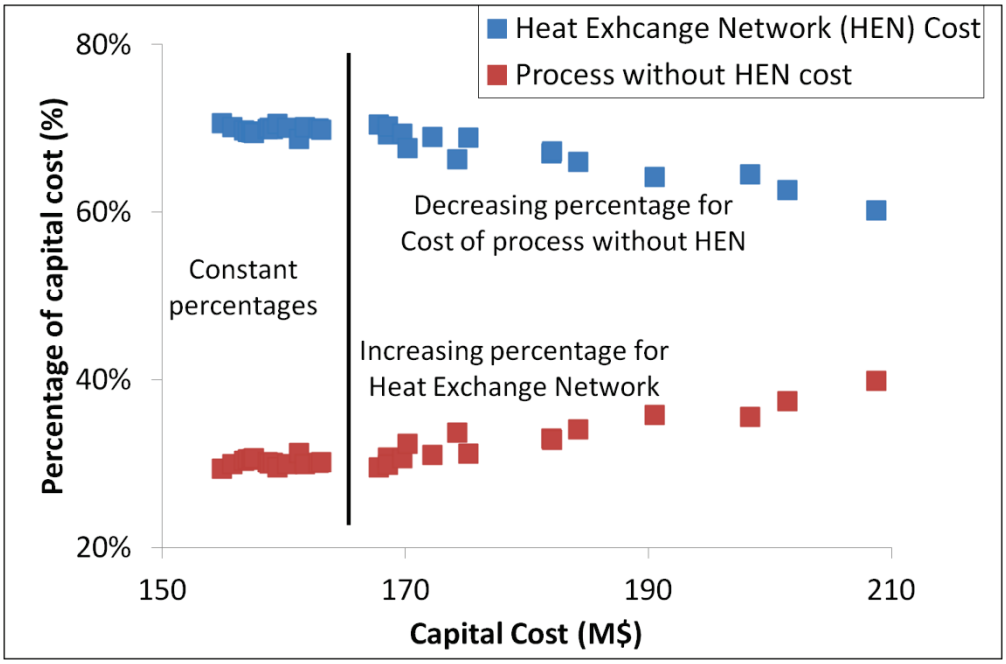

Figure 4:17 Percentage of capital cost: Relationship for Heat Exchanger Cost and Process Cost

Finally, Figure 4:18 highlights the relationship between heat exchanger cost and net power production. As we can see, a clear trade-off exists between these two variables. Nonetheless, this trade-off does not constitute a clear Pareto set, namely because of the influence of process equipment costs on the exergy efficiency-capital cost Pareto front.

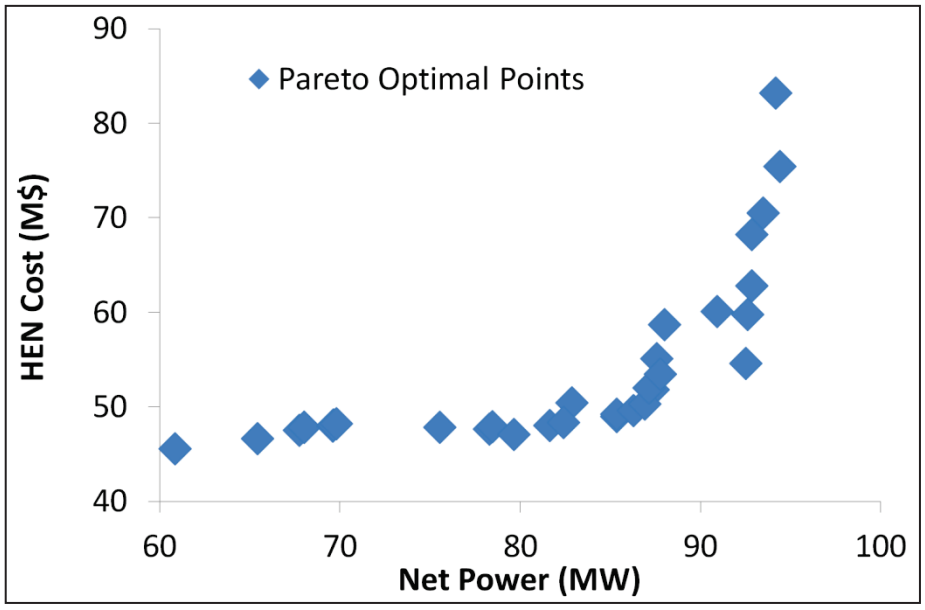

Figure 4:18 Relationship between heat exchanger cost and net power production

4.5.2.4 Obtained scope for objective functions, design variables and measured variables

The optimization yielded the previously highlighted Pareto set by investigating several possible values for the various design variables. Considering this, a direct result of the obtained convergence is a possible narrowing of the previously specified ranges for the various design variables. With this in mind, Table 4:16 highlights the scopes and operating ranges for the problem's two objective functions, five measured variables, and 33 design variables. This table contains both the initial and final ranges for the investigated design variables. On the other hand, only the final ranges are specified for the objective function and measured variables, and this because of the nature of their evaluation. As we can see, 23 of the 33 design variables saw a narrowing of their specified ranges. This is mostly true for the various vaporization rates, where this narrowing is directly related to the efficiency of multiple-effect evaporation. Moreover, the narrowing of the ranges for the various utility flow rates is mainly related to the great values associated with the initial range. This choice was directly related to a lack of knowledge concerning the various possible values. Other variables witnessed a smaller narrowing and can hence be considered as ***distance variables***. This is namely the case for the stripping column and boiler pressures, and the solvent temperature.

Table 4:16 Obtained scopes and ranges for objective functions, measured variables and design variables

Variable	Unit	Initial range	Final range	Variable	Unit	Initial range	Final range
ex_{eff}	%		[37.6; 41.7]	C_{inv}	M$		[155 ; 210]
r_{ev_1}	-	[0 ; 1]	[0; 0.8]	dT_{ev_2}	°C	[4;12]	[4; 12]
r_{ev_2}	-	[0 ; 1]	[0; 0.45]	dT_{ev_3}	°C	[4;12]	[4; 12]
r_{ev_3}	-	[0 ; 1]	[0; 0.15]	dT_{ev_4}	°C	[4;12]	[4 ; 12]
r_{ev_4}	-	[0 ; 1]	[0; 0.25]	dT_{ev_5}	°C	[4;12]	[4; 12]
r_{ev_5}	-	[0 ; 1]	[0; 0.55]	dT_{ev_6}	°C	[4;12]	[4 ; 12]
r_{ev_6}	-	[0 ; 1]	[0;0.4]	$dT_{ev_{tot}}$	°C		[32 ; 50]
p_{strip}	atm	[0.25 ; 3]	[0.25 ; 2]	x_{sgcc}	%	[0.65 ; 0.7]	[0.65 ; 0.7]
$V_{fr,rect,top}$	-	[0 ; 1]	[0.1; 1]	S/F	kg/kg	[0.5 ; 0.6]	[0.5; 0.59]
p_{rect}	atm	[0.75 ; 3.5]	[1 ; 3.5]	T_{solv}	°C	[340 ; 414]	[350 ; 403]
p_{boiler}	atm	[60 ; 100]	[75; 100]	hum_{bag}	mol.%	[0.24; 0.45]	[0.24; 0.45]
$p_{tur,1}$	atm	[12 ; 25]	[12; 25]	T_{sheat}	°C	[150 ; 300]	[155; 300]
$p_{tur,3}$	atm	[1;2]	[1; 2]	$p_{tur,2}$	atm	[2 ; 12]	[2.5 ; 10.5]
$p_{tur,5}$	atm	[0.08 ; 0.4]	[0.08 ; 0.4]	$p_{tur,4}$	atm	[0.4 ; 1]	[0.4 ; 1]
$\dot{m}_{frig,ut}$	t/h	[0 ;10^3]	[20.8; 21.2]	$\dot{m}_{cold,ut}$	t/h	[0;10^5]	[2.3 ; 2.5].10^4
$\dot{m}_{steam,2}$	t/h	[0 ;10^3]	[70 ; 332]	$\dot{m}_{steam,1}$	t/h	[0 ;10^3]	[10; 84]
$\dot{m}_{steam,4}$	t/h	[0 ;10^3]	[0 ; 139]	$\dot{m}_{steam,3}$	t/h	[0 ;10^3]	[0 ; 55]
$\dot{m}_{boiler}$	t/h	[0 ; 10^3]	[472 ; 527]	$\dot{m}_{steam,5}$	t/h	[0 ;10^3]	[159; 355]
W_{prod}	MW		[60 ; 95]	C_{HEN}	M$		[45 ;83]
$Area_{HEN}$	m^2		[44 ; 82].10^3	$\dot{m}_{et}$	t/h		[31.9 ; 32.5]

4.5.2.5 *Extraction of knee points and fragmentation: proposal and implementation of a dedicated algorithm*

As indicated in Chapter 1, knee points are interesting points in the Pareto curve namely because they represent an inflexion point therein. As a result they are capable of dividing the said curve into multiple fragments that can be analyzed separately or bundled and compared with other fragments.

By definition, a knee point is defined by the following statement in the case of two conflicting objectives where one is maximized, in our case exergy efficiency, and the other is minimized, in our case capital cost.

Before the knee point, i.e. for a smaller exergy efficiency in our case, an increase in exergy efficiency is met by a smaller increase in capital cost. In contrast, after the knee point, i.e. for a greater efficiency in our case, an increase in exergy efficiency is met by a greater increase in capital cost.

This statement can be translated into a mathematical formulation for these knee points obtained as follows. The various points are first ranked in a decreasing order with respect to exergy efficiency, i.e. an increasing order with respect to capital cost. The various objective function values are then normalized as highlighted in Equation 4:10. The variation in their values between point i-1 and point i is then computed as highlighted in Equation 4:11. A variation ratio can then be established for the point i as the ratio between the variation in normalized exergy efficiency and the normalized in investment cost.

Equation 4:10 Equation for the normalization of maximized objective functions

$$obj_{i,norm,j} = \frac{(obj_{i,value,j} - obj_{i,min,j})}{(obj_{i,max,j} - obj_{i,min,j})}$$

Equation 4:11 Equation for the variation in the value of objective function i between points j and j-1

$$\Delta obj_{i,norm,j} = obj_{i,norm,\mathrm{j}} - obj_{i,norm,j-1}$$

Equation 4:12 Variation ratio for point j

$$ratio_{var,j} = \frac{\Delta(ex_{eff})_{norm,j}}{\Delta(C_{FC})_{norm,j}} \Rightarrow \begin{cases} > 1 \Rightarrow \Delta(ex_{eff})_{norm,j} > \Delta(C_{inv})_{norm,j} \\ < 1 \Rightarrow \Delta(ex_{eff})_{norm,j} < \Delta(C_{inv})_{norm,j} \end{cases}$$

Considering this, a variation ratio greater than one indicates that the variation in the exergy efficiency is greater than that in the capital cost. In contrast, a variation ratio smaller than one indicates that the variation in capital cost is greater than that in exergy efficiency. With this in mind, we can now provide a mathematical formulation for a knee point based on the previous definition reminded here: before the knee point, a great increase in exergy efficiency is met by a small increase in capital cost, and after it a small increase in exergy efficiency is met by a great increase in capital cost. This translates into the following: the variation ratio at the knee point is greater than one (a great increase in exergy efficiency is met by a small increase in capital cost); whereas the variation ratio at the knee point is smaller than one (a small increase in exergy efficiency is met by a great increase in capital cost). This is defined in mathematical terms via Equation 4:13 in mathematical terms, where $knee_{points}$ is the set of knee points that are to be found in the curve.

Equation 4:13 Mathematical definition of a knee point

$$point_j \in knee_{points} \; iff \; ratio_{var,j} > 1 \bigwedge ratio_{var,j+1} < 1$$

Considering this, the Pareto curve approximation and its corresponding knee points and resulting fragmentation are shown in Figure 4:19. As we can see from this Figure, the obtained Non Dominated Set contains six different knee points whose values and seven different fragments with

various population counts. Moreover, Figure 4:19 highlights the two extreme points for which no better, or worst, values for the objective functions exist.

With this in mind, Table 4:17 provides the objective function values for both the knee and extreme points. This table also contains objective function values for the points that precede the first and last knee point used in order to illustrate the previous calculation procedure. As we can see, the variation ratio is equal to 1.31 at the first knee point and to 0.39 after it, whereas this ratio is equal to 1.19 at the sixth knee point and 0.09 after it, highlighting the correctness of the proposed calculation procedure.

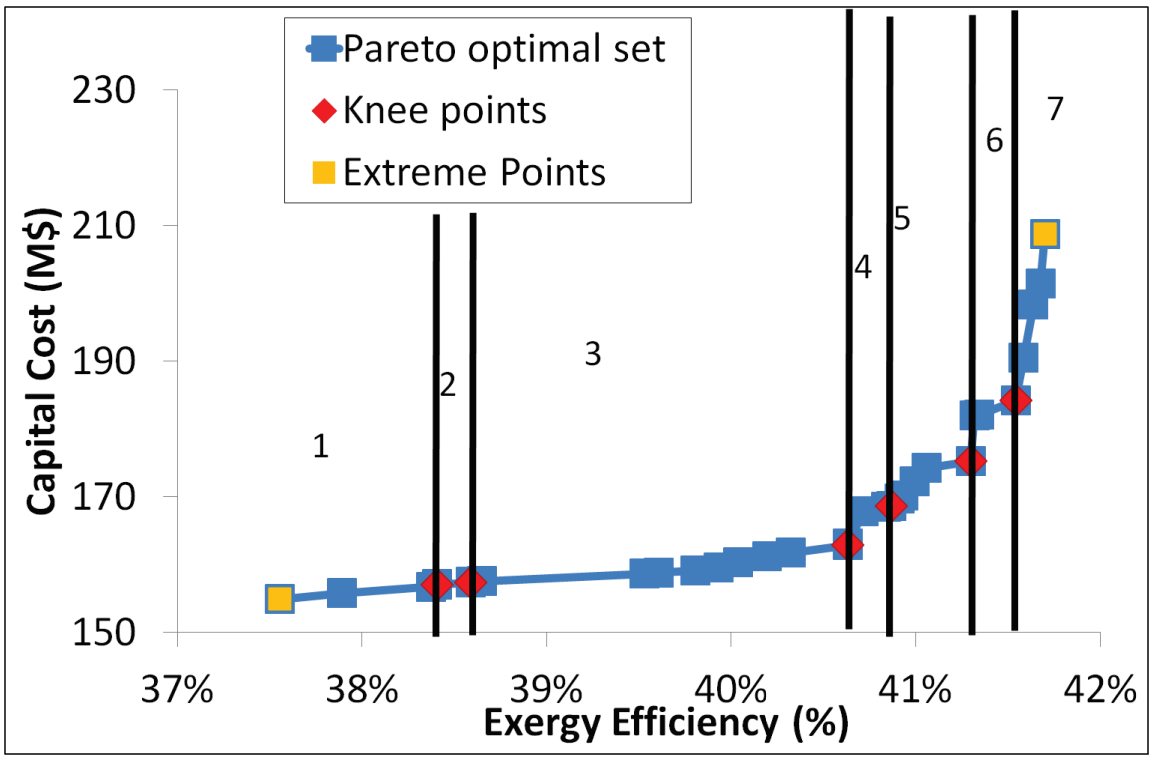

Figure 4:19 Pareto curve (capital cost vs. exergy efficiency) along with knee points and extreme points

A first observation that can be extracted from Table 4:17 is the fact that between the sixth point and the second extreme, a 0.36% increase in exergy efficiency is met by a 14% increase in capital cost. This is characteristic of many energy systems in which a great capital cost is required to obtain the efficiency values higher than a given threshold.

Table 4:17 Objective function values for knee points and extreme points

Extreme 1	37.56%	154.93	0%	0%			
Pre-Knee 1	38.37%	156.73	20%	3%			
Knee 1	38.41%	157.06	21%	4%	0.8%	0.6%	1.31
Post-Knee 1	38.41%	157.08	21%	4%	0.01%	0.03%	0.39
Knee 2	38.59%	157.33	25%	4%			
Knee 3	40.63%	162.89	74%	15%			
Knee 4	40.87%	168.56	80%	25%			
Knee 5	41.30%	175.20	90%	38%			
Pre-Knee 6	41.34%	182.07	91%	50%			
Knee 6	41.54%	184.22	96%	54%	4.8%	4.0%	1.19
Post-Knee 6	41.58%	190.54	97%	66%	1.0%	11.7%	0.09
Extreme 2	41.70%	208.72	100%	66%			

4.5.2.6 Evolution of objective function and design variable values through the various fragments

Each point obtained in the Pareto curve approximation highlighted in Figure 4:12 are associated to decision vectors with specific values for the design and measured variables. The change in these values is the prime factor behind the optimization per say and behind the variability in the Pareto optimal functions.

In this section, we will make use of the previous fragmentation in order to track the evolution of the various objective functions, design and measured variables through the obtained front. For this sake, a mean value for the different variables and functions was calculated for each fragment, as highlighted in Equation 4:14.

Equation 4:14 Expression for the mean value for a given variable or objective function in a given fragment

$$var_{mean_{frag,k}} = mean(var_j, j \in frag_k)$$

This obtained mean is then normalized according to two different strategies. The first strategy concerns both measured variables and objective functions, for which no initial bounds can be set. This strategy is highlighted in Equation 4:15. In this equation, obj designates the investigated objective function or measaured variabe, $obj_{mean_{frag,k}}$ and $obj_{norm,frag,k}$ its mean and normalized values for a given fragment$frag, k$, and $obj_{mean_{min}}$ and $obj_{mean_{max}}$ the minimum and maximum values of the previously averaged values.

Equation 4:15 Equation for the normalization of measured variables & objective functions

$$obj_{i,norm_{frag,k}} = \frac{(obj_{i,mean_{frag,k}} - obj_{i,mean_{min}})}{(obj_{i,mean_{max}} - obj_{i,mean_{min}})}$$

With this in mind, Figure 4:20 plots the variation of our two objective functions, exergy efficiency and capital cost, and our key measured variables, net power production, heat exchanger cost and the cost of the process without the heat exchange network, along the Pareto fragments. As we can see, all parameters evolve from minimal values, with zero normalized values, towards a maximum normalized value of 1. This increases nonetheless at various rates. Increase in exergy efficiency and net power production is faster for the first than for the last fragments, in contrast to cost related parameters.

The previously discussed spike in capital cost occurring between the sixth knee and the second extreme point can be easily visualized in Figure 4:20, this time between the sixth and seventh fragments.

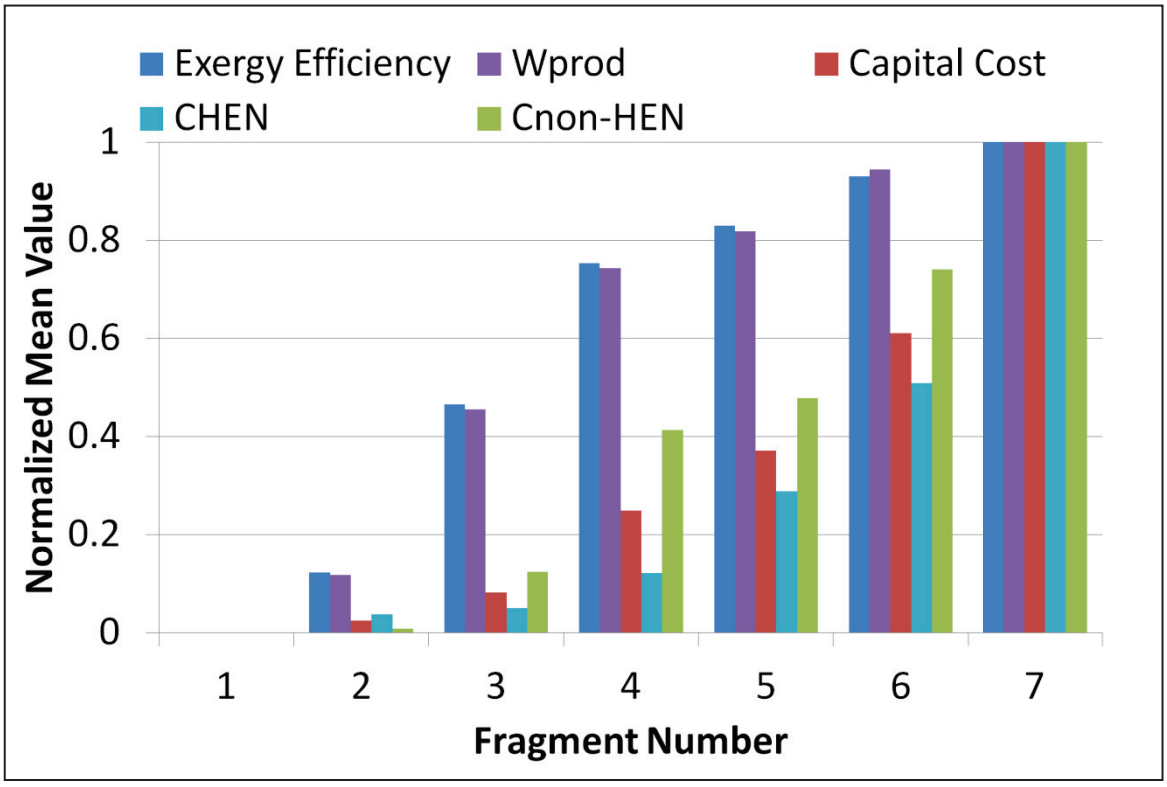

Figure 4:20 Variation of objective functions and key measured variables along Pareto fragments

The second normalization strategy concerns design variables and is highlighted In Equation 4:16. In this equation, var designates the investigated variable. $var_{mean_{frag,i}}$ and $var_{norm_{frag,i}}$ designate its mean and normalized values for a given individual i, and var_{low} and var_{up} its lower and upper bounds as specified in Table 4:13. This normalization will enable the plotting of the various

parameters in dedicated bar graphs, and will ultimate enable the tracking of the variation of their mean values along the various fragments.

Equation 4:16 Equation for the normalization of optimization variables

$$var_{norm_{frag,i}} = \frac{(var_{mean_{frag,i}} - var_{low})}{(var_{up} - var_{low})}$$

With this in mind, Figure 4:21 tracks the variation of the six evaporation rates, relative to the six evaporators, along the Pareto fragments. From this Figure, we can see that the first evaporation rate evolves from large values for the first fragments towards low values for the last fragments, in contrast with the remaining evaporators. Moreover, we can see that the third evaporator has a smaller evaporation rate compared with the remaining levels and this for all the considered fragments.

Some of the obtained results can be linked to literature, namely the evolution of the first evaporation level. In fact, high evaporation loads in the first evaporation level are linked to low exergy efficiencies and low capital costs, due to low vapor bleeding in other level. Low loads on the other hand are associated with higher exergy efficiencies and higher loads, and this due to the greater vapor bleeding in lower temperature levels.

The only exception seems to be in the third fragment where comparatively low efficiencies and capital costs are associated with high vaporization rates. This result, along with the evolution in the various evaporation rates can only be explained through an overall analysis of the system.

Figure 4:22 tracks on the other hand the variation of the temperature decrements in the various vaporization rates. As indicated earlier, these decrements do not concern the first level, whose temperature is fixed at 120 °C. From this figure, we can see that these decrements witness an overall decrease for the third and sixth evaporation levels along the various fragments. The values for the remaining evaporators on the other hand fluctuated along the fragments.

More interestingly, we see a reduction in the sum of these decrements. This is in line with the results of [28], which have observed a reduction in this value with reduced heat consumption. The increase in capital cost can however be understood by a reduction in the heat exchange temperature in the process associated with a smaller temperature decrement.

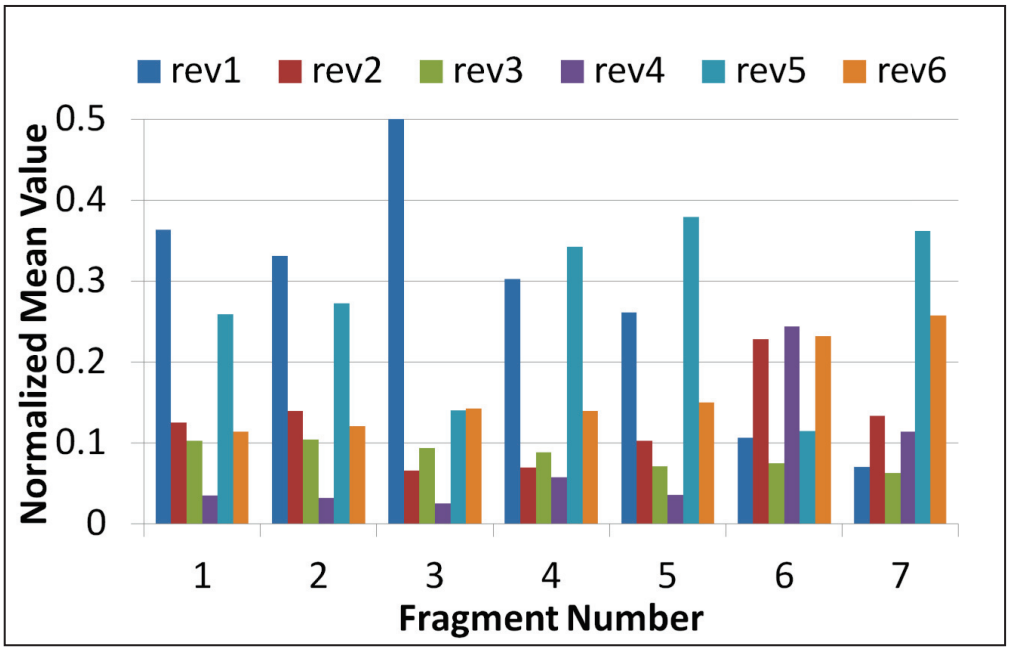

Figure 4:21 Variation of normalized mean vaporization rates along the Pareto fragments

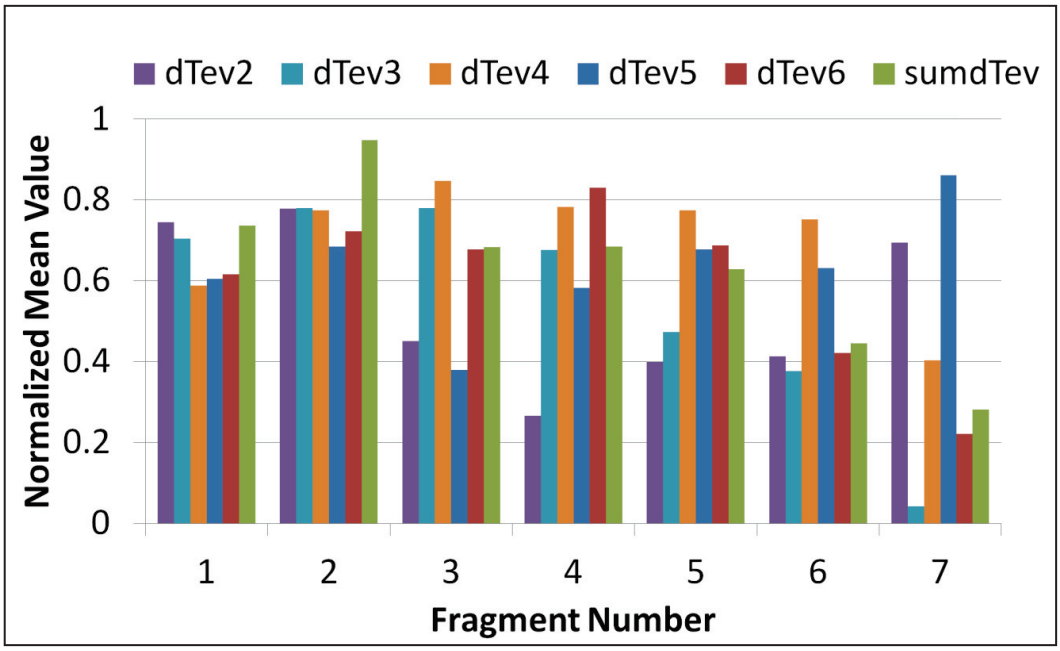

Figure 4:22 Variation of normalized mean vaporization temperature decrements along the Pareto fragments

In addition, Figure 4:23 tracks the variation of the normalized mean values for distillation and dehydration design variables along the different fragments. As we can see, the values for the stripping column pressure witnesses a visible decrease along the various fragments. The rectification column pressure on the other hand fluctuates along these fragments. However, more importantly we can see that values for stripping pressure are higher than those for rectifying

pressures in the first two fragments, denoting forward-integrated distillation. This tendency is reversed after the third fragment, where the stripping pressure drops below the rectifying pressure, denoted back-ward integrated distillation. The obtained results conform with previous literature results namely those of [44], where back-ward integrated distillation is associated with low heat consumption and high capital costs. In all cases, we can see that both these values retained values 60% smaller than their assigned maximum bound. This reflects the inadequacy of high operating pressures.

On another note, the vapor fraction in the rectification column distillate $V_{fr,rect,top}$ retains a rather constant high value along the various fragments with a drop for high efficiency high costs systems. The opposite applies for the solvent feed temperature T_{solv} which retains a rather constant low value along the various fragments with an increase for high efficiency high cost systems. The value for the solvent to feed ratio S/F fluctuates along the fragments with low values for high efficiency high cost systems.

Figure 4:24 on the other hand highlights the variation for the following design variables: post-drying bagasse humidity (hum_{bag}), boiler operating pressure (P_{boiler}), Steam superheating temperature (T_{sheat}) and sugar concentration of the concentrated sugar fraction (x_{sgcc}). As we can see, all of these variab les whitness a clear trend along the various fragments.

In fact, bagasse humidity goes from rather high values in the first fragments to small values for the final fragments. The same applies for the output sugar concentration. The opposite however is true for boiler pressure and superheating temperature. The obtained results are in line with literature results depicting a high pressure, high superheating temperature boiler with dry cake input. The case for sugar concentration was investigated solely by [87] which obtained similar results when using a 70% rather than a 65% concentration.

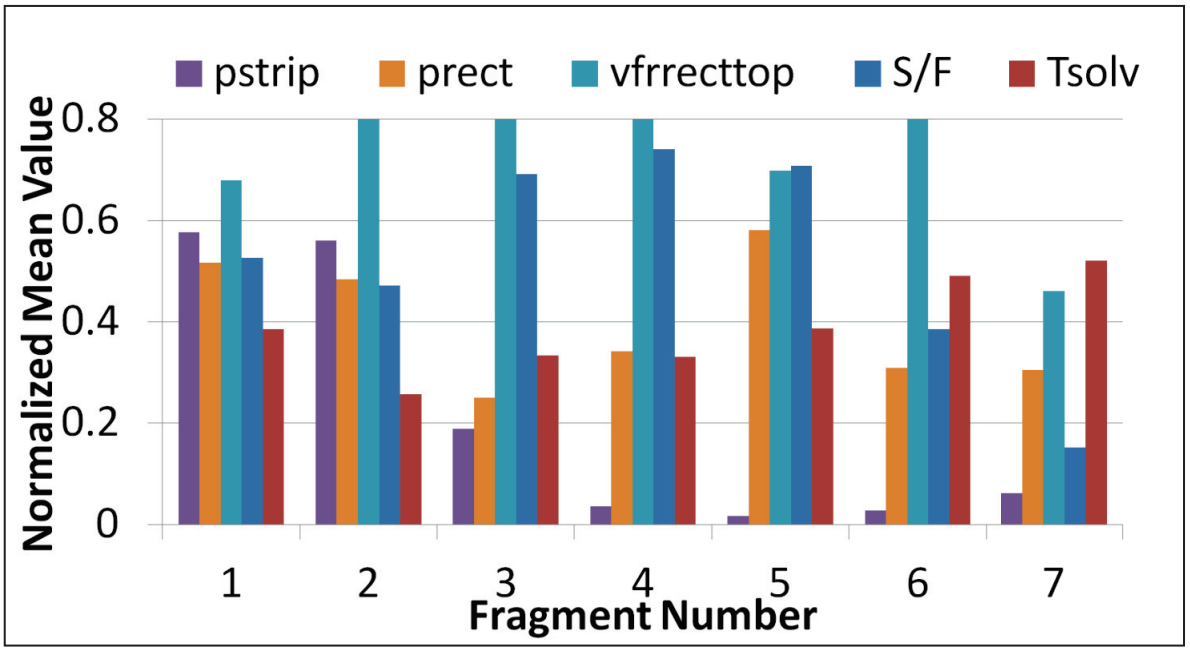

Figure 4:23 Variation of normalized mean values for distillation and dehydration design variables along the Pareto fragments

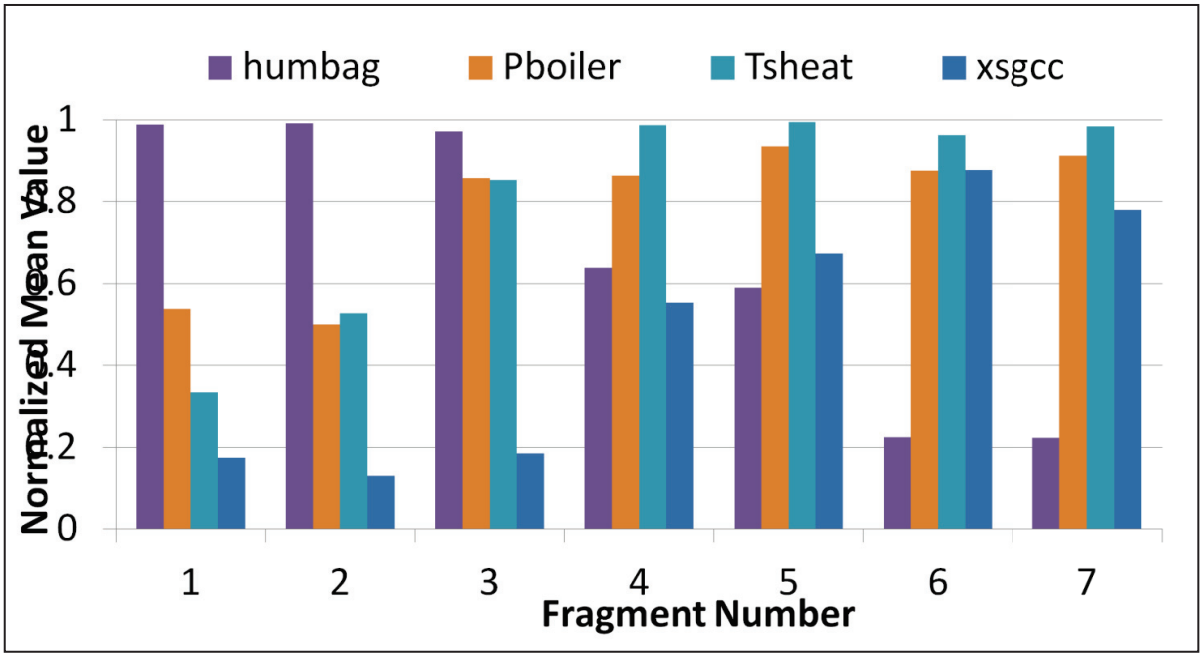

Figure 4:24 Variation of normalized values for bagasse humidity, boiler pressure, superheating temperature and sugar concentration

Figure 4:25 shows the variation in turbine pressures along the various fragments. Almost all of these variables witness a fluctuation except the fourth turbine pressure which sees an increase along the various fragments. This variation cannot however be understood without observing the variation in the corresponding steam flow rate highlighted in Figure 4:26.

We can see, from Figure 4:26, that the third and fourth turbines are employed only in the last fragment. As a result, the variation in their operating pressure for the remaining fragments does not have any impact on the study problem. Another observation is the decrease in the steam flow rate in the second turbine and its increase in the fifth turbine. This increase does not apply for the last fragment where it is met by the appearance of the 3rd and 4th turbines.

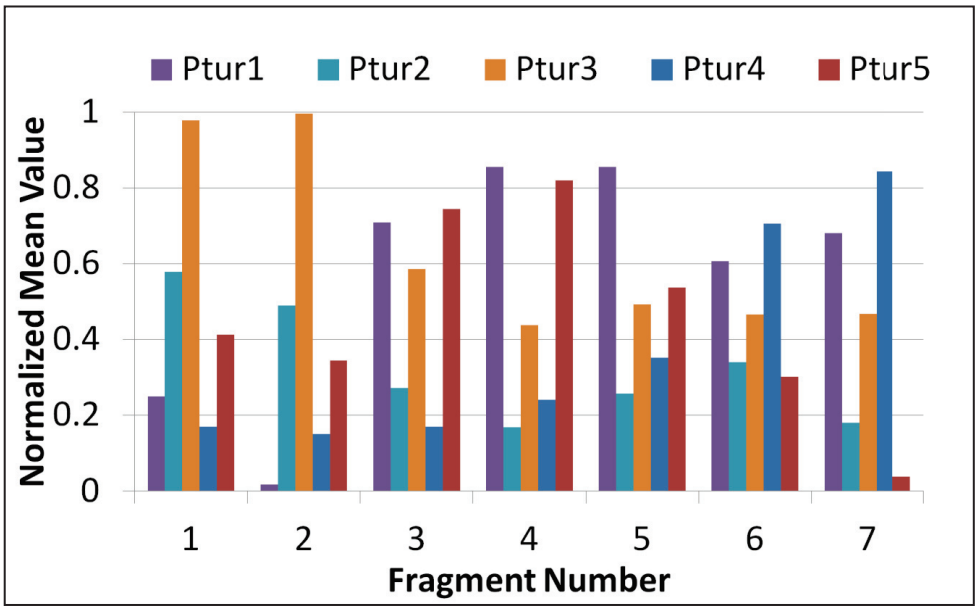

Figure 4:25 Variation of normalized values for turbine pressures

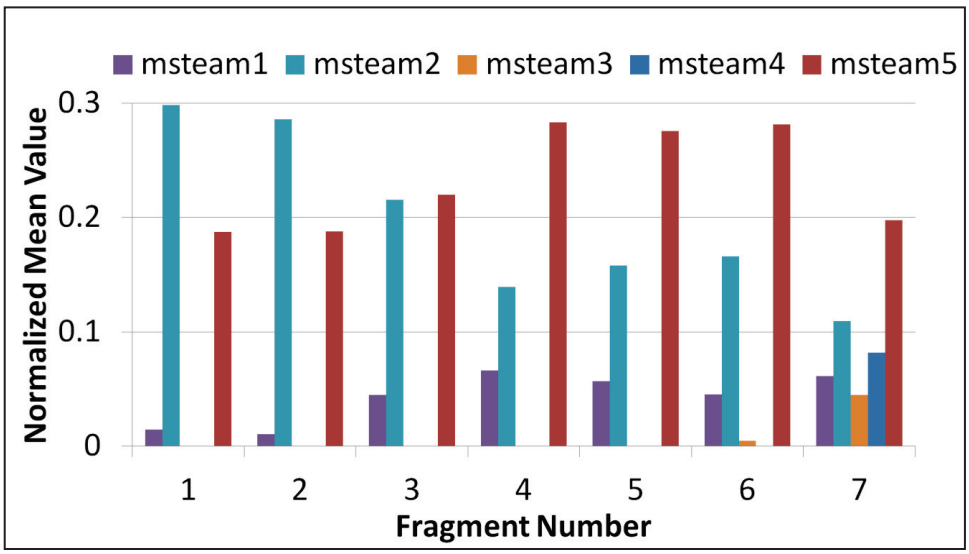

Figure 4:26 Variation of normalized mean values for steam mass flow rates

Figure 4:27 finally shows the variation in the cold and refrigeration utility requirements. These variables differ from the previous ones by the use of Equation 4:15 rather than Equation 4:16. This is because the proposed ranges were too large to be able to visualize any substantial evolution in the values of these variables. The elements of Figure 4:27 indicate that both these values fluctuate

along the fragments. We can see nonetheless that cold utility consumption decreases with higher efficiency higher cost systems. The refrigeration utility consumption can however be linked to the stripping column pressure which decreases for higher efficiency higher cost systems.

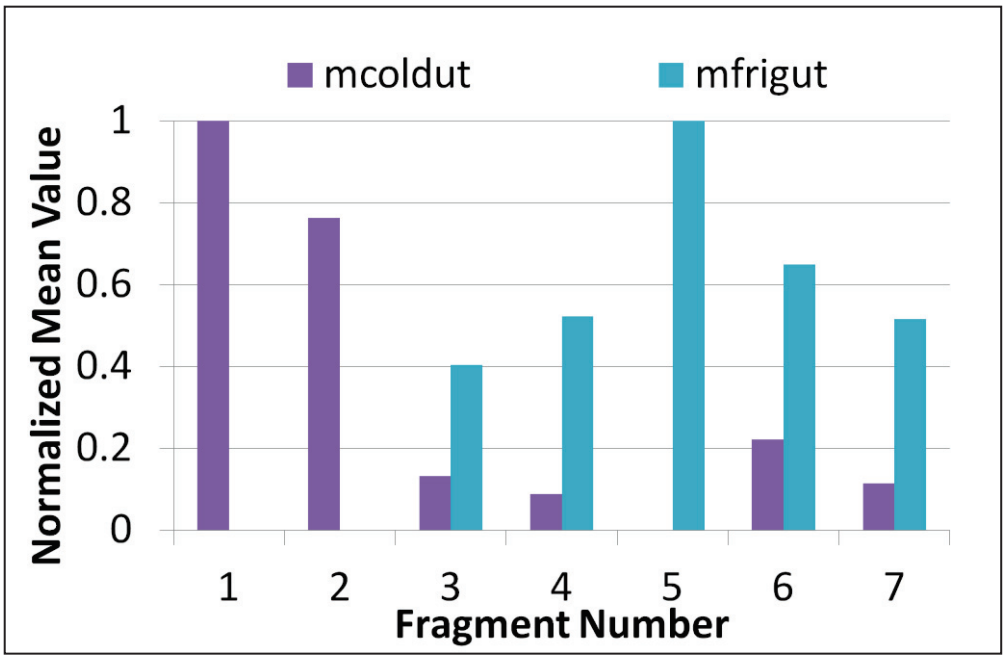

Figure 4:27 Variation of normalized mean values for utility flow rates

4.5.2.7 Classification of Variables

In addition to providing us with the trends for the various design variables, the previous methodology enables us to classify the variables using a literature defined codification. Such a codification is provided by [94] and can be broken down as follows:

- Primary position variables: their values determine the evolution of the objective functions and this in a single trend along the whole Pareto front.
- Secondary position variables: whose values determine the evolution of the objective functions albeit in a periodic trend, possibly influenced by another variable
- Floating variables: whose values fluctuate throughout the Pareto frontier
- Mixed variables: for which the evolution of their values varies throughout the front, witnessing for example a constant value in a given section, an evolution in another section and a floating in a third section.

Table 4:18 Results of variable analysis and classification

Variable Type	Nature of Trend	Investigated Variables	Related Figure	Correlation factor
Position Variable	Positive	$r_{ev_4}, r_{ev_5}, r_{ev_6}$	Figure 4:21	0.5; 0.2; 0.4
		T_{solv},	Figure 4:23	0.2
		P_{boiler}, T_{sheat}	Figure 4:24	0.7; 0.9
		p_{tur4}	Figure 4:25	0.6
		$\dot{m}_{steam,3}, \dot{m}_{steam,4}$	Figure 4:26	0.5; 0.4
	Negative	r_{ev_3}	Figure 4:21	-0.4
		hum_{bag}	Figure 4:24	-0.8
Secondary position variables	Positive	x_{sgcc}	Figure 4:24	0.7
		$\dot{m}_{steam,1}$	Figure 4:26	0.7
		$\dot{m}_{frig,ut}$	Figure 4:27	0.5
	Negative	r_{ev_1}	Figure 4:21	-0.5
		dT_{ev3}	Figure 4:22	-0.6
		p_{strip}	Figure 4:23	-0.9
		p_{tur1};p_{tur2};p_{tur3}	Figure 4:25	0.6; -0.7;-0.6
		$\dot{m}_{steam,2}$, $\dot{m}_{steam,5}$	Figure 4:26	-0.9; 0.5
		$\dot{m}_{cold,ut}$	Figure 4:27	-0.8
Floating Variables	Positive	r_{ev_2}	Figure 4:21	0.06
		dT_{ev5}	Figure 4:22	0.2
	Negative	dT_{ev2}; dT_{ev4}; dT_{ev6}	Figure 4:22	-0.3; -0.04;-0.2
		$V_{fr,rect,top}$;P_{rect}; S/F	Figure 4:23	-0.1;-0.2;-0.1
		p_{tur5}	Figure 4:25	-0.1

Considering the level of detail associated with this variable, it will be adopted for our current problem, albeit with a small modification. This modification takes into account the sign of the trend (increasing vs. decreasing) that links the variables to the objective functions. Moreover, seeing the correlation existing between the objective functions (increasing efficiency for increasing costs), trends will only be defined for one objective function, exergy efficiency in our case. Considering this as well as the content of the previous analysis, the results for our variable classification are provided in Table 4:18. This table does not have any fixed variables however, since no such variables could be deduced from the previous analysis. The correlation factor linking each variable to the exergy efficiency was also included in this table. This factor serves to assert the findings of the previous graphical analysis. As indicated by Breedel et al., this parameter should be handled with great care since it cannot determine by itself the nature of the variables. Finally, this classification is only valid given the ranges specified in Table 4:16.

4.6 Profitability evaluation: selection of optimal configuration

4.6.1 Definition of evaluated parameters and economic hypotheses

As indicated in Chapter 1, our optimal process selection method is based on a profitability analysis which seeks to identify the process with the optimal values for chosen indicators under different economic scenarios. The key profitability indicator, used in industry worldwide, is the Net Present Value. In fact, a given industrial project is said to be profitable if and only if its Net Present Value is positive. In addition, the NPV can be used to select between competing industrial alternatives, namely presented by the Pareto curve. With this in mind, a given industrial project is said to be more profitable than another project if and only if its Net Present Value is greater than that of the other project.

For these reasons, this parameter is be used in our case, mainly to select the most optimal Pareto configuration. Details concerning the calculation procedure for this parameter for a given industrial project are provided in Chapter 1. We will contend ourselves in this level with defining an additional indicator. This indicator is $maxNPV$ which represents the highest NPV value for all points belonging to the Pareto curve. This parameter allows also to pinpoint the corresponding most profitable Pareto individual, I_{profit}. Considering this, Equation 4:17 provides the formula for calculating the maximum Net Present Value whereas Equation 4:18 provides the formula for determining the most profitable Pareto alternative.

Equation 4:17 Formula for calculating the maximum feasible Net Present Value (M$)

$$maxNPV(M\$) = \max_{I \in Pareto} NPV_I(Economic\ conditions)$$

Equation 4:18 Formula for determining the most profitable Pareto alternative

$$I_{Profit} = (ex_{eff,I_{Profit}}, C_{FC,I_{Profit}})/NPV_{I_{Profit}} = maxNPV$$

Considering the importance of the said economic conditions, we provide below a definition of the various parameters entering into play in the Net Present Value calculation procedure:

- The project life time (LT, y): the number of years the plant will be in operation.
- The Salvage equipment value (SV, M$) :the equipment selling price after the project life time is done
- The construction and start-up period (t_{c-s}, y): the period needed to set up the plant before its first round of production.
- The depreciation rate (λ): linked to the loss of value of equipment, assumed to evolve in a linear manner for a given number of years.
- The days of operation per year (n_{dop}) : the number of days the plant will be in production mode, evaluated with 24h/day
- The tax rate($\mathbf{tax}_{\boldsymbol{rate}}$) imposed on the net profit after depreciation.

- The sugarcane price (SCP) evaluated in \$/t-SC.
- The leaves price (LP) also evaluated in \$/ t-leaves
- The ethanol selling price (ESP) evaluated in \$/l ethanol
- The power selling price (PSP) evaluated in \$/MWh.
- The Discount Rate (%): set by the investor to evaluate the risk associated with the project and the time value of money.

With this in mind, Table 4:19 provides information concerning the chosen economic scenarios, based on data extracted from literature, as well as the results for the different indicators under these different scenarios.

Table 4:19 Results of profitability evaluation: economic hypotheses as extracted from literature and values for chosen indicators

Article	[69]	[89]	[64]	[63]
Evaluated Scenario	1	2	3	4
Project lifetime (years)	25		20	25
Salvage equipment value (M$)	0			
Construction and start-up (years)	2			
Depreciation (years)	10- Linear			
Days of operation	167			210
Tax rate (%)	34%			
Sugarcane price (SCP) ($/TC)	19.41	23.25	20.40	28.76
Leaves Price (LP) (($/TC)	15	17.05		
Ethanol price ($/L)	0.5	0.60	0.53	0.513
Electricity price ($/MWh)	70.5	84.88	66.00	69
Discount Rate (r_{dc} %)	11%			

As we can see in Table 4:19, the provided economic indicators provide a great diversity in their values. In fact, only the salvage equipment value, the construction and start-up period, and the depreciation and tax rates are similar for all four cases. The remaining parameters vary between cases, with raw material and product prices having a specific value for each case. Nonetheless, the Discount Rate was only specified by [63], in the form of a Minimum Accepted Internal Rate of Return. However, this value was chosen for all our economic evaluations. This choice is validated by the works of Short et al. who proposed for the American Department of Energy a discount rate of 10% for all projects dealing with renewable energy production.

4.6.2 Presentation of results for all economic scenarios

We present in this section the results of the profitability analysis, as described previously. We start by highlighting in Figure 4:28 the curves present the evolution of the Net Present Value with respect to exergy efficiency across the Pareto population for all four economic scenarios. As we

can see, all four curves follow a similar trend albeit with different NPV values. As a result, an optimal profitability region similar to all scenarios can be extracted from this figure. This region is defined by the two dotted lines highlighted therein. The first line refers to an exergy efficiency value of 39.82% whereas the second refers to an efficiency of 41.31%. Moreover, a maximal profitability design point, similar to all scenarios, can be extracted from this curve, and is also represented by the solid line in Figure 4:28. This point is associated with an exergy efficiency of 40.65%.

Additionally, we can clearly see that the second scenario is the most profitable of all the scenarios, followed by the first, third and fourth. This is concluded by virtue of decreasing NPV values for all points on the curve. As a result, both the maximum Net Present Value and the number of profitable points (NPV>0) decreases when we go from the second to the first and finally the fourth scenario. Finally, all of the NPV curves present a series of peeks occurring at specific values for exergy efficiency. These peeks present local optima for the said curves. Considering this, they obtained optimal point is an additional example of such a peek.

Considering the results provided in Figure 4:28, Table 4:20 highlights the results obtained for the maximum NPV ($maxNPV$) along with its corresponding most profitable Pareto point (I_{Profit}). This table also provides the reader with an additional parameter, the number of profitable alternatives, i.e. having an NPV greater than zero.

Table 4:20 Results for NPV related indicators for all four economic scenarios

Evaluated Scenario	1	2	3	4
Number of profitable alternatives @ IRR= 11% (N_{alt})	29	32	29	15
Maximum Net Present Value @ IRR= 11% $maxNPV$ (M$)	34.3	99.8	44.9	12.0
$I_{Profit}\ (ex_{eff}; C_{inv})$	(40.65%; 163 M$)	(40.65%; 163 M$)	(40.65%; 163 M$)	(40.65%; 163 M$)

The obtained results confirm the trends observed in the previous figures. We see that Scenario 2 provides substantially better results than the other scenarios. Scenario 1 and 3 on the other hand provide almost similar results, with scenario 1 being slightly better (28 profitable individuals vs. 27; 37.3 maxNPV). Finally, scenario 4 provides the worst results for all indicators. Nevertheless, the same design point, with an exergy efficiency of 40.65% and a capital cost of 163 M$, presents the most optimal solutions for all investigated scenarios.

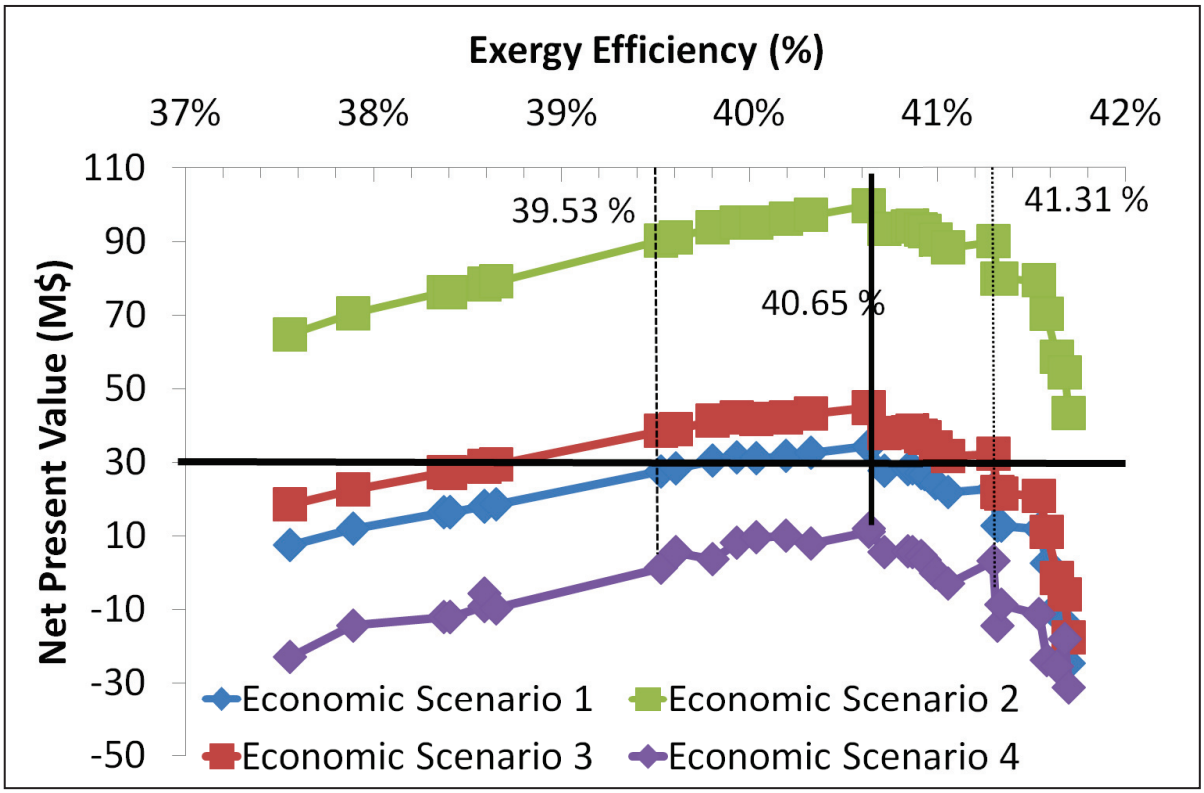

Figure 4:28 Net Present Value vs. Exergy efficiency for Pareto individuals under four different economic scenarios

4.6.3 Explanation of the variation within a specific NPV/PI curve

In this section, we try to identify the reason for the observed form of the NPV/PI curve. This can only be done by returning to the Pareto curve which served to calculate them. For this reason, we make use of Figure 4:29 which plots the Investment cost along with the Net Present Value, corresponding to the second economic scenario, against exergy efficiency for all the points on the Pareto curve. As we can see in Figure 4:29, the initial increase in Net Present Value for low exergy efficiencies is related to the gradual and small increase in capital cost for these points.

This same increase in capital costs sees then an upward spike leading to the witnessed decrease in Net Present Value. This entails that, under the chosen values for economic parameters, the increase in investment cost after the optimal design point weighs more heavily on the investment cost than the increase in exergy efficiency.

In addition, as we can see, the featured peeks, and a fortiori the peek with the highest NPV, occur at the previously highlighted knee points. This is again due to the paradigm offered by these knee points: they have a greater exergy efficiency for a similar capital cost than the point before them, and a smaller capital cost for a similar efficiency than the point after them. Considering this, the Net Present Value can be an excellent mathematical way to identify these points.

We can also notice the optimal and limit points denoting the optimality region. We can see from this figure that these points are inflexion points. More importantly we can see from our figure that our optimal point (40.65% and 163 M$) offers the best compromise between exergy efficiency and capital costs. In fact, the curve is characterized by a net increase in exergy efficiency for a small increase in capital cost for points before the optimal, whilst the opposite is true for points after it.

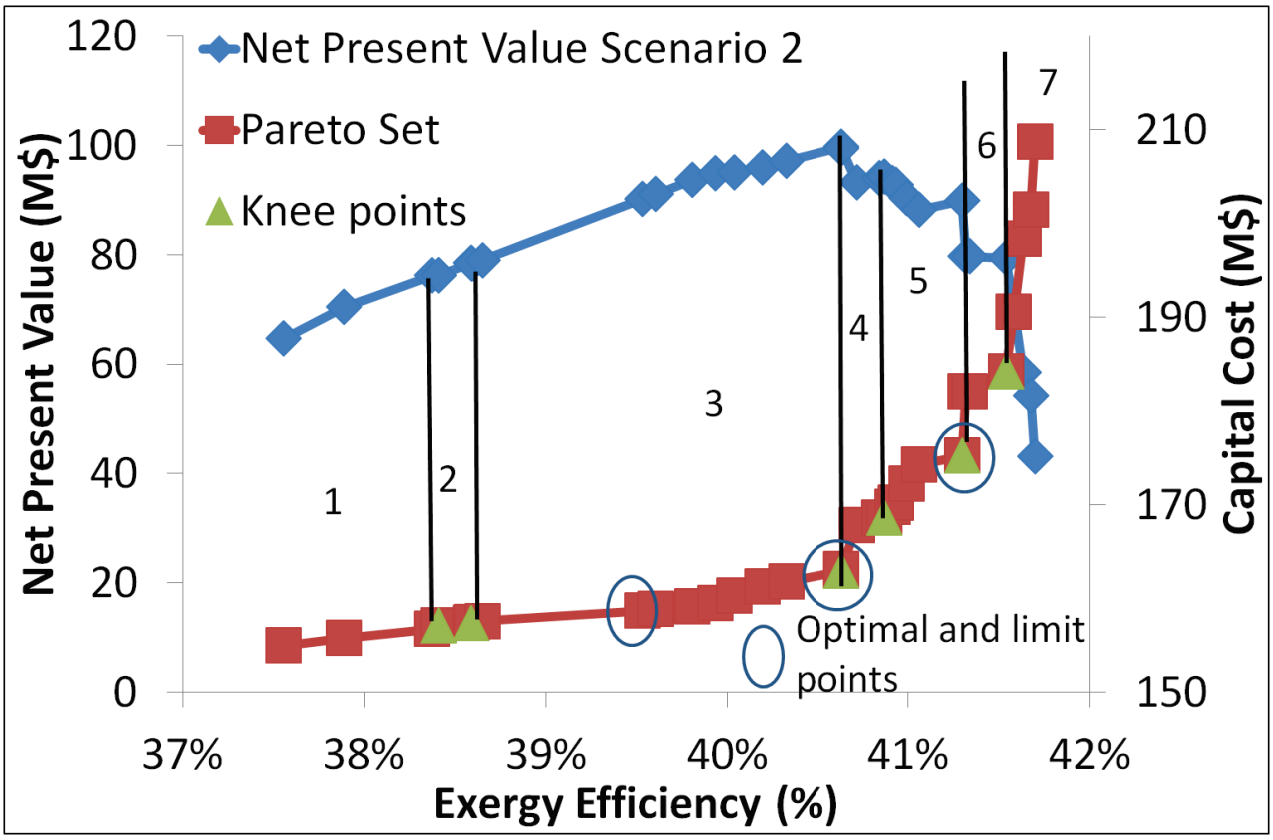

Figure 4:29 NPV vs. Exergy Efficiency & Capital cost vs. Exergy efficiency for optimal Pareto system. Identification of NPV based fragmentation

4.6.3.1 Explanation of the variation between the NPV/PI curves

In this section, we try to identify the reasons for the observed evolution between the various NPV/PI curves. Seeing that the optimal solution is the same for all considerations, the observed difference is due only to the difference in values for the economic parameters. Considering this, the optimal results observed for the second scenario can be explained by the rather high values for the products: ethanol (0.6 $/L vs. a maximum of 0.53 $/L) and electricity (84.88 $/MWh vs. a maximum of 70.5 $/MWh) and this despite the rather high value for the sugarcane price (23.25 $/t-SC). Moreover, the bad results associated with the fourth economic scenario are due to the very high sugarcane price (28.76 $/t-SC vs. a maximum of 23.25 $/t-SC), which is faced by rather mild values for ethanol and power (0.513 $/L and 69 $/MWh). Nonetheless, the main reason behind its feasibility is the rather high operating time (210 d/y vs. a standard value of 167 d/y). Finally, the similarity between the results for the first and third scenarios can be linked to the

rather close prices for sugarcane (19.41 $/t –SC and 20.4 $/t-SC), ethanol (0.5 $/L vs. 0.53 $/L) and power (70.5 $/MWh and 66 $/MW). The slightly lower value associated with the third scenario is due to the smaller project lifetime (20 vs. 25 years). From all the previously mentioned parameters, the leaves price is the only parameter that features little influence on the obtained results.

Finally, the fact that the same operating point provided optimal results for all alternatives is mainly due to the rather mild electricity prices which do not vary by a great extent. In fact by looking at the structure of the problem, we can see that the only input/output stream that evolves with exergy efficiency is power. Considering this, a higher power selling price will lead the maximal NPV towards a higher exergy efficiency cost.

As a matter of fact, a small sensitivity analysis, applied to the first scenario, yielded that only in the case of a 2.2 fold increase in electricity prices (155 $/MWh vs.70.5 $/MWh) does a higher efficiency higher cost process (41.3% ; 175M$) become more profitable than the previously obtained point. To the opposite, the same analysis yielded that only in the case of a 1.3-fold decrease in electricity prices for the first case (55 $/MWh vs. 70.5 $/MWh) does a lower efficiency lower cost process (40.04%; 160 M$) process become more profitable.

Nonetheless, it is interesting to note that both these points are peek points that pertain to the previously obtained NPV curve.

4.6.3.2 Definition and results for additional economic parameters

Even though the Net Present Value is the ultimate parameter for optimal process selection and for the evaluation of profitability, other economic indicators, dealt with in literature, will be defined in this paragraph. These indicators are detailed below with their formulas specified in Table 4:21:

- The maximum Internal Rate of Return ($maxIRR$) is the IRR value for which the Maximum Net Present Value for all individuals in the Pareto curve is equal to zero. This evaluation highlighted in Equation 4:19, is carried out under fixed economic hypotheses. For the remaining calculations, an Internal Rate of Return of 11% was assumed for all projects as highlighted in [63]. This indicator is interesting because it allows the designer to compare this project with other possible industrial projects.
- The Minimum Ethanol Selling Price ($minESP$), known in literature under the acronym $MESP$, evaluated in ($/l) is the ethanol price for which the maximum NPV for all individuals in the Pareto curve is equal to zero. This evaluation, highlighted in Equation 4:20, is realized under fixed economic hypotheses and for a constant internal rate of return. The only variable is the ethanol selling price (ESP). This indicator is interesting, because below this price no process on the Pareto curve is profitable, with all other economic indicators remaining constant. The lower this value the better.
- The Minimum Power Selling Price ($minPSP$) evaluated in ($/MW) is the electricity price for which the maximum NPV for all Pareto individuals is equal to zero. This evaluation, highlighted

in Equation 4:21, is performed under fixed economic hypotheses and for a constant internal rate of return, with the only variable being the electricity selling price (PSP). This indicator is interesting, because below this price no process on the Pareto curve is profitable, with all other economic indicators remaining constant. The lower this value the better

- The Maximum SugarCane Price ($maxSCP$) evaluated in ($/t SC) is the sugarcane purchase price for which the maximum NPV for all Pareto individuals is equal to zero. This evaluation, highlighted in Equation 4:22, is performed under fixed economic hypotheses and for a constant IRR, with the only variable being the sugarcane price (SCP). This indicator is interesting, because above this price no process on the Pareto curve is profitable. Thus, it can be concluded that the higher this value the better
- The Maximum Leaves Price ($maxLP$) evaluated in ($/t Leaves) is the leaves purchase price for which the maximum Net Present Value for all Pareto individuals is equal to zero. This evaluation, highlighted in Equation 4:23, is performed under fixed economic hypotheses and for a constant internal rate of return, with the only variable being the leaves price (LP). The higher this value the better
- Moreover, their values are calculated for the different economic scenarios as highlighted in Table 4:22. Moreover, each indicator is associated with an optimal process configuration which will also be provided in the results. Considering this, values for the various economic indicators, including the Maximum NPV, $\max NPV$, as well as the optimal configurations associated with each indicator, are provided in Table 4:22.

Table 4:21 Mathematical formulation for additional economic indicators

Economic Indicator	Mathematical Equation	Equation number
$\boldsymbol{maxIRR}$ (%)	$maxIRR(\%) = IRR / \max_{I \in Pareto} NPV_I(IRR) = 0$	Equation 4:19 Formula for the maximum internal rate of return
$\boldsymbol{MESP}$ $(\frac{\$}{\boldsymbol{l\ ethanol}})$	$MESP(\$/l) = ESP / \max_{I \in Pareto} NPV_I(ESP) = 0$	Equation 4:20 Formula for the Minimum Ethanol selling price
$\boldsymbol{MPSP}$ $(\frac{\$}{\boldsymbol{MWh}})$	$MPSP(\$/l) = PSP / \max_{I \in Pareto} NPV_I(PSP) = 0$	Equation 4:21 Formula for the Minimum Power selling price
$\boldsymbol{maxSCP}$ $(\frac{\$}{\mathbf{t-SC}})$	$maxSCP = SCP / \max_{I \in Pareto} NPV_I(SCP) = 0$	Equation 4:22 Formula for the maximum sugarcane price
$\boldsymbol{maxLP}$ $(\frac{\$}{\boldsymbol{t-leaves}})$	$maxLP = LP / \max_{I \in Pareto} NPV_I(SCP) = 0$	Equation 4:23 Formula for the Maximum Leaves price

From the obtained results, we can see that the Maximum IRR evolves in a similar manner to the Maximum NPV indicator. As a result, its value is the most optimal for the second scenario,

followed by the first, third and finally fourth. This also applies for the minimum Power selling price ($minPSP$) and maximum leaves price ($maxLP$) whose values also followst he same trend. This does not apply to other indicators such as $minESP$ and $maxSCP$, whose values follow different trends.

For example, $minESP$ has its best calue for the first scenario, followed by the second, third and fourth. The first case fares better than the second due to its smaller sugarcane price, and this despite having a smaller price for electricity. The second fares better than the third because of its higher electricity price and greater project lifetime, and this despite having a higher sugarcane price. Finally, the third case fares better than the fourth due to its smaller sugarcane price, and this despite having a smaller project lifetime and operating days per year.

$maxSCP$ on the other hand sees its best value for the second case, followed by the fourth, third and finally first. This second case fares better than the fourth thanks to its higher product prices. The fourth fares better than the third thanks to its greater operating time. And finally, the third fares better than the first thanks to its greater ethanol price.

Table 4:22 Results for various economic indicators

Evaluated Scenario	1	2	3	4
$maxNPV$ (M$)	37.3	103.5	27.7	12
$maxIRR$ (%)	13.66%	18.16%	13.25%	11.85%
Optimal configuration-I ($ex_{eff}; C_{inv}$)	(40.65%; 163 M$)	(40.65%; 163 M$)	(40.04%; 160 M$)	(40.65%; 163 M$)
$minESP$ @ IRR=11% ($/L)	0.455	0.473	0.494	0.502
Optimal configuration-I ($ex_{eff}; C_{inv}$)	(40.65%; 163 M$)	(40.65%; 163 M$)	(40.04%; 160 M$)	(40.65%; 163 M$)
$minPSP$@ IRR=11% ($/L)	48.25	21.95	48.20	63.50
Optimal configuration-I ($ex_{eff}; C_{inv}$)	(39.84%; 160 M$)	(40.04%; 160 M$)	(40.04%; 160 M$)	(40.65%; 163 M$)
maxSCP @ IRR=11% ($/L)	23.1	33.6	23.4	29.47
Optimal configuration-I ($ex_{eff}; C_{inv}$)	(40.65%; 163 M$)	(40.65%; 163 M$)	(40.04%; 160 M$)	(40.65%; 163 M$)
$maxLP$ @ IRR=11% ($/L)	71	174	62	31
Optimal configuration-I ($ex_{eff}; C_{inv}$)	(40.65%; 163 M$)	(40.65%; 163 M$)	(40.04%; 160 M$)	(40.65%; 163 M$)

This complex situation is however met by the rather constant optimal design (40.65%; 163M$) which applies for almost all cases. This design is not however the most optimal in the case of minimal electricity prices, where the optimal design is obtained for a 39.85% efficiency and 160 M$ capital cost in the first to third scenarios. This shift is due to the lowering of the electricity price. This however does not apply for the fourth case, which can only be understood in the light of a greater number of operating days per year, justifying hence the investment in a higher

efficiency process. Moreover, this same design (39.84%; 160M$) is the best for $maxIRR$ in the third scenario. This can be understood in the light of a smaller project lifetime which justifies the choice of a less efficient less expensive system.

4.6.4 Comparison with literature

In this section, we will compare the obtained results with those deduced from literature. This comparison will take into consideration the Pareto curve as well as the values for the various economic indicators.

In order to compare the Pareto curve, it is necessary to calculate the exergy efficiency of the various literature works. This is faced by the hurdle of a variable input sugarcane content which leads to a variable output ethanol rate. This issue is handled by adopting a general formula for the exergy content of sugarcane. The two main energy vectors of this stream are sucrose and bagasse (fibers) whose nominal exergy contents are 6.47 and 5.88 MWh/t. Considering this, the formulate for calculating the nominal exergy content of sugarcane is provided in Equation 4:24. Likewise, the formula for calculating the exergy content of the produced ethanol based on the common metric used in literature (l ethanol/ton sugar cane) is also provided in Equation 4:25.

Equation 4:24 Expression of nominal sugarcane exergy content as a function of fibers and sucrose content

$$ex_{cane,nom} = x_{sucrose} \times ex_{sucrose} + x_{bagasse} \times ex_{bagasse}$$
$$= 6.47 \times x_{sucrose} + 5.88 \times x_{bagasse} (\frac{MWh}{t})$$

Equation 4:25 Produced ethanol exergy content based on production rate

$$ex_{et,prod} = et_{prod} \times \dot{m}_{sugarcane} \times \rho_{ethanol} \times ex_{ethanol} (MW)$$

As a result, the exergy efficiency for each literature alternative is calculated following the formula provided in Equation 4:26.

Equation 4:26 Calculation of exergy efficiency

$$ex_{eff} = \frac{ex_{et,prod} + ex_W}{\dot{m}_{sugarcane} \times ex_{cane,nom} + \dot{m}_{leaves} \times ex_{leaves,m}}$$

Considering the previous definitions, a reminder of key literature hypotheses and results along with the additional evaluation of exergy efficiency is provided in Table 4:23. This table contains also the key hypotheses for our work along with values for fixed variables in our studied process. As we can see, our current work is the only work that makes use of multi-objective optimization for the proposed process. It is for this same reason that neither the net power production, the exergy efficiency or the investment cost were provided. Moreover, Table 4:23 consists a first comparison of sugarcane conversion technologies with the use of exergy efficiency as a

comparison function. This criterion enables to overcome the challenges to comparison posed by disparities in the content of input sugarcane.

Table 4:23 Reminder of previous literature results with the inclusion of calculated exergy efficiency

Article	[69]			[89]	[64]	[63]	[44]	Current work
Sugarcane input rate (TC/h)	500							
Leaves input rate (kg/TC)	0	0	66				0	66
Optimized process configuration		x	x	x		x	x	x
Leaves combustion			x	x	x	x		x
Heat integration							x	x
Multi-objective optimization								x
Sugarcane Sugars content (wt %)	15			15.3	15	15.86	14.44	12.5
Sugarcane Fibers Content (wt. %)	14			13	14	13	13.15	12.52
Exergy Ethanol produced (MW)	293			269	279	300	268	264
Net power produced (MW)	46.5	52.5	93	86.5	71	72	43	
Total exergy in products (MW)	339	345	386	355	350	372	311	
Nominal sugarcane exergy content (MWh/t)	1.589			1.589	1.589	1.543	1.589	1.571
Sugarcane Exergy Content (MW)	794	794	794	772	794	785	755	723
Leaves exergy content (MW)	0	0	145	0	0	0	0	145
Total input Exergy (MW)	794	794	940	917	794	931	755	868
Exergy Efficiency (%)	42.7	43.5	41.0	38.8	44.0	40.0	41.0	
Investment cost (M$)	199	202	222	263	117	165	143.3	

With this in mind, Figure 4:30 plots the variable literature points on the same exergy efficiency-capital cost graph as the previously obtained Pareto curve. As we can see, Pareto results fare better than literature ones for cases without leaves combustion, whereas results for cases omitting the use of leaves fare better, from the standpoints of both exergy efficiency and capital

costs. This might pose some questions regarding the correctness of employing the chosen objective functions, namely exergy efficiency. The second point is stressed by the greater IRR obtained for the case of leaves combustion (16.90%) when compared to their exclusion (15.90%) in the works of [69]. It should be noted nonetheless that the practice of burning leaves in the CHP system is a novel one, with the possibility of burning them on site remaining a solid practice. This leads us to questioning the advantages of the chosen leaves valorization techniques. In fact, the low efficiency associated with leaves combustion stresses all the more the low efficiency of the combined leaves and bagasse combustion system. This guides future work towards a better utilization of the input material.

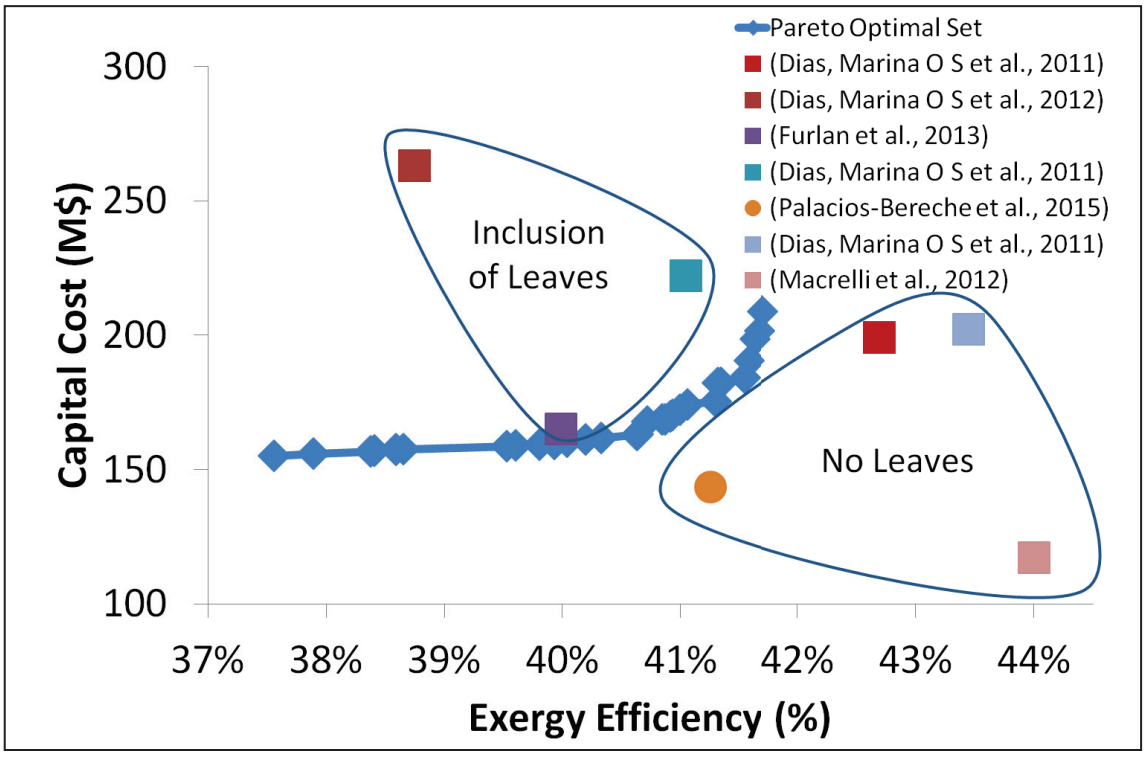

Figure 4:30 Obtained Exergy Efficiency vs. Capital Cost Pareto curve along with calculated literature results (Dias Marina OS et al.2011) [69], (Dias, Marina OS et al. 2012) [89], (Macrelli et al. 2012) [64], (Furlan et al. 2013) [63] and (Palacios-Bereche et al. 2015) [44]

Finally, a comparison of the values for the key economic indicators concerning the various scenarios with leaves combustion is provided in Table 4:24. As we can see, the results suffer from a large discrepancy due to the means in which these variables have been calculated. Nonetheless, we can clearly see the discrepancy between the values of the NPV for the case of [63]. This is due to the fact that the authors adopted a low price for their electricity, based on the spot market (40.1 $/MWh), which is lower than the minimum power selling price set at 63.5$/MWh. We on the other hand adopted a more optimistic price based on the auction market (69.2 $/MWh).

Table 4:24 Comparison of results for key economic indicators literature vs. optimal Pareto front

Article	[69]	[89]	[64]	[63]
Evaluated Scenario	1	2	3	4
MESP ($ / L ethanol)	0.288	0.37	0.264	0.29
MESP @ IRR=11% ($/L)	0.455	0.473	0.494	0.502
MPSP ($/MWh)	44.7	52.63		
MPSP @ IRR=11% ($/MWh)	48.25	21.95	48.20	63.50
maxIRR (%)	16.90%	14.90%	32.10%	7.60%
$\boldsymbol{maxIRR}$ **(%)**	13.66%	18.16%	13.25%	11.85%
NPV (M$)				-34.5
$\boldsymbol{maxNPV}$ **(M$)**	37.3	103.5	27.7	12

4.7 Conclusion

This chapter dealt with the optimization of the production of bioelectricity and bioethanol from sugarcane and sugarcane leaves in a combined distillery and cogeneration plant. This optimization followed a rigorous methodology starting from a thorough bibliographic investigation and a subsequent synthesis of associated results. The related bibliographic work was divided according to the investigated process section: distillation, dehydration, multi-effect evaporation and bagasse combustion leading to combined heat and power production, before highlighting works dealing with global process evaluation.

This was followed by a choice of objective functions, design variables and associated control ranges. The said functions were exergy efficiency which needed to be maximized and capital cost which on the other hand needed to be minimized. Design variables were related to various process steps: distillation, dehydration, evaporation and combined heat and power production. They were controlled by two sets of algorithms: the first is a Mixed Integer Linear Programming algorithm dealing with the maximization of net power production. This algorithm controlled 8 utility variables, namely mass flow rates of produced steam, cold water and refrigeration utility. Moreover, this algorithm was part of a global algorithm which controlled 25 intrinsic process parameters such as evaporation rates, temperature decrements, pressure levels, end concentrations and solvent properties.

This global algorithm was a multi-objective evolutionary optimization algorithm which explored the design space, based on error-handling, ranking and selection pressure techniques, and extracted the Non Dominated Pareto set associated with the study problem. This set was obtained after a total of 1000 evaluations and contained a total of 32 points. The exergy efficiency within the Pareto set evolved between a minimum of 37.6% and a maximum of 41.7% for a minimal capital cost of 155 M$ and a maximal cost of 209 M$. Moreover, an explanation was given for the trend followed by the curve. This explanation was based on the observed compromise between net power production, representing the extent of heat integration in the process, and heat exchanger cost, which increases with an increased heat exchange. Finally, as a result of

convergence, the operating range for a number of variables was reduced from the original range defined before the optimization step.

A fragmentation technique was then adopted based on a developed algorithm that seeks to extract curve knee points. These points present an inflection point in the curve and are as a result an indicator for a shift in operation. This step split the obtained Pareto curve into a total of seven fragments, corresponding to seven knee points. The mean value for each design variable was calculated for each fragment and its associated trend was deduced. This allowed us to split our variables into different groups. The first group deals with primary position variables (11 variables), which determine the location of the design point on the Pareto curve. These variables are bagasse humidity, evaporation rates, steam mass flow rates, dehydration solvent feed temperature along with boiler parameters namely boiler pressure and steam superheating temperature. Other categories were split secondary position variables (12 variables) whose values influenced the objective function values but to a lesser extent, and floating variables (9 variables) whose values fluctuated along the Pareto curve.

A profitability analysis using the Net Present Value economic indicator was then performed on the said curve. This analysis enabled to determine the profitability associated with each design alternative and to ultimately select the most profitable one. This analysis was also performed given four different economic scenarios extracted from literature. The obtained NPV curves highlighted similar trends albeit at different values for the NPV indicator. These trends included local optima occurring around the previously identified knee points, with a global optima occurring for all cases at an exergy efficiency of 40.65% and a capital cost of 163 M$. This relationship between NPV and knee points highlights the effectiveness of using this technique to deduce these points from an exergy efficiency-capital cost Pareto curve. The obtained similarity in trends was explained in light of a small variation in economic hypotheses, namely electricity price. It was thus shown that an increase, albeit substantial, in this price leads to a shift in the optimal operating point towards a higher efficiency higher cost design. This need for a substantial increase highlights the hurdles imposed by the associated investment costs. Multiple other economic indicators were calculated, namely the minimum selling prices and maximum prices of products (ethanol and power) and raw materials (sugarcane and leaves) along with the maximum internal rate of return. These values give the designer insights into the limits of profitability associated with the investigated curve under various economic scenarios. It was shown that the previous optimal point retained its optimality for a large number all of almost all indicators, except in specific cases where a smaller efficiency lower cost system (39.84% and 160 M$) prevailed. This was witnessed for the minimum power selling price indicator, and this namely due to the lowering in electricity price.

In the last section of this chapter, comparisons were made with literature results. These comparisons proved the validity of the proposed algorithm, and this despite the disparity in the evaluation techniques adopted in the various works.

This methodology yields a Pareto curve of optimal compromise solutions which can be used as a basis to compare other optimization works. Such works can include the use of additional variables, or the investigation of other process schemes. This curve can also be used as a basis for more detailed decision support methodologies. Only profitability, via the maximization of the NPV, was chosen in our case. In contrast, the decision maker can study the inclusion of additional environmental, societal or safety measures in his decision making procedure. As a result, the obtained Pareto set presents a great base for such works.

Chapter 5 Application of optimal process design methodology to combined distillery, hydrolysis and cogeneration process

In this chapter, we will investigate the application of the methodology for optimal process design highlighted in Chapter 1 to the process defined in Chapter 3. In a first step, we will provide a brief review of the employed methodology and the studied process. We will then present a bibliographic review of the main bibliographic works dealing with the studied process. We will then present the application of our methodology, and analyze the obtained results. Finally, comparisons will be made with results from bibliography, and conclusions will be made.

5.1 Reminder of the applied methodology

The employed methodology is presented in detail in Chapter 1. Nonetheless, a brief reminder thereof is provided in this section. Considering this, a brief description of the methodology's main points and its operating principle is provided in Figure 5:1, with further details in this paragraph. We notice on this figure the one run simulation, multi-objective optimization and optimal process selection steps. All of these steps are fed by bibliographic data which deal either with the design of the process superstructure as highlighted in Chapter 2 or to the choice of optimization variables, objective functions or selection criteria and scenario. With this in mind, the previously highlighted steps are discussed below.

5.1.1 One Run Simulation

A One Run simulation can be realized once specific values are assigned to process variables. This step starts by first performing a process simulation in ASPEN PLUS ®: the chosen values for process variables are transferred to the Aspen simulation flow sheet; mass and energy balances are performed for each process block. Convergence of this simulation occurs when all design specifications are met, and all balances are respected. In this case, values for controlled operating parameters are calculated for each unit operation as well as parameters for mass, heat and power streams.

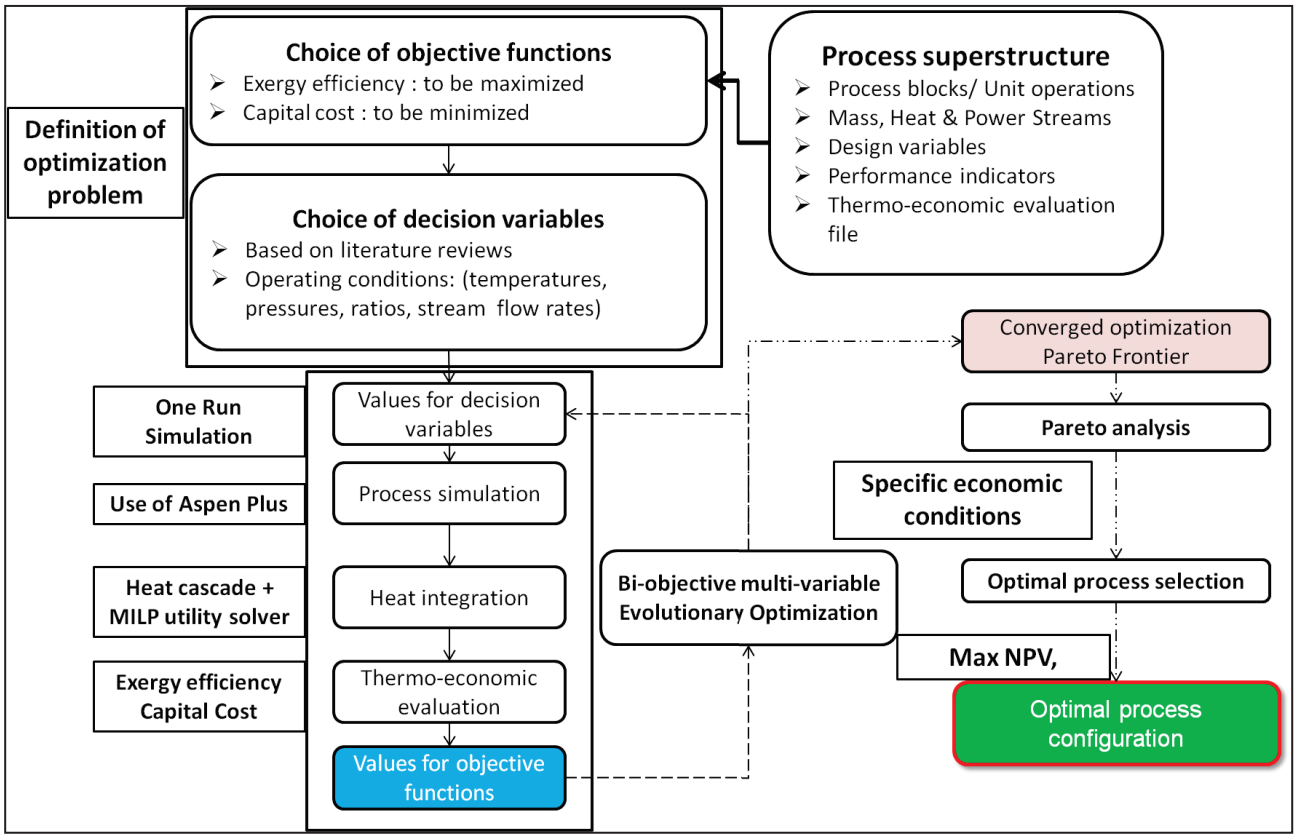

Figure 5:1 Overall scheme for proposed multi-objective optimal process design

Going from heat stream results, we proceed to resolve the process heat integration problem which consists in determining the process heat cascade and the corresponding utility system by the use of a specific linear optimization algorithm, as highlighted in [28]. This algorithm operates in two levels: in a first step, the process streams heat exchange network which minimizes external heat demand is deduced by the use of the heat cascade methodology; then the flow rate of the various utility streams is chosen such that it maximizes a chosen objective function, in our case the cogenerated power stream. Finally, this algorithm deduces also a corresponding cost for the heat exchange network.

Once this is realized, we can proceed to perform a thermo-economic evaluation based on a predefined thermo-economic calculation procedure pertaining to the studied superstructure. This evaluation takes as inputs the results of both process simulation and thermo-economic evaluation, and ultimately returns values for the process performance indicators, otherwise denoted as objective functions.

5.1.2 Process optimization

Multi-objective multi-variable evolutionary optimization can then be performed on the defined system. This optimization converges towards a Pareto set of solutions presenting a compromise between the various objectives. The chosen objective functions are as highlighted in Chapter 1 the

maximization of exergy efficiency and the minimization of capital costs. These objectives are conflicting and both contribute to the optimal design of a given process.

5.1.3 Optimal process selection

Specific analysis and selection techniques are finally applied on the obtained Pareto curve in order to deduce one single optimal process configuration. As indicated in Chapter 1, our chosen technique resorts to a profitability analysis under specific or varying economic conditions. This profitability is expressed notably by the maximization of the Net Present Value (NPV) criterion

5.2 Description of process superstructure

The studied process is the combined distillery, hydrolysis and cogeneration system for the production of conventional and cellulosic ethanol along with power cogeneration. Figure 5:2 highlights the chosen process superstructure, thoroughly described in Chapter 3. The steps highlighted in blue in this figure are in common with the conventional distillery. Such steps are: Sugarcane handling and sugar extraction, juice concentration and sterilization, fermentation, distillation and dehydration. The three last steps were grouped together for the sake of conciseness. The cold and hot utilities are also common to both the conventional distillery and the combined production process.

Moreover, the blocks highlighted in green relate to the hydrolysis section. These block include the following steps: pretreatment, hydrolysis and biodigestion coupled with gas turbine. Pretreatment ensures a breakdown of the bagasse structure with a partial hydrolysis of its hemicellulose content to xylose (C5) sugars. This step is followed by filtration and washing tasks which end up separating the solids and xylose content. The solids stream is mixed with enzymes and water and sent to the hydrolysis reactor. Two hydrolysis reactions occur therein. The predominant one concerns the partial conversion of cellulose to glucose, whilst the second concerns the hydrolysis of the remaining hemicellulose content to xylose. This reactor leaves however the lignin content, along with a significant cellulosic portion of the bagasse intact.

Various streams result from the novel section. The first is the glucose stream which is injected into the ethanol production train prior to juice concentration. The second is the unhydrolyzed bagasse stream which is injected into the combustion section. The third is the xylose stream which is converted into power.

We can also see the presence of a bagasse splitter. This splitter enables the diversion of the resulting bagasse either to combustion or to hydrolysis.

This section has also an intermediary stream between pretreatment and hydrolysis consisting in a cellulose/lignin (cellulignin) solid fraction which is submitted to hydrolysis. This splits highlights the competition that exists between these two steps which translates into a competition between increased power production and increased ethanol production.

Moreover, based on Figure 5:2, this superstructure is based on the following design choices:

- Leaves are not hydrolyzed with sugarcane bagasse. They are solely burnt as a means for heat and power cogeneration
- Mass integration between sugar streams occurs prior to the juice concentration section
- Only the biodigestion of the xylose fraction, without the distillation vinasse, is considered

With the previous analysis in mind, it is interesting to note that, as highlighted in Chapter 3 , the resulting process has many similarities with the conventional ethanol from sugarcane production process, namely in the separation levels where the previous optimization challenges and considerations hold.

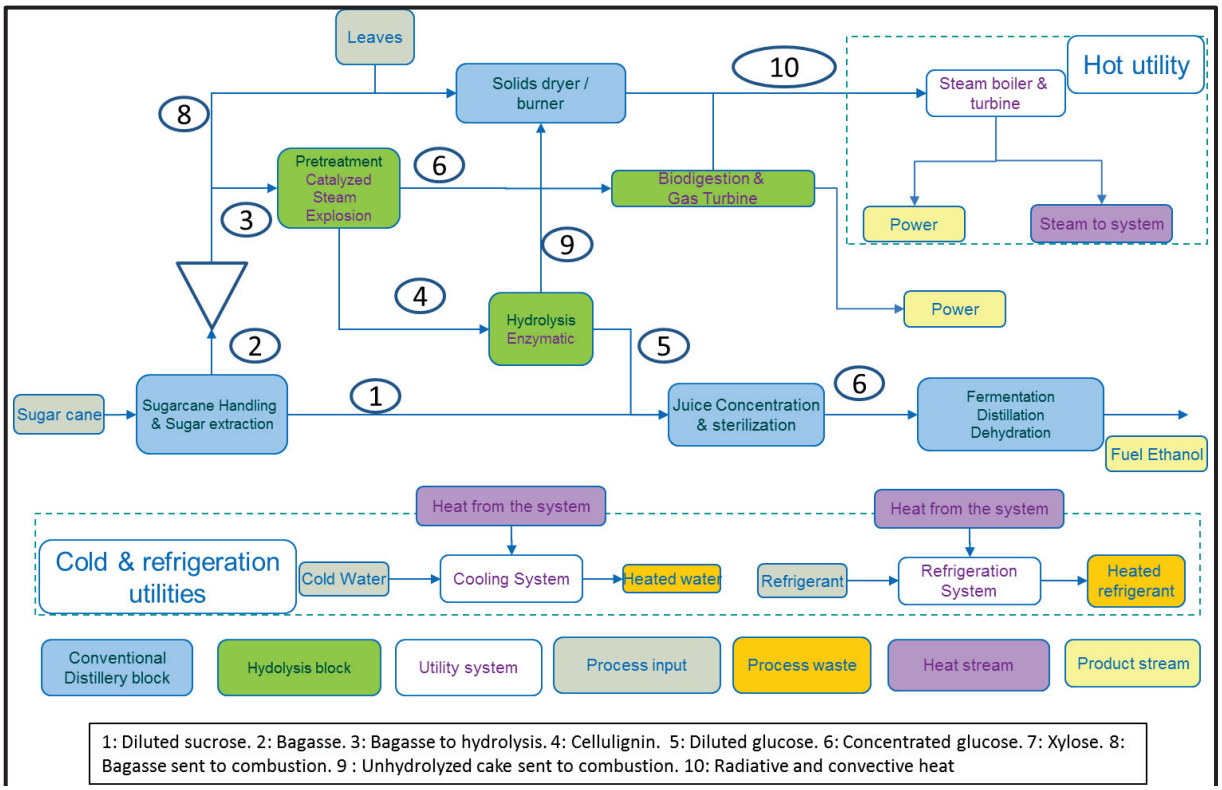

Figure 5:2 Block Flow Diagram for combined production process

5.3 Bibliography concerning process optimization

Bagasse hydrolysis and the conversion of its carbohydrate fraction, namely cellulose, to ethanol is a rather nascent technology of bagasse hydrolysis. This technology came into interest namely due to the great availability of bagasse in conventional sugarcane factories and to the impeding need of producing renewable bio-based fuels. Considering this, the optimal integration of this technology into a global sugarcane distillery and cogeneration plant is a topic of great interest in literature. As a result, this paragraph will provide a bibliographic review of research works dealing with the optimization of the performance of the combined distillery, cogeneration and hydrolysis processes. This review contains works which have dealt with configurations a bit different from

our chosen superstructure. This will help both position our optimization results within the more global research activity.

5.3.1 Investigated process designs and operating parameters

[64] performed a thermo-economic evaluation of several process configurations, based on an initial design encompassing (1) steam explosion pretreatment, (2) separate enzymatic hydrolysis and fermentation of cellulose fraction, (3) biodigestion of hemicellulose hydrolysates, (4) combustion of produced biogas and unhydrolyzed solid fraction and (5) the meeting of process heat demand by diverting the required amount of lignocellulosic material to CHP system. With this in mind, the authors investigated the following possibilities and this for a variety of solutions:

- Drying of the unhydrolyzed solid fraction or lack thereof
- Optimization of conventional distillery through heat integration or lack thereof
- Mass stream integration between bagasse hydrolysis and sugarcane juice streams or lack thereof
- Inclusion of leaves hydrolysis, which have better pretreatment/hydrolysis performance parameters, or lack thereof
- Modification of enzyme dosage, hydrolysis time and solids loading

This multiplicity led to a total of 14 different scenarios, eight of which are highlighted in the context of our work. This choice was made in order to select alternatives with disparate design conditions, enabling hence their comparison and the deduction of design rules.

[81] on the other hand considered an optimized ethanol distillery, with an optimal lignocellulosic material split enabling the meeting of process heat demand, with excess material sent to the hydrolysis section. Both bagasse and leaves were considered as lignocellulosic feed stock. Moreover, section steam explosion pretreatment and enzymatic hydrolysis, with separation of hemicellulose hydrolysates and non-hydrolyzed solids was the chosen path was chosen for bagasse conversion. With this in mind, the authors considered additional process configurations by acting on the following points:

- Varying hydrolysis parameters: solids loading and conversion efficiency. Lower yields were assumed with higher loadings.
- The investigated couples were: (5% solids loading, 80% conversion), (10%, 70%), (15%, 66%) and (20%, 50%).

Two conditions were chosen in our case. This was seen as a sufficient number in order to test the impact of an increased solids loading on the performance of the system.

On another note, [21] investigated the application of a global optimization algorithm on a mass integrated distillery, cogeneration and hydrolysis process. This algorithm was based on evolutionary multi-objective optimization, coupled with detailed process modeling, in Aspen Plus, and heat integration. The investigated design variables were: (1) the bagasse fraction diverted to

hydrolysis and (2) the outlet concentrations for the various evaporators. As we can see, hydrolysis parameters were considered as constant, contrary to the previous works. Moreover, two objective functions were chosen: (1) the maximization of ethanol production and (2) the maximization of power production. This work resulted in the generation of a Pareto set with multiple points. This set will be thoroughly discussed in a later section. However, we will contend ourselves with the choice of two different solutions: the first with a hydrolyze bagasse fraction of 16%, and the second with a fraction of 40%. The authors did not however specify the obtained results for the various evaporator concentrations.

Finally, [69] studied different process alternatives taking into account either the combustion or the hydrolysis of bagasse and leaves, for fixed process operating conditions. Two of these alternatives were taken into account in the present section and this because they deal with the hydrolysis technology chosen in the context of our work. These alternatives differ in the inclusion of leaves hydrolysis or lack thereof.

With this in mind, Table 5:1 provides a summary of the cases investigated in the main literature works dealing with ethanol production from sugarcane bagasse and its integration to the conventional ethanol and power production train. From this table, we deduce that the key investigated areas are the following:

- The adoption of an optimized distillery with optimal evaporation, distillation and cogeneration
- The mass integration of bagasse pretreatment/hydrolysis streams with conventional distillery streams
- Process heat integration through the Pinch Analysis Technique
- The inclusion of sugarcane leaves as a substrate for pretreatment/hydrolysis
- Control of hydrolysis variables: solids loading (sld_{load}) and residence time (hyd_{res}) in hydrolysis reactor, along with hydrolyzed bagasse fraction (bag_{toet}).
- Control of process variables: cake humidity (hum_{cake}) and concentrations at the outlet of evaporation levels (C_{evi}).

Concerning nomenclature, the (+) sign in Table 5:1 indicates the adoption of the proposed alternative, whereas the (-) sign indicates the lack thereof. On the other hand, the (+/-) sign indicates that the authors considered scenarios where the proposed alternative were adopted along with others where these alternatives were not considered.

Table 5:1 Design considerations, controlled parameters and number of evaluated scenarios for ethanol production from sugarcane and bagasse

Article / Considered technology	Optimization variables	Optimized distillery	Mass integration	Heat integration	Leaves Hydrolysis	# Scenarios
[64]	$sld_{load}, hyd_{res}, hum_{cake}$	+/-	+/-	-	+/-	14
[81]	sld_{load}	+	+	-	+	4
[21]	bag_{toet}, $C_{evi}\ i = 1,..,4$	+	+	+	-	2
[69]		+	+	+	+/-	2

Table 5:2 and Table 5:3 on the other hand highlight design hypotheses for chosen process configurations deduced from literature. Information included in Table 5:2 reflect variations in key design variables: lignin cake humidity ($\mathrm{hum_{cake}}$ $(\mathrm{wt.\%})$), solids loading ($\mathrm{sld_{load}}$), enzyme loading in the hydrolysis reactor ($\mathrm{enz_{load}}$), and residence time ($\mathrm{hyd_{res}}$) in the hydrolysis reactor along with the fraction of lignocellulosic material diverted for ethanol production ($\mathrm{bag_{toet}}$), and this for the investigated literature works. Information included in Table 5:3 highlight decisions made related to key design alternatives: (1) use of leaves as an additional input lignocellulosic material, (2) the use of an optimized distillery, (3) the adoption of mass integration between the two process sections and (4) the adoption of in-process heat exchange.

Moreover, the absence of information for the cake humidity variable is due to a lack of specification in the related research works. The absence of the bagasse split parameter is on the other hand due to it being a calculated variable for the related cases, as will be highlighted in the following paragraph.

Finally, we remind that all investigated works and chosen designs had the same technological path for bagasse hydrolysis. This path consisted in: steam explosion pretreatment, separation and biodigestion of xylose fraction, enzymatic hydrolysis, separation and combustion of unhydrolyzed solids along with xylose biogas, and rerouting of glucose fraction to the conventional ethanol production train.

5.3.2 Studied performance parameters along with obtained results

With the previous review in mind, we turn our attention in this paragraph to the studied performance parameters and the obtained results. Calculated parameters are the same as those for the conventional distillery: the steam consumption rate (SC (kg//TC)), the ethanol production rate (et_{prod}(L/TC)), the power production rate (W_{prod} (kWh/TC)), process energy efficiency ($\varepsilon_{\mathrm{eff}}$ (%)), and process investment cost ($\mathrm{C_{inv}}$(M$)). The main difference with the conventional distillery is the fact that the ethanol production rate is dependent on the values for design variables as well

as chosen configurations. This variable was nearly constant for the conventional distillery under fixed input conditions, regardless of the values of design variables.

Table 5:2 Select process designs with steam explosion pretreatment, enzymatic hydrolysis and pentose biodigestion: values for key design variables

Case	Article	hum_{cake} $(wt.\%)$	sld_{load} $(wt.\%)$	enz_{load}	hyd_{res} (h)	bag_{toet} (%)
1	[64]	65	7%	Low	72h	
2		20				
3					48h	
4				High	72h	
5						
6						
7						
8			7%			
9	[81]		5%		48h	
10			15%			
11	[21]		5%		24h	16%
12						40%
13	[69]		10%		72h	
14			10%		72h	

Table 5:3 Select process designs with steam explosion pretreatment, enzymatic hydrolysis and pentose biodigestion: Decision related to key design alternatives

Case	Article	Use of leaves	Optimized distillery	Mass integration
1	[64]	-	-	-
2				
3				
4				
5			+ (evaporation and distillation systems)	
6				+ (before distillation)
7				+ (before concentration)
8		+		
9	[81]			
10				
11	[21]	-	+/- (only evaporation)	+ (before fermentation)
12				
13	[69]	-	+	+ (before concentration)
14		+		

Considering this, Table 5:4 highlights the obtained results for the various parameters, for the different cases highlighted in Table 5:2 and Table 5:3. As we can see, contrary to optimization works realized on the conventional distillery, optimization works taking into account bagasse hydrolysis lead to various ethanol production rates. These various rates are accompanied by varying steam consumption rates, electricity production rates, energy efficiencies and capital costs, variations that are experienced in optimizations made to the conventional distillery.

This table also includes values for two additional parameters proper to bagasse conversion: the cellulose to glucose conversion efficiency ($\eta_{conv,cell}$) (%) and the lignocellulosic biomass split (bag_{toet}) (%). The first parameter is dependent on hydrolysis parameters namely: solids loading, residence time and enzymes loading, and reflects the extent of the hydrolysis reaction. The second parameter on the other hand depends on the totality of the parameters as highlighted in Table 5:4. Moreover, as indicated previously, this parameter can either be calculated or specified by the user. In both cases, the related value should respect the constraints imposed by meeting the process heat requirements, which vary according to design conditions and chosen configurations. This constraint yields a maximum fraction of hydrolyzed bagasse. The results highlighted in Table 5:4 for cases 1 to 10 reflect therefore the maximum amount of diverted bagasse possible for the related design parameters. Moreover, the values specified in points 11 & 12 are smaller than the maximum amount (calculated at 95%).

Table 5:4 Performance indicators and their values as deduced from literature provided in Table 5:1

Case Number	SC (kg/TC)	et_{prod} (L/TC)	W_{prod} (kWh/TC)	ε_{eff} (%)	C_{inv} (M$)	$\eta_{conv,cell}$ (%)	bag_{toet} (%)
1		98	56	59.2%	223	47%	74.6%
2		102	50	61.4%	236	47%	94%
3		101	52	61.4%	234	42%	98%
4		107	43	62.0%	237	73%	83.7%
5		113	46	64.7%	272	73%	100%
6		113	48	64.8%	260	73%	100%
7		113	46	64.9%	259	73%	100%
8		129	60	60.5%	334	73%/96%*	100%
9	750	100	80			80%	45%
10	620	110	50			60%	85%
11	398	85	160		200	69.2%	16%
12	360	88	145		250	69.2%	40%
13		101	65		276	60%	60%
14		111	93		329	60%	77%

Finally, we can see that the eight cases in Table 5:4 have two different conversion ratios. This is because the hydrolysis of the leaves cellulose fraction is more efficient than that of bagasse, namely due to the lesser lignin content in the said leaves.

Based on the obtained results, we proceed to make a pair by pair comparison in order to highlight the impact of each investigated variable or design configuration on the performance of the system.

Cases 1 & 2 differ in the inclusion of a lignin cake drying step. As a result, the cake's humidity drops from 65% to 20% between the first and second cases. The direct impact of this modification is an increase in the lower heating value of the said cake, resulting in a smaller need for burning bagasse. As a result, a greater amount of bagasse gets converted to hydrolysis (74.6% vs. 94%), leading to a greater ethanol production (98 vs. 102 L/TC), and a smaller power production (50 vs. 56 kWh/TC). Ultimately, this modification resulted in an increase in energy efficiency (59.2% vs. 61.4%) albeit accompanied with an increase in investment cost (223 vs. 236 M$). Finally, we can see that the cellulose conversion efficiency remains the same. This is due to constant hydrolysis parameters

Cases 2 & 3 differ in the use of a smaller residence time (72h vs. 48h). This decrease results in smaller conversion efficiencies (42% vs. 47%). This ultimately leads to a higher unhydrolyzed solids fraction. This fraction is then burnt, leading to a smaller need for bagasse combustion. This thus leads to a greater bagasse availability (98% vs.94%), and to overall similar results for ethanol production (102 L /TC vs. 101 L/TC), power production (50 vs. 52 kWh/TC), energy efficiency (61.4% for both) and investment (236 M$ vs. 234 M$).

Cases 2 & 4 differ in the employed enzymes loading (low vs. high). This increase results in a greater conversion efficiency (47% vs. 73%). This is contrary to the previous case and leads to a smaller unhydrolyzed solids fraction, thus a smaller combusted fraction. This leads to a greater need for bagasse combustion, highlighted by a smaller hydrolyzed bagasse fraction (94% vs. 83.7%). Nonetheless, the obtained process has a higher ethanol production rate (102 vs. 107 L/TC), a smaller power production rate (43 vs. 50 kWh/TC), for an ultimately greater efficiency (61.4% vs. 62.0%), and a comparably similar investment cost (236 vs. 267 M$).

This analysis could be repeated for all other cases with varying parameters. For the sake of conciseness, Table 5:5 presents the results of this overall analysis in the form of a table. We observe therein the 4 different performance indicators, whose desired trends are also provided, along with the 5 different design variables and the 4 changes to process configurations. The fraction of bagasse sent to hydrolysis is considered as a design variable in this case rather than a calculated variable, as is the case for [21]. The impact of each variable on the chosen performance parameters was evaluated based on an analysis of investigated literature results, with the constraint of having all other parameters constant.

Table 5:5 Definition of the combined process optimization problem as deduced from literature

		Comments and indications as deduced from literature					
Performance indicators + desired trends	↗ et_{prod} ↗ W_{prod} ↗ ε_{eff} ↘ C_{inv}	Greater conversion efficiency, greater profit from sales **Lower initial investment, lower maintenance costs**					
Process section	**Optimization variables**	**Key trends**					
		Compared cases	et_{prod}	W_{prod}	ε_{eff}	C_{inv}	**Driving Force**
Process variables	hum_{cake}	**1 & 2**	↗	↘	↗	↗	**↗ LHV_{cake}, ↗ bagasse availability**
	hyd_{res} ↗	**2 & 3**	=	=	=	=	**↗ $\eta_{conv,cell}$ ↗ bagasse availability**
	enz_{load} ↗	**3 & 4**	↗	↘	↗	=	**↗ $\eta_{conv,cell}$, ↘ bagasse availability**
	sld_{load} ↗	**9 & 10**	↗	↘			**↘$\eta_{conv,cell}$, ↘ SC , ↗ bagasse availability**
	bag_{toet} ↗	**11 & 12**	↗	↘		↗	**↗ hydrolysis, ↘ combustion**
Process design	**Optimized distillery (in-process heat exchange)**	**4 & 5**	↗	↗	↗	↗	**↘ SC, ↗ bagasse availability**
	Mass integration	**5 & 6**	=	=	=	↘	**Less equipment**
		6 & 7	=	=	=	=	
	Use of leaves	**7 & 8, 13 & 14**	↗	↗	↘	↗	**Inclusion of an additional lignocellulosic material**

5.3.3 Results of profitability analysis

We concentrate in this section on the profitability analysis made by the different authors on the various considered alternatives. For this reason, we start by specifying the various economic hypotheses made by these authors. These hypotheses are provided in Table 5:6. We recall most of the hypotheses used in conventional distilleries: the project lifetime, the equipment salvage value, the plant construction and start-up period, equipment depreciation, days of operation, taxes, discount rates, along with the prices of input and output materials. The only difference resides in the addition of the enzyme cost parameter. This is due to the inclusion of this component as a raw material for the bagasse hydrolysis process.

Moreover, two formulations were adopted for this cost. The first is in $ / L cellulosic ethanol produced, i.e. ethanol coming from cellulose hydrolysis, and $/ t enzymes, which is relative to the actual enzymes consumption. The complexity of the first formulation is evidenced in the works of

[64] where multiple enzyme dosages are employed leading to case by case values for this cost. Finally, we can spot the absence of hypotheses related to the works of [81]. This is because of the fact that this work did not include any such profitability analysis.

With this in mind, we present in Table 5:7 the results of the profitability analysis applied to the various investigated cases, along with the ethanol production rate. We recall parameters in common with the conventional distillery. Such parameters include the Minimum Ethanol Selling Price, expressed in $/L ethanol, the Minimum Power Selling Price, expressed in $/MWh, which present the market prices for the related products below which the various configurations become unprofitable, with all other parameters remaining constant. Other parameters are the Internal Rate of Return (IRR) and the Net Present Value (NPV), which are direct measures of the profitability of the various alternatives. This table however includes an additional parameter, not found in the case of a conventional distillery: the minimum selling price for cellulosic ethanol (MESP- cellulosic) evaluated in $/L produced cellulosic ethanol. This parameter reflects the market price for the ethanol fraction issued from hydrolyzed fraction below which the various cases become unprofitable.

A quick analysis of Table 5:7 along with the previous ones yields the following:

- A greater power production rate can be associated with an increase in MESP and a reduction in IRR (cases 1→8).
- Nonetheless, this decrease is slightly reversed by the inclusion of mass-integration (cases 6 and 7), and this due to the lower associated investment cost, for similar values for other parameters.
- Also, cases 13 & 14 show that the inclusion of leaves hydrolysis may lead to
- Nonetheless, all of the realized modifications led to a smaller cellulosic ethanol cost (cases 1→8).
- A comparison of cases 11 & 12, referring to [21], against other parameters shows that a electricity price (51 $/MWh vs. 86 and 70.6 $/MWh) is hugely detrimental for the minimum ethanol selling price (greater than all other cases for a smaller production rate)
- The inclusion of leaves going from case 13 to case 14 leads to a slight reduction in MESP accompanied however with a slight increase in MPSP. The reduction in MESP is contrary to the results witnessed between cases 7 & 8. This is due to the fact that similar hydrolysis rates were adopted for bagasse and leaves in the case of [69], whereas a greater rate was adopted for leaves in the case of [64].

Table 5:6 Main hypotheses for profitability analysis of the various investigated cases

Article	[64]	[21]	[69]
Project lifetime (years)	20	25	25
Salvage equipment value (M$)	0		0
Construction and start-up (years)	1		2
Depreciation (years)	10- Linear		10- Linear
Days of operation	200	200	167
Tax rate (income and social contributions)	34%		34%
Discount rate (%)	10%	10%	
Sugarcane price ($/TC)	19.5	31.17	19.41
Sugarcane Trash Price ($/ton leaves)	13	15.02	15
Enzyme price ($/ton enzyme or $ / L cellulosic ethanol)	($/L) Given for each evaluated case	1250 $ /t	0.15 $ /L
Ethanol price ($/L)	0.53	0.72	0.5
Electricity price ($/MWh)	86	51	70.5

Table 5:7 Main results of profitability analysis of the various investigated cases

Case Number	et_{prod} (L/TC)	MESP ($/L ethanol)	MPSP ($ / MWh)	IRR (%)	NPV M$	MESP cellulosic ($/ L cellulosic ethanol)
1	98	0.43		15.7%		1.55
2	102	0.44		15.4%		1.36
3	101	0.45		15.0%		1.45
4	107	0.46		14.5%		1.19
5	113	0.49		12.7%		1.16
6	113	0.48		11.5%		1.12
7	113	0.48		13.4%		1.11
8	129	0.52		11.4%		0.99
9	100					
10	110					
11	85	0.52				2
12	88	0.61				2.6
13	101	0.319	40.58	12.6%		
14	111	0.317	41.3	12.2%	-30.0	

5.3.4 Application of evolutionary optimization methods

In this final bibliographic section, we turn our attention to the application of evolutionary multi-objective optimization to the investigated problem, more specifically the works of [21] This work, with related results highlighted in Table 5:1, applied the previously discussed evolutionary multi-objective optimization coupled with process simulation and heat integration methodology to the

studied combined production process. The authors chose the maximization of power production, evaluated in kWh/t cane, and the maximization of ethanol production, evaluated in l/t cane, as objective functions for the optimization problem. Optimization variables on the other hand included the fraction of bagasse sent to hydrolysis section (bag_{toet}) and four additional variables related to the concentrations at the outlet of each step of the glucose multiple-effect evaporation system. Whereas the first variable influences both objective functions, the remaining variables have an impact on power production and this by virtue of the vapor bleeding mechanism highlighted in 2.3.2. Moreover, this work differs from others by considering this hydrolyzed bagasse as free optimization variables, whose value is set by the optimization algorithm rather than calculated as a result of heat integration. This enables the variable to have values other, namely smaller, than the maximum amount set by the heat integration problem.

With this in mind, Figure 5:3.(a) highlights the results of the multi-objective optimization. Similar to the previously highlighted results, electricity production decreases with increased ethanol production. Moreover, an inflection point can be observed at around 89 l ethanol/ t cane. In fact, electricity production drops sharply after this point, faced by a smaller increase in ethanol production. Moreover, the obtained results provide a wider panel of various solutions that the various case by case simulations previously realized. As a matter of fact, points 11 & 12 of Table 5:2 and beyond refer to specific points on the said curve.

The authors later realized an economic evaluation of the various points on this optimal compromise curve. The key investigated variable was the total annual production cost (C_t) evaluated in M$ as highlighted in Equation 5:1, where C_{inv} is the annualized investment cost, C_{enz}, $C_{sugarcane}$ and C_{leaves} the total enzyme, sugarcane and leaves purchase cost. C_{elec} on the other hand refers to an algebraic formulation of the electricity cost, with it taking negative values in the case of power production, reflecting a smaller total cost due to an additional source of revenue, and positive values in the case of power consumption, reflecting an additional process input. This variable is compared against the total ethanol cost ($C_{ethanol}$), with ethanol being considered as the main process product. Finally, all of these variables were evaluated under the economic conditions highlighted in Table 5:6.

Equation 5:1 Expression for total production cost[21]

$$C_t = C_{inv} + C_{enz} + C_{sugarcane} + C_{leaves} + C_{elec}\ (M\$/y)$$

Figure 5:3.(b) highlights the evolution of these various parameters with the bagasse fraction sent to hydrolysis. We can see in a first step that the leaves and sugarcane costs are fairly constant, which is consistent with a constant input flow rate for these variables. All other variables on the other hand whiteness an increase with an increased hydrolyzed bagasse fraction. In fact, a higher hydrolyzed fraction leads to a higher ethanol production, a greater enzyme use, a greater investment cost and a smaller power production/greater power consumption. Finally, the

obtained results indicate that the process is profitable ($C_{ethanol} > C_t$) for hydrolyzed bagasse fractions smaller than c.a. 65%, under the chosen economic parameters.

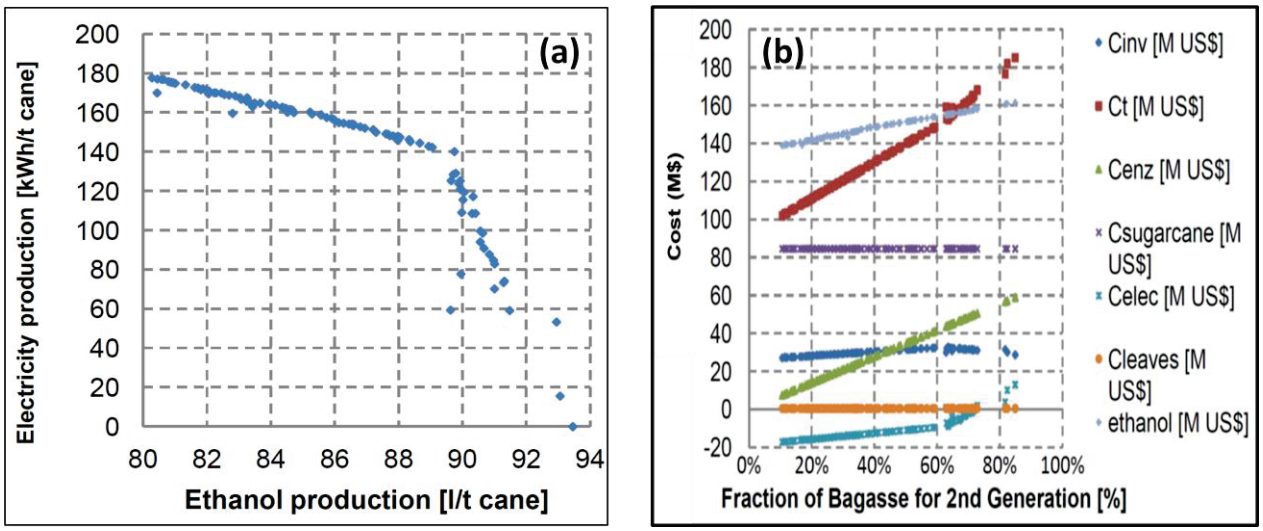

Figure 5:3 (a) Results of multi-objective optimization work applied on the studied process and (b) Evolution of costs of various components with fraction of bagasse sent to hydrolysis [21]

5.3.5 Conclusions about the bibliography

We can retain the following points from the previous bibliographic analysis. We start by stating the complexity of the studied problem due to the presence of multiple competing functions and variables.

This bibliographic review pinpointed key optimization variables pertaining both to the hydrolysis section and to the distillery per say. The control of both parameters leads to optimized alternatives. These parameters were nonetheless specified for a maximal hydrolyzed bagasse fraction.

This bibliography also showed the advantages brought by mass integrating both ethanol production streams, namely on the investment cost. Moreover the best result was found when integration occurred prior to the juice concentration step.

The hydrolysis of leaves on the other hand was found to have a negative impact on the evaluated functions, namely due to the greater investment associated with its inclusion.

Finally, the multi-objective evolutionary optimization coupled with process and heat integration enables a greater exploration of the design space than a simple case by case evaluation. This optimization made also possible the setting of the hydrolyzed bagasse fraction. However, this optimization failed to include other hydrolysis and distillery based optimization variables and was not performed based on conventional objective functions, i.e. exergy efficiency and capital costs.

With this in mind, we believe that a multi-objective optimization with investment cost and exergy efficiency as objective functions, and chosen hydrolysis and distillery parameters as optimization variables, will lead to a greater exploration of the various possibilities and ultimately to more optimal configurations.

5.4 Definition of framework for optimization work

We provide in this section a definition of the framework for the optimization work. This framework includes: the choice of the objective functions along with their calculation method, the choice of optimization variables and the adaptations made to the optimization algorithm.

5.4.1 Defining the objective functions

Having defined the optimization problem and the studied process, we turn our attention towards the optimization problem per say. With this in mind, we focus our attention in this section on the objective functions and their associated equations. These objective functions, whose validity was previously discussed in Chapter 1 are reminded in Table 5:8. We recall then the process exergy efficiency and investment cost. Whereas the definition of investment cost is simple, exergy efficiency reflects the extent of the conversion of input materials into useful products.

Table 5:8 Reminder of chosen objective functions and their desired evolution

Objective function name	Function description	Desired evolution
ex_{eff}	Process exergy efficiency	Maximization
C_{FC}	Fixed Capital Cost	Minimization

5.4.1.1 Calculation of process exergy efficiency

As indicated in Chapter 1, exergy efficiency is calculated as the ratio of the exergy of product streams to that of input streams. It is hence an indicator of the process' conversion efficiency, and ultimately of its profitability.

Considering this, Table 4:12 highlights the exergy input/output balance for the studied process. Input streams include: sugarcane, leaves and enzymes. Output streams on the other hand include ethanol and power production. Mass flow rates are expressed in tones/hour $\left(\frac{t}{h}\right)$ whereas energy rates are expressed in Megawatts (MW). Moreover, nominal exergy contents are expressed in $\frac{MWh}{t}$ for mass streams whereas it is unit less for power streams. The final exergy is the multiplication of the specific rate by the nominal exergy content and is expressed in MW, as indicated in Chapter 1.

Finally, considering the exergy contents of the various input and output streams defined in Table 4:12, Equation 5:2 provides the literal equation for the exergy efficiency of the combined production process.

Equation 5:2 Literal expression of exergy efficiency for combined production process

$$ex_{eff} = \frac{Ex_{Prod}}{Ex_{in}} = \frac{Ex_{ethanol} + Ex_{W_{out}}}{Ex_{cane} + Ex_{leaves} + Ex_{enz}} = \frac{\dot{m}_{ethanol} \times ex_{ethanol} + W_{out} \times ex_{W_{out}}}{\dot{m}_{cane} \times ex_{cane} + \dot{m}_{leaves} \times ex_{leaves} + \dot{m}_{enz} \times ex_{enz}}$$

Table 5:9 Exergy balance for the combined sugarcane distillery, hydrolysis and cogeneration process

Component	Flow rate	Nominal exergy content	Total exergy content (MW)
Input streams			
Sugarcane	$\dot{m}_{cane}(\frac{t}{h})$	$ex_{cane} = 1.445\ (\frac{MWh}{t})$	$Ex_{cane} = \dot{m}_{cane} \times ex_{cane}$
Leaves	$\dot{m}_{leaves}\ (\frac{t}{h})$	$ex_{leaves} = 4.4\ (\frac{MWh}{t})$	$Ex_{leaves} = \dot{m}_{leaves} \times ex_{leaves}$
Enzymes	$\dot{m}_{enz}\ \left(\frac{t}{h}\right)$	$ex_{enz} = 6.11\ (\frac{MWh}{t})$	$Ex_{enz} = \dot{m}_{enz} \times ex_{enz}$
Output streams			
Ethanol	$\dot{m}_{ethanol}\ (\frac{t}{h})$	$ex_{ethanol} = 8.21\ (\frac{MWh}{t})$	$Ex_{ethanol} = \dot{m}_{ethanol} \times ex_{ethanol}$
Power production	$W_{out}(MW)$	$ex_{W_{out}} = 1\ (-)$	$Ex_{W_{out}} = W_{out} \times ex_{W_{out}}$

5.4.1.2 Calculation of process capital cost

As indicated in Chapter 1, capital costs are another key objective function used for process evaluation and optimization. In fact, this function provides an indication about the required investment. Considering this, this function is calculated for our objective function as the sum of the capital costs of the various process blocks, to which is added the cost of the heat exchange network. Moreover, in order to avoid a repetition in the calculation of heat exchange equipment, the cost of certain equipment was excluded from the calculation route related to the block's costs. As a result, Equation 4:3 provides a literal equation for the Grass Root Capital cost for a given process configuration ($C_{capital,GR}$).

Equation 5:3 Literal equation for the calculation of process capital cost

$$C_{FC} = C_{capital,GR} = \sum_{i=1}^{N_{blocks}} C_{capital,GR_i}\ (excluding\ steam\ boiler, reboilers\ and\ evaporators) + C_{HEN,GR}\ (A_{hen,tot})(M\$)$$

5.4.2 Choice of optimization variables

We turn our attention in this section to the choice of the various optimization variables and their associated intervals The said optimization variables are chosen from amongst the various process

variables. Moreover, these variables can pertain either to the MILP heat integration algorithm or to the global optimization algorithm. In addition, each of these variables is associated with a search space from which related values are extracted. Considering this, the choice and range of the optimization variables ultimately determines the design space for the optimization problem.

With this in mind, we base our choice for the various optimization variables on the previously realized bibliographic review. This review indicated that, under a constant predefined configuration, the controlled variables pertain either to the distillery per say, to the cogeneration system, or to the hydrolysis section.

Having already studied the optimization the distillery and cogeneration systems in depth in Chapter 4, we decided to keep the same variables and the same ranges as highlighted in Chapter 4 for these sections.

For the hydrolysis section on the other hand, we chose to control the variables investigated in literature, namely: the solids loading, the hydrolysis residence time and the fraction of bagasse diverted to the hydrolysis section. The enzyme loading was however kept at its maximum value. This was realized in the hopes of designing processes with higher ethanol yields, and was motivated by the rather small contribution of enzymes to the total production cost as highlighted in [21].

Considering this, Table 5:10 provides details concerning the optimization variables and their variation ranges. This problem has a total of 28 optimization variables controlled by the outer Evolutionary Multi-Objective Optimization (EMOO) algorithm. These variables pertain to the various process sections. Table 5:11 on the other hand highlights the 8 optimization variables controlled by the inner MILP problem. These variables pertain to mass flow rates in the different hot and cold utility systems.

Table 5:10 Optimization variables and associated bounds for combined process multi-objective optimization problem

Section	Variable names	Unit	Variables description	$N_{var,MOO}$	min_{val}	max_{val}
Evaporation	r_{ev_i}	-	Vaporization rates in evaporators	6	0	1
	dT_{ev_i}	°C	Temperature difference in evaporators	5	4	12
	x_{sgcc}	kg/kg	Juice concentration at the concentration outlet	1	0.65	0.7
Distillation	p_{strip}	atm	Stripping & rectifying column pressure	1	0.25	3
	p_{rect}	atm		1	0.75	3.5
	$V_{fr,rect,top}$	mol/ mol	Vapor fraction in rectifying top	1	0	1
Dehydration	S/F	kg/kg	Solvent to feed ratio	1	0.5	1.75
	T_{solv}	°C	Solvent input temperature	1	365	470
Hydrolysis	sld_{load}	wt. %	Solids loading in reactor	1	0.05	0.2
	hyd_{res}	h	Residence time in reactor	1	24	96
	bag_{toet}	-	Fraction of hydrolyzed bagasse	1	0.05	0.95
Cake drying	hum_{bag}	mol/mol	Bagasse humidity	1	0.2	0.45
Boiler and steam turbine	p_{tur_1}	atm	Pressure in turbine levels and boiler	1	12	25
	p_{tur_2}	atm		1	2	12
	p_{tur_3}	atm		1	1	2
	p_{tur_4}	atm		1	0.4	1
	p_{tur_5}	atm		1	0.08	0.4
	P_{boiler}	atm		1	60	100
	T_{sheat}	°C	Superheating Temperature	1	150	300
$N_{var,MOO}$				28		

Table 5:11 Optimization variables and associated bounds for Mixed Integer Linear Programming heat integration problem

Section	Variable code names	Unit	Variables description	N_{var}	min_{val}	max_{val}
Boiler and steam turbine	$\dot{m}_{water}$, $\dot{m}_{steam,i}$	t/h	Boiler water steam cooling water and refrigeration flow rates	6	0	10^3
Refrigeration utility	$\dot{m}_{cold,ut}$	t/h		1	0	10^5
Cold utility	$\dot{m}_{frig,ut}$	t/h		1	0	10^3
$N_{var,MILP}$				8		

5.4.3 Choice of measured variables

On another hand, just as for the optimization of the conventional distillery and cogeneration system, five additional parameters were also measured. These parameters are defined in Table 5:12: the ethanol production rate, net power production, the heat exchanger area, the heat exchanger cost and the cost of the process without the heat exchanger. These parameters were chosen because they are directly related to the chosen objective functions. Another reason for this choice is the presence of a conflict between some of these variables. Such a conflict was evidenced in the previous bibliographic review for the case of ethanol and power production. The various other relationships will be highlighted in later sections.

Table 5:12 Process variables measured in Multi-Objective optimization problem

Variable names	Variables description
$\dot{m}_{et}$ **(t/h)**	Ethanol mass flow rate
W_{prod} **(MW)**	Total net power production
$Area_{HEN}$ **(m^2)**	Area of heat exchanger network
C_{HEN} **(M$)**	Cost of heat exchange network
$C_{non-HEN}$**(M$)**	Process capital cost without heat exchange network

5.4.4 Model preparation

In this section, we present the main points introduced to the multi-objective optimization model in order to ensure that the model converges to optimal feasible and physical solutions and this in a reasonable time span.

5.4.4.1 Constraints imposed on distillery related variables

In a first place, seeing that the problem encompasses the distillery and the cogeneration section, the same design constraints imposed on these sections and presented in Chapter 4 apply in our case. These points are reminded below:

- In the case of a vaporization rate for a given evaporator equal to zero, the heat duty of both the condensation and cooling streams associated to the said evaporator are also set to zero
- The refrigeration system is used in the case of low temperatures in the purge stream related to the stripping column. In fact this stream requires cooling in order to extract the carbon dioxide stream. With low pressure levels, cooling temperatures might be too low and thus require the use of a refrigeration unit.
- The variation in evaporation temperature is defined by two bounds: the first in relation with the sucrose degradation temperature set at 120°C. The second is in relation to the lower permissible pressure which yields a minimal temperature at 50°C. As a result, the maximal temperature difference is set at 70 °C. None the less, this constraint is always respected with the chosen values for the design variables.
- In order to respect the constraints imposed on the vaporization rates, the various rates proposed by the algorithm are first normalized by dividing each specific original value by the sum of the original values, as highlighted in Equation 4:4. This new value is then returned to the optimizer as the actual value for these variables.

Equation 5:4 Equation for the correction of the vaporization rates

$$r_{ev,i,corrected} = \frac{r_{ev,i,proposed}}{\sum_{i=1}^{6} r_{ev,i,proposed}}$$

In the case of sub-atmospheric pressure in the rectifying column, the vapor content in the column's distillate is set to zero so to prevent the use of a compressor to bring the pressure up to atmospheric level. In fact, this alternative is to be avoided because it requires both additional investment in compressor and additional power consumption

5.4.4.2 Impact of solids loading and hydrolysis time on cellulose to ethanol conversion

As indicated in the previous bibliographic review, a key calculated parameter that influences the rest of the problem is the conversion yield of the hydrolysis conversion reaction. From all the considered optimization variables, this yield is solely dependent on two variables: hydrolysis yield and solids loading. This dependence was emphasized in the various research works. Thus, in order to correctly represent this dependence, a correct model for this relationship needed to be adopted.

For this reason, we made use of the results obtained by [71], which were previously used in Chapter 3to initialize our studied model. In fact, in this work, the authors measured the impact of various variables on the hydrolysis reaction. However, rather than focusing on the conversion yield per say, the authors turned their attention to a more specific parameter: $GlcEq$ expressed in g glucose /L and which equates to the sugar concentration in the reaction output stream. Considering this, both parameters were evaluated for various values of the following parameters: solids loading, hydrolysis time, enzymes loading and agitation speed. Seeing that both the enzymes loading and agitation speed are constant in our case, values for the hydrolysis yields were

recorded in a first step for constant agitation speeds of 200 rpm as highlighted in Table 5:13. These results confirm the fact that a higher enzymes loading, a smaller solids loading and a greater hydrolysis time all contribute to a greater conversion yield. However, the evolution of the glucose equivalent concentration follows a more tortuous path.

In the following sections we will turn our attention, just in the case of [71] towards this glucose concentration which will be our calculated variable. On the other hand, the hydrolysis yield is calculated by a design specification in the Aspen simulation with the goal of respecting this glucose concentration.

Table 5:13 Recorded results for various reaction conditions for an agitation power of 200 rpm [71]

Enzyme dosage (g enzyme /g cellulose)	Solids loading (wt. %)	Residence time (h)	Conversion yield (%)	Glucose concentration (g/L)
0.025	20%	24h	13.4	14.9
0.025	5%		25.6	7.1
0.0625	12.50%		41.8	26.7
0.1	20%		51.6	57.2
0.1	5%		66.8	18.6
0.025	20%	72h	23.8	26.5
0.025	5%		33.2	9.2
0.0625	12.50%		62.8	43.6
0.1	20%		69.2	76.8
0.1	5%		92.5	25.7
0.025	20%	96h		35.3
0.025	5%			10.5
0.0625	12.50%			55.7
0.1	20%			89.0
0.1	5%			30.2

Considering this, and in order to model the time dependence of this parameter, we considered our cellulose conversion reaction as a first-order reaction with kinetic factor k_{hyd} as highlighted in Equation 5:5, with $GlcEq \ \ in\ g/l, hyd_{Res}\ in\ h\ \&\ hyd_{Res_0} = 24h$.

Equation 5:5 Cellulose hydrolysis conversion yield as a function of residence time

$$GlcEq\ (hyd_{Res}) = GlcEq\left(hyd_{Res_0}\right) \times e^{k_{hyd}\left(hyd_{Res} - hyd_{Res_0}\right)}$$

Based on Equation 5:5, and the results deduced from [71], Table 5:14 provides results for the kinetic coefficient for the various evaluated cases. As we can see, the table does not contain information about the residence time. This is due to the first order reaction, where the kinetic coefficient is independent of the residence time. This table also includes values for the initial

glucose output concentration $GlcEq\left(hyd_{Res_0}\right)$= $GlcEq_0$, which also is solely dependent on the enzyme dosage and solids loading.

Table 5:14 Results for hydrolysis conversion efficiencies under various reaction conditions for an agitation power of 200 rpm

Enzyme dosage (g enzyme /g cellulose)	Solids loading (wt. %)	Kinetic factor (h-1)	$GlcEq\left(\mathrm{hyd}_{\mathrm{Res}_0}\right) = GlcEq_0$
0.025	20%	0.0120	14.9
0.025	5%	0.0054	7.1
0.0625	12.50%	0.0102	26.7
0.1	20%	0.0061	57.2
0.1	5%	0.0068	18.6

By taking into account the dependence of the kinetic factor and the initial conversion yield on the enzyme dosage and solids loading, Equation 5:5 can be expressed as highlighted in Equation 5:6.

Equation 5:6 Cellulose hydrolysis conversion yield as a function of residence time

$$GlcEq(hyd_{Res}, sd_{load}, enz_{load}) = GlcEq_0(sd_{load}, enz_{load}) \times e^{-k_{hyd}((sd_{load}, enz_{load})(hyd_{Res} - hyd_{Res_0})}$$

With this in mind, a correct modeling of both the kinetic factor (k_{hyd}) and the initial glucose concentration $GlcEq\left(hyd_{Res_0}\right)$, as a function of the solids loading and enzyme dosage, is sufficient to correctly model the actual glucose concentration ($GlcEq(hyd_{Res})$) for any combination of solids loading, enzyme dosage and hydrolysis residence time. The relationship between these two parameters and the solids loading and enzyme dosage can be modeled by the use of a quadratic approximation as highlighted in Equation 5:7.

Equation 5:7 Approximation of hydrolysis reaction parameters using quadratic model

$$var(sd_{load}, enz_{load}) = a_{var} + b_{var} \times sd_{load} + c_{var} \times enz_{load} + d_{var} \times sd_{load}^2 + e_{var} \times enz_{load}^2 + f_{var} \times enz_{load} \times sd_{load}$$

The values of the various coefficients were sought so that the modeled variable values approximate as much as possible the experimental values. This was realized by virtue of the least squares method. The obtained values for the various variables for the two parameters, kinetic coefficient and initial conversion yield are highlighted, with the associated precision, in Table 5:15.

Table 5:15 Values for quadratic model parameters approximating values for hydrolysis kinetic factor and default glucose concentration

Parameter	Kinetic factor (k_{hyd})	Default glucose concentration($GlcEq_0$)
a_{var}	-0.003	0.09
b_{var}	0.154	77.58
c_{var}	0.097	28.40
d_{var}	-0.377	-376.07
e_{var}	-0.386	-95.62
f_{var}	-0.629	2737.72
Least Square Precision	8.8E-9	1.06E-07

Now considering that the enzyme loading is set at the constant value of 0.1 g enzyme/ g cellulose in our model, Equation 5:7 is now transformed by the adoption of a constant enzymes loading as in Equation 5:8. This equation ultimately becomes a solely solids loading-dependent equation with new parameters as highlighted in Equation 5:9. The novel coefficients are then calculated for each parameter as highlighted in Equation 5:9. With this in mind, the values of the novel coefficients are specified in Table 5:16.

Equation 5:8 Approximation of hydrolysis reaction parameters using quadratic model and constant enzymes loading

$$var(sd_{load}, enz_{load_0}) = \left(a_{var} + c_{var} \times enz_{load_0} + e_{var} \times enz_{load_0}^2\right) + \left(b_{var} + f_{var} \times enz_{load}\right) \times sd_{load} + d_{var} \times sd_{load}^2$$

Equation 5:9 Approximation of hydrolysis reaction parameters with sole dependence on solids loading

$$var_{enz_{load_0}}(sd_{load}) = a'_{var} + b'_{var} \times sd_{load} + c'_{var} \times sd_{load}^2$$

Table 5:16 Values for quadratic approximation coefficients

Parameter	Kinetic factor (k_{hyd})	Default glucose concentration($GlcEq_0$)
a'_{var}	0.0031	1.972924
b'_{var}	0.0907	351.3489
c'_{var}	-0.3772	-376.071
Least Square Precision	3E-09	5E-08

This glucose equivalent was then met within the Aspen Simulation by controlling the yield of the cellulose hydrolysis reaction. With this in mind, we provide in Table 5:17 a comparison between literature and calculated conversion efficiencies for various cases. We spot a large disparity between the results, namely due to various pretreatment conditions and possibly enzymes

loading. This disparity is however minimal for residence times of 48h. Finally, It is however to see that a greater solids loading leads to a smaller conversion efficiency whereas a greater hydrolysis time leads to a greater conversion efficiency.

Table 5:17 Comparison between literature and calculated conversion efficiencies for various cases

Research work	sd_{load}	hyd_{Res}	Lit	Calc
[81]	0.05	48	80%	72%
	0.15	48	44%	44%
[69]	0.1	72	60%	73%
[64]	0.07	48	66%	65%
	0.07	72	73%	80%

With the previous results in mind, we acknowledge the inaccuracies associated with our performed model, inaccuracies that are further aggravated by a paucity of related research works.

5.4.4.3 Relationship between heat consumption and bagasse diversion

As indicated earlier, a key issue addressed in literature concerns the amount of bagasse diverted for subsequent hydrolysis. This amount is usually by a minimum combusted fraction which is used to meet process heat requirements. In the works of [64, 69, 81] this constraint was met by performing a local optimization loop which fixed the combusted bagasse fraction at the minimum required value, or diversely the hydrolyzed bagasse fraction at the maximum possible value.

[21] [21]on the other hand set this parameter as a free variable that was controlled by the multi-objective optimization algorithm. This same scheme is adopted in our work as can be seen in Table 4:13. Moreover, considering the fact the process heat balance is resolved at the heat integration level, the following statements can be made:

- The heat integration problem will not be resolved in the case of excessive bagasse hydrolysis.
- This is due to the absence of any additional hot utilities, and occurs despite the combustion of the unhydrolyzed solid fraction and the produced biogas stream.
- This leads to a non-convergent simulation, which by virtue of the elitist nature of the algorithm, will be discarded in the course of the optimization
- Power cogeneration occurs in the case of a value for the hydrolyzed bagasse fraction, lower than the maximum value

5.4.4.4 Reminder of main modifications made to optimization algorithm

We briefly remind in this section, the main modifications made to the used optimization algorithm. The employed algorithm was introduced in Chapter 1 and the performed modifications were highlighted in Chapter 4. These modifications include:

- Error handling namely concerning non-convergent simulations, disrespect of design specifications and the failure to solve the related heat integration problem

- Selection pressure namely with the greater probability of choosing fitter individuals as progenitors for later individuals
- Parallelization made possible on a multi-processor Windows® platform

5.5 Results of multi-objective optimization

We will present in this section the results for the performed optimization run. Considering this, we will first highlight the obtained Pareto set, before seeking to understand the key factors behind it. We will also investigate the various optimization variables and try to extract rules for designing Pareto optimal solutions.

5.5.1.1 Presented of obtained Pareto set

Turning our attention to the obtained optimal solutions, Figure 4:12 provides a graphical representation of the final Non-Dominated (Pareto) Set for the combined production process optimization problem. As we can see the exergy efficiency evolves between a minimal value of 39.2% and a maximal value of 44.3%. Capital costs on the other hand evolve between a minimal value of 220 M$, corresponding to the smallest exergy efficiency and a maximal value of 393 M$, corresponding to the greatest exergy efficiency. A clear observation can be made at this level: the scope of variation of capital cost is greater than that of exergy efficiency (79% for the first vs. 13% for the second).

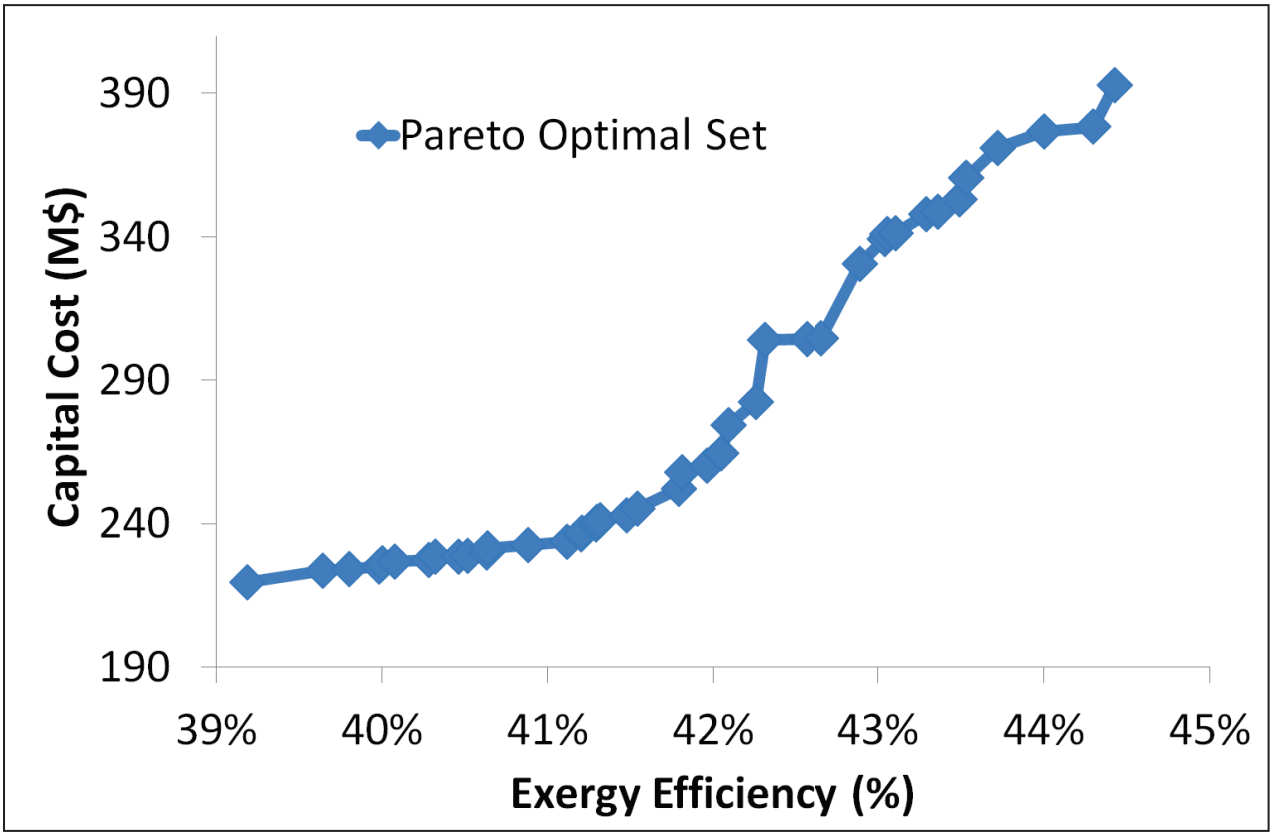

Figure 5:4 Pareto optimal set for combined distillery, hydrolysis and cogeneration configuration

5.5.2 Explanation of the obtained results: analysis of measured variables

The obtained trade-off curve can be explained by taking a closer look at the measured variables. Considering this, we will firs interest ourselves with exergy efficiency related variables before concentrating on capital cost variables.

5.5.2.1 Exergy efficiency related variables

Exergy efficiency is influenced by both input and output exergy rates. Whereas exergy input rate has two constant components, sugarcane and leaves intake, exergy output rate depends directly on the optimization problem. Considering this, Figure 5:5.(a) plots the relationship between the exergy efficiency and output exergy ex_{out}, expressed as the sum of output ethanol exergy and the net power. We can see a nearly linear relationship (R^2=0.9967). The observed linearity is due to the constant sugarcane and leaves input, as indicated previously, along with the small impact of enzymes, the third key process input. With this in mind, we focus our attention on the two constituents of output exergy, ethanol and power, whose relationships to exergy efficiency are highlighted in Figure 5:5.(b) and Figure 5:5.(c) respectively. As we can see, the Pareto curve is highlighted by a nearly constant ethanol production rate for small exergy efficiencies (<41.8% c.a.), followed by a continuous increase in ethanol production for higher efficiencies. This is countered by an increase in power production for smaller efficiencies (<41.8% c.a.), followed by a decrease in this production for higher efficiencies. The relationship between ethanol production and net production is more specifically highlighted in Figure 5:5.(a). As we can see, points before the critical point whiteness a variable power production for a nearly constant ethanol production, whereas points after it whiteness a decrease in power production for an increase in ethanol production.

This can be explained as follows: for points before the critical point, the main driving force is process heat integration, similar to the case of the conventional distillery + cogeneration highlighted in Chapter 4. On the other hand, the driving force for points to the right of the critical point is the production of ethanol from bagasse. The split of the Pareto space according to these driving forces is highlighted in Figure 5:5.(d). This figure also highlights cases, visualized by the encircled areas, where the two driving forces play roles outside their area of dominance. As a matter of fact, both areas are associated with nearly constant ethanol production rates for variable power production rates. For the area with predominant heat integration, this is characteristic of a variable ethanol production rate. Likewise, for the area with predominant ethanol production, this is characteristic of a varying heat integration potential.

Considering this, the problem can be stated differently: multiple optimal heat integration possibilities exist for each ethanol production rate. This formulation raises a series of questions both highlighted and addressed below:

- Why are higher ethanol production rates associated only higher efficiencies

This is evidenced by observing Figure 5:5.(b). This trend can be explained considering a combination of the bi-objective nature of the optimization problem, and of the specificities of bagasse hydrolysis. The first point, i.e. the bi-objective nature, leads to the fact that if two points have similar efficiency, the point with the lowest cost is chosen by the optimization algorithm. The second point links the increased ethanol production to an increased cellulose hydrolysis rate, which is associated with a greater investment cost than the cogeneration case, as evidenced from literature. Considering this, a point with a higher ethanol production and a lower power production might have the same efficiency as a point with a smaller ethanol production and a greater power production, but will surely have a greater capital cost. This is why the Pareto curve does not contain points with a high ethanol production rate and a small exergy efficiency.

- Why was the critical value obtained for an exergy efficiency of 41.8%?

In order to handle the first point, we turn our attention to the distillery + cogeneration optimization case. This is because of the similarity between this case and the cases to the left of the critical point, with concerns to a constant ethanol production rate. With this in mind, the distillery + cogeneration optimization case returned the various possibilities for an optimal process heat integration with regards to exergy efficiency and capital costs. Moreover, maximum efficiency for this case was equal to this value as highlighted in Chapter 4. Considering a constant ethanol production, this value reflects the greatest possible power production rate, which in turn reflects the greatest potential for both heat integration and net power production.

By comparing these results to our current results, we can see that our critical point has a similar efficiency evaluated at 41.8%. We can thus understand this point as the maximum potential for heat integration and subsequent power production offered by the conventional + cogeneration process. Beyond this point, greater ethanol production is required to obtain a higher efficiency. This result characterizes the greater efficiency of the bagasse hydrolysis technique when compared to combustion.

- Why is there only a limited number of heat integration possibilities for larger exergy efficiencies?

The presence of this limited number is associated to the bi-objective nature of the optimization problem and to the limits of the investigated process. In this context, the first point presents a lower bound whereas the second point presents an upper bound.

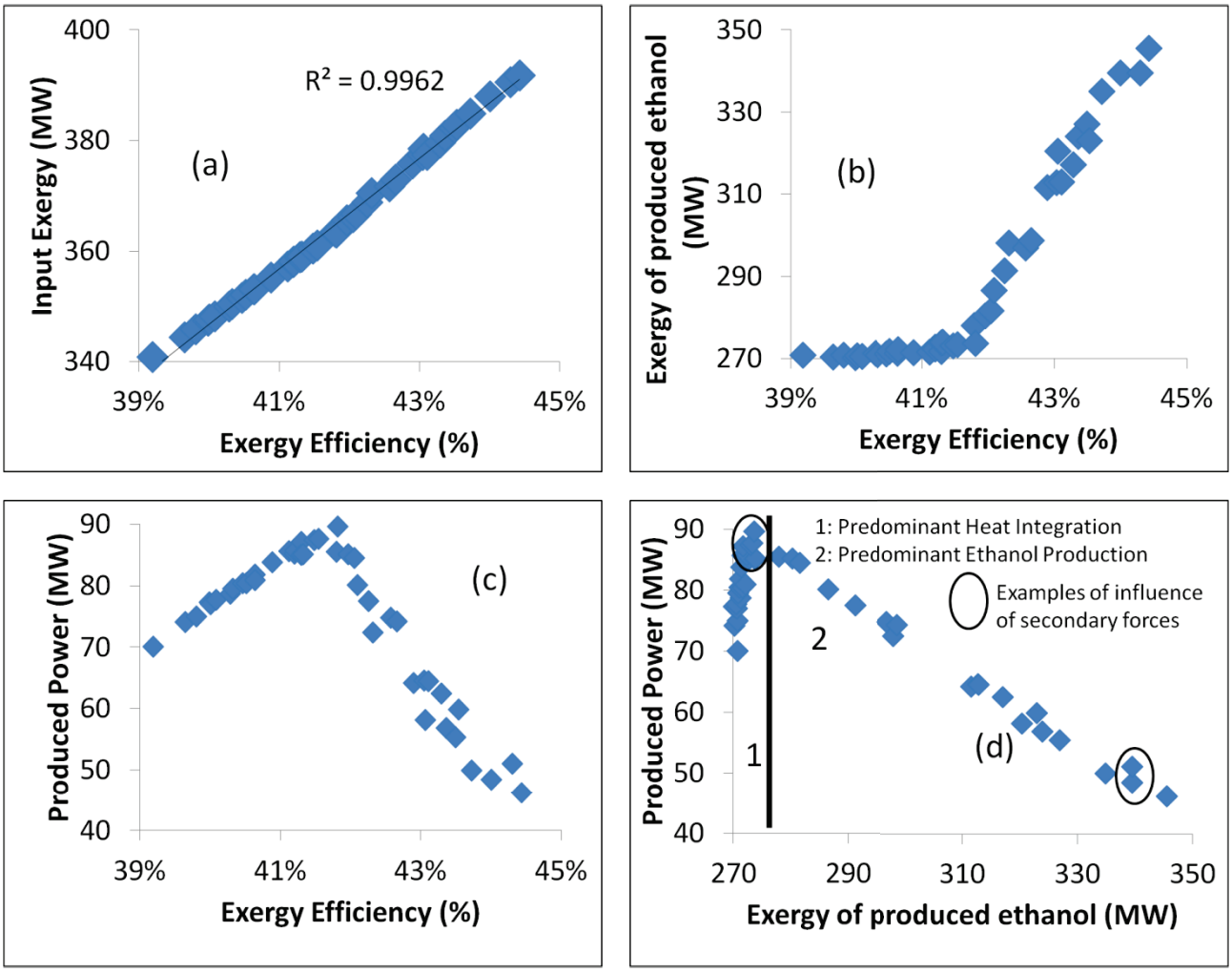

Figure 5:5 Relationships for optimal points between (a) exergy efficiency and produced exergy content (MW), (b) exergy efficiency and ethanol exergy content (MW), (c) exergy efficiency and net power production (MW), and (d) ethanol exergy and net power production.

Considering the first point, it is the chosen objective functions, and namely efficiency that present a limit. In fact, only (ethanol production/power production) couples presenting an exergy efficiency equal to or higher than that of a lower ethanol production point can potentially make their way to the Pareto curve. This eliminates hence all solutions with a lower electricity production rate for a similar ethanol production rate.

The process limits on the other hand provide an upper bound by the fact that no higher electricity production rate can be obtained for a given ethanol production rate than the one obtained in this work. The presence of this limit is emphasized by the presence of capital costs as objective function which would have eliminated the most costly alternative between two alternatives presenting similar efficiencies.

5.5.2.2 Capital cost related variables

As highlighted in Equation 4:3, capital costs are calculated as the sum of the cost of the heat exchange network and the cost of the process without this network. Considering this, Figure 5:6.(a) Equation 5:7 highlights the relationship between process capital cost and HEN cost for all optimal points, whereas Figure 5:6.(b) highlights the relationship between process capital cost and the cost of the remaining sections (i.e. process excluding heat exchange network cost). Equation 5:7. We can immediately spot the linear relationship existing between the capital cost and the process w/o HEN cost ($R^2 = 0.9927$). This can be related to the rather small contribution of the HEN cost to the total cost, evaluated at an average of 20%, contrasted by the greater contribution of the rest of the process (evaluated at an average of 80%).

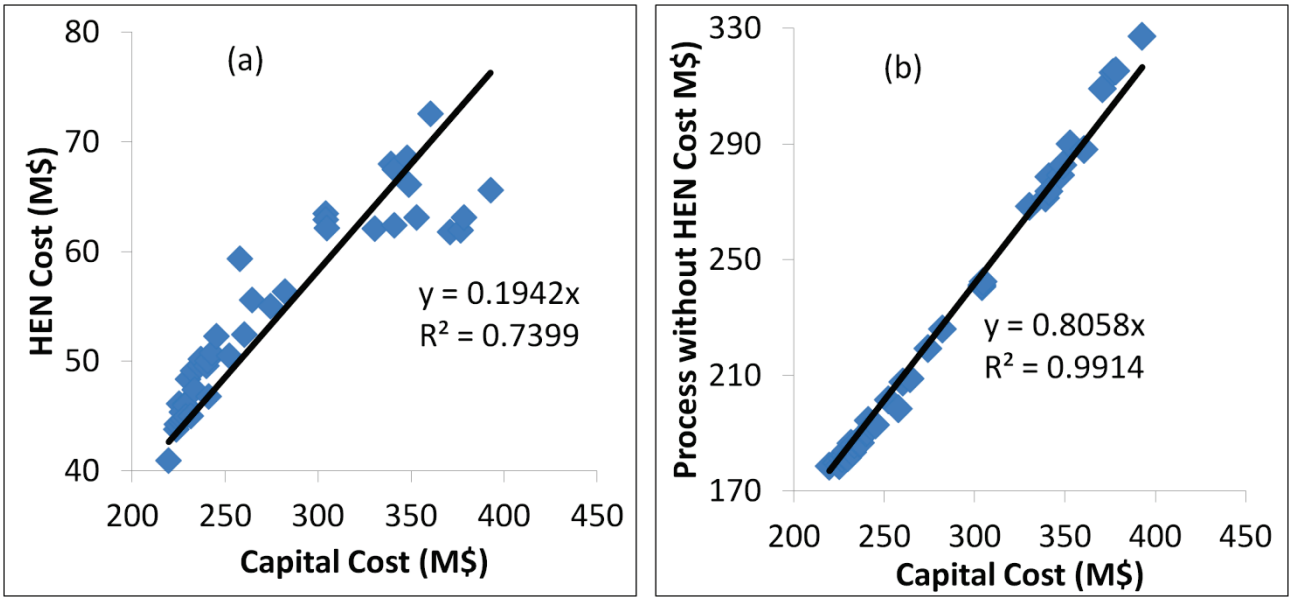

Figure 5:6 Relationship between capital costs and its constituents: (a) HEN cost, (b) process cost w/o HEN

5.5.3 Explanation of the obtained results: analysis of design variables

5.5.3.1 Obtained scope for objective functions, design variables and measured variables: distance variables

The optimization yielded the previously highlighted Pareto set by investigating several possible values for the various design variables. Considering this, a direct result of the obtained convergence is a possible narrowing of the previously specified ranges for the various design variables. With this in mind, Table 4:16 highlights the scopes and operating ranges for the problem's two objective functions, four measured variables, 8 MILP variables and 29 MOO design variables. This table contains both the initial and final ranges for the investigated MOO design variables. On the other hand, only the final ranges are specified for the objective functions, measured variables and MILP variables, and this because of the nature of their evaluation. As we can see, 15 of the 29 MOO variables saw a narrowing of their specified ranges. These variables are

referred to as ***distance variables*** because they can provide a direct idea of the presence or lack thereof of a point on the Pareto curve.

For example, a point with a solid's loading of 5% will not be present on the curve, and this regardless of its values for the other variables. Likewise, a point with a stripping column pressure of 1 atm will also be absent from the curve, and this also regardless of its values for other variables. On the other hand, a point that has values for its distance variables within the specified optimal ranges might have a change of being on the Pareto curve.

Therefore, based on the results highlighted in Table 4:16, a Pareto point has the following attributes concerning optimization variables:

- Not very high evaporation rates in the first level (0 – 0.8) vs. (0-1)
- Low evaporation rates in second, third and sixth levels (0 - 0.3) vs. (0-1)
- Low to mild evaporation rates in the fourth and fifth evaporators (0 – 0.4(0.45)) vs. (0-1)
- Low stripping pressure (0.25-0.65) atm vs. (0.25 -3) atm initially
- Mild to low rectifying column pressures (0.75-1.6) atm vs. (0.75 – 3.5) atm initially
- High steam superheating temperatures (290-300) °C vs. (150 – 300) °C initially
- Mild to high hydrolysis solids loadings (10-19.5) % vs. (2 – 20)% initially
- Mild to high hydrolysis residence times (34-96) h vs. (24 – 96)h initially
- Not very high temperature decrements in the third evaporator (4-10.5) °C vs. (4 – 12) °C initially
- Not very high sugar concentrations at the outlet of the evaporation section (0.65-0.68) wt.% vs. [0.65-0.7) wt% initially
- Not very high pressures in the fourth turbine level (0.4 – 0.65) atm vs. (0.4 – 1) atm. initially
- Mild pressures in the second turbine level (2.5 - 10.5) atm vs. (2 - 12) atm initially

Table 5:18 Obtained scopes and operating ranges for objective functions, measured variables and design variables

Variable name	Unit	Initial operating range	Final operating range	Variable Name	Unit	Initial operating range	Final operating range
ex_{eff}	%		[39.2; 44.4]	C_{inv}	M$		[155 ; 210]
r_{ev_1}	-	[0 ; 1]	[0; 0.8]	dT_{ev_2}	°C	[4;12]	[4; 12]
r_{ev_2}	-	[0 ; 1]	[0; 0.3]	dT_{ev_3}	°C	[4;12]	[4; 10.5]
r_{ev_3}	-	[0 ; 1]	[0; 0.3]	dT_{ev_4}	°C	[4;12]	[4 ; 12]
r_{ev_4}	-	[0 ; 1]	[0; 0.4]	dT_{ev_5}	°C	[4;12]	[4; 12]
r_{ev_5}	-	[0 ; 1]	[0; 0.45]	dT_{ev_6}	°C	[4;12]	[4 ; 12]
r_{ev_6}	-	[0 ; 1]	[0;0.3]	$dT_{ev_{tot}}$	°C		[32 ; 50]
p_{strip}	atm	[0.25 ; 3]	[0.25 ; 0.65]	x_{sgcc}	wt. %	[0.65 ; 0.7]	[0.65 ; 0.68]
$V_{fr,rect,top}$	-	[0 ; 1]	[0; 1]	S/F	kg/kg	[0.5 ; 0.6]	[0.5; 0.6]
p_{rect}	atm	[0.75 ; 3.5]	[0.75 ; 1.6]	T_{solv}	°C	[340 ; 414]	[340 ; 414]
p_{boiler}	atm	[60 ; 100]	[60; 100]	hum_{bag}	mol.%	[0.3; 0.45]	[0.3; 0.45]
T_{sheat}	°C	[150 ; 300]	[290; 300]	$p_{tur,1}$	atm	[12 ; 25]	[12; 25]
$p_{tur,2}$	atm	[2 ; 12]	[2.5 ; 10.5]	$p_{tur,3}$	atm	[1;2]	[1; 2]
$p_{tur,4}$	atm	[0.4;1]	[0.4 ; 0.65]	$p_{tur,5}$	atm	[0.08 ; 0.4]	[0.08 ; 0.4]
bag_{toet}		[0.05; 0.95]	[0.05;0.95]	sld_{load}	wt.%	[2; 20]	[10;19.5]
res_{hyd}	H	[24;96]	[34;96]				
$\dot{m}_{frig,ut}$	t/h		[18.7; 20.8]	$\dot{m}_{cold,ut}$	t/h		[1.1 ; 2.3].10^4
$\dot{m}_{steam,1}$	t/h		[0; 100]	$\dot{m}_{steam,2}$	t/h		[25 ; 300]
$\dot{m}_{steam,3}$	t/h		[0 ; 100]	$\dot{m}_{steam,4}$	t/h		[0 ; 70]
$\dot{m}_{steam,5}$	t/h		[76; 390]	$\dot{m}_{boiler}$	t/h		[359 ; 490]
W_{prod}	MW		[46 ; 90]	C_{HEN}	M$		[40 ; 73]
$Area_{HEN}$	m^2		[44 ; 80].10^3	$\dot{m}_{et}$	t/h		[32.9 ;10]

5.5.3.2 Extraction of knee points and fragmentation of Pareto curve

We now proceed to a fragmentation of the Pareto curve with respect to the various knee points as defined in Chapter 1. This fragmentation will ultimately enable us to determine the evolution of the various variables on the Pareto curve.

We make thus use of the algorithm highlighted in Chapter 4 and obtain the fragmentation and knee points as highlighted in Figure 5:7. As we can see, we have 10 knee points which result in 11 Pareto curve fragments as provided in Figure 5:7.

Moreover, Table 5:19 specifies both actual and normalized objective function values for the various knee and extreme points. From these values, we can see that the exergy efficiency grows fast for the first knee points, in contrast with a small growth for the capital cost. In fact, exergy efficiency witnesses a 52% growth between the first extreme point and the fifth knee, whereas the

capital cost witnesses a mere 23% increase between these two points. On the other hand, exergy efficiency witnesses a 48 % increase between the fifth knee and the second extreme point, in contrast to the capital cost which increased by 77%. This increase can be understood in light of the increasing role played by bagasse hydrolysis.

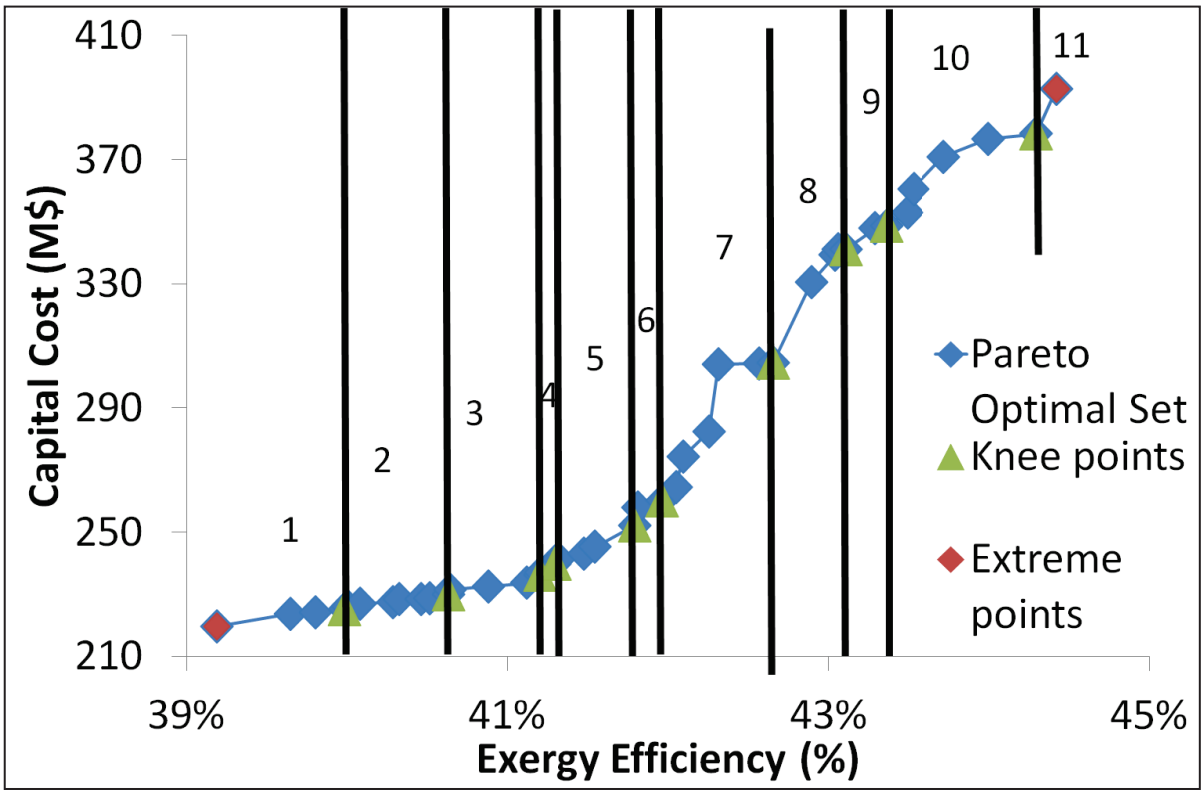

Figure 5:7 Fragmentation of the Pareto curve with respect to knee points

Table 5:19 Objective function values for knee points and extreme points

Point Name	ex_{eff}	C_{inv}	$ex_{eff_{norm}}$	$C_{inv_{norm}}$	Point Name	ex_{eff}	C_{inv}	$ex_{eff_{norm}}$	$C_{inv_{norm}}$
Extreme 1	39.2%	219	0%	0%	Knee 6	42.0%	260	53%	23%
Knee 1	39.9%	225	15%	3%	Knee 7	42.7%	304	66%	49%
Knee 2	40.6%	229	28%	6%	Knee 8	43.1%	353	75%	70%
Knee 3	41.1%	236	38%	10%	Knee 9	43.4%	348	80%	75%
Knee 4	41.3%	239	40%	12%	Knee 10	44.3%	378	98%	92%
Knee 5	41.8%	252	50%	19%	Extreme 2	44.4%	392	100%	100%

5.5.3.3 Evolution of design variable values through the various fragments

The various Parents points, objective were grouped into 11 different clusters as a result of this fragmentation, with each cluster containing the corresponding maximum efficiency knee point. A different approach was adopted than that highlighted in 4.5.2.6. In fact, in this case, the minimum,

mean and maximum values were then calculated for each design variable and this for each cluster. The evolution of these values along the various clusters was then investigated for each variable. The observation of these trend lines enabled us to categorize the different variables as follows:

- Primary position variables: whose values determine the evolution of the objective functions and this in a single trend along the whole Pareto front.
- Secondary position variables: whose values determine the evolution of the objective functions albeit in a periodic trend, possibly influenced by a primary position variable
- Fixed variables or distance variables have their values converge to a fixed value or to a narrow range. As a result, their distance from these values determines the distance of the objective function from the Pareto set.
- Floating variables: whose values fluctuate throughout the Pareto frontier
- Mixed variables: for which the evolution of their values varies throughout the front, witnessing for example a constant value in a given section, an evolution in another section and a floating in a third section.

Considering this, we will base our variable visualization on this categorization. Each variable will be visualized for an increasing fragment number, which is synonymous to a greater exergy efficiency and greater capital cost.

In conclusions, the method utilized in this section and that employed in 4.5.2.6 are both equally useful in determining the evolution of the variables. A more detailed comparison of these two methods can help identify the most suitable one, or possibly move towards a third methodology. This however lies outside the scope of this current thesis.

5.5.3.4 Evolution of primary position variables

Position variables help identify the position of a given Pareto point on the related Pareto curve. Considering this, primary position variables evolve in a regular manner throughout the Pareto space, or the Pareto fragments in our case. Our study problem has two such variables: bag_{toet} and $\dot{m}_{cold,ut}$, as evidenced by their evolution along the various fragments highlighted in Figure 5:8.(a) and Figure 5:8.(b) respectively.

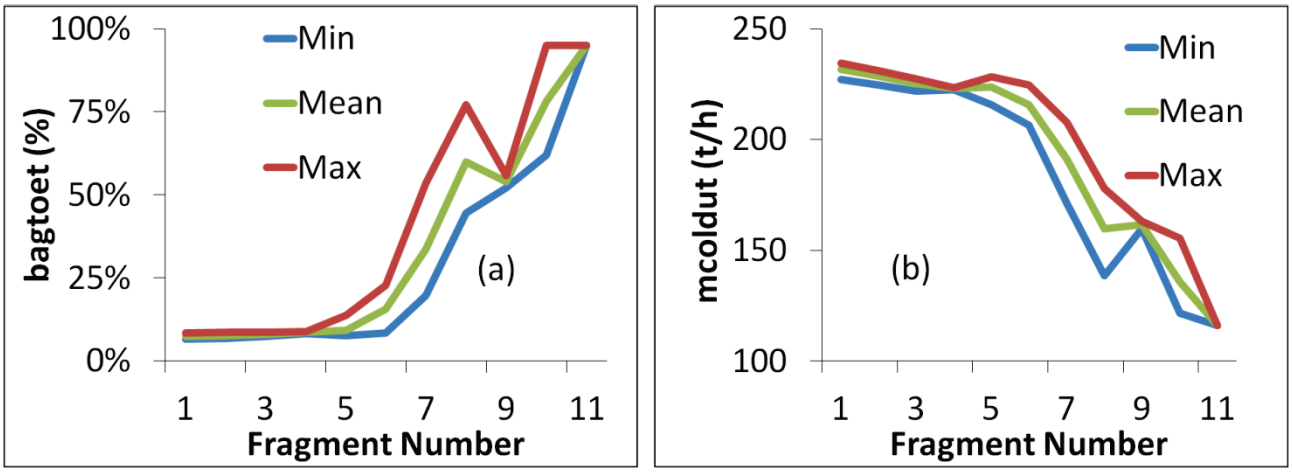

Figure 5:8 Evolution of key position variables: (a) fraction of bagasse diverted for hydrolysis and ethanol production $bag_{toet}(\%)$, and (b) cold water flow rate $\dot{m}_{cold,ut}$ $(\frac{t}{h})$

The first variable bag_{toet} is the amount of bagasse diverted for hydrolysis. This variable is the main behind the proposed optimization. In fact, a higher hydrolyzed bagasse fraction leads to a greater ethanol production, which as highlighted earlier is equivalent with a greater efficiency and greater cost. Its status as a primary position variable is thus self-evident. Finally, the presence of a rather constant fraction for the initial fragments is characteristic of the heat integration step, which is predominant for smaller efficiencies as indicated previously.

The second variable on the other hand is the required cold utility flow rate, $\dot{m}_{cold,ut}$ evaluated in tonnes/hour. Its status as a primary position variable is due to its direct relation to the first variable bag_{toet}. In fact, a greater hydrolyzed bagasse fraction leads to a smaller heat production through combustion, and thus to a smaller requirement for a cold utility. This heat is in fact transformed into ethanol.

Finally, a change in the trend can be witnessed for both variables at various points of their respective curve. This change of slope is characteristic of the effect of secondary position variables, which will be discussed in the next section. None the less, it can be deduce that exergy efficiency and capital costs are greater for a greater hydrolyzed bagasse fraction and a smaller cold utility consumption.

5.5.3.5 Evolution of certain secondary position variables

Secondary position variables are an additional example of position variables. Their variation occurs however in a periodic trend, in opposition to the constant trend for the primary position variables.

5.5.3.5.1 Hydrolysis related variables

A first example of such variables are those related to the hydrolysis section, namely: the hydrolysis residence time hyd_{res} and (b) the solids loading in the hydrolysis reactor (sld_{load}), as evidenced by their evolution highlighted in Figure 5:9.(a) and Figure 5:9.(b) respectively.

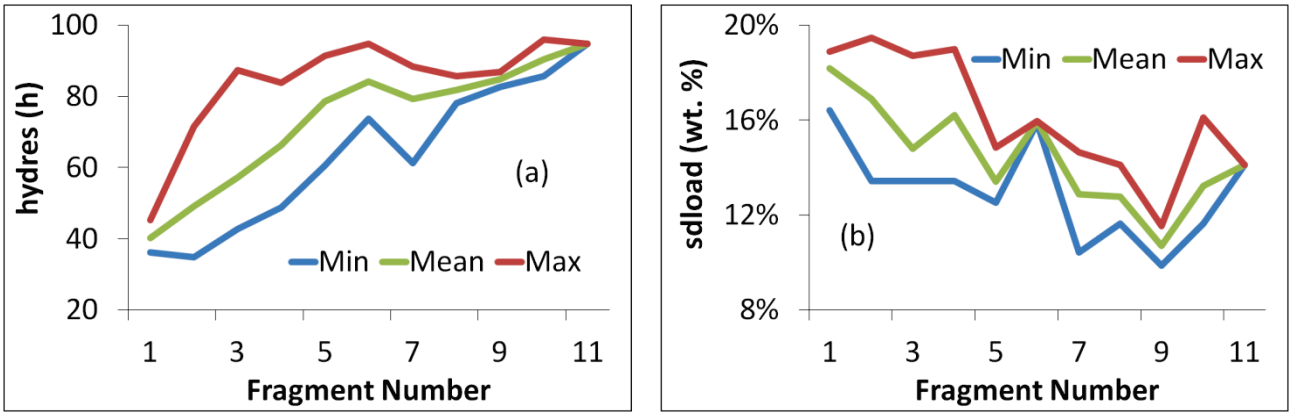

Figure 5:9 Secondary variables related to hydrolysis section : (a) the hydrolysis residence time $(hyd_{res})(h)$ and (b) the solids loading in the hydrolysis reactor $(sld_{load}(wt.\%))$

As can be seen in Figure 5:9.(a), the hydrolysis residence time follows an increasing trend. This is due to the greater hydrolysis yield associated with greater residence times, which ultimately results in a higher ethanol production. Also a higher residence time leads to a need for a greater number of hydrolysis reactors, which is synonymous with a greater investment cost.

The solids loading on the other hand follows a decreasing trend as highlighted in Figure 5:9.(b). This is also due to the greater hydrolysis yield associated with a smaller solids loading. Smaller solids loadings are also associated with a greater input flow rate to the reactors, leading to an even greater number of reactors, also synonymous with a greater investment cost.

The status of these variables as secondary position variables is due to the variation in the trends observed at the sixth and tenth fragments for the hydrolysis residence time and at the fifth and ninth fragments for the solids loading. Both cases can be related to spikes in the hydrolyzed bagasse fraction, observed for the fifth and ninth fragments. Such spikes lead to an increase in ethanol production, a decrease in electricity production and an increase in investment cost if all parameters were left the same. Such modifications are tampered down by using higher solids loadings and lower hydrolysis times. Moreover, we can deduce from the obtained results that the solids' loading is more critical than the hydrolysis time. This is because (1) it changes its trend first; (2) it sees the greatest variation in its value at the critical points.

5.5.3.5.2 Distillery related variables

We turn our attention now to variables related to the distillery. The variables first such variables to be classified as secondary position variables are the vaporization rates in the first (r_{ev_1}) and fifth (r_{ev_5}) evaporation levels. This is evidenced by their evolution in Figure 5:10.(a) , and Figure 5:10.(b) respectively.

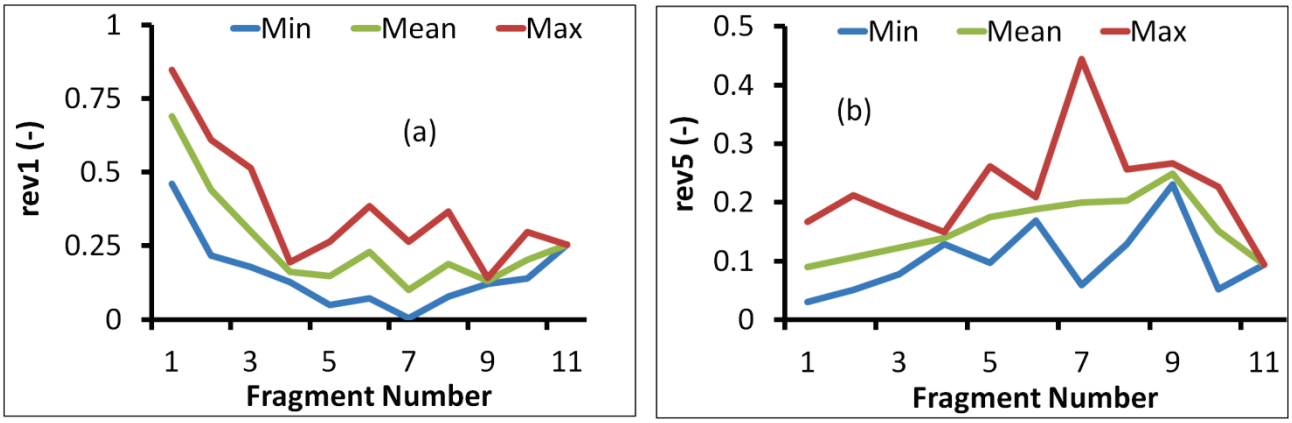

Figure 5:10 Secondary variables related to the distillery: (a) first level r_{ev_1}, and (b) fifth level r_{ev_5}

As we can see, r_{ev_1} follows a decreasing trend. This is due to the increase of both costs and exergy efficiency with a greater vapor bleeding, as highlighted in Figure 5:10. However, as we can see this trend has certain discontinuities namely at the fifth and eighth fragment. This can also be linked to the spike in bagasse consumption watered down by a greater use of this less expensive level.

r_{ev_5} on the other hand follows an increasing trend until the eighth fragment after which it witnesses a steady decline, except for the last fragment. This can be understood in light of a smaller role for the first level for initial fragments and the greater role in the final fragments.

5.5.3.6 Classification of variables

After having highlighted the two key position variables along with some position variables, we proceed to a classification of all of the variables in accordance with their nature, primary position, secondary position and floating. This classification is highlighted in Table 5:20. Again, as was done in Chapter 4, these variables are divided into positive and negative trends, trends that are recorded with respect to exergy efficiency. The hydrolyzed bagasse fraction remains the main influential variable, along with the cold utility flow rate. 22 secondary variables exist and include hydrolysis parameters, utility steam rates, column pressures, certain vaporization parameters and turbine pressures. 16 floating variables exist and include boiler parameters, dehydration parameters amongst with other process variables.

Finally, even though the correlation factor between each variable and exergy efficiency is specified in Table 5:20, this parameter should be taken only as a possible indicator of the variable's impact and nature.

Table 5:20 Results of variable analysis and classification

Variable Type	Nature of Trend	Investigated Variables	Correlation factor
Position Variable	Positive	bag_{toet}	0.91
	Negative	$\dot{m}_{cold,ut}$	-0.93
Secondary position variables	Positive	r_{ev_5}, hyd_{res}, p_{tur1}	0.23, 0.8, 0.39
		$\dot{m}_{steam,1}$, $\dot{m}_{steam,3}$, $\dot{m}_{steam,4}$	0.57, 0.5, 0.21
	Negative	r_{ev_1}, dT_{ev4}, dT_{ev5}	-0.62, -0.67, -0.25
		sld_{load}, p_{strip}, p_{rect}	-0.6, -0.31, -0.2
		hum_{bag}, p_{tur2}, p_{tur3}	-0.65, -0.62, -0.48
		$\dot{m}_{steam,2}$, $\dot{m}_{steam,5}$; $\dot{m}_{water}$	-0.2, -0.52, -0.8
Floating Variables	Positive	r_{ev_2}, r_{ev_3}, r_{ev_4}, r_{ev_6}	0.55, 0.351, 0.08, 0.23
		dT_{ev2}; dT_{ev3}; dT_{ev6}	0.59, 0.49, 0.49
		S/F, T_{solv}, $\dot{m}_{frig,ut}$	0.01, 0.33, 0.17
	Negative	x_{sgcc}, $V_{fr,rect,top}$	-0.13, -0.1
		p_{tur4}, p_{tur5}	-0.13, -0.14
		P_{boiler}, T_{sheat}	-0.17, -0.27

5.6 Selection of optimal solutions: profitability analysis

As indicated in Chapter 1 and previously performed in Chapter 4, our optimal process selection method is based on a profitability analysis. This analysis seeks to identify the process with the optimal values for chosen indicators under different economic scenarios.

5.6.1.1 Definition of evaluated parameters and economic hypotheses

The key profitability indicator, used in industry worldwide, is the Net Present Value (NPV). Moreover, the NPV can be used to select between competing industrial alternatives, namely those presented by the Pareto curve. With this in mind, a given industrial project is said to be more profitable than another if and only if its Net Present Value is greater than that of the other project.

For these reasons, this parameter is used in our case, mainly to select the most optimal Pareto configuration. Such an alternative (I_{Profit}) has the maximum value for the Net Present Value ($maxNPV$) as highlighted in Equation 4:17 and Equation 5:11.

$$maxNPV(M\$) = \max_{I \in Pareto} NPV_I(Economic\ conditions)$$

Equation 5:10 Formula for calculating the maximum feasible Net Present Value (M$)

$$I_{Profit} = (ex_{eff,I_{Profit}}, C_{inv,I_{Profit}})/NPV_{I_{Profit}} = maxNPV$$

Equation 5:11 Formula for determining the most profitable Pareto alternative

Moreover, as evidenced from Equation 4:17, the various values of the NPV, along with the value for $maxNPV$, and ultimately the most profitable alternative I_{Profit} all depend on the chosen values for the various economic indicators.

Considering the importance of the latter indicators, we provide below a definition of the various parameters entering into play in the Net Present Value calculation procedure for the distillery + hydrolysis + cogeneration case:

- The project life time (LT, y): the number of years the plant will be in operation.
- The Salvage equipment value (SV, M$) :the equipment selling price after the project life time is done
- The construction and start-up period (CSU, y): the period needed to set up the plant before its first round of production.
- The depreciation rate (λ): linked to the loss of value of equipment, assumed to evolve in a linear manner for a given number of years.
- The days of operation per year (n_{dop}) : the number of days the plant will be in production mode, evaluated with 24h/day
- The tax rate(tax_{rate}) imposed on the net profit after depreciation.
- The sugarcane price (SCP) evaluated in $/t-SC.
- The leaves price (LP) evaluated in $/ t-leaves
- The enzyme price (EP) evaluated in $/t-enzyme
- The ethanol selling price (ESP) evaluated in $/l ethanol
- The power selling price (PSP) evaluated in $/MWh.
- The Discount Rate (%): set by the investor to evaluate the risk associated with the project and the time value of money.

With this in mind, we make use of literature data made available in Table 5:6, and reminded in Table 4:19. As we can see, cells with red fonts can be found in this table. These cells represent the absence of data concerning certain parameters. In order to circumvent this, we assumed for these cells values similar to those for the remaining cases. This was straightforward for parameters with similar results for all cases. This is the case for the salvage equipment value, the construction and start-up period and the tax rate. Choices were however made of parameters with various values, like the construction period, the discount rate and the enzymes price. These choices fell on the most conservative of all values and this to guarantee a certain degree of caution.

Moreover, the choice of the enzyme price to be evaluated in $/L cellulosic ethanol did not seem very sordid for us, mainly seeing that different ethanol production rates could be obtained for constant enzyme rates, and this by varying the solids loading or hydrolysis yield. For this reason, the evaluation in $/t-enzyme consumed was retained.

Table 5:21 Economic hypotheses as extracted from literature and values for chosen indicators

Article	[69]	[64]	[21]	[63]
Evaluated scenario	1	2	3	4
Project lifetime (years)	25	20	25	25
Salvage equipment value (M$)	0	0	0	0
Construction and start-up (years)	2	1	2	2
Depreciation (years)	10- Linear	10- Linear	10- Linear	10-Linear
Days of operation	167	200	200	210
Tax rate (income and social contributions)	34%	34%	34%	34%
Discount rate (%)	10%	10%	10%	11%
Sugarcane price ($/TC)	19.41	19.5	31.17	28.76
Sugarcane Trash Price ($/ton leaves)	15	13	15.02	17
Enzyme price ($/ton enzyme)	1680	1680	1250	1680
Ethanol price ($/L)	0.5	0.53	0.72	0.51
Electricity price ($/MWh)	70.5	86	51	69

5.6.1.2 Presentation of results for all economic scenarios

We present in this section the results of the profitability analysis, as described previously. We start by highlighting in Figure 5:11 the curves presenting the evolution of the Net Present Value with respect to exergy efficiency across the Pareto population for all four economic scenarios. As we can see in a first glance, all the scenarios follow a similar trend. In fact, as can be seen in Figure 5:11, the NPV curves have greater NPV values for low-efficiency, low-cost systems compared to high-efficiency, high-cost systems. Also, it can be seen that the NPV value changes little up until a certain value, before beginning a steep descent towards lower values. In fact, by contrasting the two sections, the first section witnesses an average difference of 13M$ between the minimum and maximum values. The second section on the other hand witnesses an average difference of 250 M$ between these two values. Finally, the critical value not surprisingly none other than the critical value observed in Figure 5:5, corresponding to an exergy efficiency of 41.8% and a capital cost of 245 M$. More specifically, this value sets the limit between the absence and the presence of bagasse hydrolysis.

Moreover, as we can see in Figure 5:11, some economic conditions provide better overall results than others. This is the case for the second and third economic scenarios, which in fact yield positive NPV results for low efficiency, low cost systems. This result is due to their respective economic conditions. In fact, by combining Table 4:19 and Figure 5:11, we can see that the better results for the second economic scenario are due to its smaller sugarcane price, combined with its

greater electricity price. The better results for the third economic scenario on the other hand are due to its great ethanol price. Disparities however still exist between these two scenarios.

First, the second scenario provides better results for low exergy efficiency low cost systems, where heat integration is predominant. This is mainly due to its higher electricity price (86 $/MWh vs. 51$/MWh), coupled with its smaller sugarcane price (19.5 $/MWh vs. 31.7 $/MWh).

Second, the third economic scenario provides better results for high efficiency, high cost systems, where ethanol production is predominant. This is mainly due to its higher ethanol price (0.72 $/L vs. 0.53 $/L).

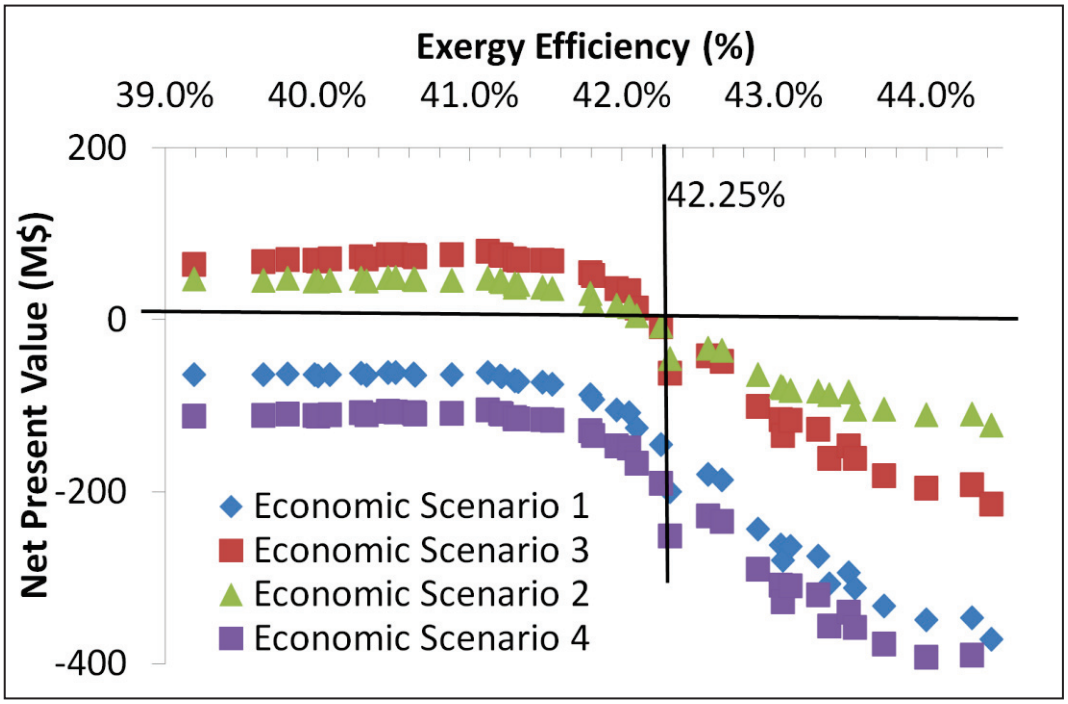

Figure 5:11 Net Present Value vs. Exergy efficiency for Pareto individuals under four different economic scenarios

Finally, this change occurs after the Pareto point characterized by an exergy efficiency of 42.22% and a capital cost of 282 M$. This point is characterized by a shift in the annual operating margins, as highlighted in Figure 5:12. In fact, before this point, the margin is greater for the second economic scenario, whilst this value is greater for the third scenario after this point. This highlights an additional effect of the chosen economic conditions on the obtained Net Present Value profile, and ultimately the nature of the optimal values.

In contrast to these profiles, the first scenario has lower NPV values due to its smaller number of operating days (167 vs. 200 & 210 days /year). The fourth scenario however has the worst results due to its low ethanol price coupled with its great sugarcane price (0.51 $/L and 28.76 $/L respectively).

All of these previous analyses lead to the great role played by market parameters on both the profitability of the Pareto curve and the evolution of the NPV along the said curve.

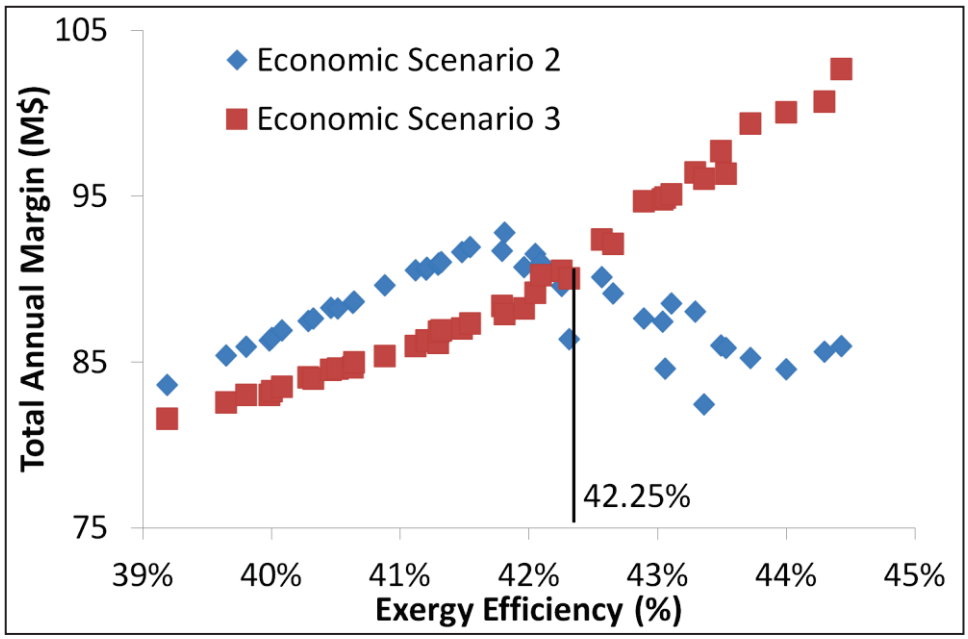

Figure 5:12 Evolution of total margin along Pareto curve for second and third economic scenario

5.6.1.3 Presentation and discussion of most profitable solutions

As indicated earlier, the most profitable Pareto solution is that which presents the maximum value for the NPV under chosen economic conditions. With this in mind, Table 5:22 records the most profitable point for each scenario, along with its corresponding NPV value, and its coordinates on the Pareto front. As we can see, the maximum NPV is obtained for the second case, followed by the third, then the first and finally the fourth. These values can be understood in light of the explanations provided in the previous paragraph.

On a second note, concerning the nature of the optimal solution, we distinguish two different optimal points: (41.1%,234M$) for cases 2 & 4 and (40.4%,228M$) for cases 1 & 3. All of these points correspond to rather low efficiency low cost systems, which as highlighted in 5.5.2 are associated with low, rather constant ethanol production rates. These results can be understood as follows.

Table 5:22 Results for NPV related indicators for all four economic scenarios

Evaluated Scenario	1	2	3	4
Maximum Net Present Value (M$)	-61.3	79.8	48.7	-105.4
$I_{Profit}\,(ex_{eff}; C_{inv})$	(40.4%; 228 M$)	(41.1%; 234 M$)	(40.4%; 228 M$)	(41.1%; 234 M$)

A higher efficiency alternative was obtained for cases 2 & 4. This was due to a combination of high electricity price and great operating days. The first prerequisite lacks for case 4 which has the smallest electricity price, whereas the second prerequisite lacks for case 1, which has the smallest number of operating days.

5.6.1.4 Definition and results for additional economic parameters

Even though the Net Present Value is the ultimate parameter for optimal process selection and for the evaluation of profitability, other economic indicators, dealt with in literature, will be defined in this paragraph and their values highlighted for the different economic scenarios. These said indicators are detailed below with their calculation formulas specified in Table 5:23.

- The maximum internal rate of return ($maxIRR$) is the Internal Rate of Return value for which the Maximum Net Present Value for all individuals in the Pareto curve is equal to zero. This evaluation highlighted in Equation 4:19, is carried out under fixed economic hypotheses. The default discount rate will be chosen for the remaining calculations. This indicator is interesting because it allows the designer to compare this project with other possible industrial projects.
- The Minimum Ethanol Selling Price ($minESP$), known in literature under the acronym $MESP$, evaluated in ($/l ethanol produced) is the ethanol price for which the maximum Net Present Value for all individuals in the Pareto curve is equal to zero. This evaluation, highlighted in Equation 4:20, is realized under fixed economic hypotheses and for a constant internal rate of return. The only variable is the ethanol selling price (ESP). This indicator is interesting, because below this price no process on the Pareto curve is profitable, with all other economic indicators remaining constant. Considering this, the lower this value the better.
- The Minimum Power Selling Price ($minPSP$) evaluated in ($/MW) is the electricity price for which the maximum Net Present Value for all Pareto individuals is equal to zero. This evaluation, highlighted in Equation 4:21, is performed under fixed economic hypotheses and for a constant internal rate of return, with the only variable being the electricity selling price (PSP). This indicator is interesting, because below this price no process on the Pareto curve is profitable, with all other economic indicators remaining constant. Again, the lower this value the better.
- The Maximum SugarCane Price ($maxSCP$) evaluated in ($/t SC) is the sugarcane purchase price for which the maximum Net Present Value for all Pareto individuals is equal to zero. This evaluation, highlighted in Equation 4:22, is performed under fixed economic hypotheses and for a constant internal rate of return, with the only variable being the sugarcane price (SCP). This indicator is interesting, because above this price no process on the Pareto curve is profitable. Thus, it can be concluded that the higher this value the better.
- The minimum required days of operation per year $mindop$ evaluated in (days/year) is the number of operating days per year for which the Net Present Value for all Pareto individuals is equal to zero. This evaluation, highlighted in Equation 4:23, is performed under fixed economic hypotheses and for a constant internal rate of return, with the only variable being the number of days of operation (SCP). This indicator is interesting, because profitability actually increases

with a greater number of days. Thus below this number no process on the Pareto curve is profitable. Thus, it can be concluded that the lower this value the better.

Table 5:23 Mathematical formulation for additional economic indicators distillery + hydrolysis + Rankine Cycle

Economic Indicator	Mathematical Equation	Equation number
$\boldsymbol{maxIRR}$ (%)	$maxIRR(\%) = IRR/\max_{I \in Pareto} NPV_I(IRR) = 0$	Equation 5:12 Formula for maximum feasible internal rate of return
$\boldsymbol{minESP\ or\ MES}$ **($/L ethanol)**	$MESP(\$/l) = ESP/\max_{I \in Pareto} NPV_I(ESP) = 0$	Equation 5:13 Formula the Minimum Ethanol selling price ($/l ethanol)
$\boldsymbol{minPSP\ or\ MPS}$ **($/MWh)**	$MPSP(\$/MW) = PSP/\max_{I \in Pareto} NPV_I(PSP) = 0$	Equation 5:14 Formula the Minimum Power selling price ($/MWh)
$\boldsymbol{minESP - cell}$ **($ / L cellulosic ethanol)**	$minESP - cell = ESP - cell / \max_{I \in Pareto} NPV_I(ESP - cell) = 0$	Equation 5:15 Formula for the Minimum cellulosic ethanol selling price ($/L cellulosic ethanol)
$\boldsymbol{maxSCP}$ **($/t-SC)**	$maxSCP = SCP/\max_{I \in Pareto} NPV_I(SCP) = 0$	Equation 5:16 Formula for the Maximum Sugarcane price ($/ t - SC)
$\boldsymbol{mindop}$ **(days / year)**	$\text{mindop} = dop/\max_{I \in Pareto} NPV_I(dop) = 0$	Equation 5:17 Formula for the minimum number of operating days days/year)

We can notice that the two parameters concerning leaves price and enzymes price were omitted. This is because these two components affect little the profitability of the process. In fact, under the constant chosen economic conditions, no actual price for these variables results in a zero NPV for the maximum NPV value.

With this in mind, each indicator is associated with an optimal process configuration which will also be provided in the results. Considering this, Table 4:22 provides values for the various economic indicators, including the Maximum NPV,$\max NPV$, as well as the optimal configurations associated with each indicator, and this for the various economic scenarios.

As we can see, $maxIRR$ evolves in a similar manner as $maxNPV$, with the third and second alternatives having the best values, and the first and fourth trailing behind. This is because the IRR is, as the maxNPV, an indicator of profitability.

The minimum ethanol selling price minESP on the other follows a different trend. In fact, it is lowest for case 2, with cases 1, 4 and 3 falling behind. The supremacy of cases 1 &2 can be understood in relation to their low sugarcane price. Finally, case 3 has a higher price than case 4 due to its lower electricity price.

The minimum power selling price, minPSP sees its best value for case 3 followed by cases 2, 1 & 4. The supremacy of case 3 can be understood in light of its high ethanol price, whereas the value for case 2 can be understood in light of a smaller sugarcane cost. The high prices obtained for cases 1 & 4 can be understood in light of the small number of operating days per year for the first case, and the high sugarcane price in the second.

The maximum sugarcane purchase price, maxSCP, has its best value for case 3 followed by cases 2, 3 and 4. The supremacy of case 3 is also due to the high ethanol price, whereas the better results for cases 2 and 4 can be understood in light of their number of operating days. This low number in case 1 ultimately leads to it having the smallest value.

The minimum operating days, mindop, has its best values for case 2, followed by cases 3, 1 and 4. The supremacy of case 2 is due to its high electricity price and low sugarcane price. The second best results for case 3 are due on the other hand to its high ethanol price. Finally, case 4 is worst due to its high sugarcane price.

It should also be noted that a difference exists between initially profitable and initially non-profitable cases. In fact, the first cases see an increase in $maxSCP$ and $maxIRR$, and a decrease in $minESP$, $minPSP$ and $mindop$, whereas the opposite is observed for the latter cases. This is due to the impact of the different indicators on the Net Present value. For example, a higher IRR leads to a higher actualization and ultimately a lower NPV. Thus profitable systems see an increase in their IRR in order to attain the point of zero NPV. A lower IRR on the other hand leads to a higher NPV. As a result, profitable systems see a reduction in their IRR in order to attain the point of zero NPV.

Moreover, as can be seen in Table 4:22, the search for these optimal values for the different indicators may lead to a change in the nature of the optimal solution, for certain scenarios. This is the case for the following indicators $maxIRR$, $minESP$, $minPSP$ and $mindop$, and for scenarios 1, 2 & 3. These modifications were obtained as follows. for non-profitable scenarios, namely Case1, this search lead to greater efficiency systems, whereas this search lead to lower efficiency systems for profitable scenarios, namely Cases 2 & 3. This is due both to the nature of the used indicator and the nature of the Pareto curve.

Concerning the Internal Rate of Return (IRR), the following is true: a lower IRR value leads to a lower actualization, which ultimately gives more weight to annual profits made in later years. Its decrease may make more efficient, more costly projects, more interesting, whereas its increase may lead to less efficient projects being more interesting. The first situation is highlighted in case 1

where a greater efficiency project is obtained for a lower IRR, and the second in case 2 where a lower efficiency project is obtained for a higher IRR. The same applies for the number of operating days, $mindop$. In fact, a higher number of days leads to a greater annual profit, making more efficient systems more interesting, with the opposite being true for a smaller number.

Concerning the minimum ethanol selling price ($minESP$): the impact of this parameter can be understood in light of the varying ethanol production rate, which tends to increase with increasing efficiency, albeit slowly for low efficiency systems. With this in mind, a lower selling price leads to the consideration of a less efficient less costly system, as for case 3. Likewise, a higher price leads to the consideration of a more efficient system, as for case 1. The same logic can be applied for the minimum Power selling price ($minPSP$). This is due to the fact that also low efficiency systems whiteness an increase in power production. Considering the great variability in this parameter for such systems, its modification led to a change in most optimal systems for cases 1,2 and 3.

Table 5:24 Results for various economic indicators under different scenarios distillery + hydrolysis + Rankine Cycle

Evaluated Scenario	1	2	3	4
$maxNPV$ (M$)	-61.3	79.8	48.7	-105.4
Optimal configuration ($ex_{eff}; C_{inv}$)	(40.4%; 228 M$)	(41.1%; 234 M$)	(40.4%; 228 M$)	(41.1%; 234 M$)
$maxIRR$ (%)	7.07%	13.81%	12.19%	5.45%
Optimal configuration ($ex_{eff}; C_{inv}$)	(41.1%; 234 M$)	(41.1%; 234 M$)	(39.2%; 220 M$)	(41.1%; 234 M$)
$minESP$ ($/L)	0.567	0.46	0.675	0.615
Optimal configuration ($ex_{eff}; C_{inv}$)	(41.1%; 234 M$)	(41.1%; 234 M$)	(39.2%; 220 M$)	(41.1%; 234 M$)
$minPSP$ ($/L)	104	51	25	119
Optimal configuration ($ex_{eff}; C_{inv}$)	(41.1%; 234 M$)	(40.4%; 228 M$)	(40.4%; 228 M$)	(41.1%; 234 M$)
maxSCP ($/L)	13.74	25.41	35	20.33
Optimal configuration ($ex_{eff}; C_{inv}$)	(40.4%; 228 M$)	(41.1%; 234 M$)	(40.4%; 228 M$)	(41.1%; 234 M$)
$mindop$ (days/year)	199	168	178	288
Optimal configuration ($ex_{eff}; C_{inv}$)	(41.1%; 234 M$)	(41.1%; 234 M$)	(39.2%; 220 M$)	(41.1%; 234 M$)

5.6.1.5 Definition and results for cellulosic ethanol price parameter

It can be seen from the previous analysis that all the previous results pertained to low efficiency, low-cost systems. As highlighted earlier, these systems have a small fraction of hydrolyzed bagasse. This indicates that this alternative is not competitive under the chosen economic indicators. For this reason, we will consider hereafter, an additional indicator, highlighted below:

- The Minimum cellulosic ethanol selling price ($minESP - cellulosic$) evaluated in ($/L cellulosic ethanol produced) is the selling price of the ethanol fraction produced from cellulosic glucose for which the maximum Net Present Value for all individuals in the Pareto curve is equal to zero. This evaluation, highlighted in Equation 5:15, is realized under fixed economic hypotheses, including a fixed sugarcane ethanol price, and for a constant internal rate of return. The only variable is the cellulosic ethanol selling price (ESP-cellulosic). This indicator is interesting, because cellulosic ethanol might have a different market price than regular ethanol in the case of commercialization. Also, like for other variables, below this price no process on the Pareto curve is profitable. Considering this, the lower this value the better.

Table 5:25 highlights the results obtained for the four different scenarios. As for the previous table, this table contains both the value for the $minESP$ along with the related optimal configuration. As we can see, this variable converges to a zero value for the two profitable cases 2 & 3. This zero value leads to a modification in the nature of the optimum for case 3. This highlights the importance of ethanol price for this case. The optimal solution remains the same for case 2, and this because of the small overall ethanol price.

Initially non-profitable solutions on the other hand lead to non-null, almost equal values for the ethanol selling price. These values were moreover associated with the most efficient, most costly, highest ethanol producing process alternative. This highlights the all or nothing nature of the hydrolysis alternative. This is emphasized by the absence of an intermediary solution. This is due to the very high slope of the ethanol-vs.-power curve observed for the ethanol producing sections of the Pareto curve. This curve is reminded, along with its associated linear regression, in Figure 5:13. As we can see, for each 1 MW of power lost, 1.63 MW of ethanol is produced. This implies that the loss of value due to a smaller power consumption can be compensated by the increase in ethanol production given adequate ratios between the prices of the two products. Moreover, seeing that the increase in ethanol price has the greatest impact on the last alternative, and that all alternatives were initially non profitable, it is this alternative that ultimately hits the zero NPV value first.

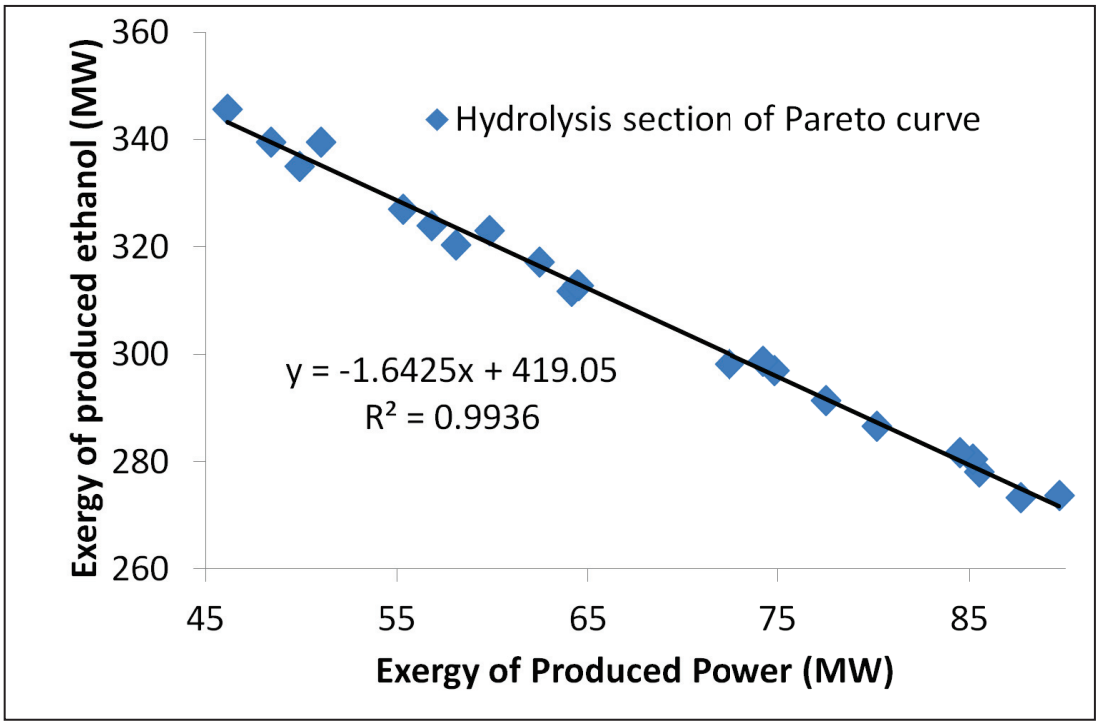

Figure 5:13 Evolution of ethanol production vs. power production for ethanol producing alternatives

Table 5:25 Results for cellulosic ethanol price indicator along with related optimal solutions

Evaluated Scenario	1	2	3	4
$minESP - cellulosic$ ($/L cellulosic ethanol)	1.76	0	0	1.72
Optimal configuration $(ex_{eff}; C_{inv})$	(44.4%; 393 M$)	(41.1%; 234 M$)	(36.9%; 224 M$)	(44.4%; 393 M$)

5.6.1.6 Use of NPV as a comparison tool: modified minimum selling prices

As observed in Table 5:25, no minimum selling price for cellulosic ethanol could be obtained for cases 2 & 3. This is because both alternatives were originally profitable, mainly for their power producing alternatives. With this in mind, we adopted a different approach based on an equation of profitability between alternatives.

This approach will seek to modify the chosen economic conditions in order to equate the profitability of the ethanol producing alternatives with that of the power producing ones. Considering this, and looking at the nature of the two problems, this equation is only made possible by controlling the ethanol selling price. In fact, as highlighted earlier, the power producing alternatives will remain more profitable than their ethanol producing counterparts in case of an increased power price, reduced sugarcane price, modified internal rate of return, or increased days of operation.

With this in mind, two cases are hence possible: (1) control the ethanol price by setting both cellulosic and sugarcane ethanol at an equal price and (2) control only the cellulosic ethanol price

by keeping the sugarcane ethanol at a constant price. Both cases will be thus investigated in this section.

This leads to the definition of two additional parameters: the modified minimum ethanol selling price ($mminESP$), defined in Equation 5:18, and the modified cellulosic ethanol selling price ($mminESPc$), defined in Equation 5:19. It should be noted that the cellulosic ethanol selling price is equal to the sugarcane ethanol selling price in the first equation, whereas the sugarcane ethanol selling price is constant in the second equation. Moreover $Pareto1$, refers to the power producing sections of the algorithm, whereas $Pareto2$ refers to the hydrolysis producing sections.

Equation 5:18 Formula for calculating the Modified minimum ethanol selling price

$$mminESP(\frac{\$}{l}) = ESP / \max_{I \in Pareto1} NPV_I(ESP) - \max_{I \in Pareto2} NPV_I(ESP) = 0; ESPc = ESP$$

Equation 5:19 Formula for calculating the Modified minimum cellulosic ethanol selling price

$$mminESPc\left(\frac{\$}{l\ cellulosic\ ethanol}\right) = \frac{ESPc}{\max_{I \in Pareto1} NPV_I(ESPc)} - \max_{I \in Pareto2} NPV_I(ESPc) = 0; ESP = cte$$

Both these variables are of key importance because they determine the prices beyond which the most profitable hydrolysis alternative becomes more profitable than the most profitable power producing alternative. Considering this, the calculated results for the 4 investigated scenarios are highlighted in Table 5:26. This table contains along with the values for the controlled variables, the corresponding maxNPV, along with the two optimal solutions, pertaining to the two Pareto sections ($Pareto1$ & $Pareto2$).

Multiple conclusions can be made concerning the obtained results. First, we can clearly see that the two variables converge towards a similar optimal value obtained for each economic scenario. This is because it is the cellulosic ethanol fraction only that determines the profitability of the various alternatives for varying ethanol prices, with other parameters remaining constant.

Moreover, both evaluations yield similar optimal alternatives for each economic scenario. Plus, whereas the extreme point (44.4%; 393 M$) was always found to be the most optimal hydrolysis alternative, the nature of the optimal power producing alternative changed between the alternatives. This again can be related to the values of the remaining economic parameters. What can be extracted however is the fact that higher ethanol prices lead to higher efficiency power producing systems. This is because of the small variation in ethanol production between the different alternatives.

Table 5:26 Results for cellulosic ethanol price indicator along with related optimal solutions for Pareto solutions for the combined distillery + cogeneration + hydrolysis process

Evaluated Scenario	1	2	3	4
$mminESP(\frac{\$}{l})$	1.63	1.5	1.3	1.45
$maxNPV$ (M$)	951	1165	670	886
Optimal configuration $Pareto1$ $(ex_{eff}; C_{inv})$	(41.17%; 236 M$)	(38.72%; 252 M$)	(40.43%; 228 M$)	(38.72%; 252 M$)
Optimal configuration $Pareto2$ $(ex_{eff}; C_{inv})$	(44.4%; 393 M$)	(44.4%; 393 M$)	(44.4%; 393 M$)	(44.4%; 393 M$)
$mminESPc\ (\frac{\$}{l\ cellulosic\ ethanol})$	1.63	1.5	1.3	1.46
$maxNPV$ (M$)	-35	108	65	-80
Optimal configuration $Pareto1$ $(ex_{eff}; C_{inv})$	(41.17%; 236 M$)	(41.17%; 236 M$)	(40.43%; 228 M$)	(38.72%; 252 M$)
Optimal configuration $Pareto2$ $(ex_{eff}; C_{inv})$	(44.4%; 393 M$)	(44.4%; 393 M$)	(44.4%; 393 M$)	(44.4%; 393 M$)

5.7 Comparison with literature

In this section, we will compare the obtained results with those deduced from literature. This comparison will take into consideration the Pareto curve as well as values for measured variables along with certain economic indicators.

5.7.1 Compare with the multi-objective optimization works of *[21]*

A key research work is the multi-objective optimization performed by [21] on a process that is fairly similar to our investigated one, with process simulation, thermal integration and evolutionary optimization being integral parts of the methodology.

The authors considered the maximization of ethanol production and the maximization of power production as conflictive objective functions, in place of exergy efficiency and capital cost. Moreover, they considered a smaller number of alternatives. In fact, they compared a total of 5 MOO variables contrary to 28 variables in our case. These variables related to the hydrolyzed bagasse fraction as well to four variables relating to the sugar content at the outlet of evaporation levels.

5.7.1.1 Comparison in an ethanol production vs. power production graph

Considering this, the optimization results for the two works are plotted on Figure 5:14 in an ethanol production versus power production graph, with the first variable evaluated in L/TC and the second in kWh/TC.

A first remark that can be made is that the results for [21] do not have the initial power production zone. This is mainly related to the choice of the objective functions. In fact, the power production

zone, obtained in the context of our work, displays similar power production levels as certain higher ethanol producing alternatives. The goal chosen by [21] to maximize both ethanol production and power production leads hence to the elimination of these alternatives. This was not however the case for our work since these alternatives presented both smaller exergy efficiencies as highlighted in Figure 5:5, and consequently small capital costs as highlighted in Figure 5:4

Another remark is the inflection of the curve observed in the case of [21] at an ethanol production rate of around 90 L/TC, after which electricity production severely drops for a small increase in ethanol production. This inflection is not observed in our case where higher ethanol and higher electricity production rates are obtained. This can be related to the greater number of variables that are included in the optimization run in our case. The control of these variables leads to a combination of optimal heat integration and optimal hydrolysis reaction conditions.

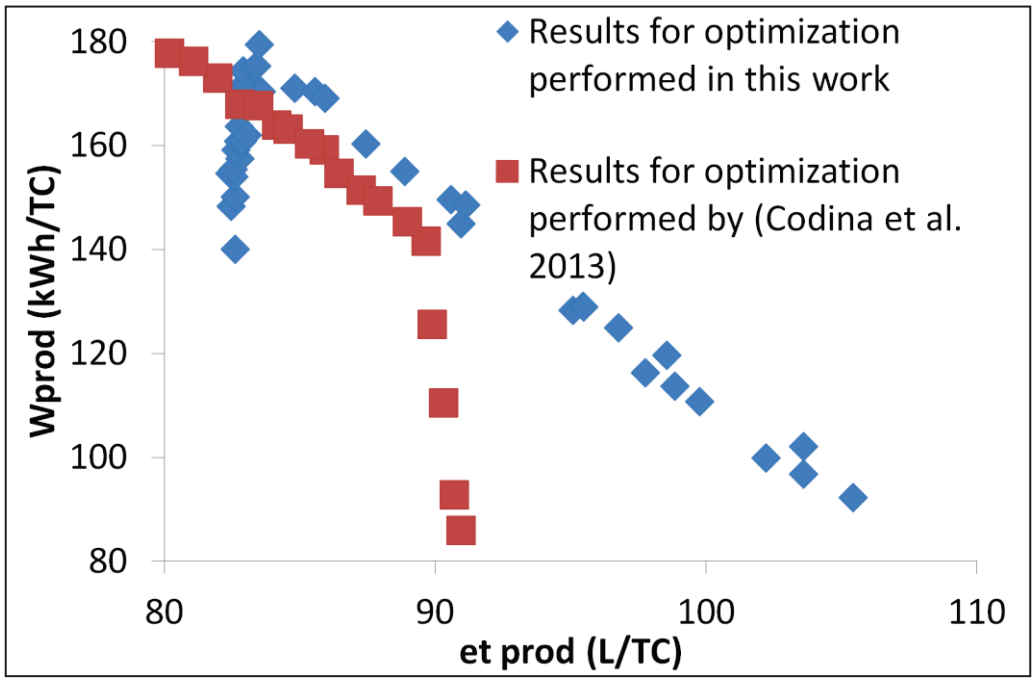

Figure 5:14 Optimization results current optimization vs. (Codina et al.2013) [21] plotted in ethanol production vs. power production graph

5.7.1.2 Comparison in an exergy efficiency vs. capital cost graph

On another note, we chose certain points with corresponding cost evaluations provided by the authors. These points were then transcribed in an exergy efficiency-capital cost graph, where they were plotted alongside the Pareto curve obtained in our work. This combination is highlighted in Figure 5:15. As we can see, our optimization provides better results than those obtained by [21] namely for higher ethanol, lower power producing systems.

It is however interesting to see that the first two points lie rather closely to the obtained Pareto curve. Nonetheless, these points represent disparate results concerning power and ethanol

production from their closest Pareto point. In fact the first point sees an ethanol production of 85 L/TC met by a power production equal to 160 kWh/TC. Nonetheless, its closest Pareto point has an ethanol production of 83 L/TC and a power production of 170 kWh/TC. Likewise, the second point has an ethanol production of 88 L/TC and a power production of 145 L/TC, whereas its closest point has an ethanol production of 83.5 L/TC and a power production of 175 L/TC

Finally, the bad results for the two remaining cases can be understood in light of their low efficiencies, which as we believe is due both to constant hydrolysis parameters, set at low levels, and to the scarcity of heat integration related design variables included in the optimization run. Their high costs are related to great amount of hydrolysis occurring therein, leading to high ethanol production rates.

Finally, the disparity in the obtained capital costs is due to the assumptions made in the calculation of these costs in both cases. Seeing that no detailed analysis was given for the cost calculation method, we were not able to make a decent comparison between the two cases.

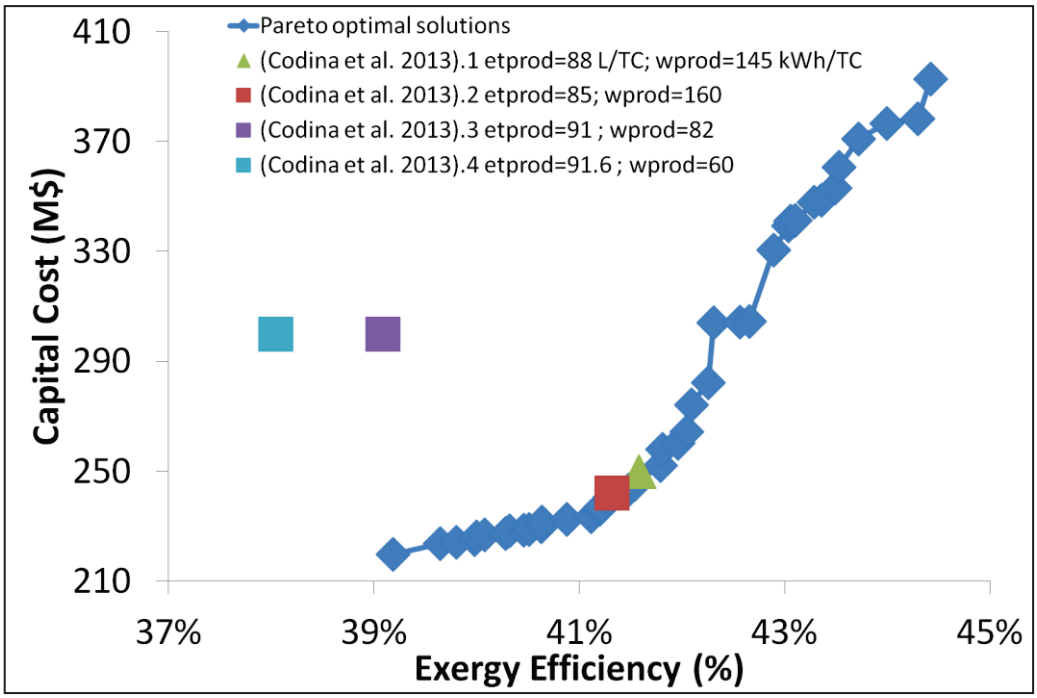

Figure 5:15 Optimization results: current optimization vs. (Codina et al. 2013) [21] plotted in exergy efficiency vs. capital cost graph

5.7.2 Compare with other research works making use of bagasse hydrolysis

In the current paragraph, we focused our attention on optimizing a process superstructure utilizing one of the most advanced bagasse hydrolysis technology. This technology consists in the following steps: (1) steam explosion pretreatment of bagasse fraction, leading to the partial hydrolysis of hemicellulose, (2) separation of hemicellulose hydrolysates and subsequent biodigestion and combustion of biogas in a gas turbine, (3) enzymatic hydrolysis of pretreated

lignocellulosic material leading to the partial hydrolysis of cellulose and lesser hydrolysis of hemicellulose residue, (4) separation of unhydrolyzed lignin and subsequent combustion along with bagasse fraction and leaves, and finally (5) mixing of obtained glucose stream with sugarcane juice prior to evaporation and subsequent ethanol production.

Nonetheless other technologies exist on the market. These technologies include the following traits: additional hydrolysis of leaves, use of more advanced pretreatment technologies and co-fermentation of hemicellulose hydrolysates (xylose) and glucose (from sugarcane and hydrolyzed cellulose). All of these technologies have the advantages of producing higher ethanol rates, using the same input material. These alternatives were however hypothesized by the various authors and lacked at the time, and still now, solid research basis. Regardless of this character, they can still provide design targets for later optimization works dealing with the combined distillery, cogeneration through Rankine cycle and bagasse (and leaves) hydrolysis plants.

Considering this, Figure 5:16 plots the results for these various works, alongside those of [21], against our Pareto optimal set. As we can see, all of the "futuristic" scenarios provide better results than our Pareto optimal set. With this in mind, the consideration of additional technological routes within our superstructure or additional design variables within our optimization algorithm may ultimately lead to a restructuring of this Pareto space.

Finally, the basic design assumptions are highlighted in Table 5:27, along with the results for ethanol production, power production, exergy efficiency and capital cost for the five different futuristic scenarios. From this table we can deduce that the main characteristic of these technologies is the high ethanol production rate associated with a low capital cost, with 2 results providing rather high power production rates ([64] 2 and [69].1.

Table 5:27 Design considerations and results for the futuristic hydrolysis scenarios

Article	**[64]**		**[69]**		
Scenario	1	2	1	2	3
Additional Leaves hydrolysis	+	+	+	+	+
Xylose fermentation	-	-	-	-	+
Novel pretreatment/hydrolysis technologies	-	+	-	+	+
Ethanol production (L/TC)	129	114.46	110.7	113.7	131.5
Power Production (kWh/TC)	60	106	92.8	62.3	72.7
Exergy efficiency (%)	48%	46%	44%	43%	50%
Capital Cost (M$)	334	234	329	286	281

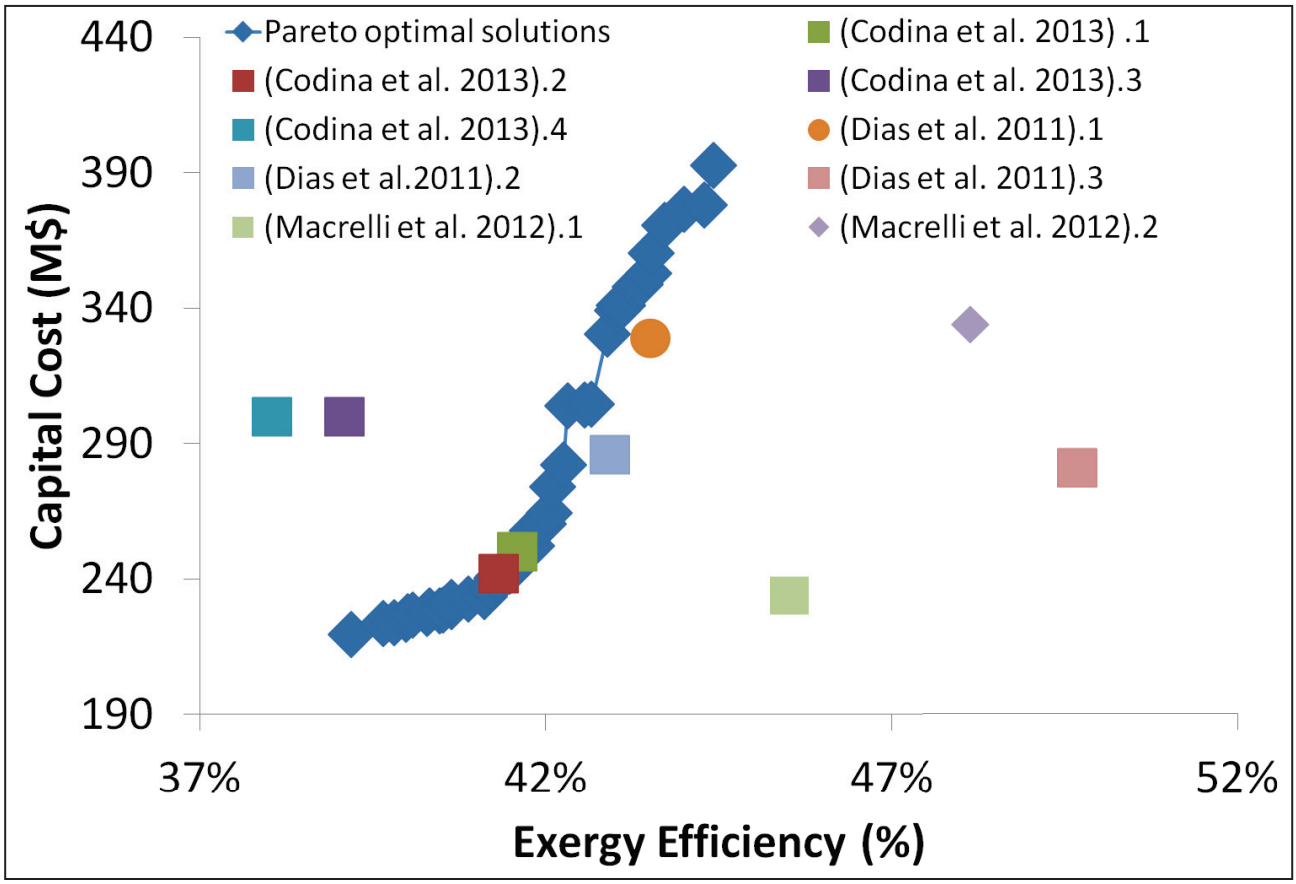

Figure 5:16 Otained Pareto optimal results (distillery + cogeneration + enzymatic hydrolysis) vs. Various research results (Codina et al. 2013) [21], (Dias et al. 2011) [69] and (Macrelli et al. 2012) [64]

5.8 Compare with distillery + cogeneration using Rankine Cycle optimization results

The use of bagasse for hydrolysis and subsequent ethanol alternative is ultimately in competition with its use for heat and power cogeneration using a Rankine cycle. Considering that the latter technology was studied using the same methodology in Chapter 4, we can plot the two optimization results in one exergy efficiency-capital cost graph. This graph is highlighted in Figure 5:17. The obtained results highlight first the higher exergy efficiencies obtained with the inclusion of the hydrolysis system. This greater efficiency comes however at the cost of a higher capital cost. Considering this, the points pertaining to the encircled area and the distillery + cogeneration + hydrolysis case can be automatically excluded due to their higher cost and similar efficiencies when compared to similar points pertaining to the distillery + cogeneration case.

With this in mind, we can construct a global Pareto curve combining these two cases, and this by the removal of the aforementioned points. This curve, highlighted in Figure 5:18 can be split into two sections. The first relates to the distillery + cogeneration case and is characterized by small efficiencies and small capital costs. The second relates to the distillery + cogeneration + hydrolysis case and is characterized by higher efficiencies and higher capital costs. Furthermore, the second

section is more efficient yet more costly with a 70M$ increase in capital cost between the most expensive distillery + cogeneration alternative and the least expensive distillery + hydrolysis + cogeneration alternative. This increase, compared to the 0.3% increase in exergy efficiency highlights the high impact of hydrolysis on investment cost.

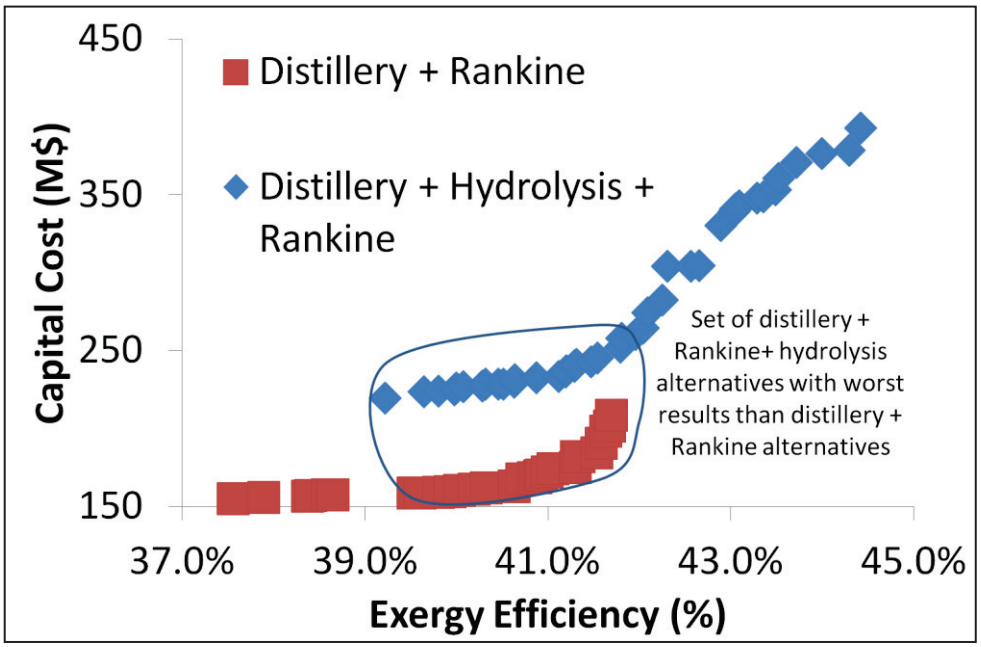

Figure 5:17 Comparison between Pareto results for distillery + Rankine cogeneration and distillery + Rankine cogeneration + hydrolysis cases

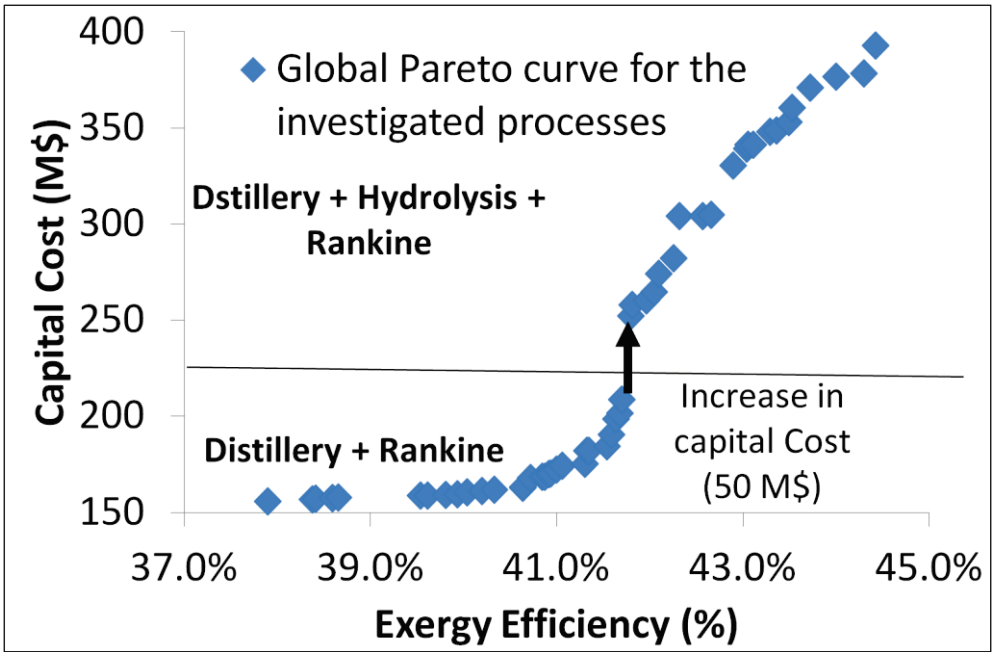

Figure 5:18 Pareto curve combining Pareto-optimal results for distillery + Rankine cogeneration + hydrolysis systems

Consequently, the previous Pareto set analysis and subsequent optimal point selection can be performed on the obtained Pareto curve, leading to a whole different set of possible optimal solutions and of values for the various economic indicators.

With this in mind, Figure 5:19 plots the Net Present Value of the configurations in the combined Pareto set highlighted in Figure 5:18 against their exergy efficiency for the four economic scenarios highlighted in Table 5:21. As we can see this graph can be split into two sections: the distillery + cogeneration alternatives with efficiencies ranging from 37% to 41.7% and the distillery + cogeneration + hydrolysis alternatives with efficiencies ranging from 41.8% to 44.42%. The first set has rather positive NPV values highlighting their profitability, whereas the second set has rather negative values, indicating its low profitability. Finally, we see the existence of a maximum for the NPV at 40.65%, the same as the value recorded in 4.6.2.

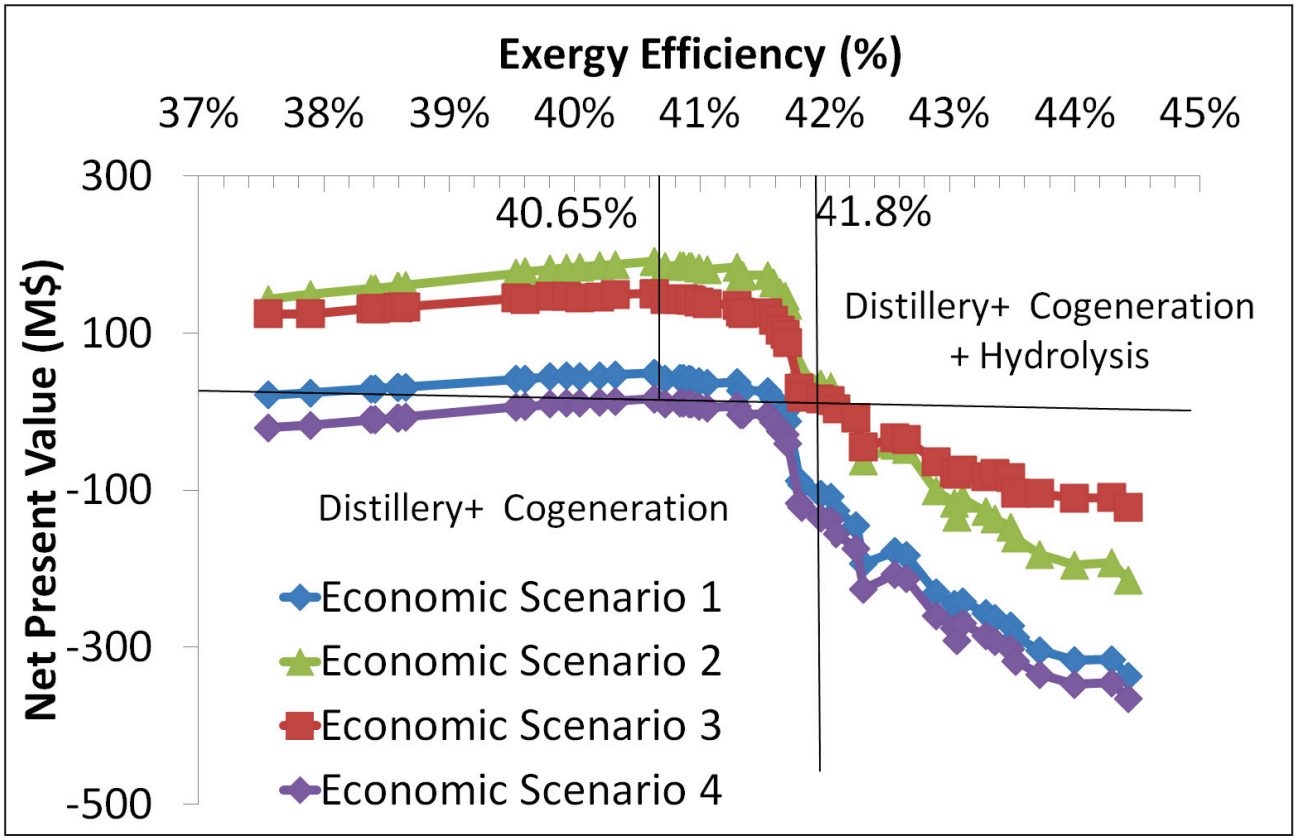

Figure 5:19 Net Present Value vs. Exergy efficiency for individuals of the combined Pareto set under four different scenarios

The low profitability of the second set can be remediated by the use of the modified minimum cellulosic selling price as indicated in 5.6.1.6 and Equation 5:19. The NPV profiles after the seeking of this parameter are provided in Figure 5:20. As we can see, the NPV value witnesses an increase for all scenarios for all configurations pertaining to the second section. This is due to the increase in selling price of the cellulosic ethanol. We can also see that all scenarios witness a maximum NPV for a maximum efficiency of 44.42%. This result is also met in Table 5:26. This point represents

both the highest ethanol production rate, the highest capital cost and the lowest electricity production rate.

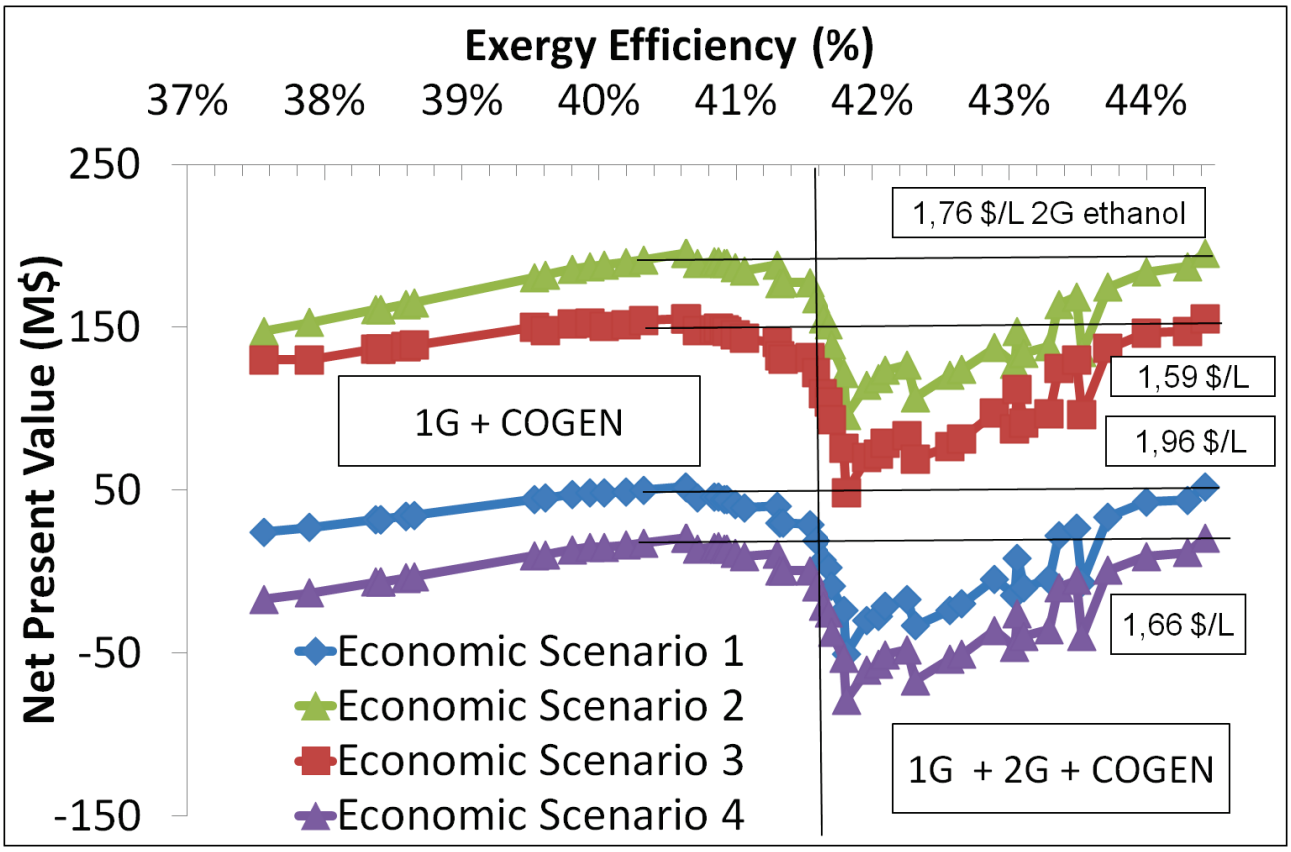

Figure 5:20 Net Present Value vs. Exergy efficiency for individuals of the combined Pareto set under four different scenarios with modified minimum ethanol selling price

Table 5:28 finally provides the result of this operation along with the obtained cellulosic ethanol selling prices and NPV values. We can see that these prices are higher than those obtained in Table 5:26. This is mainly due to the more prosperous distillery + cogeneration alternatives. We can also see that these values vary with the investigated scenarios. This dependence is however outside the scope of our work.

Table 5:28 Results for cellulosic ethanol price indicator along with related optimal solutions for the comparison of the two studied processes

Evaluated Scenario	1	2	3	4
$mminESPc\ (\frac{\$}{l\ cellulosic\ ethanol})$	1.96	1.76	1.59	1.66
$maxNPV$ (M$)	52.16	195.63	155.48	20.80
Optimal configuration $Pareto1$ $(ex_{eff}; C_{inv})$	(40.65 %; 163 M$)	(40.65 %; 163 M$)	(40.65 %; 163 M$)	(40.65 %; 163 M$)
Optimal configuration $Pareto2$ $(ex_{eff}; C_{inv})$	(44.4%; 393 M$)	(44.4%; 393 M$)	(44.4%; 393 M$)	(44.4%; 393 M$)

5.9 Summary

This chapter dealt with the optimization of the production of bioelectricity and bioethanol from sugarcane by using : (1) a conventional distillery design, (2) a heat and power cogeneration by the combustion of leaves and bagasse coupled with a Rankine cycle and (3) a bagasse hydrolysis section for the extraction and conversion of cellulosic fraction to fermentable glucose, with the use of hemicellulose hydrolysates for the generation of burnt biogas and the use of unhydrolyzed solids as fuel for the cogeneration system.

This optimization followed a rigorous methodology starting from a thorough bibliographic investigation and a subsequent synthesis of associated results. Parts of this optimization were similar to those dealt with in Chapter 4 concerning the optimization of the distillery + cogeneration process, and were not hence handled in this chapter. The related bibliographic work was thus concentrated solely on the hydrolysis section. With this in mind, the various design considerations were recorded along with the different obtained results.

Design considerations included modifying design variables such as the hydrolyzed bagasse fraction, the solids loading and residence time in the hydrolysis reactor. These considerations contained also the presence or lack thereof of leaves hydrolysis, heat integration and mass integration between the hydrolysis and distillery sections.

Obtained results contained ethanol and power production rates, along with investment costs and multiple economic indicators pertaining mainly to the selling price of the two process products: ethanol and power.

This analysis was followed by a choice of objective functions, design variables and associated control ranges. The said functions were exergy efficiency which needed to be maximized and capital cost which on the other hand needed to be minimized. Design variables were related to various process steps: distillation, dehydration, evaporation, combined heat and power production, and ultimately hydrolysis. They were controlled by two sets of algorithms: the first is a Mixed Integer Linear Programming algorithm dealing with the maximization of net power production. This algorithm controlled a total of 8 utility variables, namely the mass flow rates of produced steam, boiler water, cold water and refrigeration utility. Moreover, this algorithm was part of a global multi-objective evolutionary optimization algorithm. This algorithm controlled a total of 28 process parameters, containing three Hydrolysis related parameters. These parameters were: the amount of bagasse diverted to hydrolysis, the solids loading in the hydrolysis reactor and the residence time in the said reactor.

This optimization run was based on error-handling, ranking and selection pressure techniques. It was also based on a modeling for the impact of solids loading and residence time on the conversion yield in the hydrolysis reactor. Thanks to this optimization, we extracted the Non Dominated Pareto set associated with the study problem. This set contained a total 44 points. The

exergy efficiency within the Pareto set evolved between a minimum of 39.3% and a maximum of 44.3% for a minimal capital cost of 220 M$ and a maximal cost of 392 M$. Moreover, an explanation was given for the trend followed by the curve. This explanation was based on the observed compromise between net power production, representing the extent of bagasse combustion in the process, and ethanol production, representing the extent of bagasse hydrolysis. Considering this, it was found that a greater ethanol production was associated with greater capital costs. Moreover, these forces ended up playing complementary roles in certain sections of the curve. Finally, this analysis helped extract a critical point at an efficiency of 41.8% and a capital cost of 245 M$. This point's criticality is due to it separating the ethanol producing sections from the power producing ones.

An additional result of the convergence is the narrowing of the initial operating range for a number of variables. These variables were therefore denoted as distance variables since they help determine the closeness or remoteness of a given alternative to the optimal set. For the investigated process, such variables include mainly: operating pressures for the columns, stressing the need for low pressure columns, solids loading in hydrolysis reactor, stressing the need for using rather high values for this variable, and finally the steam superheating temperature in the boiler, stressing the need for using rather high values for this variable as well.

A fragmentation technique was then adopted based on a specific algorithm developed in Chapter 4. This algorithm seeks to extract curve knee points. These points present an inflection point in the curve and are as a result an indicator for a shift in operation. This step split the obtained Pareto curve into a total of twelve fragments, corresponding to eleven different knee points.

The Pareto points were then regrouped according to their respective fragments. The mean, minimum and maximum value for each objective function, design variable and measured variable was then calculated and this for each fragment. The obtained results were then analyzed in order to study the impact of the various variables. This study led to a further categorization of these variables into primary position variables, secondary position variables and floating variables. The first two variables have a direct impact on the evolution of the objective function values, with primary variables following a constant trend, and secondary variables a changing trend along the Pareto curve. Floating variables on the other hand have a lesser extent and they see their values evolve rather randomly across the curve.

Considering this, two primary position variables were recorded, namely the fraction of hydrolyzed bagasse and the cold utility flow rate, with the first following an increasing and the second a decreasing trend. The critical point at 41.8% and 245M$ was also found to be the point below which the hydrolyzed bagasse fraction witnesses a net increase in its value, indicating the predominance of the bagasse hydrolysis system.

Key secondary position variables included the solids loading and residence time in the hydrolysis reactor, along with evaporation rates in the first and fourth levels, steam flow rates, cake humidity

amongst others. Floating variables finally included evaporation rates in the remaining levels, boiler parameters and dehydration variables amongst others.

A profitability analysis using the Net Present Value economic indicator was then performed on the said curve. This analysis enabled to determine the profitability associated with each design alternative and to ultimately select the most profitable one. This analysis was performed for four different economic scenarios extracted from literature. The obtained NPV curves highlighted similar trends albeit at different values for the NPV indicator. These trends included a more profitable initial power producing section, followed by a decreasing profitability for higher efficiency higher cost, ethanol producing sections. This initial power producing section witnessed positive results for the second and third economic scenarios, with the ethanol producing sections witnessing negative NPV values for all the investigated scenarios, rendering them non-profitable alternatives. Considering this, the maximum profitability point was found for points with low efficiency and low capital cost. The $maxNPV$ point was thus found to be positive for the second and third case, and negative for the first and fourth cases, making the first cases profitable and the lat non-profitable.

Nonetheless, the evolution of the Pareto curves was accompanied with a small shift in profitability for higher ethanol producing sections. In fact, whereas the second scenario was the most profitable for electricity producing systems, the second scenario was the most profitable for higher ethanol producing alternatives. This was understood in light of the chosen values for the different economic indicators, which ultimately lead to a variation in the obtained operational margin. With this in mind, the shift in the evolution of the curves occurred at an exergy efficiency of 42.2% and a capital cost of 282 M$.

In a second time, multiple other economic indicators were calculated, namely the minimum selling prices products (ethanol and power) and maximum prices of raw materials (sugarcane) along with the maximum internal rate of return and the minimum number of operating days. These values give the designer insights into the limits of profitability associated with the investigated curve under various economic scenarios. It was shown that the low electricity producing alternatives retained their profitability when compared to the ethanol producing alternatives. Moreover, it was observed that the required minimum ethanol and power selling prices increased for non-profitable scenarios and decreased for profitable one. This is related to the impact of these prices on the profitability. The same applied for the number of days of operation per year, whereas the opposite was true for the sugarcane price and the internal rate of return.

Considering this, only one parameter helped the optimal design move towards higher ethanol producing alternatives, and this parameter was the selling price for the cellulosic ethanol, i.e. the ethanol fraction issued from bagasse hydrolysis. The obtained optimal solution corresponded to the point with the highest exergy efficiency and highest capital cost. This point also presented the highest ethanol production and lowest power production rates. This result was understood in light

of the increase in ethanol production that was greater than the corresponding decrease in power production for higher ethanol producing systems. This situation led to the higher profit realized by the highest ethanol producing point. This change in the nature of the optimal solution was however only possible for the initially non-profitable solutions.

Two novel parameters were introduced for the case of the initially profitable solutions. Those parameters are the modified ethanol selling price and the modified cellulosic ethanol selling price. They can be understood as the prices beyond which the most profitable ethanol producing alternative becomes more profitable than the most profitable power producing alternative. Considering this, an increase in this price will lead to an increase in the NPV of all of the investigated solutions, with the higher ethanol producing sections witnessing the greatest increase. Ultimately, the most profitable ethanol producing solution was also the highest ethanol producing alternative, stressing all the more the predominance of this alternative over other ethanol producing possibilities.

In the last section of this chapter, comparisons were made with literature results. A first comparison was made with another work which also performed a multi-objective optimization on the studied process. Results were compared in an ethanol production vs. power production and an exergy efficiency vs. capital cost diagram. Both diagrams highlighted the supremacy of our optimal cases, whilst stressing the importance of correctly evaluating the various capital costs under consideration.

A comparison was then made with futuristic bagasse hydrolysis scenarios also extracted from literature. Such alternatives highlighted better results for the considered objective functions, inevitably leading to higher profitability results. The main hurdle for their use remains however the success of their implementation on both research and pilot scales.

The last comparison was made between the obtained Pareto curves for the distillery + cogeneration + hydrolysis case and for the distillery + cogeneration case. It was found that these curves had mutually exclusive curves, namely concentrated around the power producing alternatives. The higher cost for such alternatives obtained for the distillery + hydrolysis + Rankine Cycle led to their subsequent elimination. This resulted in a mega-Pareto curve including alternatives related to both the first and second design case. It is interesting to note that the same methodology applied in this chapter could be applied on this newly obtained curve.

5.10 Conclusion

In conclusion, the current chapter provided another application of the proposed methodology, to a more complex process structure than in Chapter 4. The application of this methodology led to the generation of a Pareto set better than the ones obtained in literature, namely in concerns to its diversity and scope. The inclusion of additional process alternatives or design variables in the proposed methodology may lead to even better results. These novel variables and designs should

however be deduced from either a detailed systems analysis or a detailed bibliographic review, before their inclusion. Key possibilities include: the hydrolysis of leaves, the inclusion of more advances pretreatments and the fermentation of hemicellulose hydrolysates.

General Conclusion

The need for a structured methodology for optimal process design has been a key issue for design engineers ever since the advent of chemical engineering. This is due both to the complexity of processes, involving a great number of design conditions and unit operations, and to the complexity of their evaluation, namely with regards to competition between efficiency and costs.

Of all the possible methodologies, one technique has come out strong with extensive application in literature. This technique relies on a sequencing of three key steps as highlighted Figure 1, with a multi-objective multivariate optimization step at its core.

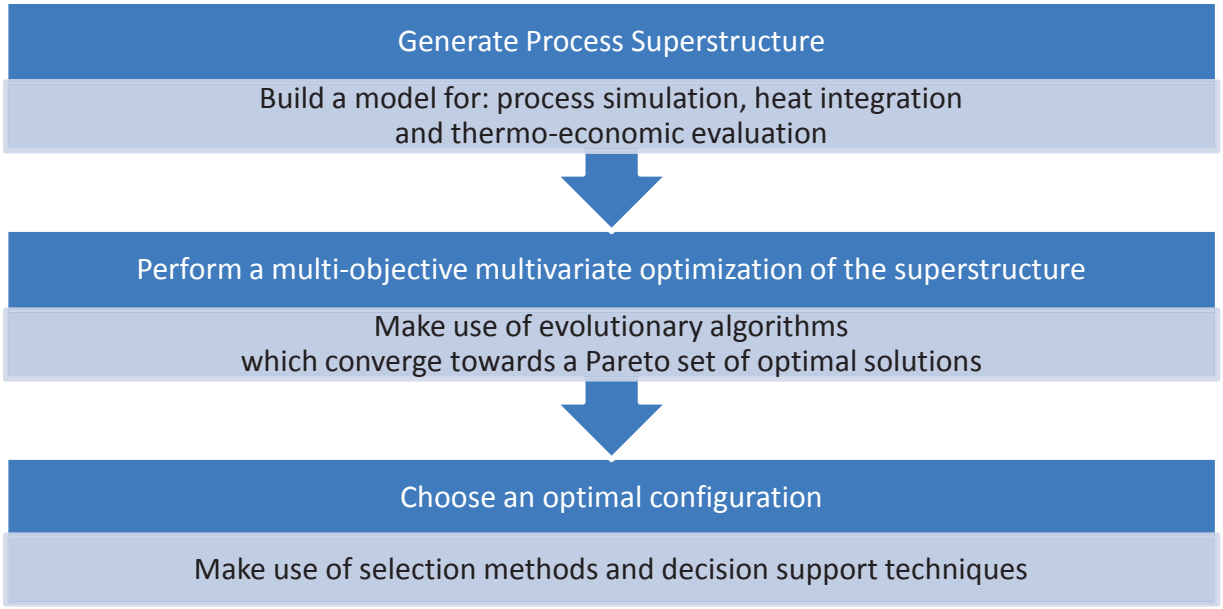

Figure 1 Summary of multi-objective method for optimal process design

Considering this, this thesis dealt with the further development of this methodology.

This was realized through its application to two studied processes:

- A combined distillery, biomass combustion and Rankine cycle process for the production of ethanol and power. The ethanol production in this process is constant. Considering this, optimization works in literature have dealt with the increase in net power production and the decrease in capital costs. This was realized by acting on both distillery, combustion and CHP parameters, with heat integration being the driving force.
-

- A process similar to the first albeit with the addition of a hydrolysis step, for an enhanced ethanol production. This leads to a competition between bagasse hydrolysis and bagasse combustion, and to a reduction in power production. Considering this, optimization works in literature have dealt with the increase in ethanol production, the increase in net power production and the decrease in capital costs. This was realized by acting on hydrolysis parameters as well as distillery, combustion and CHP parameters as in the first process.

With this in mind, Figure 2 highlights the previously cited steps in the form of a block flow diagram. In this diagram, the steps common to both processes are highlighted in white, whereas hydrolysis steps are indicated in blue, with dotted lines for their related input/output streams.

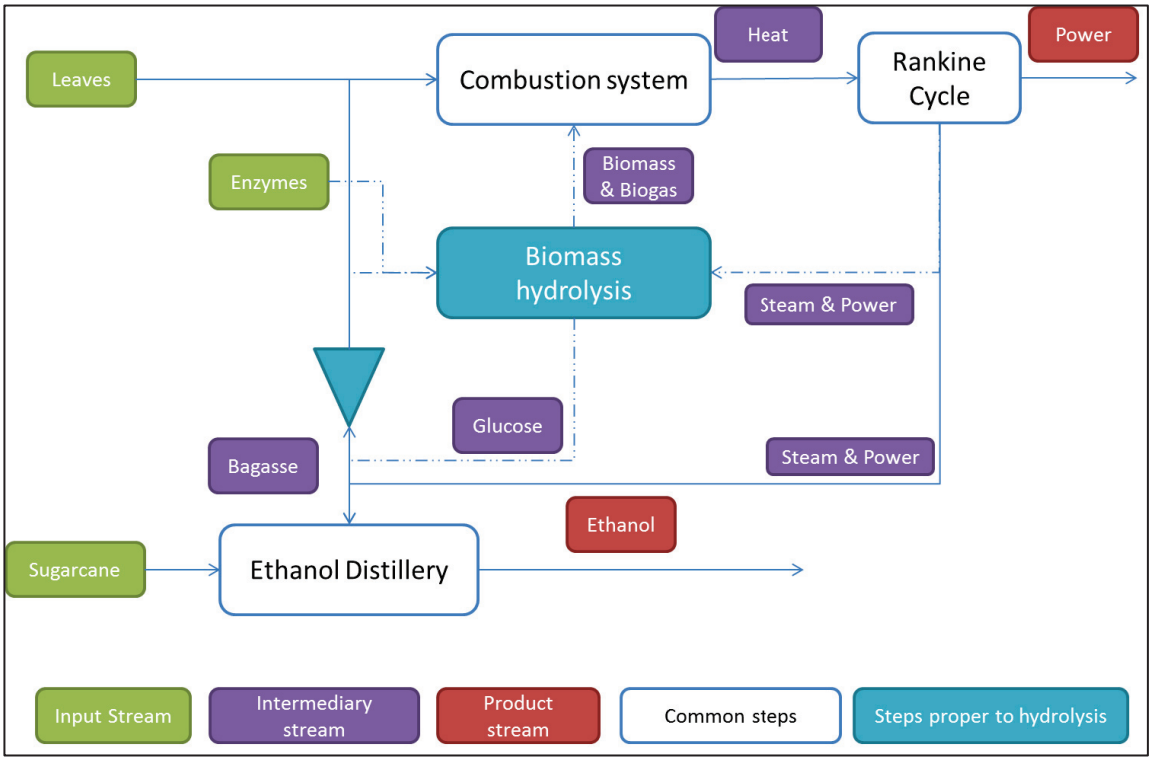

Figure 2 Block diagram for the two studied processes

The ethanol distillery converts input sugarcane into ethanol through the following steps: sugarcane juice extraction, concentration and fermentation, and ethanol distillation and dehydration.

The combustion system on the other hand converts input fuel, bagasse and leaves, to heat through the following steps: bagasse dryer and biomass (bagasse and leaves) incinerator. In the case of the second process, output biomass is also inputted to the drying step, with an additional biogas burning step.

The Rankine cycle draws heat from the combustion and converts it to lower level steam and electricity. Its main goal is to fuel the various process steps, with the possibility of producing surplus power.

The hydrolysis process converted input bagasse into: glucose for ethanol production and biomass and biogas for heat production. This was realized by a sequence of steam-explosion and enzymatic hydrolysis.

Considering this, the thesis was structured as follows. In the first chapter, we presented and defended the various steps of the methodology. This defense was based both an extensive literature review. In the second and third chapters we presented the process simulation and evaluation flowsheets for the two investigated processes respectively. These flowsheets were the basis for the next two chapters. The fourth and fifth chapters consisted in the application of the methodology presented in Chapter 1 to the two processes defined in Chapters 2 and 3.

In this final section we will present the main conclusions of this thesis work. These conclusions are highlighted in the table below which reiterates the structure of the methodology, and highlights the results of its application to our processes.

Main Conclusions for process superstructure step	Application to studied processes
Step I : Generate process superstructure	
The development of a correctly modeled process flowsheet enables a faithful representation of reality.	The process flowsheets for our two studied processes were modeled in Aspen Plus®. This was realized by using a hierarchal approach consisting in blocks with unit operations therein. The related thermodynamic models, operating parameters and design specifications were deduced from literature. A configuration is defined by a choice of values for the various parameters.
The choice of adequate objective functions enables an integral evaluation of the process	Exergy efficiency and capital costs were the two investigated objective functions. These functions reflect the conflict between profit and capital costs.
The use of detailed calculation procedures for the objective functions enables a faithful evaluation of a given process configuration	Exergy efficiency was calculated as the ratio of the exergy contents of products (power and ethanol) to that of input materials (sugarcane, leaves and enzymes in the case of hydrolysis).Capital costs were calculated as the sum of the cost of the various equipment evaluated by the use of correlations presented by the Chauvel manual for process evaluation.
The inclusion of a heat integration step is an essential part of any evaluation procedure	This step enables the modeling of in-process heat exchanges, the calculation of required utility rates and the estimation of the heat exchanger capital cost. It intervenes rightly after process simulation has converged and before the process evaluation step. An MILP algorithm coupled with the heat cascade technique was adopted for this purpose. In our case, the MILP model was solved with the goal of maximizing power production.

Step II : Perform multi-objective optimization	
The choice of the optimization variables, whose values are to be controlled, and their associated variation ranges is also an important issue.	These variables were chosen after a bibliographic review of optimization works related to the studied processes.33 variables were chosen for the first process and 36 for the second. Operating ranges were also defined for each variable. These variables were related to the various steps previously discussed. A decision vector is defined as a set of values for the optimization variables. A given decision vector defines thus a possible process configuration.
The inclusion of measured variables in the optimization run is a recommended action. This is emphasized if these variables have a direct link with the objective functions	Four variables were chosen for the first process: the net power and ethanol production rates, the heat exchange network cost, and the cost of the process without the heat exchange network. These variables were also chosen for the second
Evolutionary algorithms were the chosen technique for the desired bi-objective optimization	These algorithms start with an initial number of configurations chosen randomly. This initial number is evolved through given operations towards a final set of optimal compromise solutions. These operations include: ranking, removal and creation.
The heat integration algorithm behaves as a slave optimizer	Through its MILP optimization, the MILP optimizer seeks the utility configuration with the highest power production, for a given process configuration. This configuration is defined by a choice of values for the optimization variables.
The shape of the obtained Pareto curve reflects the nature of the investigated process	Both curves presented an increase in exergy efficiency accompanied with a more important increase in capital costs. Both curves presented inflection points after which the capital cost witnessed a spike in its value. The first curve contained a total of 32 points, whereas the second a total of 44 points
The comparison of measured variables against objective functions enables an understanding of the optimization results.	For the first process, exergy efficiency increased in a linear manner with power production, similarly to capital costs and heat exchange network cost. These results reflected the fact that more integrated alternatives result in a higher efficiency, albeit at higher cost. The second process resulted in overall higher efficiency higher cost systems. For the second process, net power hit a maximum for a critical exergy efficiency value before decreasing for higher efficiencies. Ethanol production on the other hand remained constant for

	lower efficiency systems before increasing for higher efficiency ones. Capital costs increased in a linear fashion with the process equipment costs (without heat exchange network). These results reflect a greater hydrolysis rate for higher efficiency, higher cost systems. The critical exergy point signals the taking into effect of hydrolysis, at the expense of cogeneration
The calculation of the final ranges for the optimization variables enables the designer to identify distance variables	These variables see their values converge towards a specific subset of the initial population. They reflect common thus characteristics of the optimal points. They also indicate the closeness of a given configuration to optimal conditions. 14 distance variables were recorded for the first process, and 15 for the second.
The fragmentation of the Pareto enables an understanding of the obtained Pareto curve	This fragmentation splits the curve into regions defined by the various knee points. Knee points are points where, a great increase in one variable is contrasted with a small increase in the other. A total of 7 fragments were identified for the first process, whereas 12 were identified for the second.
The visualization of statistical values for optimization variables along the fragments enables an understanding of their impact on process performance	The calculated statistical values were the mean, the minimum and the maximum. They were calculated for each variable in each fragment. These values were then plotted against the number of fragments in order to visualize their evaluation along the Pareto curve
The categorization of the design variables enables a further understanding of the optimization results, and of the characteristics of optimal solutions.	Primary position variables determine the position of a given point on the Pareto curve. 11 primary position variables were recorded for the first process and only 2 for the second process Secondary position variables determine the position of the point on the Pareto curve, only after knowing the value of the primary position variables. 12 secondary position variables were recorded for the first process and 18 for the second. Floating variables see their values vary randomly across the curve. 10 such variables were recorded for the first process and 16 variables for the second.
Step III : Select optimal configuration	
The Net Present Value as a selection criterion enabled the selection of the most profitable process configuration., through an integral economic evaluation.	The NPV can be evaluated for each alternative and for every economic scenario. Its calculation passes through an evaluation of operating costs, total revenues, total net profit and discounted cash flows. For this endeavor, an 11% discount rate was chosen

	for the first process, whereas a 10% rate was chosen for the second.
	The NPV combines optimization results with operation hypotheses and market conditions to provide an integral and overall assessment of each Pareto optimal alternatives. In our case, these hypotheses and conditions were taken from previous literature works for the two investigated processes. This resulted in a total of 4 scenarios for each process. An NPV trend can hence be ascribed for each scenario. Similar trends for the NPV were observed for both processes and for all of the scenarios albeit with varying NPV values. Nonetheless, a selected modification in the value of certain conditions may lead to a modification in the trend. The selected optimal result is the one that maximizes the NPV across the Pareto curve. The nature of the optimal point and its corresponding NPV value depend on the chosen economic parameters. Points with mild efficiencies and mild capital costs were seen to have the highest NPV values. Also, maximum NPV values were associated with the points preceding the spike in capital cost.
Additional economic indicators can also be used as selection criteria albeit with caution	These indicators include the minimum selling prices of products, the maximum purchase price of raw materials, the maximum discount rate, or the minimum number of operating days These criteria were defined as the limit at which the most profitable Pareto solution had a zero NPV value ($maxNPV$=0). For initially profitable solutions, this lead to a lower product selling price and a lower number of operating days (higher raw material price and higher discount rate). The opposite occurred for initially non profitable solutions. The nature of the most profitable solution was prone to change with the chosen indicator. This was the case for net power production and number of operating days per year for the first process with the addition of the ethanol price for the second. Higher values of these variables lead to higher efficiency systems and vice versa

	These values remain of a hypothetical nature but can help the designer in making comparisons and predictions between different economic scenarios.
The use of modified minimum product selling prices was presented as a better indicator than the conventional minimum selling price	These prices are the limit at which the most profitable high efficiency high cost system becomes as profitable as the most profitable mild efficiency mild cost alternative. Seeing that high efficiency high cost systems are initially less profitable than their mild efficiency mild cost counterparts, the obtained prices are higher than the original ones. For our second process, this resulted in a threefold increase of the ethanol selling price The required increase in these prices stresses the need for obtaining Pareto optimal points with better results for the investigated objective functions.

Perspectives

We finish off this section with perspectives for later developments both in the methodology and in the investigated process:

- The success of this methodology passes by the improvement of the multi-objective optimization algorithm.
- Substitute the stopping criterion with a criterion more dependent on the desired outcome, mainly the number or the ratio of Pareto optimal solutions in the final population.
- Include the possibility of a free number of individuals in the living population. This will help the optimization algorithm evolve towards a decently sized Pareto curve.
- Include a strategy for point creation and removal which is dependent on the obtained results. This will enable the algorithm to balance between exploration and exploitation phases in a way to guarantee optimal convergence.
- Include deterministic optimal points in the initial random population, which was generated in our case in a random fashion. This inclusion might enable a faster and more reliable convergence for the algorithm. These points can either be deduced from literature, or constructed through a detailed process analysis.
- Another success factor is the development of the method for novel process simulation tools.
- As of today, this method is mainly applicable to Vali® and Aspen Plus®, with the work in this thesis performed solely on the latter. This development will enable its application to a greater number of processes mainly those developed under ProII® for the petrochemical industry.
- A key issue at this level is parallelization. In fact, in the course of this thesis parallelization was made using the CPU. It is however possible to use a GPU. This however requires the use of a Linux platform, something that is not available today with Aspen®. This might be an additional point of study for a faster evaluation time.
- A future perspective is the further development of the process selection scheme, and underlying profitability analysis.
- Take into account an evolution in the prices of raw materials and products along the project lifetime.
- Consider various financing schemes, namely debt and annualization of capital cost.
- Include the effect of plant location on the economic evaluation, namely cost of supply of raw material and of selling of products.
- Concerning the investigated process schemes, possible additions might be:

- Distillation: the inclusion of an additional level in parallel to the stripping column; the variation of the outlet ethanol concentrations from the different distillation columns.
- Cogeneration: the inclusion of a biomass gasification step for higher power production, albeit at a higher capital cost.
- Fermentation: the study of fermentation reactors with a higher glucose input content. This will help split the separation load between the distillation and separation sections
- Hydrolysis : these various alternatives stand as interesting leads:
- The inclusion of reactor volumes and dimensions as optimization variables might help move the process towards less costly alternatives.
- The inclusion of an additional pretreatment, delignification, step might increase the cellulose conversion rate, albeit at the expense of a higher investment cost.
- Another alternative is the inclusion of the stripping column vinasse stream in the sugar stream inputted to the biodigestor
- The inclusion of the co-fermentation of C5 and C6 sugars for an even higher ethanol production at a seemingly similar cost.
- The inclusion of an enzyme production section: these enzymes are considered as purchased items, but there is a possibility for producing them in-house.
- Study the effect of various conditions for the input material, namely: sugarcane content, fibers content and water content, on the performance of the system.
- Study the possibility of water treatment and recycling on process performance.
- Consider constraints on safety in the process evaluation scheme.
-

At the end, we conclude our thesis with a citation from the great author and thinker George Bernard Shaw, highlighting the endless perspectives every scientific or even human endeavor leaves behind it:

“Science never solves a problem without creating ten more”

References

1. Wells GL, Rose LM: *The Art of Chemical Process Design*. *Volume 2*. Elsevier; 1986.

2. Smith R: *Chemical Process Design and Integration*. 2006.

3. Dimian AC, Bildea CS, Kiss AA: *Integrated Design and Simulation of Chemical Processes*. *Volume 35*. Elsevier; 2014.

4. Smith RM: *Chemical Process: Design and Integration*. Chichester, West Sussex, England: Wiley; 2005.

5. Gassner M, Maréchal F: **Thermo-economic process model for thermochemical production of Synthetic Natural Gas (SNG) from lignocellulosic biomass**. *Biomass and Bioenergy* 2009, **33**:1587–1604.

6. Szargut J, Morris DR: **Calculation of the standard chemical exergy of some elements and their compounds, based upon sea water as the datum level substance**. *Bull Polish Acad Sci Tech Sci* 1985, **33**:293–305.

7. Gassner M, Maréchal F: **Thermo-economic optimisation of the polygeneration of synthetic natural gas (SNG), power and heat from lignocellulosic biomass by gasification and methanation**. *Energy Environ Sci* 2012, **5**:5768.

8. Gassner M, Maréchal F: **Methodology for the optimal thermo-economic, multi-objective design of thermochemical fuel production from biomass**. *Comput Chem Eng* 2009, **33**:769–781.

9. Ulrich GD: *A Guide to Chemical Engineering Process Design and Economics*. University of Michigan: Wiley; 1984.

10. Turton R, Bailie RC, Whiting WB, Shaeiwitz JA: *Analysis, Synthesis and Design of Chemical Processes*. Pearson Education; 2008.

11. Chauvel A, Fournier G, Raimbault C: *Manual of Process Economic Evaluation*. Editions Technip; 2003.

12. Peters M, Timmerhaus K, West R: *Plant Design and Economics for Chemical Engineers*. McGraw-Hill Education; 2003. [*McGraw-Hill Chemical Engineering Series*]

13. Towler GP, Sinnott RK: *Chemical Engineering Design: Principles, Practice, and Economics of Plant and Process Design*. Oxford, Waltham, Mass.: Butterworth-Heinemann; 2013. [*Butterworth Heinemann*]

14. Brown T: *Engineering Economics and Economic Design for Process Engineers*. Taylor & Francis; 2006.

15. Azzaro-Pantel C, Ouattara A, Pibouleau L: **Ecodesign of Chemical Processes with Multi Objective Genetic Algorithms**. *Multi-Objective Optim Chem Eng Dev Appl* 2013:335–367.

16. Savic D: **Single-objective vs Multiobjective Optimisation for Integrated Decision Support**. *Proc First Bienn Meet Int Environ Model Softw Soc* 2002:7–12.

17. Dewulf J, Van Langenhove H, Muys B, Bruers S, Bakshi BR, Grubb GF, Paulus DM, Sciubba E: **Exergy: its potential and limitations in environmental science and technology.** *Environ Sci Technol* 2008, **42**:2221–2232.

18. Rosen M a., Dincer I, Kanoglu M: **Role of exergy in increasing efficiency and sustainability and reducing environmental impact**. *Energy Policy* 2008, **36**:128–137.

19. Sánchez ÓJ, Cardona C a.: **Trends in biotechnological production of fuel ethanol from different feedstocks**. *Bioresour Technol* 2008, **99**:5270–5295.

20. Gomez A, Pibouleau L, Azzaro-Pantel C, Domenech S, Latgé C, Haubensack D: **Multiobjective genetic algorithm strategies for electricity production from generation IV nuclear technology**. *Energy Convers Manag* 2010, **51**:859–871.

21. Ensinas A V, Codina V, Marechal F, Albarelli J, Aparecida M: **Thermo-Economic Optimization of Integrated First and Second Generation Sugarcane Ethanol Plant**. *Chem Eng Trans* 2013, **35**:523–528.

22. Toffolo a., Lazzaretto a.: **Evolutionary algorithms for multi-objective energetic and economic optimization in thermal system design**. *Energy* 2002, **27**:549–567.

23. Roosen P, Uhlenbruck S, Lucas K: **Pareto optimization of a combined cycle power system as a decision support tool for trading off investment vs. operating costs**. *Int J Therm Sci* 2003, **42**:553–560.

24. Pozo C, Guillén-Gosálbez G, Sorribas A, Jiménez L: **Identifying the Preferred Subset of Enzymatic Profiles in Nonlinear Kinetic Metabolic Models via Multiobjective Global Optimization and Pareto Filters**. *PLoS One* 2012, **7**:e43487.

25. Leyland GB: **Multi-objective optimisation applied to industrial energy problems**. 2002.

26. Gomez A: **Optimisation technico-économique multiobjectif de systèmes de conversion d'énergie: cogénération électricité-hydrogène à partir d'un réacteur nucléaire de IVème génération.** Institut National Polytechnique; 2008.

27. Peduzzi E, Tock L, Boissonnet G, Maréchal F: **Thermo-economic evaluation and optimization of the thermo-chemical conversion of biomass into methanol**. *Energy* 2013, **58**:9–16.

28. Morandin M, Toffolo A, Lazzaretto A, Maréchal F, Ensinas A V., Nebra S a.: **Synthesis and parameter optimization of a combined sugar and ethanol production process integrated with a CHP system**. *Energy* 2010, **36**:3675–3690.

29. Linnhoff B, Ahmad S: **Cost optimum heat exchanger networks—1. Minimum energy and capital using simple models for capital cost**. *Comput Chem Eng* 1990, **14**:729–750.

30. Maréchal F, Kalitventzeff B: **Identification of the optimal pressure levels in steam networks**

using integrated combined heat and power method. *Chem Eng Sci* 1997, **52**:2977–2989.

31. Maréchal F, Kalitventzeff B: **A Methodology for the Optimal Insertion of Organic Rankine Cycles in Industrial Processes**. In *2nd International Symposium of Process Integration*. Hallifax, Canada; 2004.

32. Ahmad S, Linnhoff B, Smith R: **Cost optimum heat exchanger networks—2. targets and design for detailed capital cost models**. *Comput Chem Eng* 1990, **14**:751–767.

33. Xu L, Yang J: *Introduction to Multi-Criteria Decision Making and the Evidential Reasoning Approach*. Manchester: Manchester School of Management; 2001.

34. Lai Y-J, Liu T-Y, Hwang C-L: **TOPSIS for MODM**. *Eur J Oper Res* 1994, **76**:486–500.

35. Bouyssou D: **Outranking Methods**. In *Encyclopedia of optimization*. Edited by Floudas CA, Pardalos PM. Springer; 2001:1919–1925.

36. Fülöp J: **Introduction to decision making methods**. In *BDEI-3 Workshop, Washington*. Citeseer; 2005.

37. Chen H, Wen Y, Waters MD, Shonnard DR: **Design guidance for chemical processes Using environmental and economic assessments**. *Ind Eng Chem Res* 2002, **41**:4503–4513.

38. Mokeddem D, Khellaf A: **Pareto optimal solutions for multicriteria optimization of a chemical engineering process using a diploid genetic algorithm**. *Int Trans Oper Res* 2008, **15**:51–65.

39. Dias MOS, Da Cunha MP, MacIel Filho R, Bonomi A, Jesus CDF, Rossell CE V: **Simulation of integrated first and second generation bioethanol production from sugarcane: Comparison between different biomass pretreatment methods**. *J Ind Microbiol Biotechnol* 2011, **38**:955–966.

40. Wooley RJ, Putsche V: **Development of an ASPEN PLUS Physical Property Database for Biofuels Components**. *Victoria* 1996(April):1–38.

41. Dias MOS, Ensinas A V., Nebra S a., Maciel Filho R, Rossell CE V, Maciel MRW: **Production of bioethanol and other bio-based materials from sugarcane bagasse: Integration to conventional bioethanol production process**. *Chem Eng Res Des* 2009, **87**:1206–1216.

42. Ensinas A V., Nebra S a., Lozano M a., Serra L: **Design of evaporation systems and heaters networks in sugar cane factories using a thermoeconomic optimization procedure**. *Int J Thermodyn* 2007, **10**:97–105.

43. Higa M, Freitas AJ, Bannwart AC, Zemp RJ: **Thermal integration of multiple effect evaporator in sugar plant**. *Appl Therm Eng* 2009, **29**:515–522.

44. Palacios-Bereche R, Ensinas A V., Modesto M, Nebra S a.: **Double-effect distillation and thermal integration applied to the ethanol production process**. *Energy* 2015, **82**:512–523.

45. Lazzaretto A, Morandin M, Toffolo A: **Methodological aspects in synthesis of combined sugar and ethanol production plant**. *Energy* 2012, **41**:165–174.

46. Basso LC, Rocha SN, Basso TO: *Ethanol Production in Brazil: The Industrial Process and Its Impact on Yeast Fermentation*. INTECH Open Access Publisher; 2011.

47. Batista FRM, Follegatti-Romero L a., Bessa LCB a., Meirelles AJ a.: **Computational simulation applied to the investigation of industrial plants for bioethanol distillation**. *Comput Chem Eng* 2012, **46**:1–16.

48. Bessa LCB a., Batista FRM, Meirelles AJ a.: **Double-effect integration of multicomponent alcoholic distillation columns**. *Energy* 2012, **45**:603–612.

49. Bessa LCB a., Ferreira MC, Batista E a. C, Meirelles AJ a.: **Performance and cost evaluation of a new double-effect integration of multicomponent bioethanol distillation**. *Energy* 2013, **63**:1–9.

50. Ponce GHSF, Alves M, Miranda JCC, Maciel Filho R, Wolf Maciel MR: **Using an internally heat-integrated distillation column for ethanol–water separation for fuel applications**. *Chem Eng Res Des* 2015, **95**:55–63.

51. Bastidas P a, Gil ID: **Comparison of the main ethanol dehydration technologies through process simulation**. *20th Eur Symp Comput Aided Process Eng* 2010:1–4.

52. Meirelles A, Weiss S, Herfurth H: **Ethanol Dehydration By Extractive Distillation**. *J Chem Technol Biotechnol* 1992, **53**:181 – 188.

53. Errico M, Rong BG: **Synthesis of new separation processes for bioethanol production by extractive distillation**. *Sep Purif Technol* 2012, **96**:58–67.

54. Errico M, Rong B-G, Tola G, Spano M: **Optimal Synthesis of Distillation Systems for Bioethanol Separation. Part 2. Extractive Distillation with Complex Columns**. *Ind Eng Chem Res* 2013, **52**:1620–1626.

55. GarcìÌa-Herreros P, GoÌmez JM, Gil ID, RodriÌguez G: **Optimization of the design and operation of an extractive distillation system for the production of fuel grade ethanol using glycerol as entrainer**. *Ind Eng Chem Res* 2011, **50**:3977–3985.

56. Vázquez-Ojeda M, Segovia-Hernández JG, Hernández S, Hernández-Aguirre A, Kiss AA: **Design and optimization of an ethanol dehydration process using stochastic methods**. *Sep Purif Technol* 2013, **105**:90–97.

57. Vázquez-Ojeda M, Segovia-Hernández JG, Ponce-Ortega JM: **Incorporation of Mass and Energy Integration in the Optimal Bioethanol Separation Process**. *Chem Eng Technol* 2013, **36**:1865–1873.

58. Sosa-Arnao JH, Correa JLG, Silva MA, Nebra SA: **Sugar cane bagasse drying- a review**. *Int sugar J* 2006, **108**:381.

59. Ensinas A V, Arnao JHS, Nebra SA: **Increasing energetic efficiency in sugar, ethanol, and electricity producing plants**. In *Sugarcane bioethanol: R&D for productivity and sustainability*. Edited by Luis Augusto Barbosa Cortez. Blucher Sao Paulo; 2010:583–600.

60. Sosa-Arnao JH, Nebra SA: **Bagasse dryer role in the energy recovery of water tube boilers**. *Dry Technol* 2009, **27**:587–594.

61. Dias MOS, Junqueira TL, Jesus CDF, Rossell CEV, Maciel Filho R, Bonomi A: **Improving second generation ethanol production through optimization of first generation production process from**

sugarcane. *Energy* 2012, **43**:246–252.

62. Dias MOS, Modesto M, Ensinas A V., Nebra S a., Filho RM, Rossell CEV: **Improving bioethanol production from sugarcane: evaluation of distillation, thermal integration and cogeneration systems**. *Energy* 2011, **36**:3691–3703.

63. Furlan FF, Filho RT, Pinto FH, Costa CB, Cruz AJ, Giordano RL, Giordano RC: **Bioelectricity versus bioethanol from sugarcane bagasse: is it worth being flexible?** *Biotechnol Biofuels* 2013, **6**:142.

64. Macrelli S, Mogensen J, Zacchi G: **Techno-economic evaluation of 2nd generation bioethanol production from sugar cane bagasse and leaves integrated with the sugar-based ethanol process**. *Biotechnol Biofuels* 2012, **5**:22.

65. Bolliger R, Favrat D, Marechal FF: **Advanced Power Plant Design Methodology using Process Integration and Multi-Objective Thermo-Economic Optimisation**. *ECOS 2005, 18th Int Conf Effic Cost, Optim Simul Environ Impact Energy Syst* 2005, **2**:777–784.

66. Alves M, Ponce GHSF, Silva MA, Ensinas A V: **Surplus electricity production in sugarcane mills using residual bagasse and straw as fuel**. *Energy* 2015, **91**:751–757.

67. Ojeda K, Ávila O, Suárez J, Kafarov V: **Evaluation of technological alternatives for process integration of sugarcane bagasse for sustainable biofuels production-Part 1**. *Chem Eng Res Des* 2011, **89**:270–279.

68. Maréchal F, Kalitventzeff B: **Targeting the optimal integration of steam networks: Mathematical tools and methodology**. *Comput Chem Eng* 1999, **23**(SUPPL. 1):5133–5136.

69. Dias MOS, Cunha MP, Jesus CDF, Rocha GJM, Pradella JGC, Rossell CEV, Maciel Filho R, Bonomi A: **Second generation ethanol in Brazil: Can it compete with electricity production?** *Bioresour Technol* 2011, **102**:8964–8971.

70. Damartzis T, Zabaniotou a.: **Thermochemical conversion of biomass to second generation biofuels through integrated process design-A review**. *Renew Sustain Energy Rev* 2011, **15**:366–378.

71. Ramos LP, da Silva L, Ballem AC, Pitarelo AP, Chiarello LM, Silveira MHL: **Enzymatic hydrolysis of steam-exploded sugarcane bagasse using high total solids and low enzyme loadings.** *Bioresour Technol* 2014, **175C**:195–202.

72. Carrasco C, Baudel HM, Sendelius J, Modig T, Roslander C, Galbe M, Hahn-Hägerdal B, Zacchi G, Lidén G: **SO2-catalyzed steam pretreatment and fermentation of enzymatically hydrolyzed sugarcane bagasse**. *Enzyme Microb Technol* 2010, **46**:64–73.

73. Quintero J a., Moncada J, Cardona C a.: **Techno-economic analysis of bioethanol production from lignocellulosic residues in Colombia: A process simulation approach**. *Bioresour Technol* 2013, **139**:300–307.

74. Chiaramonti D, Prussi M, Ferrero S, Oriani L, Ottonello P, Torre P, Cherchi F: **Review of pretreatment processes for lignocellulosic ethanol production, and development of an innovative method**. *Biomass and Bioenergy* 2012, **46**:25–35.

75. Alvira P, Tomás-Pejó E, Ballesteros M, Negro MJ: **Pretreatment technologies for an efficient bioethanol production process based on enzymatic hydrolysis: A review**. *Bioresour Technol* 2010, **101**:4851–4861.

76. Mariano AP, Dias MOS, Junqueira TL, Cunha MP, Bonomi A, Filho RM: **Utilization of pentoses from sugarcane biomass: Techno-economics of biogas vs. butanol production**. *Bioresour Technol* 2013, **142**:390–399.

77. Gassner M, Marechal F: **Increasing Conversion Efficiency in Fuel Ethanol Production from Lignocellulosic Biomass by Polygeneration – and a Paradoxon between Energy and Exergy in Process Integration**. *23rd Int Conf Effic Cost, Optim Simul Environ Impact Energy Syst (ECOS 2010) proceedings, B 2* 2010(june):1–6.

78. **Final Report Summary - CANEBIOFUEL (Conversion of sugar cane biomass into ethanol)** [http://cordis.europa.eu/result/rcn/53336_en.html]

79. Palmqvist E, Hahn-Hägerdal B, Galbe M, Larsson M, Stenberg K, Szengyel Z, Tengborg C, Zacchi G: **Design and operation of a bench-scale process development unit for the production of ethanol from lignocellulosics**. *Bioresour Technol* 1996, **58**:171–179.

80. Humbird D, Mohagheghi A, Dowe N, Schell DJ: **Economic impact of total solids loading on enzymatic hydrolysis of dilute acid pretreated corn stover.** *Biotechnol Prog* 2010, **26**:1245–1251.

81. Dias MOS, Junqueira TL, Rossell CE V., Maciel Filho R, Bonomi A: **Evaluation of process configurations for second generation integrated with first generation bioethanol production from sugarcane**. *Fuel Process Technol* 2013, **109**:84–89.

82. Seabra JE a., Macedo IC: **Comparative analysis for power generation and ethanol production from sugarcane residual biomass in Brazil**. *Energy Policy* 2011, **39**:421–428.

83. Errico M, Rong B-G, Tola G, Spano M: **Optimal synthesis of distillation systems for bioethanol separation. Part 1: Extractive distillation with simple columns**. *Ind Eng Chem Res* 2013, **52**:1612–1619.

84. Kiss A a., Suszwalak DJ-. PC: **Enhanced bioethanol dehydration by extractive and azeotropic distillation in dividing-wall columns**. *Sep Purif Technol* 2012, **86**:70–78.

85. Luo H, Bildea CS, Kiss A a.: **Novel Heat-Pump-Assisted Extractive Distillation for Bioethanol Purification**. *Ind Eng Chem Res* 2015, **54**:2208–2213.

86. Urbaniec K, Zalewski P, Zhu XX: **A decomposition approach for retrofit design of energy systems in the sugar industry**. *Appl Therm Eng* 2000, **20**:1431–1442.

87. Ensinas A V., Nebra S a., Lozano M a., Serra LM: **Analysis of process steam demand reduction and electricity generation in sugar and ethanol production from sugarcane**. *Energy Convers Manag* 2007, **48**:2978–2987.

88. Palacios-Bereche R, Ensinas A V, Modesto M, Nebra SA: **Mechanical vapour recompression incorporated to the ethanol production from sugarcane and thermal integration to the overall process applying pinch analysis**. *Chem Eng Trans* 2014, **39**:397–402.

89. Dias MOS, Junqueira TL, Cavalett O, Cunha MP, Jesus CDF, Rossell CEV, Maciel Filho R, Bonomi A: **Integrated versus stand-alone second generation ethanol production from sugarcane bagasse and trash**. *Bioresour Technol* 2012, **103**:152–161.

90. Hatzakis I: **Multi-objective evolutionary optimization in time-changing environments**. Massachusetts Institute of Technology; 2007.

91. Noraini M, Geraghty J: **Genetic algorithm performance with different selection strategies in solving TSP**. In *World Congress on Engineering*. *Volume II*; 2011:4–9.

92. Al Jadaan O, Rao CR, Rajamani L: **Improved selection operator GA**. *J Theor Appl Inf Technol* 2008, **4**:269–277.

93. **Multicore - Parallel processing on multiple cores** [http://fr.mathworks.com/matlabcentral/fileexchange/13775-multicore-parallel-processing-on-multiple-cores]

94. Brownlee A, Wright J: **Solution analysis in multi-objective optimization**. In *First Building Simulation and Optimization Conference*; 2012:317–324.